DOKUZ EYLÜL UNIVERSITY
GRADUATE SCHOOL OF NATURAL AND APPLIED SCIENCES

ACTIVE POWER FILTERS BASED ON NEURAL NETWORKS FOR POWER QUALITY

by

Kadir VARDAR

October, 2011

İZMİR

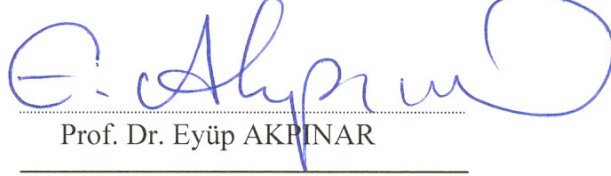# ACTIVE POWER FILTERS BASED ON
NEURAL NETWORKS FOR POWER QUALITY

A Thesis Submitted to the
Graduate School of Natural and Applied Sciences of Dokuz Eylül University
In Partial Fulfillment of the Requirements for the Degree of Doctor of
Philosophy in Electrical and Electronics Engineering,
Electrical and Electronics Program

by
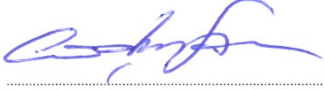**Kadir VARDAR**

October, 2011
İZMİR

Ph.D. THESIS EXAMINATION RESULT FORM

We have read the thesis entitled "**ACTIVE POWER FILTERS BASED ON NEURAL NETWORKS FOR POWER QUALITY**" completed by **KADİR VARDAR** under supervision of **PROF.DR. EYÜP AKPINAR** and we certify that in our opinion it is fully adequate, in scope and in quality, as a thesis for the degree of Doctor of Philosophy.

Prof. Dr. Eyüp AKPINAR

Supervisor

Prof. Dr. Coşkun SARI

Thesis Committee Member

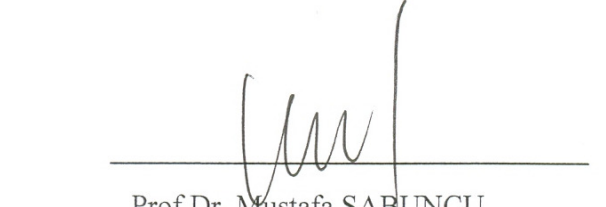Yrd. Doç. Dr. Tolga SÜRGEVİL
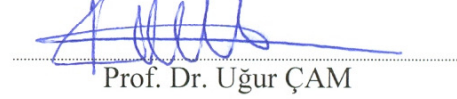
Thesis Committee Member

Doç. Dr. Mehmet Timur AYDEMİR

Examining Committee Member

Prof. Dr. Uğur ÇAM

Examining Committee Member

Prof.Dr. Mustafa SABUNCU
Director
Graduate School of Natural and Applied Sciences

ACKNOWLEDGMENTS

ACTIVE POWER FILTERS BASED ON NEURAL NETWORKS FOR POWER QUALITY

ABSTRACT

In this thesis, a 20 kVA shunt active power filter (APF) prototype was designed for power quality application. Primarily, harmonic detection methods for generating reference currents have been investigated. The advantages and disadvantages of several methods found in the literature have been discussed on the basis of simulation results. Adaptive linear neuron (ADALINE) method based shunt active filter structure is analyzed. This method is compared to the instantaneous reactive power theory (IRPT) method using direct current control technique. The direct and indirect current control techniques are applied in ADALINE method. The performances of direct and indirect current control techniques are compared. TMS320F2812 digital signal processor is used as a central processing unit in experimental works. Also, a systematic design approach is developed for rapid prototype system in a reliable procedure. The self-developed codes on DSP were tested with Simulink; therefore, any possible error in the controller implemented within software is eliminated before connecting the power converter to the supply. The designed shunt APF prototype has been tested successfully in industrial environment and laboratory. The modularity of shunt active power filters is examined for high power applications. The configurations and methods for parallel operation of APFs are analyzed with simulation and results are discussed.

Finally, the hysteresis current controller is modeled with APF first time for stability analysis and design of dc link PI controller. The results of linear model are compared with the detailed simulation results. Also, analysis of system has been done in order to designing compensation capacitor with APF.

Keywords: Active power filters, ADALINE, Digital signal processor applications, Harmonics detection methods, Parallel operation of active filter, Rapid prototyping, Hysteresis Current Controller.

GÜÇ KALİTESİ İÇİN YAPAY SİNİR AĞI TABANLI AKTİF GÜÇ FİLTRESİ

ÖZ

Bu tezde, güç kalitesini geliştirmek için 20 kVA paralel aktif güç filtresi (AGF) tasarlanmıştır. Öncelikle, referans akımın üretimi için harmonik çıkarım metotları incelendi. Literatürde bulunan bazı metotların avantaj ve dejavantajları simulasyon sonuçları ile tartışıldı. Adaptif doğrusal neron (ADALINE) metot tabanlı AGF yapıları analiz edildi. Bu metot, direk akım kontrolü için anlık reaktif güç teorisi (ARGT) metodu ile karşılaştırıldı. ADALINE metodu direkt ve endirekt akım kontrolü için uygulandı. Direk ve endirekt akım kontrol tekniklerinin performansları karşılaştırıldı. Deneysel çalışmalarda merkezi işlemci olarak TMS320F2812 dijital sinyal işlemcisi kullanıldı. Ayrıca, hızlı prototipleme için güvenli bir sistematik tasarım yaklaşımı geliştirildi. Yazılmış olan DSP kodu, güç çevirici yapısı şebekeye bağlanmadan önce yazılımda olası hatalara karşı Simulink ile test edilmiştir. Tasarlanan aktif filtre prototipi endüstriyel ortamda ve laboratuarda başarıyla test edilmiştir. Yüksek güçlü uygulamalar için aktif güç filtrelerinin modülerliği incelenmiştir. AGF'lerin paralel çalışması metot ve konfigürasyonları simülasyonlarla analiz edildi ve sonuçlar tartışıldı.

Son olarak, ilk kez histerezis akım kontrolcülü APF kararlılık analizi ve DC hat PI kontrolcüsü tasarımı için modellendi. Doğrusal modelin sonucu detaylı simülasyon sonuçları ile karşılaştırıldı. Ayrıca, kompanzasyon kapasitörlü APF tasarımı için sistemin analizi yapıldı.

Anahtar Kelimeler: Aktif güç filtreleri, ADALINE, Dijital sinyal işlemci uygulamaları, Harmonik çıkarım metotları, Aktif filtrelerin paralel çalıştırılması, Hızlı prototipleme, Histerezis akım kontrolcüsü.

CONTENTS

CHAPTER ONE
INTRODUCTION

An ideal ac power system has a single constant frequency and specified voltage levels of constant magnitudes. However, this situation is difficult to achieve in practice. The deviations from a perfect sinusoidal waveform like variations in the magnitude or the frequency are namely power quality problems. These power quality problems appear in different forms as harmonic distortion, transients, voltage variations, voltage flicker, etc.

The harmonics from power quality problems are current or voltage that are usually integer multiples of fundamental frequency in power system. For example, if the fundamental frequency 50Hz, then 3rd is 150Hz, 5th is 250Hz. In order to quantify this distortion, the term of Total Harmonics Distortion (THD) is used. The THD value is the square root of the summation of the effective value's square from all the harmonics currents, and divided by the value of the fundamental current (Emadi, 2005).

The passive filters are used in order to minimize the harmonic distortion level (Arrillaga et al, 1985). They consist of passive energy storage elements (inductors and capacitors) arranged in such a way to provide a low impedance path to the ground for the harmonic components. However passive filter have some limitation like designing separate filter for each harmonic frequency, flowing current into the filter at the fundamental frequency, causing resonance in power system.

The APFs have been widely used to control harmonic distortion in power systems. The APFs use power electronics converters (such as PWM voltage or current source converters) in order to inject harmonic components to the electrical network that cancel out the harmonics in the source currents caused by non-linear loads. The concept of active power filtering was first introduced in 1971 by Sasaki and Machida (Sasaki & Machida, 1971) who proposed implementation based on linear amplifiers. In 1976, (Gyngyi & Strycula, 1976) proposed a family of active

1

power filter systems based on PWM current source inverter (CSI) and PWM voltage source inverter (VSI).

APFs are also used in the solution of reactive power compensation and load balancing besides harmonics compensating capability. They have a significant advantage over the passive filters since they do not cause resonance problems in the network. A conceptual survey on APF topologies, control methods and practical applications can be found in the literature.

The performance of shunt APFs depends on the DC link voltage level, value of boost inductance, value of DC link capacitor, switching filter inductance, source inductance, load type (consisting of current source or voltage source type of harmonics), and the harmonic detection methods for generating current references. An essential part in the current controller is to generate the reference signals within a minimum time delay and accurately (Akagi, 1994, 1996), (Singh et al, 1999), (Emadi, 2005), (Vardar et al, 2009a), (Rechka, 2002) as much as possible. The accuracy is affected by the sampling period that is determined by the execution time of program in digital signal processor (DSP).

There are several methods to extract the harmonics from the load current. Performance of the method is a function of characteristics of the digital filter and execution time of programmable device. The time delay created by digital filter increased attention on application of neural network (Zhao & Bose, 2004) and predictive based applications. Adaptive linear neuron (ADALINE) method which is a feedforward neural network is used to eliminate the delay with its simple structure. In literature, ADALINE method is already proposed as a harmonic estimation technique (Osowski, 1992), (Vazquez & Salmeron, 2003), (Valiviita & Ovaska, 1998), (Abdeslam et al, 2005), (Boudjedaimi, 2008), but the experimental verifications of the results are not given while the simulations are reported on the APFs. The experimental results are reported in this thesis first time and compared to the other techniques. The weighting factor in this method is set forth for magnitude and phase angle of each harmonic component is taken into account.

The purpose of this thesis is to design a shunt active power filter based on ADALINE method for power quality improvement. Firstly, ADALINE and other methods are simulated by MATLAB and compared to each other in order to specify the advantages and disadvantages in terms of response time and filtering capability against the variations in frequency, phase, and amplitude of load currents. ADALINE and the selected two methods that are IRPT and SRF methods have been programmed in the DSP and simulated in the Matlab. The design procedure is developed before testing the code on physical system by co-operating MATLAB-DSP. Thus, the proper operation of the DSP is guaranteed through simulations.

The designed 20 kVA shunt APF prototypes are tested in an industrial plant and laboratory by using these three methods and direct/indirect current control techniques. Then, the designed prototypes are connected in parallel and modularity of APF is investigated. Finally, the shunt APF with hysteresis current controller's model is linearized first time for determining the DC link PI controller parameters.

This thesis is organized as follows:

In Chapter 2, the source of harmonic, its effect and limitation of it on power system are introduced. Harmonic mitigation methods are given as passive and active filters. The structures of active power filter are classified as types of voltage source and current source according to source types, the series, shunt, hybrid, and UPQC according to connection types, direct an indirect according to current measurement point. The current control techniques are listed as the hysteresis, delta modulation, ramp comparison (linear), and predictive controllers.

In Chapter 3, the Fast Fourier Transform and Kalman Filter method as frequency domain techniques and Instantaneous Reactive Power Theory, Single-phase Instantaneous Reactive Power method, Synchronous Reference Frame method, Generalized Integral method, Adaptive Filter method, Delayless Filtering based on Neural Network, Adaptive Linear Neuron method and Wavelet method as the time

domain techniques are presented in details. These methods are simulated by using MATLAB and the results are compared.

In Chapter 4, a design procedure for shunt APF using MATLAB/Simulink and TMS320F2812 DSP is presented. The procedure contains the modeling of the system in Simulink, testing the developed self-developed code on DSP with Simulink model as simultaneous operation. The ADALINE, IRPT, and SRF methods are programmed for testing designed 20 kVA shunt APF prototype. The algorithms and used design techniques of software are presented in details. The hardware of system and circuit schemes are given. The designed filter is tested under various conditions like as balanced, unbalanced, load variations, and transient states. The results are reported and discussed in this chapter.

The modularity of shunt active power filters (APF) is considered to be the most advantageous feature that allows parallel operation of a number of modules. From the viewpoint of reliability, flexibility, and efficiency, modular filtering approach is quite appropriate for high power applications. This configuration allows various control schemes to be employed, namely power and frequency splitting and capacity limitation control. In Chapter 5, these configurations and methods for parallel operation of APFs are analyzed in PSCAD and results are discussed.

In Chapter 6, the hysteresis current controller is modeled with active power filter (APF) for stability analysis and design of dc link PI controller. The results of linear model are compared with the detailed simulation results during starting period of the APF. The stable operating ranges of system parameters like hysteresis band width, filter inductance, dc link capacitor and sampling frequency are verified by the detailed dedicated simulation program in Matlab/Simulink interlinked to TMS320F2812. The results have shown that the linear model correctly predicts the stability of the system and provides the feasible solution for PI controller parameters from Routh-Hurwitz criteria. Also, the dynamic response of the starting is measured from the APF and compared to simulation result. Then, the effect of compensation capacitors on performance of shunt APF and power system is analyzed by modeling.

Finally, the conclusions on operation of designed shunt APF and performance of methods are given in Chapter 7. The contributions of thesis are briefly summarized. The some recommendations for future work are also presented.

A contribution of this thesis is that the indirect current control technique has been applied first time with Adaline Method in this work. Also, the application of Adaline on active power filters is experimentally verified for direct current control technique. A well established algorithm based on Matlab-DSP co-processing is developed here for the safety code generation. A 20 kVA shunt APF has been designed and tested successfully for ADALINE, IRPT, and SRF methods in laboratory and industrial environments. A linear model of a shut active power filter which contains hysteresis current controller is obtained using the synchronously rotating reference frame. This model is used to find out stability limits according to filter inter inductance, hysteresis band width and switching frequency. The stability range of DC link PI controller is found by applying Routh-Hurwitz criteria.

CHAPTER TWO
HARMONICS AND POWER QUALITY

2.1 Harmonics as a Power Quality Problem

Harmonics are qualitatively defined as sinusoidal waveforms having frequencies that are integer multiples of fundamental frequency. In power system engineering, the term harmonics is widely used to describe the distortion for voltage or current waveforms. It was detected as early as the 1920s and 30s (Akagi, 1994).

The quantity of harmonics is defined as total harmonic distortion (THD) for voltage or current waveforms. The THD equations of voltage and current are given in equation (2.1) and (2.2), respectively:
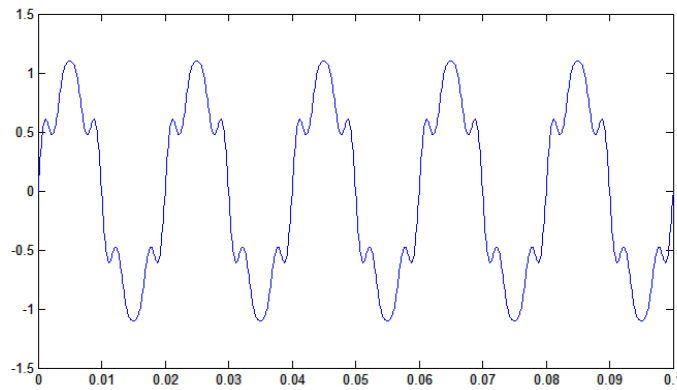
Figure 2.1 A sample waveform with harmonics as per unit.

$$THD_V = 100 \cdot \frac{\sqrt{\sum_{h=2}^{\infty} V_h^2}}{V_1} \tag{2.1}$$

$$THD_I = 100 \cdot \frac{\sqrt{\sum_{h=2}^{\infty} I_h^2}}{I_1} \tag{2.2}$$

Where, V_1 and I_1 are rms value of fundamental component, V_h and I_h are rms value of harmonic component.

6

IEEE 519-1992 standard specifies limits on voltage and current harmonic distortion for different voltage levels. Table 2.1 shows the IEEE 519 recommended voltage distortion. Table 2.2 lists recommended current distortion depending on customer load in relation to the system short circuit capacity.

Table 2.1 Harmonic voltage distortion limits at PCC.

Bus Voltage at PCC (V)	Individual Harmonic Voltage Distortion (%)	Total Voltage Distortion THD_V (%)
$V \leq 69kV$	3.0	5.0
$69kV \leq V \leq 161kV$	1.5	2.5
$V > 161kV$	1.0	1.5

Table 2.2 Harmonic current distortion limits at PCC.

I_{SC}/I_L	$h < 11$	$11 \leq h < 17$	$17 \leq h < 23$	$23 \leq h < 35$	$35 \leq h$	THD_I
$V \leq 69kV$						
<20	4.0	2.0	1.5	0.6	0.3	5.0
20-50	7.0	3.5	2.5	1	0.5	8.0
50-100	10.0	4.5	4.0	1.5	0.7	12.0
100-1000	12.0	5.5	5.0	2.0	1.0	15.0
>1000	15.0	7.0	6.0	2.5	1.4	20.0
$69kV \leq V \leq 161kV$						
<20	2.0	1.0	0.75	0.3	0.15	2.5
20-50	3.5	1.75	1.25	0.5	0.25	4.0
50-100	5.0	2.25	2.0	1.25	0.35	6.0
100-1000	6.0	2.75	2.5	1.0	0.5	7.5
>1000	7.5	3.5	3.0	1.25	0.7	10.0
$V > 161kV$						
<50	2	1.0	0.75	0.3	0.15	2.5
>51	3.5	1.75	1.25	0.5	0.25	4.0

2.1.1 Harmonic Sources

In the power system, harmonic distortion is caused by the nonlinear characteristics of the devices and loads. These nonlinear loads generate harmonic currents, which upon passing through different impedances and produce voltage harmonics. The voltage harmonics are propagate in power system and affect all of components (Emadi, 2005).

Harmonic sources can be classified into three categories: saturable devices, arcing devices, and power electronic devices. The transformers are the saturable devices, the arc furnaces, arc welders and discharge type lighting (fluorescent) can be given as arcing devices (Arrillaga et al,1985), (Greenwood, 1999).

The magnetization curve of a transformer is nonlinear and hence its operation within the saturation region causes distortion of the magnetizing current. Therefore, transformer is not a significant source of harmonics under normal operating in linear operating region. In saturation region magnetizing current increases and shows nonlinear characteristic. Motors can also generate harmonic currents in order to produce a magnetic field but it is less compared to transformer due to effect of air gap. The magnetizing characteristic of motors is much more linear compared to the transformer due to the presence of air gap.

A fluorescent lambs produce significantly amount of 3th, 5th, 7th, and 9th order harmonics. The arc furnaces are one of the high harmonic distortion devices in electrical power system. Its current is not periodic and it contains noninteger order of harmonics.

In power electronic equipment, the switching of the semiconductor devices is responsible for the nonlinear characteristic. The power electronic equipment includes adjustable speed drives (ASD), DC power supplies, battery chargers, electronic ballasts, and many other single or three phase rectifier-inverter applications. The ASDs have considerably high harmonics of order 5th and 7th. AC/DC rectifiers and

inverters produce $n \cdot p \pm 1$ order harmonics. Where, $2 \cdot p$ is number of rectifier/inverter pulses and $n = 1,2,3,...$. For example, a three phase rectifier has 6 pulses as typical and produces harmonics of order 5th, 7th, 11th, 13th, .. etc.

2.1.2 Effect of Harmonics

Harmonics can cause a variety of undesired effects in power systems like as signal interference, overvoltages, and circuit breaker failure, as well as equipment heating, malfunction, and damage.

These undesired effects caused by harmonics are listed as below:

- Cause reading error in measurement instrument.
- Interference with telecommunication systems.
- Increase heating losses and cause mechanical oscillations in induction and synchronous machines.
- Overvoltages and excessive currents on the system from resonance to harmonic voltages or currents in the network.
- Failure of capacitor banks due to dielectric breakdown or reactive power overload.
- Dielectric breakdown of insulated cables resulting from harmonic overvoltages in the system;
- Signal interference and relay malfunction, particularly in solid state and microprocessor-controlled systems;
- Interference with large motor controllers and power plant excitation systems;
- Unstable operation is occurred in circuit of zero crossing detecting and latching.
- 3rd harmonic increase neutral current.

2.2 Harmonic Mitigation Methods

Nowadays, due to the increase in the use of nonlinear loads in the distribution systems, large amounts of distorted current and voltage waveform exist. Mitigation or cancellation of these harmonics can be done by using passive or active structures.

2.2.1 Passive Filters

Passive harmonic filters have been used for harmonic mitigation for a long time which are made of inductive, capacitive, and resistive elements. The passive filters are divided in four types according to their characteristic as low-pass, high-pass, band-pass, and tuned filters, where, tuned filter is designed to eliminate one specific harmonic.

There are many problems for using passive filter like as large size, weight, fixed compensation, resonance problems with elements of system, and cause significant distortion in the voltage. (Akagi, 2005)
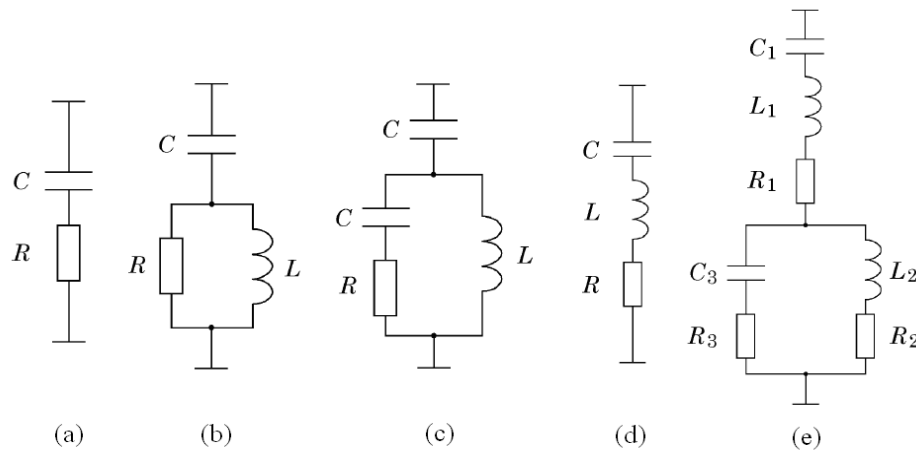

Figure 2.2 Some of structures of passive filter; high pass, a) first order b) second order c) third order, tuned filter, d) single tuned e) double tuned.

2.2.2 Active Filters

The active power filters have been widely used to control harmonic distortion in power systems. The APFs use power electronics converters (such as PWM voltage or

current source converters) in order to inject harmonic components to the electrical network that cancel out the harmonics in the source currents caused by non-linear loads. They have a significant advantage over the passive filters since they do not cause resonance problems in the network. Besides harmonics compensating capability, APFs are also used in the solution of reactive power compensation and load balancing.

APF's can be classified according to converter type, topology, and the number of phases. The converter types of APF are two types as Voltage Source Inverter (VSI) and Current Source Inverter (CSI). Single phase (two wire) and three phase (four wire) are used according to number of phase. There are four type topologies as shunt, series, hybrid, and unified. In active filters, desired elimination harmonics are detected by using different harmonic elimination methods and these methods are presented in chapter 3. The reference current is found with harmonic extraction method. The actual current is produced by using current control techniques like as hysteresis, pwm, predictive, and ramp comparison techniques. The reference current may be supply current for indirect control technique or may be filter current for direct control technique.

2.2.2.1 Shunt Active Power Filters

The most popular type active power filter is shunt or parallel active filter. The shunt APF can be voltage or current source, single or three phase. Power circuit of shunt APF consists of voltage or current source inverter. Block diagram of shunt APF is given in Figure 2.3 that used for elimination of harmonics produced by nonlinear load (Peng, 1998), (Akagi, 2005), (Emadi, 2005).

A shunt APF produce compensation current and the current of their losses for charging DC link capacitor at fundamental frequency. The compensation current is inverse of harmonic current of nonlinear loads. Shunt APF is more appropriate to use with the load as harmonic current source.

The shunt APF can perform the reactive power compensation and balancing loads. The additional filters are connected in parallel. With modular structure, power can be shared between the modules and one of each module can compensated different harmonics. Modularity is one of most important advantages of shunt APFs.
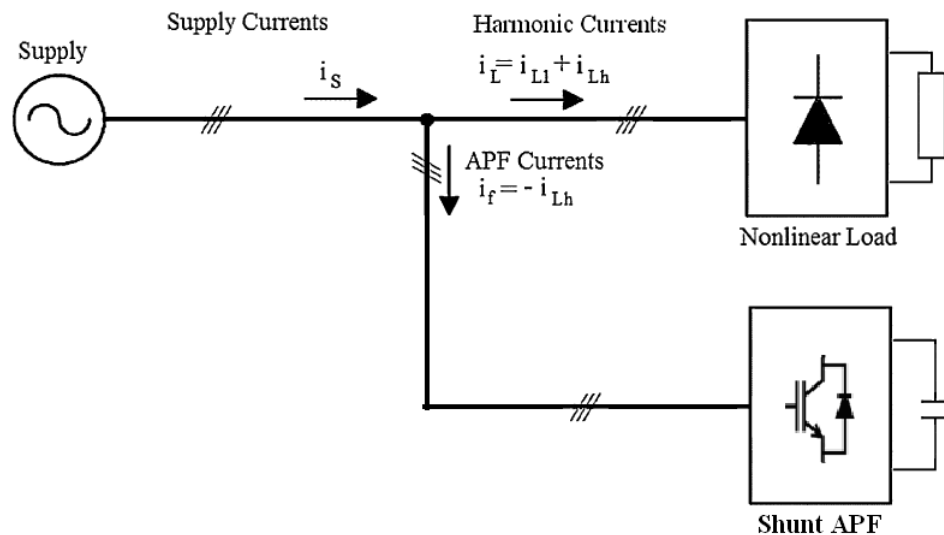
Figure 2.3 A shunt APF block scheme.

2.2.2.2 Series Active Power Filters

Figure 2.4 shows the connection scheme of a series APF. It is connected to the power system through coupling transformer and operates like as voltage source which is used to cancel the voltage harmonics of load. Therefore, series APF is widely preferred together with voltage source type harmonic sources such as diode rectifier with capacitive load (Peng, 1998), (Akagi, 2005), (Emadi, 2005).

Series APFs are used less than shunt APFs since it contains a high current rated transformer. Also, the series APFs can do regulating and balancing of AC voltages.
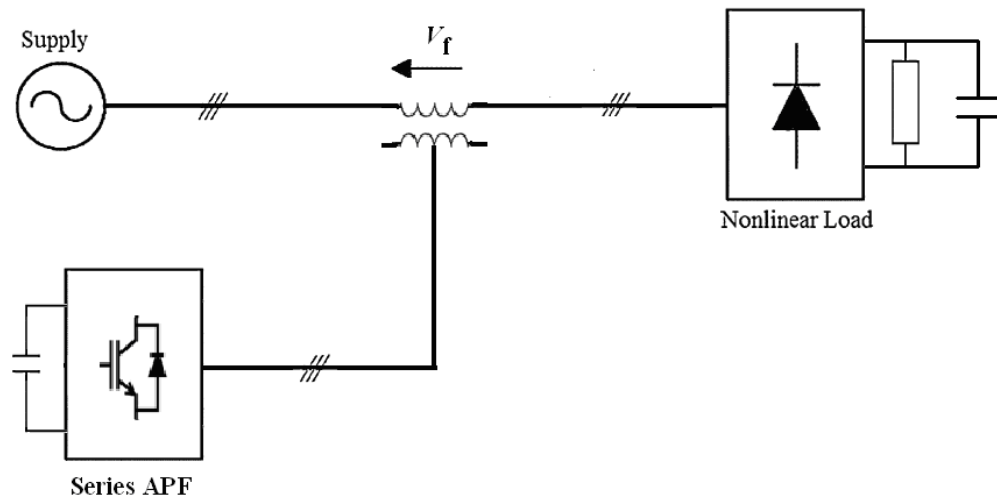
Figure 2.4 A series APF block scheme.

2.2.2.3 Hybrid Active Power Filters

The hybrid active power filter is combination of active and passive filters in order to reduce the cost of the compensation. The passive filters are used to cancel the most relevant harmonics of the load, and the active filter is dedicated to improve the performance of passive filters or to cancel other harmonics components. As a result, the total cost decreases without reduction of efficiency. Figure 2.5 and 2.6 shows the more usual hybrid active filter topologies (Peng, 1998), (Akagi, 2005), (Emadi, 2005).
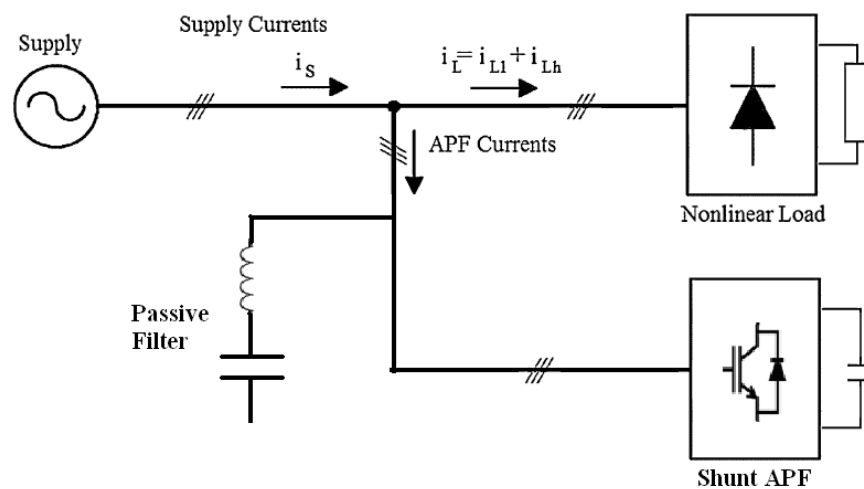
Figure 2.5 The hybrid filter that is combination of shunt APF and parallel passive filter.
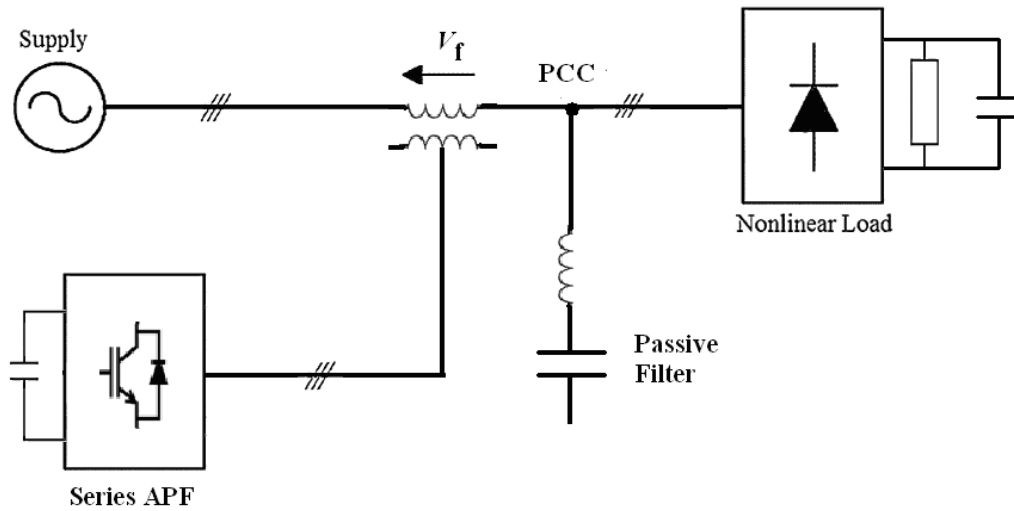
Figure 2.6 The hybrid filter that is combination of series APF and parallel passive filter.

2.2.2.4 Unified Power Quality Conditioners

UPQCs are effective devices to improve power quality which consist of series and shunt active filter. Series active filter suppresses and isolates voltage harmonics and regulates voltage at point of common coupling (PCC). Shunt APF compensates current harmonics and reactive power. Also, regulation of DC link voltage performs by shunt APF. The structure of UPQC can be shown in Figure 2.7 (Peng, 1998), (Emadi, 2005).
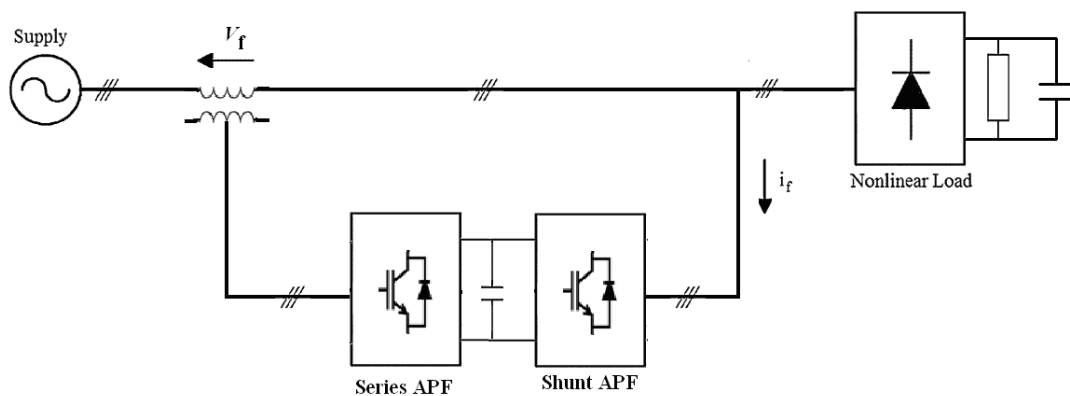
Figure 2.7 Block scheme of unified power quality conditioners.

2.3 Classification of Active Power Filters

2.3.1 Current Source Active Power Filter

The structure of current source inverter (CSI) is given in Figure 2.8. The CSI based active filter uses an inductor as DC energy storage element at DC side of converter. In these filters, DC current of the energy storage inductor must be greater than the maximum amplitude of load harmonic current. If the current of DC inductor is very small, the filter cannot perform proper compensation (Emadi, 2005), (Routimo et al, 2007).
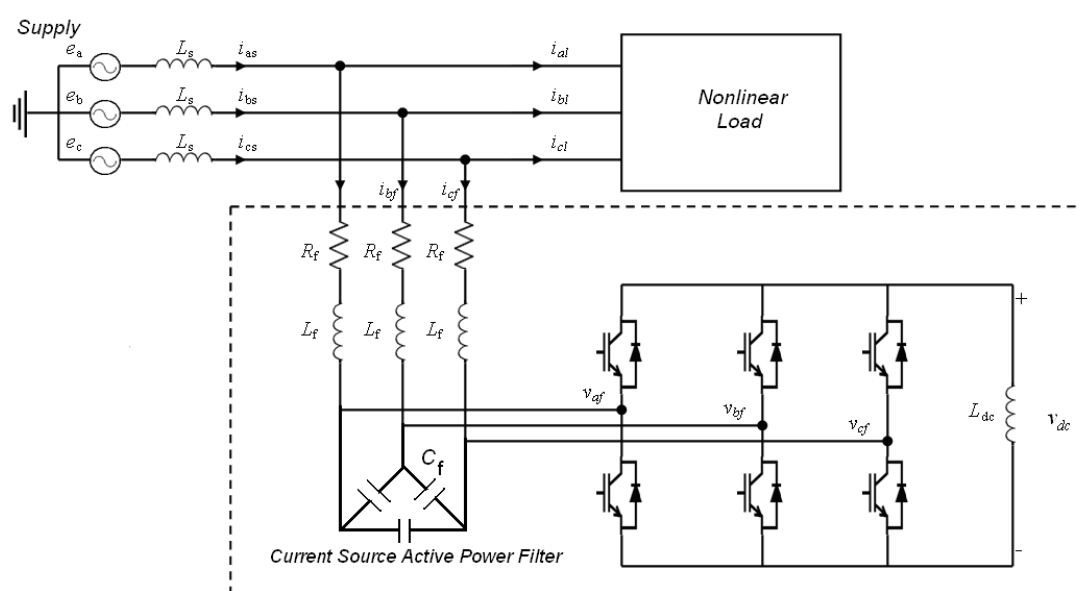
Figure 2.8 The scheme of CSI shunt active power filter.

2.3.2 Voltage Source Active Power Filter

The voltage source inverter (VSI) uses a capacitor as DC energy storage element at DC side of converter and its structure is given in Figure 2.9. In these filters, DC voltage of the energy storage capacitor must be greater than the maximum supply voltage. For proper operation of filter, DC link voltage should be 1.5 times that of the supply maximum voltage. And, DC link capacitor should be large enough to limit the

voltage ripple on DC link. Where, filter inductance links the filter and system. For controllability of active filter, this inductor should not be large. On the other hand, inductor should be very small due to increasing switching ripples. Therefore, an appropriate value for this inductance should be found (Emadi, 2005), (Routimo et al, 2007).
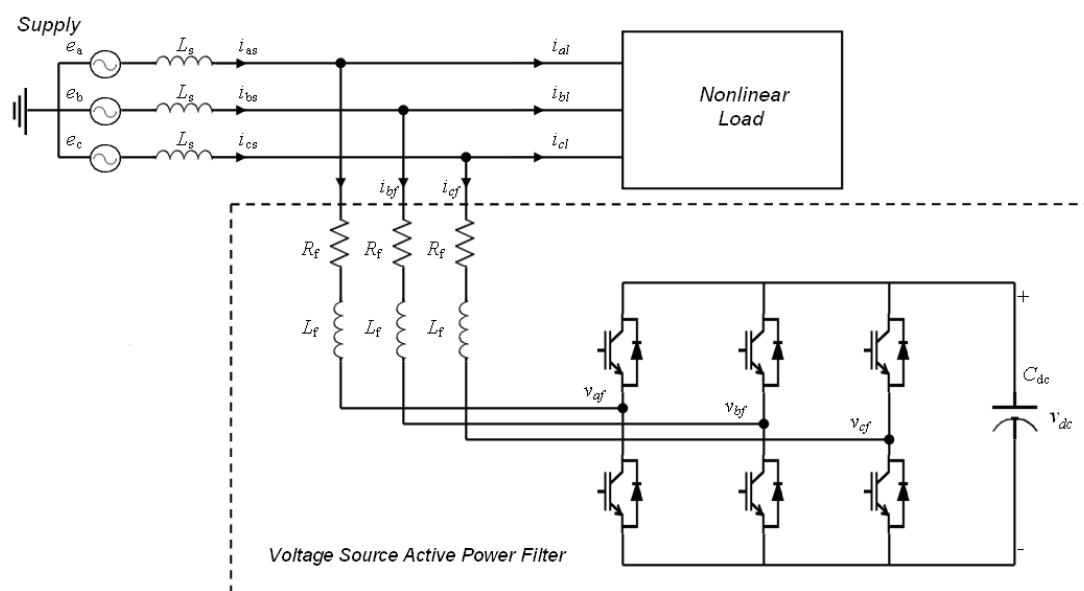
Figure 2.9 The scheme of VSI shunt active power filter.

2.4 Classification of Current Control Techniques

The current control techniques play an important role in performance of active power filters. There are several types of current control techniques such as delta modulation, hysteresis, linear (ramp comparison) and predictive controllers. All the current control methods operate in the stationary reference frame while the some of current control techniques and varieties like as linear controllers operating in the rotational frame of reference. These current control techniques are briefly explained below.

2.4.1 Delta Modulation Current Control Technique

The basic structure of a Delta Modulator is shown in Figure 2.10. It looks quite similar to that of a hysteresis controller, but operating principle is quite different. In

fact, only error sign is detected by comparators, whose outputs are sampled at a fixed rate so that inverter status is kept constant during each sampling interval. Thus, no pulse width modulation is performed, but only basic voltage vectors can be generated by the inverter for a fixed time. The effect of discretization is that, when synthesizing periodic waveforms, a non negligible amount of sub-harmonics is generated. Thus, a delta modulator should switch at a frequency about ten times higher than a PWM modulator. Also, delta modulators are very simple and insensitive to the load parameter (Malesani & Tomasin, 1993).
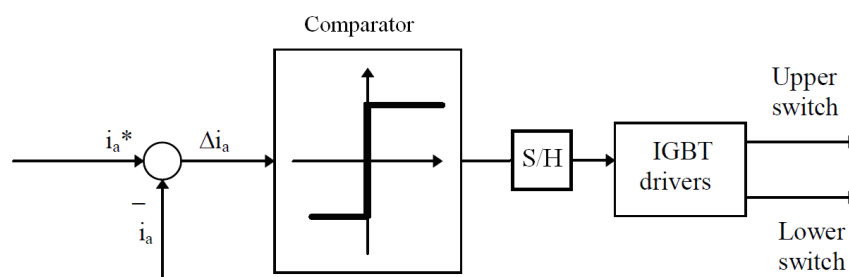
Figure 2.10 Block scheme of Delta modulation

2.4.2 Hysteresis Current Control Technique

The hysteresis current control method is widely used a control method in time domain. Hysteresis controllers utilize a hysteresis band in comparing the actual current with the reference current and produces directly the drive commands for the switches when the error exceeds an assigned band. Block scheme of hysteresis control technique is given in Figure 2.11. The advantages of this technique are high simplicity, good accuracy, outstanding robustness and a response speed limited only by switching speed and load time constant. The some characteristics of hysteresis current control such as the variable switching frequency are considered in many applications as unfavorable. Also, the variable switching frequency causes to spreading white noise along whole harmonic spectrum of supply current for active power filter applications and performance of THD is decreased. As a result, design of the switching ripple filter is complicated and the undesired resonances may be generated on power system (Malesani & Tomasin, 1993), (Casaravilla et al, 2002), (Grandy et al, 1990), (Nabae et al, 1996).
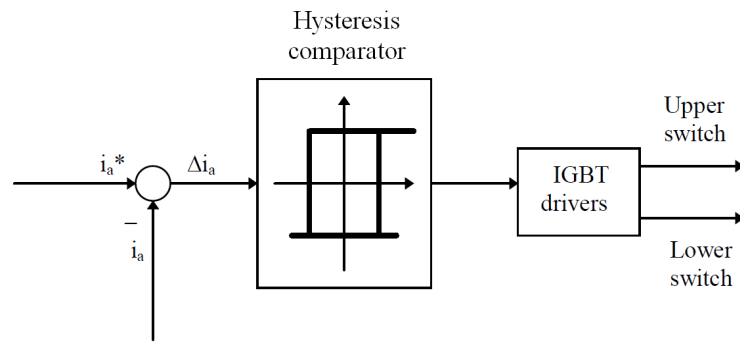
Figure 2.11 Block scheme of hysteresis current control technique

Figure 2.12 shows the ramping of the current between the two hysteresis band limits where the upper hysteresis limit is the sum of the reference current and the maximum error or the difference between the upper limit and the reference current and for the lower hysteresis limit, it is the subtraction of the reference current and the minimum error. Supposing the value for the minimum and maximum error should be the same. As a result, the hysteresis bandwidth is equal to two times of current error. (Ingram & Round, 1997)
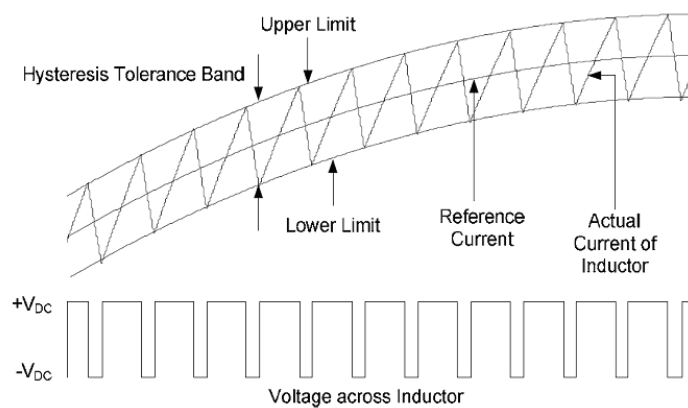
Figure 2.12 Operation of hysteresis current control technique

2.4.3 Linear Current Control Technique

The linear (ramp-comparison) current controller uses proportional-integral (PI) error compensators and compares the current error to a fixed frequency triangular carrier to generate the switching signals for the active filter. The block diagram of this

method is given in Figure 2.13 (Brod & Novotny, 1985),(Kazmierkowski & Malesani, 1998), (Malesani & Tomasin, 1993),
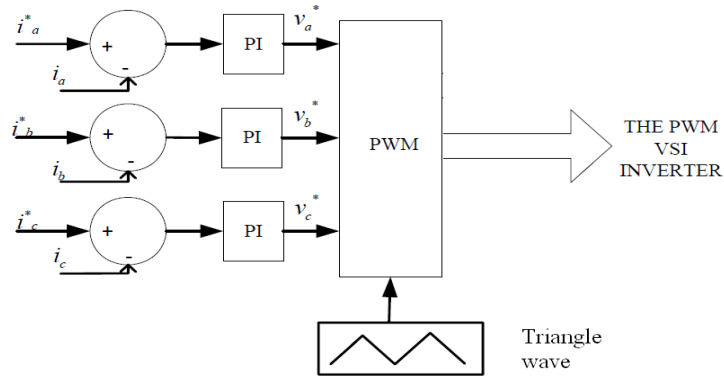
Figure 2.13 Block scheme of linear current control technique

Figure 2.14 shows the inverter output voltage resulting for the comparison between the control signal u_{ref} and the triangular carrier $u_{carrier}$. If the control signal is higher than the triangular waveform, the switches are activated to apply u_{dc} to the output. On the other hand, if the control signal is lower than the triangular carrier, an output voltage equal to $-u_{dc}$ is produced.
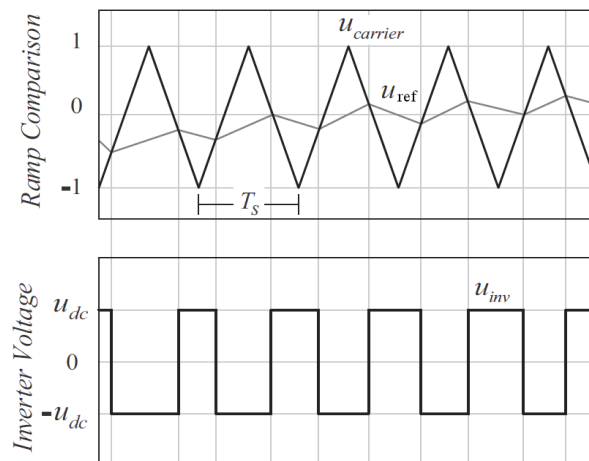
Figure 2.14 Operation of linear current control technique

In linear current controller, the switching frequency is constant, since the triangular carrier is operated with a fixed frequency. However, despite this main

advantage, the control concept has inherent amplitude and phase tracking error, as the PI controller has to process AC signals. Furthermore, it can be affected by stability requirement of the current feedback loop which is highly dependent to load parameters. Generally, linear current control technique operates in stationary and rotating reference frame (Malesani & Tomasin, 1993).

2.4.4 Predictive Current Control Technique

The basic idea of the predictive current controller is to perform a fast and accurate control loop that selects the optimum control action among all possibilities, to fulfill a certain predefined criteria (Kennel & Linder, 2000). This decision is based on the knowledge of actual variable measurements and load parameters. The typical structure of a predictive current controller is shown in Figure 2.15. The "Load Model" block provides the actual load states to the "Prediction and Decision", which is considered the heart of a predictive control system. Based on the comparison of actual states and references, the optimum switching state is selected according to the decided criteria, which can be for example minimum switching frequency, minimum response time or minimum current distortion (Kernel& Linder, 2000), (Holtz & Stadtfeld, 1983).
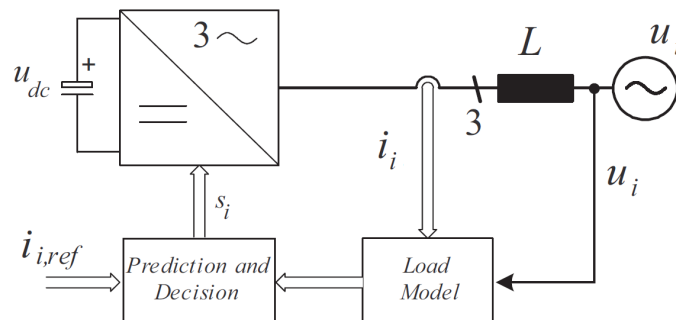
Figure 2.15 Block scheme of predictive current control technique

2.5 Direct and Indirect Current Techniques

2.5.1 Direct Current Technique of Shunt APF

In the direct current technique as being shown in Figure 2.16, the switching signals of IGBT in shunt APF are obtained by comparing reference three phase filter currents (sum of harmonics and compensation current of DC link voltage) and measured filter currents in the HCCs. Here, the reference filter currents can be estimated by using any harmonic extraction methods on load current (Singh et al, 1998,1999,2007), (Dixon & Ooi, 1988).
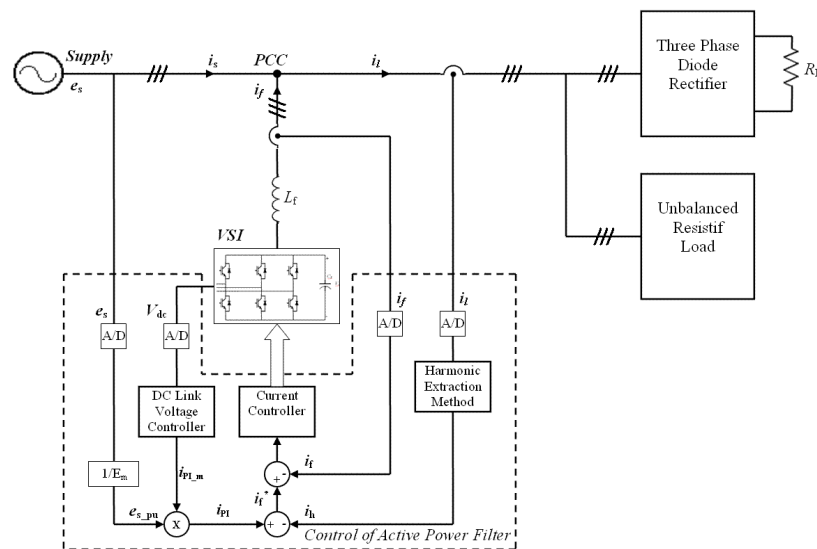
Figure 2.16 Single line diagram of direct current controller.

2.5.2 Indirect Current Technique of Shunt APF

The block diagram given in Figure 2.17 shows the indirect current technique used in control of APF. The currents are measured from load and supply sides. The switching signals of IGBT are controlled by comparing the reference supply current, which is estimated from the fundamental component of load current, and actual (measured) supply currents in the HCC (Singh et al, 1998,1999,2007), (Dixon & Ooi, 1988).
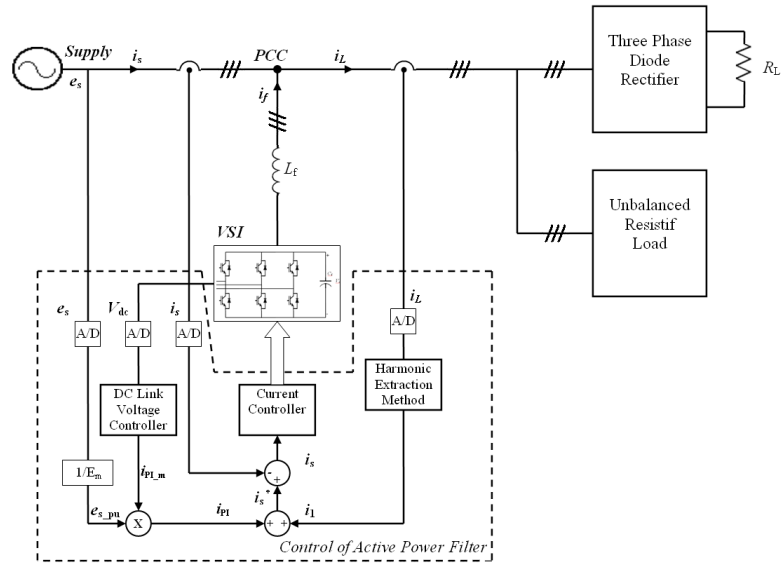
Figure 2.17 Single line diagram of indirect current controller.

CHAPTER THREE
HARMONIC EXTRACTION METHODS

3.1 Introductory Remarks

In the process of harmonic compensation, detection of the load current harmonics is one part, while the generation of compensating harmonic currents by means of converter switching is the other part of APF. The performance of active power filters depends on the harmonic detection methods for generating current references, current control method, and dynamic characteristics of APF power converter circuit. Of all these criteria related to design of APF, generation of current references constitutes an important part that affects the filtering performance since any inaccurate phase and magnitude of reference currents yields to incorrect compensation and hence performance degradation (Han et al, 2005),(Ovaska et al, 2005),(Valiviita & Ovaska, 1998). Some of the loads such as arc furnaces in power system are varying very fast. Therefore, the response time of APFs when compensating the harmonics of rapidly changing loads should be considered as a critical parameter. So, a fast and accurate detection of harmonic components in current or voltage waveforms is essential in APFs for varying loads. Many harmonic detection methods were proposed and their performances were evaluated in papers that can be found in the literature (Rechka et al, 2002a, 2002b,2003), (Asiminoaei et al, 2005), (Girgis et al,1991), (Tepper et al, 1996).

There are several methods for extracting the harmonics content of a non-sinusoidal load current. Generally, the harmonic extraction methods can be classified as frequency domain or time domain techniques. The frequency domain techniques investigated in this chapter are Fast Fourier Transform (FFT) and Kalman Filter method. The time domain techniques include Instantaneous Reactive Power Theory (IRPT), Single-phase Instantaneous Reactive Power method, Synchronous Reference Frame (SRF) method, Generalized Integral method, Adaptive Filter method,

Delayless Filtering based on Neural Network, Adaptive Linear Neuron (ADALINE) method and Wavelet method.

In this chapter, these methods are simulated in MATLAB and compared to each other in order to specify the advantages and disadvantages in terms of response time and filtering capability against the variations in frequency, phase, and amplitude of load currents.

3.1.1 Frequency Domain Harmonic Extraction Methods

3.1.1.1 Fast Fourier Transform Method

The amplitude and phase information of the harmonic series in a periodic signal can be calculated by using the Fourier analysis (Rechka, 2002a, 2002b).

$$\overline{X}_h = \sum_{n=0}^{N-1} x(n) \cdot \cos\left(\frac{2\pi.h.n}{N}\right) - j \cdot \sum_{n=0}^{N-1} x(n) \cdot \sin\left(\frac{2\pi.h.n}{N}\right) \tag{3.1}$$

$$\overline{X}_h = X_{hr} + j \cdot X_{hi} \tag{3.2}$$

$$\left|\overline{X}_h\right| = \sqrt{X_{hr} + j \cdot X_{hi}} \tag{3.3}$$

$$\varphi_h = \arctan\left(\frac{X_{hi}}{X_{hr}}\right) \tag{3.4}$$

Where, N is number of sample in a period, x(n) value of input at the point of n, X_h is h^{th} harmonic component vector. X_{hr} real part of this vector and X_{hi} is imaginary part and also φ_h is phase angel.

Fast Fourier Transform (FFT) is an efficient algorithm for computing the Discrete Fourier Transform (DFT) of discrete signals. The FFT reduces the amount of time for calculation by using the number of sampled points N, which is a power of two. This method is preferred in some digital signal processing applications if the waveform is processed on-line using microcontrollers having a higher clock

frequency. The basic operational principle of an APF requires extracting harmonics to be eliminated (or minimized) from the entire current waveform of the load. Therefore, the FFT is a powerful tool for harmonic analysis in active power filters as well. The drawback of this application is the execution time of the algorithm implemented in processor, because it needs sampled data over one period to estimate the spectrum of harmonics. If the load current varies in every period or in every few periods, the FFT algorithm may not provide sufficient information on-line to follow the harmonic content of the load.

3.1.1.2 Kalman Filter Method

This algorithm provides the estimate of the electrical magnitudes from their sampled values in a response time of less than one sampling interval. Kalman Filter method is applied by using equations below. (Moreno et al, 2002)

$$x_{k+1} = \phi_k \cdot x_k + \nu_k \tag{3.5}$$

$$z_k = [H_k] \cdot x_k + \omega_k \tag{3.6}$$

Kalman gain is calculated and estimated measurement is updated according to equations below.

$$x_{k+1}^- = \phi_k \cdot \hat{x}_k \tag{3.7}$$

$$P_{k+1}^- = \phi_k \cdot P_k \cdot \phi_k^T + Q_k \tag{3.8}$$

$$K_k = P_k^- H_k^T (H_k P_k^- H_k^T + R_k)^{-1} \tag{3.9}$$

$$\hat{x} = \hat{x}_k^- + K_k (z_k - H_k \hat{x}_k^-) \tag{3.10}$$

$$P_k = (I - K_k H_k) P_k^- \tag{3.11}$$

If number of harmonic component is n_f, state transition matrix is given in equations (3.12) and (3.13).

$$\phi_k = \begin{bmatrix} M_1 & .. & 0 \\ .. & .. & .. \\ 0 & .. & M_{nf} \end{bmatrix} \tag{3.12}$$

$$M_i = \begin{bmatrix} \cos(i\omega\Delta t) & -\sin(i\omega\Delta t) \\ \sin(i\omega\Delta t) & \cos(i\omega\Delta t) \end{bmatrix} \tag{3.13}$$

and

$$H_k = \begin{bmatrix} 1 & 0 & 1 & 0 & . & . & . & . & 1 & 0 \end{bmatrix} \tag{3.14}$$

Where, Δt is sampling time interval, x_k: State vector at instant k and it has nx1 dimension. ϕ_k: State transition matrix with nxn dimension, z_k: is measurement variable at instant (scalar).

H_k: has 1xn dimension and the matrix which gives ideal relation (without noise) between the measurements and state vector at the instant k. P_k is error covariance matrix, υ_k : noise signal, Q_k : covariance matrix of υ_k. The real-time algorithm of Kalman filter is given in Figure 3.1.

Entering previously $\hat{x}_k^-$ estimation and P_k^- error covariance

Kalman Gain Computing
$$K_k = P_k^- H_k^T (H_k P_k^- H_k^T + R_k)^{-1}$$

$$x_{k+1}^- = \phi_k \cdot \hat{x}_k$$
$$P_{k+1}^- = \phi_k \cdot P_k \cdot \phi_k^T + Q_k$$

Updated estimate with measurement Z_k
$$\hat{x} = \hat{x}_k^- + K_k (z_k - H_k \hat{x}_k^-)$$

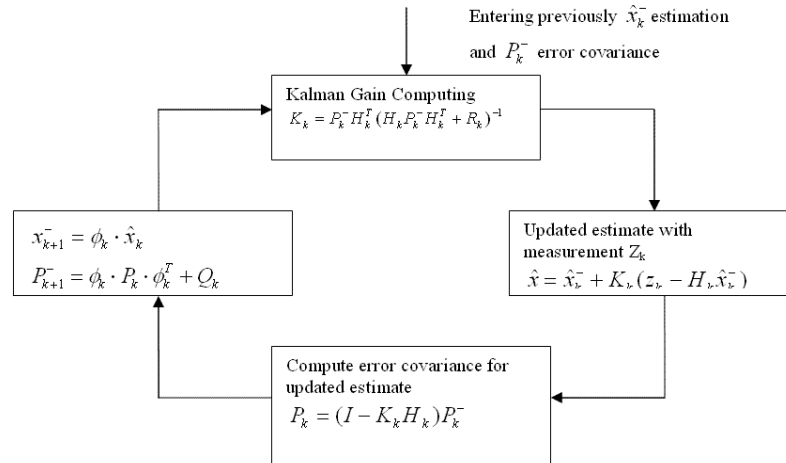Compute error covariance for updated estimate
$$P_k = (I - K_k H_k) P_k^-$$

Figure 3.1 Block diagram of Kalman filter.

3.2.1 Time Domain Harmonic Extraction Methods

3.2.1.1 Instantaneous Reactive Power Theory Method (IRPT)

In a three-phase system, harmonic current components can be found by using the IRPT (Rechka, 2002a, 2002b) as shown in the block diagram in Figure 3.2. The dc and ac components in these instantaneous active and reactive powers are due to fundamental and harmonic currents of the load, respectively. The power values of the dc components are filtered out by two high-pass filters. Thus, the remaining part is extracted as active and reactive powers caused by the load harmonic currents. Here it must be noted that the delay of response is based on filters' performance. Using the output of filters, the reference currents for each phase of the APF are generated, first in stationary alfa-beta coordinates and then in abc variables using Clarke's transformation.

$$
\begin{bmatrix} v_d^s \\ v_q^s \end{bmatrix} = \sqrt{\frac{2}{3}} \cdot \begin{bmatrix} 1 & -\frac{1}{2} & -\frac{1}{2} \\ 0 & \frac{\sqrt{3}}{2} & -\frac{\sqrt{3}}{2} \end{bmatrix} \cdot \begin{bmatrix} v_a \\ v_b \\ v_c \end{bmatrix} \tag{3.15}
$$

$$
\begin{bmatrix} i_{Ld}^s \\ i_{Lq}^s \end{bmatrix} = \sqrt{\frac{2}{3}} \cdot \begin{bmatrix} 1 & -\frac{1}{2} & -\frac{1}{2} \\ 0 & \frac{\sqrt{3}}{2} & -\frac{\sqrt{3}}{2} \end{bmatrix} \cdot \begin{bmatrix} i_{La} \\ i_{Lb} \\ i_{Lc} \end{bmatrix} \tag{3.16}
$$

Instantaneous active and reactive powers are calculated by using following equations:

$$
\begin{bmatrix} p_L \\ q_L \end{bmatrix} = \frac{3}{2} \cdot \begin{bmatrix} v_d^s & v_q^s \\ -v_q^s & v_d^s \end{bmatrix} \cdot \begin{bmatrix} i_{Ld}^s \\ i_{Lq}^s \end{bmatrix} = \begin{bmatrix} \bar{p}_L + \tilde{p}_{Lh} \\ \bar{q}_L + \tilde{q}_{Lh} \end{bmatrix} \tag{3.17}
$$

$$
\begin{bmatrix} i_{df}^{s\,*} \\ i_{qf}^{s\,*} \end{bmatrix} = \frac{1}{v_d^{s\,2} + v_q^{s\,2}} \cdot \begin{bmatrix} v_d^s & -v_q^s \\ v_q^s & v_d^s \end{bmatrix} \cdot \begin{bmatrix} -\tilde{p}_{Lh} \\ -\tilde{q}_{Lh} \end{bmatrix} \tag{3.18}
$$

$$
\begin{bmatrix} i^{*}_{af} \\ i^{*}_{bf} \\ i^{*}_{cf} \end{bmatrix} = \sqrt{\frac{2}{3}} \cdot \begin{bmatrix} 1 & 0 \\ -\dfrac{1}{2} & \dfrac{\sqrt{3}}{2} \\ -\dfrac{1}{2} & -\dfrac{\sqrt{3}}{2} \end{bmatrix} \cdot \begin{bmatrix} i^{s}_{df}{}^{*} \\ i^{s}_{qf}{}^{*} \end{bmatrix} \tag{3.19}
$$

This method does not take zero sequence components and hence the effect of unbalanced voltages and currents into account. The IRPT is widely used for three-phase balanced non-linear loads, such as rectifiers.
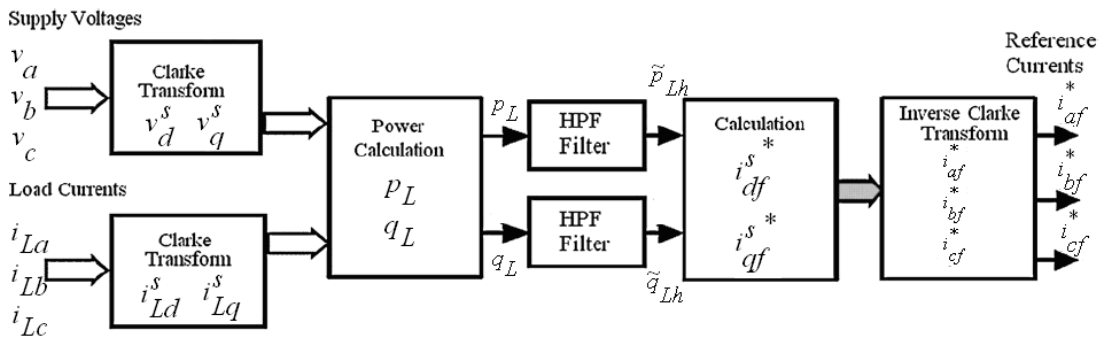
Figure 3.2 Block diagram of IRPT method.

3.2.1.2 Single Phase Instantaneously Reactive Power Theory Method

The application of active power filters in a single-phase system independent of load level also needs the reference waveform of harmonics in load current. The time varying source voltage $v(t)$ and load current $i(t)$ can be written in complex form as given in equations (3.20) and (3.21).(Haque & Ise, 2002), (Khadkikar et al,2009)

$$
\bar{v}(t) = v \cdot e^{j(\beta(t))} = v \cdot [\cos(\beta(t)) + j \cdot \sin(\beta(t))] = v_r(t) + j \cdot v_i(t)] \tag{3.20}
$$

$$
\bar{i}(t) = i \cdot e^{j(\psi(t))} = i \cdot [\cos(\psi(t)) + j \cdot \sin(\psi(t))] = i_r(t) + j \cdot i_i(t)] \tag{3.21}
$$

Where, $\bar{v}(t)$ and $\bar{i}(t)$ *are* instantaneous space vectors of current and voltage. The magnitude and phase of these vectors may change in time. These vectors can be

resolved into two components on real and imaginary axes which provide amplitude and angular position of the vector.
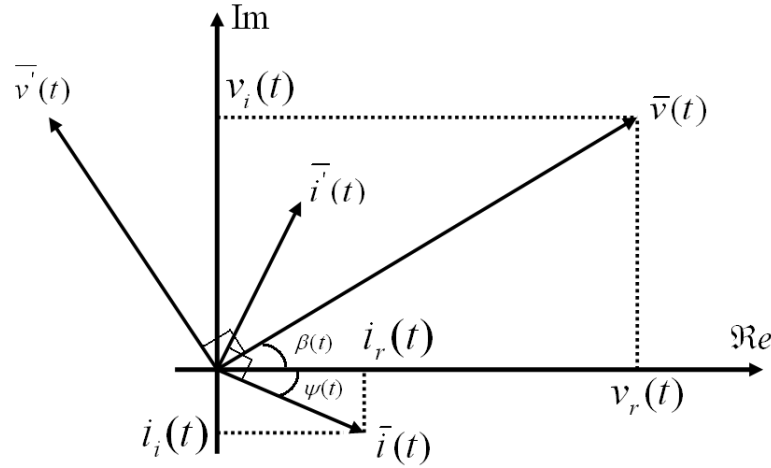
Figure 3.3 Instantaneous space vectors of current and voltage.

$\overline{v}^{'}(t)$ and $\overline{i}^{'}(t)$ are defined as the space vectors in Figure 3.3 leading source voltage and load current by $\pi/2$ respectively.

Single phase instantaneous complex power can be written as follows.

$$S = \overline{v}(t) \cdot \overline{i}^{*}(t) \tag{3.22}$$

Where $i^{*}(t)$ is called complex conjugate of instantaneous space vector of $i(t)$. By substituting equations (3.20) and (3.21) into the equation (3.22), the following equation can be obtained for complex power.

$$S = \left[v_r(t) \cdot i_r(t) + v_i(t) \cdot i_i(t) \right] + j \cdot \left[v_r(t) \cdot i_i(t) - v_i(t) \cdot i_r(t) \right] = p + j \cdot q \tag{3.23}$$

$$p = \overline{p} + \tilde{p} \tag{3.24}$$

$$q = \overline{q} + \tilde{q} \tag{3.25}$$

The real part is the single phase instantaneous active power while the imaginary part is the single phase instantaneous reactive power. The power transferred at the

higher frequencies of current than fundamental one can be extracted. This is achieved by employing a high pass filter on real and imaginary parts of the complex power. The output of high pass filters are defined as $\tilde{p}$ and $\tilde{q}$ referring to the instantaneous active and reactive powers due to harmonics. Hence, the reference current for the active power filter can be obtained as follows:

$$i_{ref} = \frac{\left[\tilde{p} \cdot v_r(t) - \tilde{q} \cdot v_i(t)\right]}{\left[v_r^2(t) + v_i^2(t)\right]} \tag{3.26}$$

The main advantage of this method is the ability to generate sinusoidal reference for each phase in the case of current imbalance in a three-phase system. IRPT can be applied to single-phase system by creating two virtual currents and two virtual voltages that have the same magnitude as the measured voltage and current and displaced by 120° phase shift. (Pinto et al, 2007)
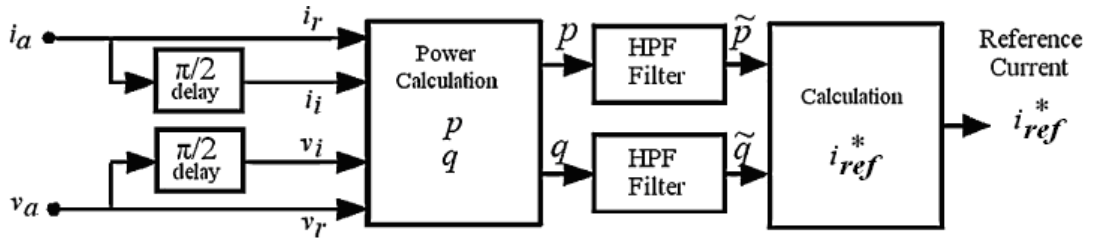
Figure 3.4 Block diagram of Single Phase PQ theory.

3.2.1.3 Synchronous Reference Frame (SRF) Method

Synchronous reference frame (SRF) method (Bhattachharya et al, 1998) is based on Park transformation and shown in Figure 3.5. There are mainly two blocks corresponding to positive and negative sequence controllers. The positive sequence component of load current is transformed to d^e- q^e axes by generating positive sequence phase information $+\theta_e$ from PLL circuit. The detail of mathematical implementation of PLL software in the synchronization of three-phase system is given in (Aiello et al, 2007) and its application in Matlab simulations can be found in

package program. AC quantities in positive sequence waveform include all harmonic components while dc quantity is fundamental component of load current. The negative sequence component of load current is also transformed to d^e - q^e axes by generating negative sequence phase information $-\theta_e$ from the PLL. If voltages and currents in the three-phase system are balanced, the output of this block will be zero. As long as it is not the aim to compensate current imbalance in the load currents, the negative sequence current components are subtracted from the reference current waveforms and the active filter only compensates the load current harmonics.
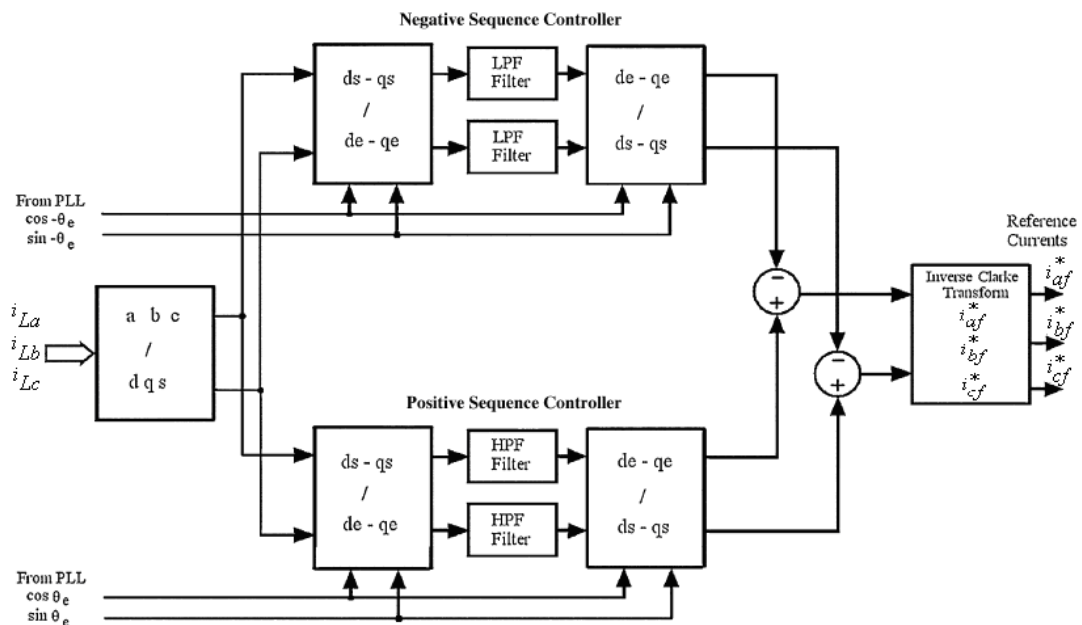
Figure 3.5 Block diagram of SRF Method

In application of APF, the execution time in the DSP is a most important parameter in order to increase performance of filtering. According to literature and experimental works, the most important factor reducing the speed of IRPT method is the structure of high order low-pass filter. In SRF method, the filter used can be designed as lower order, therefore DC component is passed and it can be operated at faster frequency than IRPT method. SRF method is applied only using positive sequence which can operate fast for balanced load. Since the sampling time is increased, the shunt APF is showed high performance.
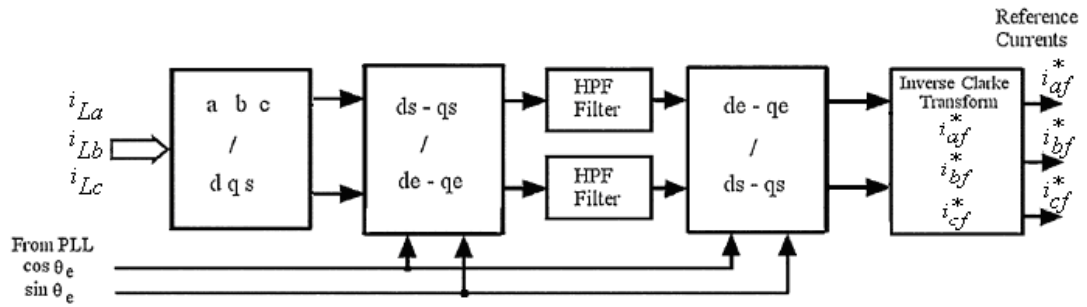
Figure 3.6 Another application of SFR method for balanced system.

In literature, another application is selective harmonic elimination technique which is given in Figure 3.7. The desired harmonics are obtained separately and compensated. For example, when the separation of 5th order harmonic is carried out, θ_e is obtained by using PLL then it is multiplied by -5 since 5th order harmonic has negative sequence (rotates in opposite direction to fundamental). When the load current is transformed by $-5 \cdot \theta_e$, 5th order harmonic current appears in DC quantity. This DC quantity is filtered out by using a LPF and it is transformed to stationary reference frame. The reference current is obtained by summing up the other harmonics eliminated like as 7th, 11th and 13th, etc.

Figure 3.7 The selective harmonic elimination application with SFR method.

The transformation between reference frames are done by using the equations below.

$$\begin{bmatrix} i_{Ld}^{s} \\ i_{Lq}^{s} \end{bmatrix} = \sqrt{\frac{2}{3}} \cdot \begin{bmatrix} 1 & -\frac{1}{2} & -\frac{1}{2} \\ 0 & \frac{\sqrt{3}}{2} & -\frac{\sqrt{3}}{2} \end{bmatrix} \cdot \begin{bmatrix} i_{La} \\ i_{Lb} \\ i_{Lc} \end{bmatrix} \tag{3.27}$$

$$\begin{bmatrix} i_{Ld}^{e} \\ i_{Lq}^{e} \end{bmatrix} = \begin{bmatrix} -\sin(\theta_{e}) & \cos(\theta_{e}) \\ \cos(\theta_{e}) & \sin(\theta_{e}) \end{bmatrix} \cdot \begin{bmatrix} i_{Ld}^{s} \\ i_{Lq}^{s} \end{bmatrix} \tag{3.28}$$

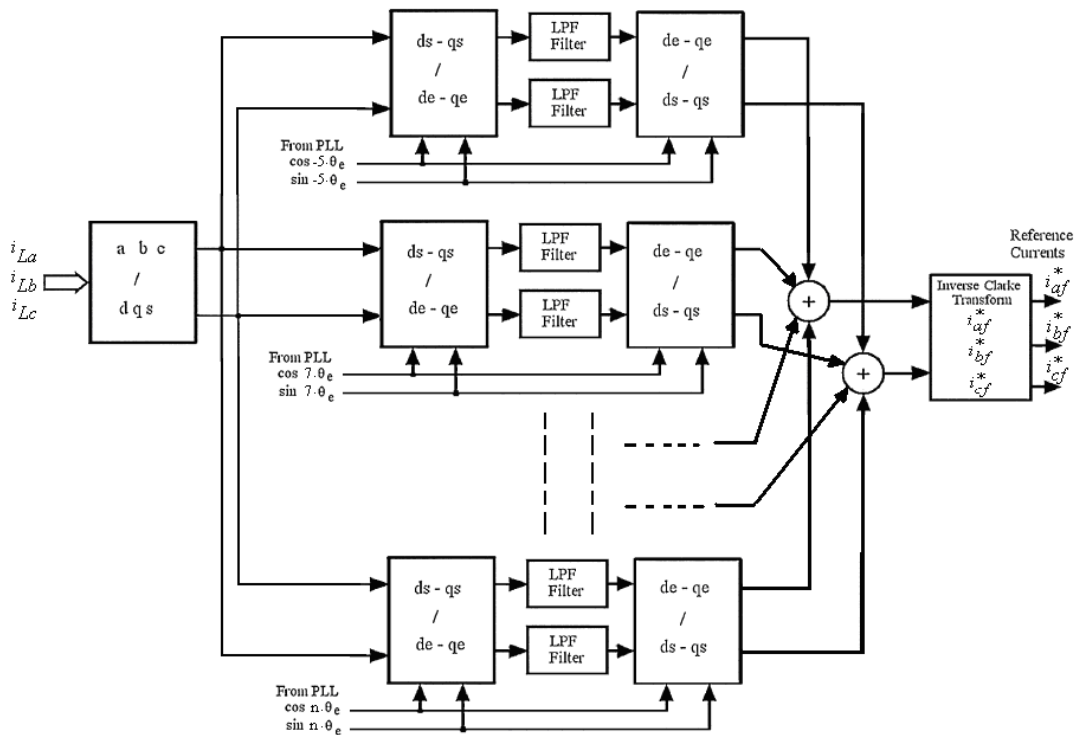$$\begin{bmatrix} i_{df}^{s\,*} \\ i_{qf}^{s\,*} \end{bmatrix} = \begin{bmatrix} -\sin(\theta_{e}) & \cos(\theta_{e}) \\ \cos(\theta_{e}) & \sin(\theta_{e}) \end{bmatrix} \cdot \begin{bmatrix} i_{df}^{e\,*} \\ i_{qf}^{e\,*} \end{bmatrix} \tag{3.29}$$

$$\begin{bmatrix} i_{af}^{*} \\ i_{bf}^{*} \\ i_{cf}^{*} \end{bmatrix} = \sqrt{\frac{2}{3}} \cdot \begin{bmatrix} 1 & 0 \\ -\frac{1}{2} & \frac{\sqrt{3}}{2} \\ -\frac{1}{2} & -\frac{\sqrt{3}}{2} \end{bmatrix} \cdot \begin{bmatrix} i_{df}^{s\,*} \\ i_{qf}^{s\,*} \end{bmatrix} \tag{3.30}$$

3.2.1.4 Generalized Integral Method

The IRPT method has faster response to the transients of load current; however, it may cause a steady-state error for the noncontinuous load current waveform. A three-phase rectifier load has this type of variation during the commutation of diodes, if the overlap angle is negligible. The generalized integral method has a good tracking capability for non-continuous load current (Asiminoaei et al, 2005). A generalized integral method implements the integration in time by using a second order transfer functions, which will give an infinite gain at the selected resonant frequency. There is a transfer function for each harmonic frequency and each behaves as independent band-stop (notch) filters as being shown for three harmonic frequencies in Figure 3.8. This technique can be used successfully for each phase

current of three-phase system even though the load is unbalanced, if the harmonic content of the load is known.
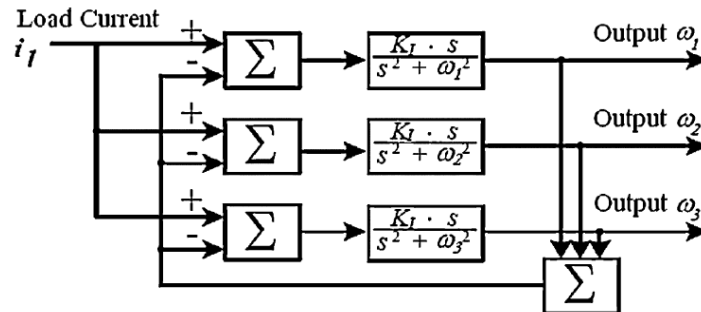
Figure 3.8 Block diagram of generalized integral method.

3.2.1.5 Adaptive Filter Method

The load current and supply voltage are input to the digital adaptive filter. In this method, the load current may be written in terms of real, reactive and harmonic components as follows (Ozdemir, 2004):

$$i(t) = i_p(t) + i_q(t) + i_h(t) \tag{3.31}$$

Where, $i_p(t)$, $i_q(t)$, and $i_h(t)$ are real, reactive, and harmonic currents, respectively. This method extracts the real and reactive components, which are respectively in phase with and 90° phase shifted with respect to supply voltage. The rest of the load current is the harmonic component. The change of supply frequency does not affect the response of the filter. The MATLAB/Simulink scheme of the adaptive digital filter is given in Figure 3.9. There are two branches, which are "upper branch" and "lower branch" evaluating active and reactive current components, respectively in the block diagram shown below. Harmonic current component is obtained by subtracting these currents from total load current.
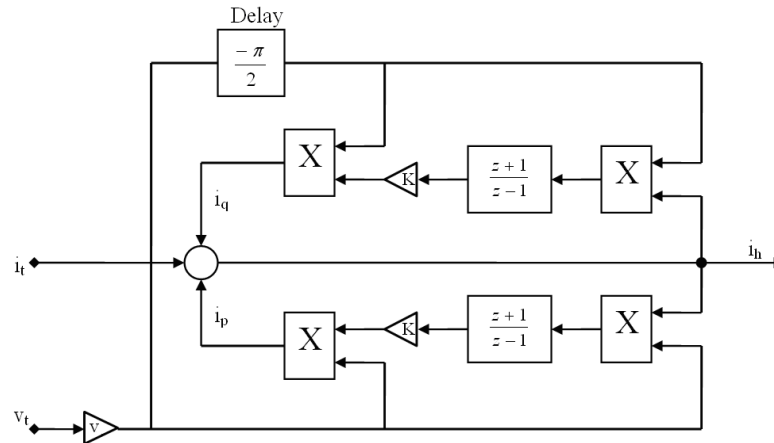
Figure 3.9 Structure of Digital adaptive filter.

3.2.1.6 Delayless Filtering Based on Neural Network

A delayless filtering application of feed forward neural network has been also used in the extraction of harmonics from load current. The delay due to filtering is an important parameter, which affects the load current tracking. The structure of three-phase square-wave delayless filtering by neural network can be found in (Zhao & Bose, 2004) and shown in Figure 3.10.
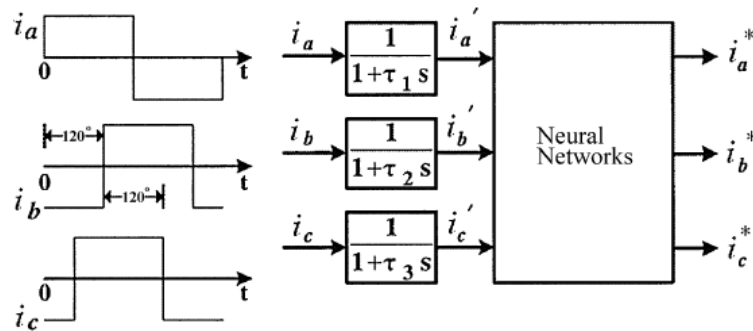
Figure 3.10 Block diagram of neural networks method.

In simulations, training set is produced in Matlab as offline. Time constants of the low pass filter are $\tau_1 = \tau_2 = \tau_3 = 0.002$ sec. The training is completed after 1000 iterations and mean square error is obtained as MSE=1.9e-6. Designed feed forward neural network is formed 3, 10 and 3 neurons in the input layer, hidden layer and output layer, respectively.
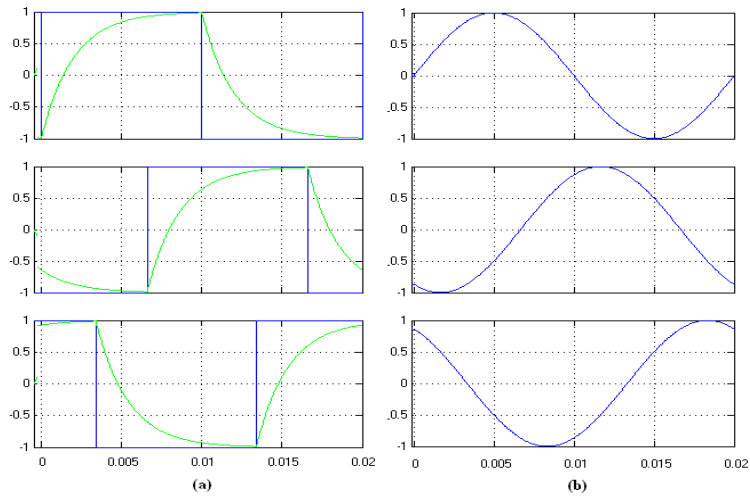
Figure 3.11 (a) Input data set i and i' for networks, (b) Target data
set for network.

This technique uses three-phase currents together in time therefore the harmonics
of unbalanced three-phase load cannot be estimated properly.

3.2.1.7 Wavelet Method

The wavelet decomposition and reconstruction algorithm is used for detecting the
harmonics in load current. Discrete Meyer wavelet is used as mother wavelet due to
its orthogonal and bi-orthogonal properties to generate reference signal for APF.
Simulation results show that the wavelet algorithm can abstract the fundamental
component of supply currents effectively. The sequence $f(n)$ obtained after
digitizing original signal $f(t)$, can be decomposed into an approximate signal a_j and
a detail signal d_j in specific frequency bands. The original signal can be expressed
as

$$f(n) = d_1(n) + a_1(n) = d_1(n) + d_2(n) + a_2(n) = \sum_{j=1}^{M} d_j(n) + a_M(n) \qquad (3.32)$$

Where, $a_j(n) = a_{j+1}(n) + d_{j+1}(n)$. Hence, the fundamental current component can
be obtained from one of the detail or approximate signals that are decomposed in the

frequency range of interest. The wavelet application on the harmonic detection is given in (Liu et al, 2006), (Yalazan, 2007) for pulsating load currents.

3.2.1.8 Adaptive Linear Neuron (ADALINE) Method

The ADALINE method (Pecharanin et al, 1994),(Dubey et al, 2005) has only a feed forward neuron. The basic block of this network having n inputs and a single output is shown in Figure 3.12. The relation between input and output variables is given in equation (3.33).

$$y = \sum_{n=1}^{N} W_n . X_n + b \qquad (3.33)$$

Where, W_n are the weighting values, X_n are inputs of neuron, n is number of inputs and b is bias value.
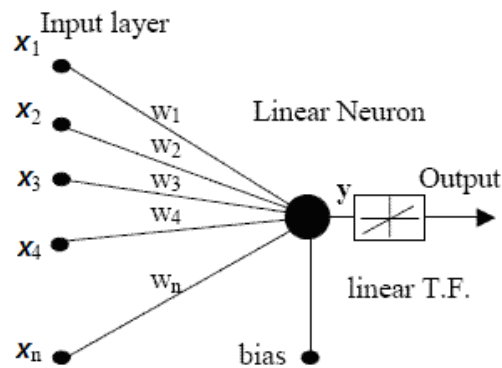
Figure 3.12 Structure of the ADALINE

Two different approaches are reported for the separation of fundamental waveform from harmonics by using ADALINE. In the first approach, inputs are defined as a function of *sin* and *cos* values based on the Fourier analysis, hence the output is the sum of load current harmonics in time. And weighting factors (magnitudes and phase of harmonics) are adjusted online according to error minimization (Osowski, 1992), (Vazquez & Salmeron, 2003), (Valiviita & Ovaska, 1998), (Abdeslam et al, 2005), (Boudjedaimi et al, 2008). In the second one, the

inputs are the data sampled from load current during the half of period. Output is the instantaneous value of fundamental component of load current. Weighting factors should be estimated to provide relation between inputs and output. Off-line training of neural network (Pecharanin et al, 1994) is performed by using the m-file written in Matlab in order to reduce the execution time of program on DSP. The m-file is written here by taking the expected harmonics (including even harmonics) and fundamental components of load current into consideration. Therefore, the response of the ADALINE here is depending on the selected harmonic components. The other technique would be using the sampled load current in a half of the period (one frame) as inputs and training neural network such that the output will be the fundamental component. The block diagram of training algorithm given in Figure 3.13 has the variables defined below.
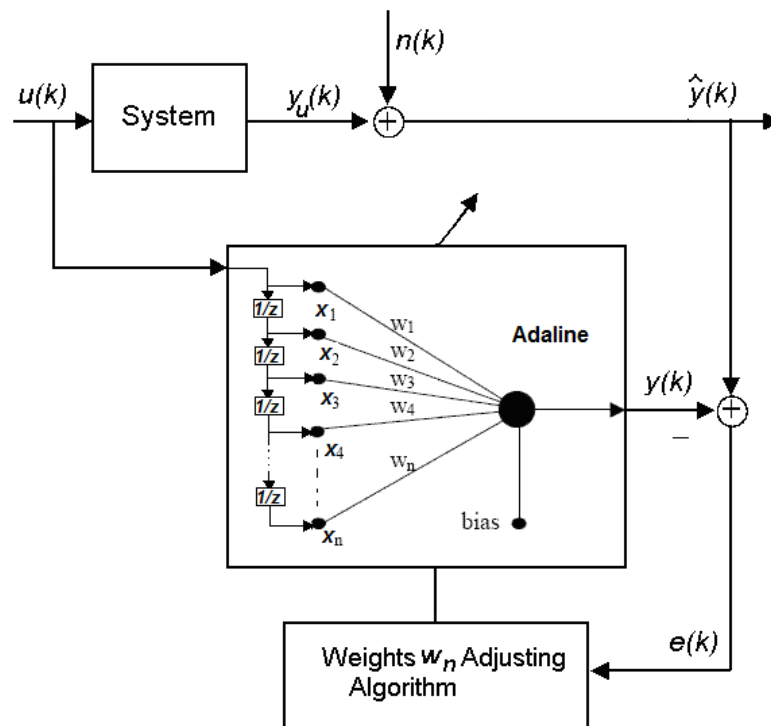
Figure 3.13 Block scheme of data

$$X_n = \begin{bmatrix} u(k) & u(k-1) & u(k-2) & .. & u(k-n) \end{bmatrix}$$

$$W_n = \begin{bmatrix} W_1 & W_2 & W_3 & .. & W_n \end{bmatrix}$$

$\hat{y}(k)$: reference output,

$u(k)$: input of system.

$n(k)$: noise component

$y_u(k)$: ideal output of the system

$e(k)$: the error

The input vector contains the data sampled in the half of the period; the relation between the number of inputs, fundamental frequency and the sampling frequency may be given in equation (3.34):

$$f_s = 2 \cdot n \cdot f_1 \tag{3.34}$$

The sampling frequency should be at a value such that the waveform of harmonics is predicted within a good accuracy. The error function in training process is defined as given in equation (3.35) using the gradient descent method.

$$E = \frac{1}{2} \sum_{f=I}^{F} \left\| y_f - \hat{y}_f \right\|^2 \tag{3.35}$$

Where, F is the total number of data used for training. The gradient of error is given in equation (3.36).

$$\nabla E = \left(\frac{\partial E}{\partial W_1}, \frac{\partial E}{\partial W_2}, ..., \frac{\partial E}{\partial W_n} \right) \tag{3.36}$$

In training process, each weight is updated using the increment given in equations (3.37) and (3.38).

$$\Delta W_n = \gamma \frac{\partial E}{\partial W_n} \tag{3.37}$$

$$W_n(k+1) = W_n(k) + \Delta W_n \tag{3.38}$$

Where, k is iteration number, γ is learning constant and equals to 0.01 for this application.

The training has been accomplished for the input signals at various amplitude and frequencies. The input signals are selected at different fundamental frequencies between 45 and 55 Hz and at the orders of 5th, 7th, 11th, and 13th harmonics having various magnitudes. In addition, the training signals are perturbed with white noise having a variance of 0.01 in order to obtain a better noise rejection. The output is considered as the instantaneous value of the fundamental waveform. The input data during training is sampled at 6 kHz, training of the neural network is completed after 4000 iterations and the MSE is obtained as $1.02132*10^{-5}$. The training is terminated when the error falls below the desired level (Rojas, 1996).

3.3 Simulation of Harmonic Extraction Methods

The methods outlined above are simulated in MATLAB/ Simulink environment under different operating conditions and their performances are summarized in Table 3.1. The case study is performed at three-stages: In the first interval, the load current has 0.75 pu fundamental component at 50 Hz, 0.2 pu 5th harmonic and 0.08 pu 7th harmonic components during 0.0–0.1 s of simulation time. The second interval is between 0.1 and 0.2 s and the fundamental component of the load current is increased to 1.0 pu at 0.1 s. Finally, during 0.2–0.3 s, the fundamental frequency of the load current is set to 45Hz and the responses of the methods against such a frequency deviation are investigated as shown in Figure 3.14. In simulations, the supply voltages are assumed to be balanced and sinusoidal. The entire block diagrams of Matlab simulations and system parameters are given in Appendix.
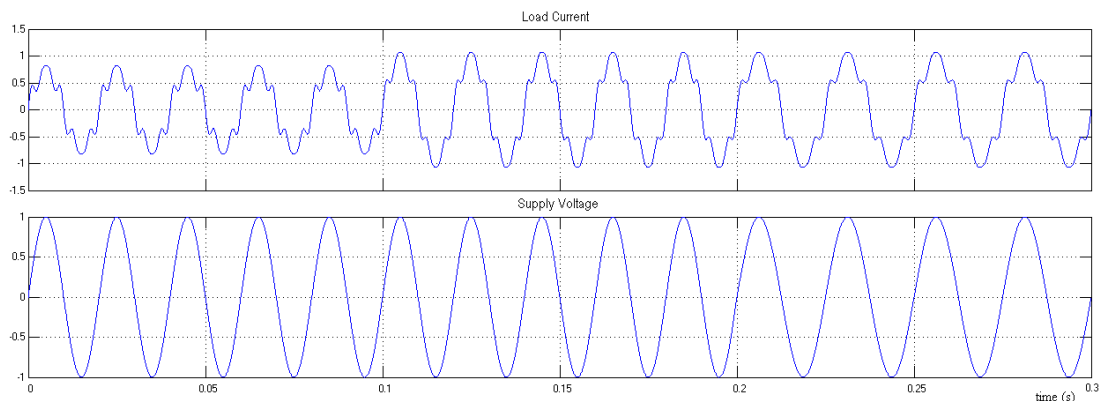
Figure 3.14 Load current and supply voltage in simulation works.

Figure 3.15 and Figure 3.16 shows the results for FFT method and Kalman filter method, respectively. FFT method responds to amplitude variation in one-cycle and produces incorrect results when supply frequency deviates. FFT method is vulnerable to frequency deviations. In general, frequency domain methods respond to load variations in one supply cycle and require a large amount of computation. Therefore, either PLL or zero-crossing algorithms should be implemented within the FFT technique in order to estimate the harmonics correctly due to the variation of frequency of the supply. Kalman filter method is applied to an adequate result could not be obtained.
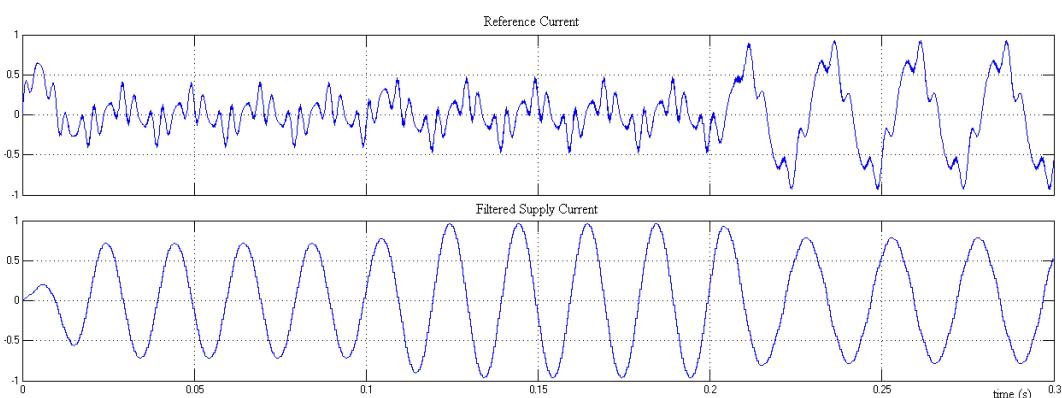
Figure 3.15 Simulation result of FFT method
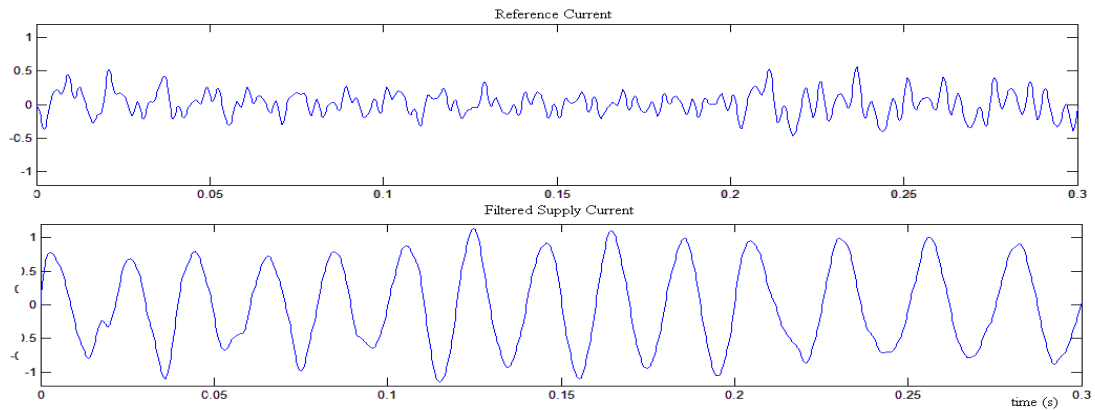
Figure 3.16 Simulation result of Kalman Filter method

The simulation results for IRPT, single-phase PQ method, and SRF methods are shown in Figure 3.17, 3.18, and 3.19, respectively. In IRPT method, the duration of transient response against the load variations takes one complete cycle, while it takes 2.5 cycles in SRF method. IRPT method is insensitive to frequency deviations and its performances mainly depend on low-pass filter characteristics. IRPT method also produces incorrect reference currents under load current imbalance since it distributes any current imbalance to other phases. However, since the negative sequence controller block detects any imbalance in the load currents and subtracts negative sequence component from the reference currents in SRF method, the active filter reference currents are produced such that they only compensate the load current harmonics. The SRF method is also capable to generate the reference current for active power filter at a prespecified frequency by setting the rotating reference frame speed to the same frequency.
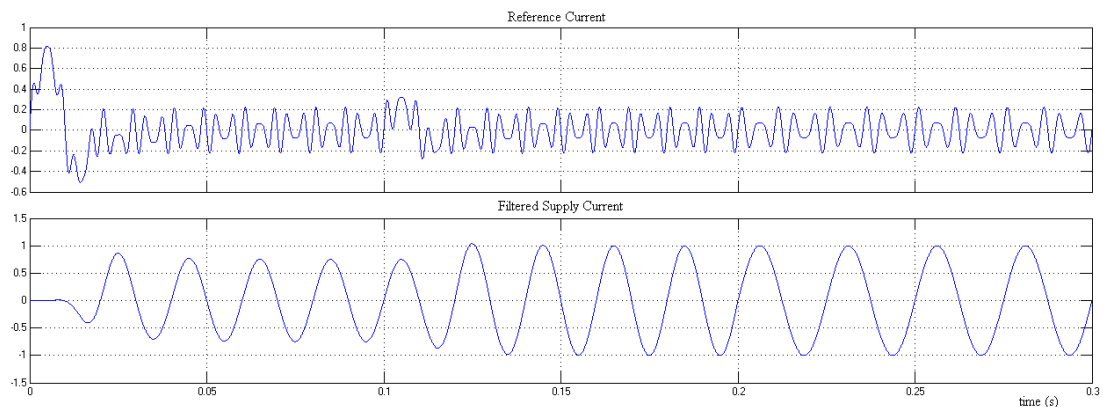
Figure 3.17 Simulation result of IRPT method.
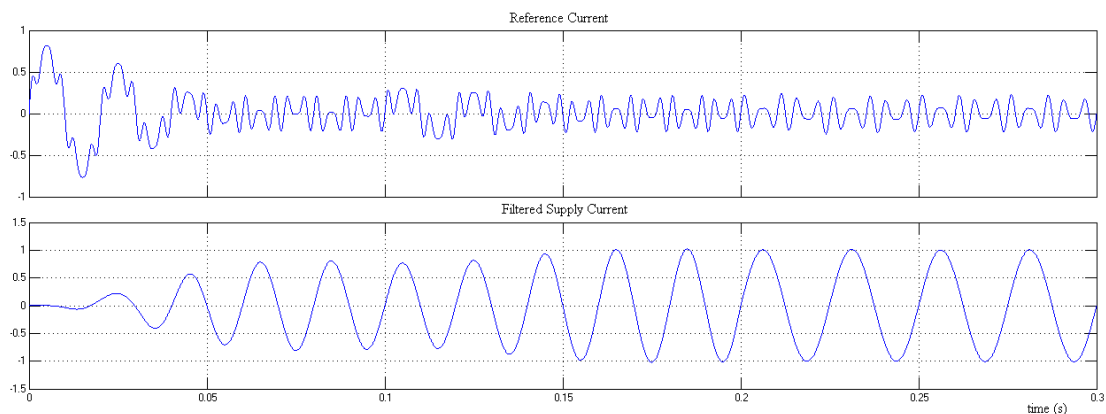
Figure 3.18 Simulation result of SRF method.

In single-phase PQ method, the duration of the transient response against amplitude variation is observed to be half cycle. This method produces incorrect reference currents under frequency deviation. Because the leading source voltage and load current by $\pi/2$ is needed to obtain imaginary axis components.
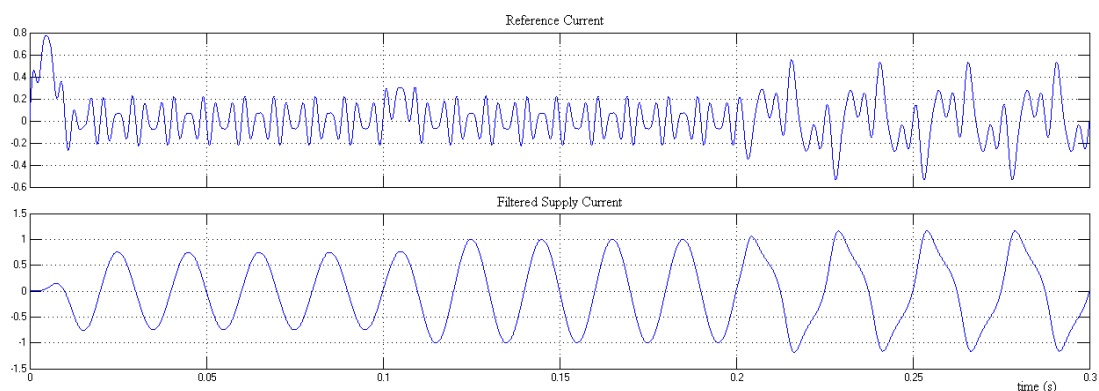
Figure 3.19 Simulation result of single phase PQ theory method.

Generalized integral method produces a 1.5 cycle delay at its output as shown in Figure 3.20. There is a trade off between the filtering performance and response time, since it is dependent on the filter bandwidth. Its performance against the frequency variations is not satisfactory due to fixed cut-off frequencies of notch filters.
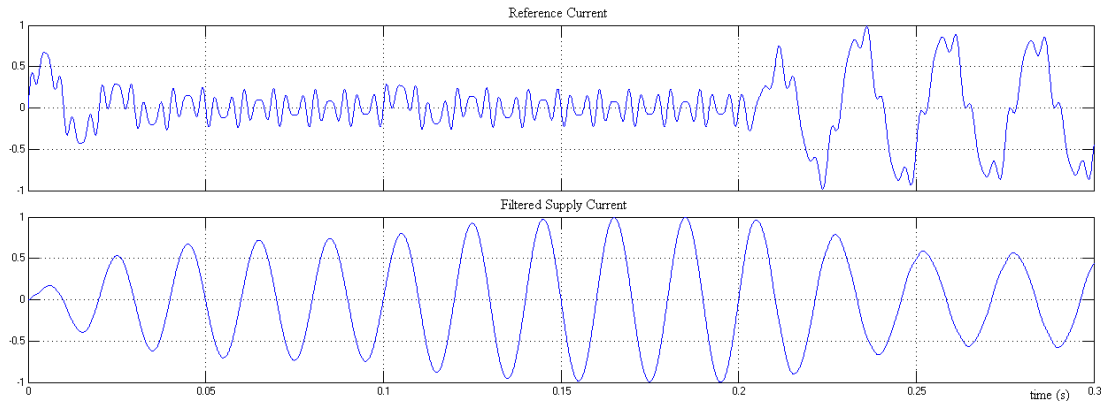
Figure 3.20 Simulation result of Generalized Integral method.

Adaptive filter method produces output in approximately 1 cycle delay as shown in Figure 3.21. Filter cut-off frequency varies depending on the supply frequency and hence its performance against frequency deviations is good due to its adaptive structure.
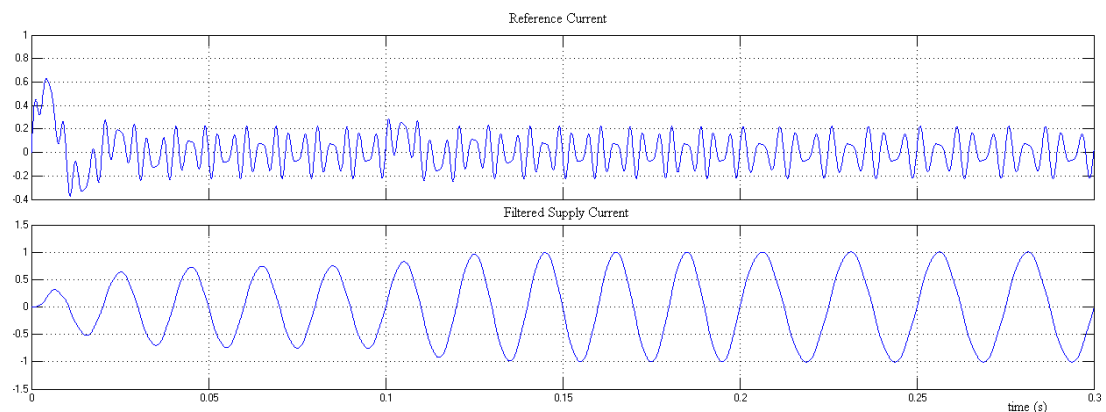
Figure 3.21 Simulation result of Adaptive Filter method.

The results for Delayless filtering based on neural network method are shown in Figure 3.22. Designed feed forward neural network is formed by 3, 10 and 3 neurons in the input layer, hidden layer and output layer, respectively. The offline training set is produced in Matlab offline. The training is completed after 1000 iterations and mean square error is obtained as $1.9 \times 10-6$. In the results, it was observed that the current reference produced by this method is not capable to compensate all harmonic contents in the load current waveform. When the total harmonic distortion of the load current is high, this method is unable to extract the fundamental component.
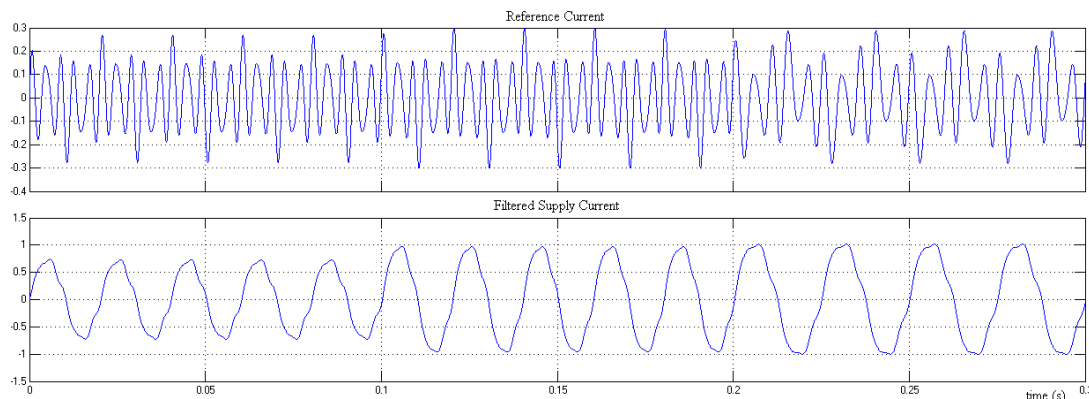
Figure 3.22 Simulation result of NN based Delayless filtering method.

The results of adaptive linear neuron method are shown in Figure 3.23. The response of the method against load variations, both in amplitude and frequency, is satisfactory. It produces a response at delay of one quarter cycle during load transients. Its performance is dependent on training data and best performance is obtained when the network is trained with all possible load conditions.
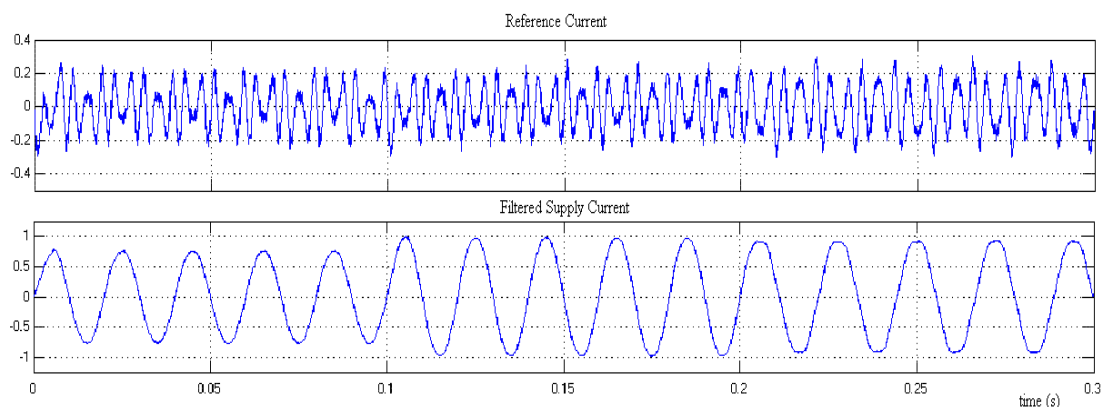
Figure 3.23 Simulation result of Adaline Method.

Wavelet method produces a response at delay of one quarter cycle as shown in Figure 3.24j. Its response to amplitude and frequency variations in load currents is fast and quite satisfactory. But their implementations in the DSP create a long execution time.

3.4 Result of Simulations and Comparisons.

The simulation results of all applied methods are given in Figure 3.24 as the bulk for comparison purposes. Where, it can be see that, best response time is shown with ADALINE method. Also, IRPT and SRF methods have remarkable response depending on characteristic of digital filter used. IRPT method works only under the three-phase balanced load condition. SRF method works only in three-phase systems and it uses for unbalanced load. ADALINE can work for single or three phase system. Fundamental component of load current can be extracted almost delayless by using this method. But, it depends training data and mathematical complexity increasing with high sampling time. IRPT method is very sensitive to noise in sampling of supply voltages. In this method, digital filter takes time in computation. Only, SRF, FFT, Generalized integral methods can be employed for selective harmonic elimination. (Dubey et al, 2005)

Three methods out of ten have been selected to be programmed in the digital signal processing unit based on the criteria such that the algorithm can be implemented for three-phase system with a faster response against frequency, load variation and unbalanced loading. These methods are the IRPT, SRF, and ADALINE. The IRPT is preferred because its transient response is faster. The ADALINE can be implemented for single-phase and unbalanced systems because of its good response to frequency variation. Although the wavelet algorithm is good for frequency variation, it was not implemented due to its complexity for implementation and large number of mathematical calculations. The performance comparison of all methods is given in Table 3.1.
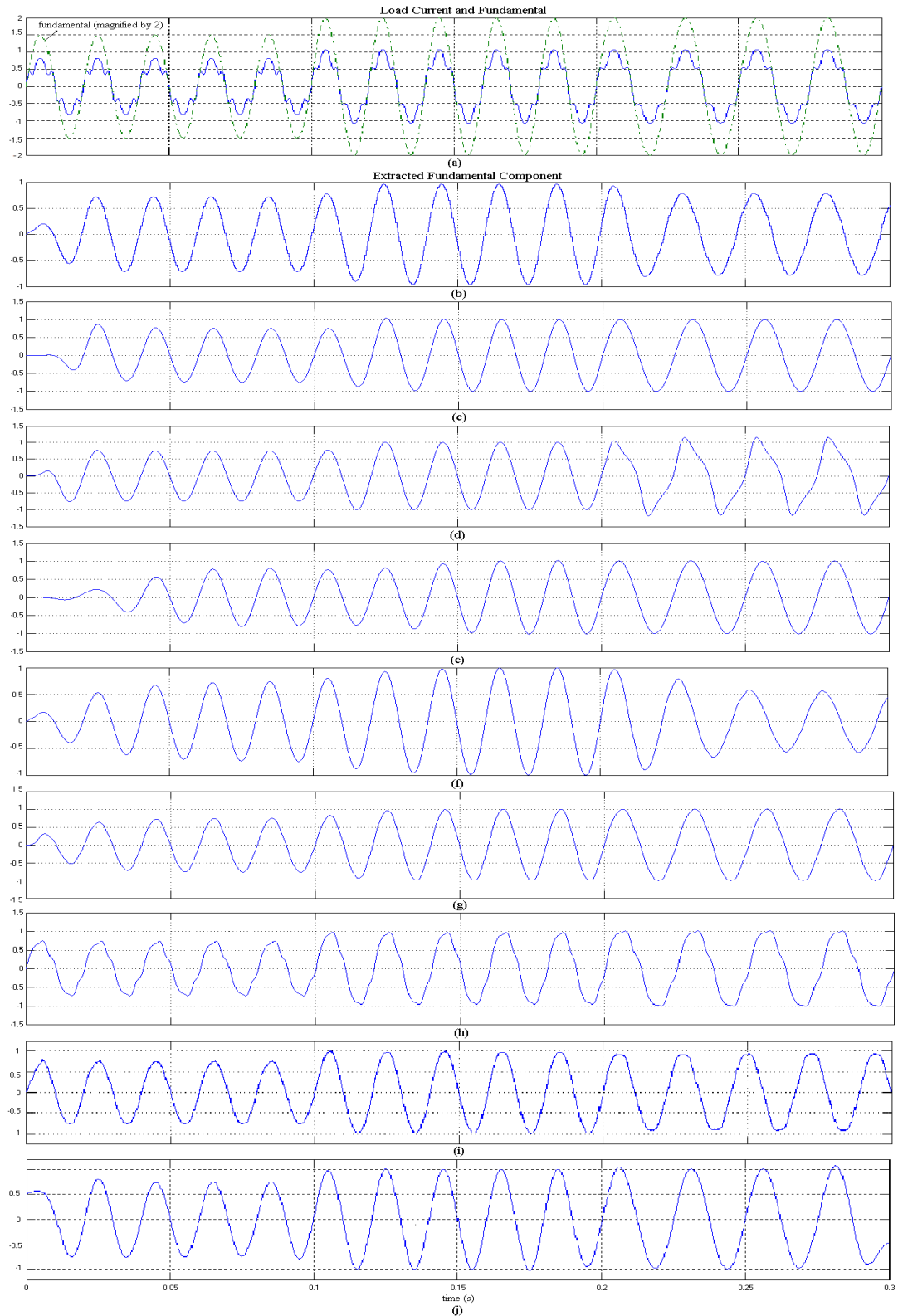
Figure 3.24 Simulation results for the investigated methods; (a) load current and fundamental waveform (b) FFT (c) IRPT (d) single-phase PQ (e) SRF (f) generalized integral method (g) adaptive filter method (h) delayless filter based on NN (i) ADALINE (j) wavelet method.

Table 3.1 Performance comparison of the harmonic extraction methods.

Method	Application	Calculation Complexity	Noise immunity	Accuracy	Response time	Performance against frequency variations	Limitation
DFT	1/3-phase	few (depends on number of samples, N)	bad (anti-aliasing filter is required)	good	slow (one-complete cycle)	bad	
IRPT	3-phase only	few	depends on HPF	good (depends on HPF)	depends on HPF time response	bad	Requires balanced system, not suitable for SHE
Single-phase pq	1/3-phase	few	depends on HPF	good (depends on HPF)	depends on HPF time response	bad	not suitable for SHE
SRF	3-phase only	complex	depends on PLL and HPF	Good (depends on PLL and HPF)	depends on PLL and HPF time response	good (due to PLL)	Can be employed for SHE also (due to PLL)
Generalized integral method	1/3-phase	complex	depends on filter band width	depends on filter band width	depends on filter band width	Bad (due to fixed notch filter frequencies)	Can be employed for SHE
Adaptive filter method	1/3-phase	few	depends on filter band width	depends on filter band width	depends on filter band width	good (due to adaptive structure)	
Delayless NN filter	1/3-phase	complex	Good at low distortion	good at low THD	good	bad	Requires offline training of the network
ADALINE	1/3-phase	complex	good	considerably good	very good	good	Requires offline training of the network
Wavelet	1/3-phase	complex	good	good	very good	good	

CHAPTER FOUR
DESIGN OF SHUNT ACTIVE POWER FILTER PROTOTYPE AND EXPERIMENTAL WORKS

4.1 Introductory Remarks

Nowadays, many power electronics devices are integrated with digital signals processors (DSP) that offer a generic structure and implementation of complex calculations required in a wide range of applications (Aredes et al, 2005), (Ozdemir et al, 2007), (Yanbo et al, 2006). While the DSPs offer better solution to the control of many complex systems, developing a DSP code and testing it on the real system requires additional effort and attention since the design of power electronics systems contains a background of inter-disciplinary knowledgebase (Balog et al, 2005).

In the design procedure of such devices, it is often necessary to construct the complete system model to investigate its performance through computer simulations before implementing. In (Dawande et al, 1997), it was noted that the use of hardware in simulation of the power electronics converter is essential. The inclusion of DSP based design into computer simulations can be carried out by using the program of DSP and co-operation with PC. In recent years, the use of automatic code generation tools has become widespread. These tools can be used effectively to make a rapid prototyping and hardware-in-the-loop testing of controllers possible (Defour et al, 2005). From this point of view, the Embedded Target tools that integrate the MATLAB/Simulink and Texas Instruments TMS320C2000 DSP platforms are useful to develop and validate the designs rapidly. These tools are used to generate a program in C-language for real-time implementation of the Simulink model and also provide a flexibility to test the generated or self developed code with other Simulink models (The Mathwork, 2003a).

In this chapter, a design procedure for shunt APF using MATLAB/Simulink and TMS320F2812 DSP is presented. The procedure contains the modeling of the system

in Simulink testing the developed code on DSP with Simulink model, and experimental tests are carried on the prototype system. So that, the procedure described here can still provide an efficient and safe way in testing the DSP codes prepared for real system implementation. The proper operation of the DSP is guaranteed through simulations before testing the code on physical system. Also, hardware and software structures of designed shunt active power prototype are given in this chapter. Finally, prepared 20 kVA shunt APF prototype have been tested at laboratory and industrial conditions by using direct and indirect current control techniques with ADALINE, IRPT, SRF harmonic extraction methods.

4.2 Implementation of Shunt APF

4.2.1 Hardware Design

In the power converter part of the hardware, SEMIKRON SKM75GB123D and SKYPER 32PRO dual igbt driver modul were used. This driver module is equipped with built-in gate drive circuits and protection circuits for short-circuit, overheating, and supply under-voltage protection. The three-phase voltage and current waveforms are measured via Hall-effect voltage transducers (LV-25P) and current transducers (LA100P). The measured voltage and current waveforms are input to ADC ports of the TMS320F2812 DSP by conditioning these signals to 0-3V ADC voltage levels. An anti- aliasing filter and 10K resistor were used between output of signal conditioning circuit and ADC input of DSP for properly sampling signal. These circuits given in Appendix B. Prepared circuits have been placed in a cabinet and the cabling has been done. In cabinet, Siemens S7-200 PLC is used as a main controller for management of DC power supply, supply of DSP, main contactor, and start/stop buttons. The photographs of the elements of hardware are given in Figure 4.1-4.7.
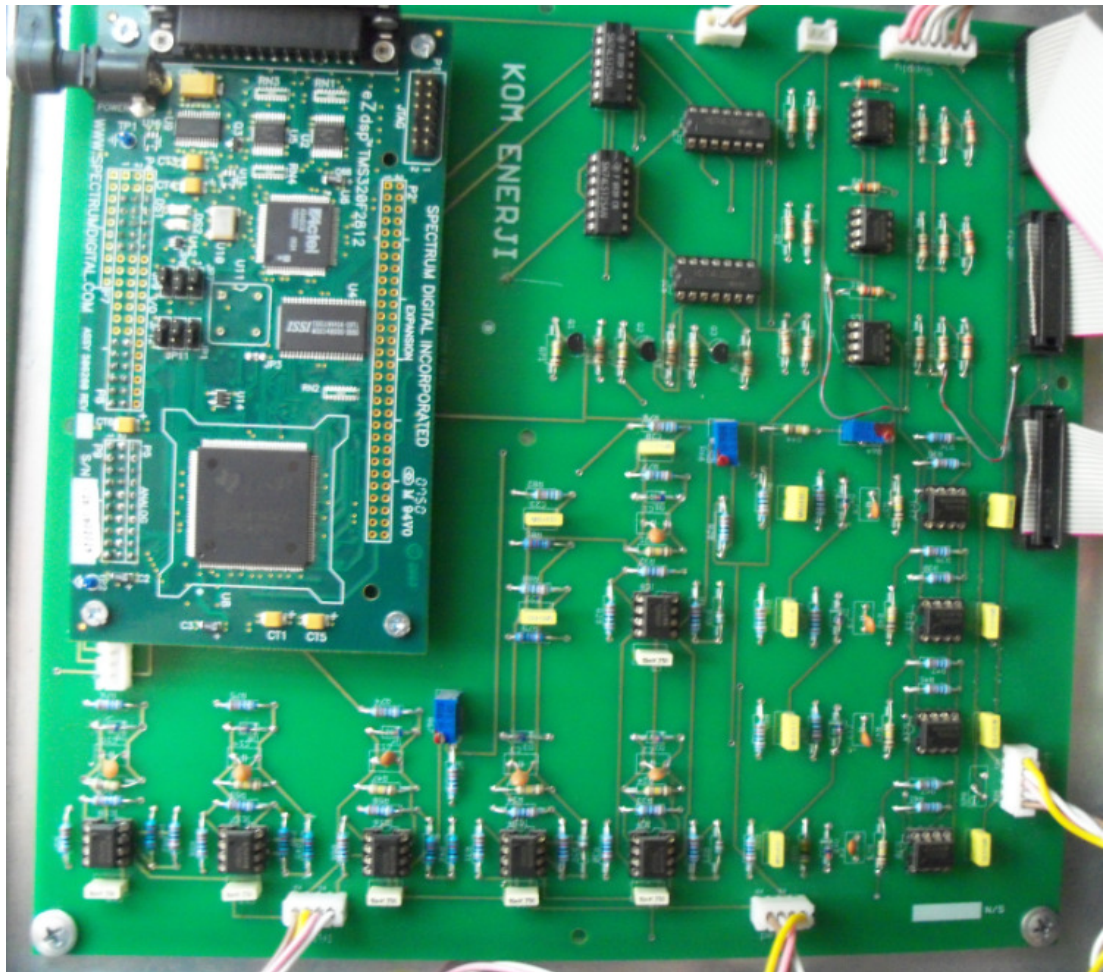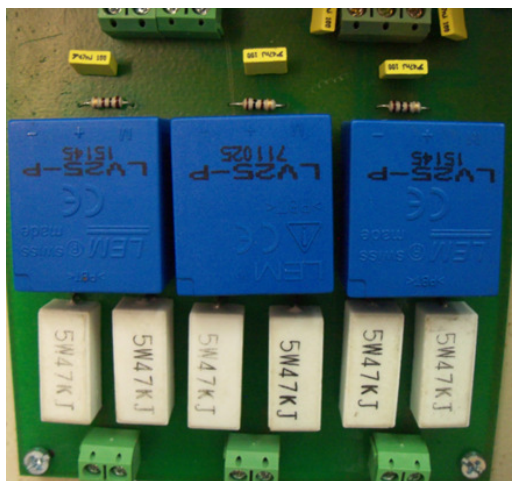
Figure 4.1 DSP and main control card.
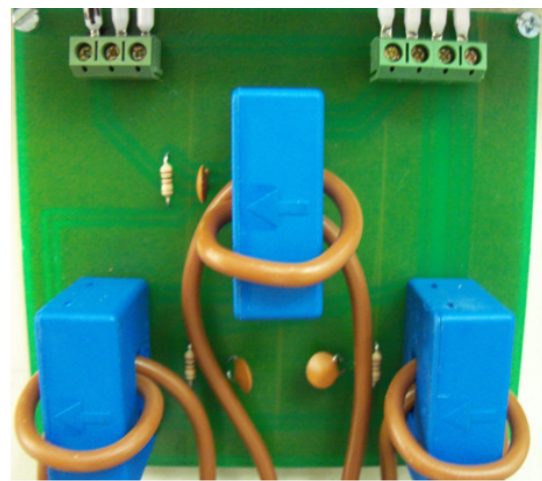
Figure 4.2 a) Voltage measurement card, b) Current measurement card.
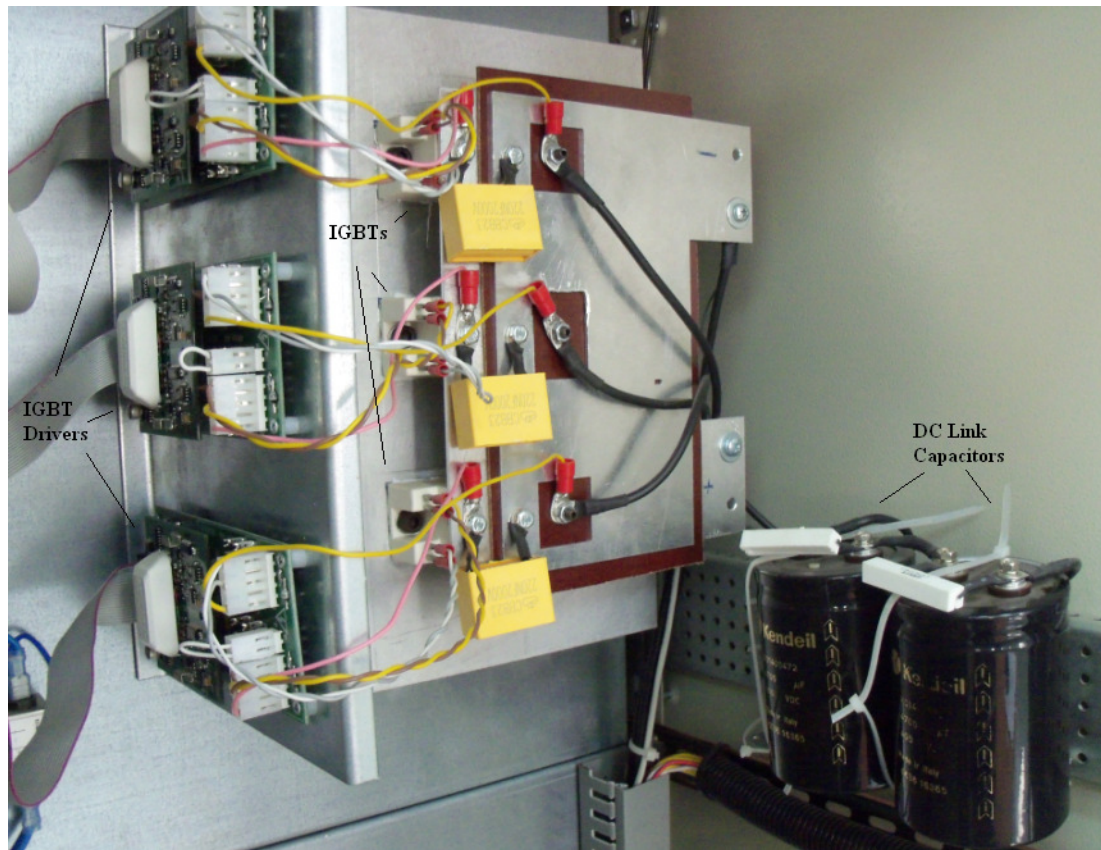
Figure 4.3 The circuit of power module and drivers.
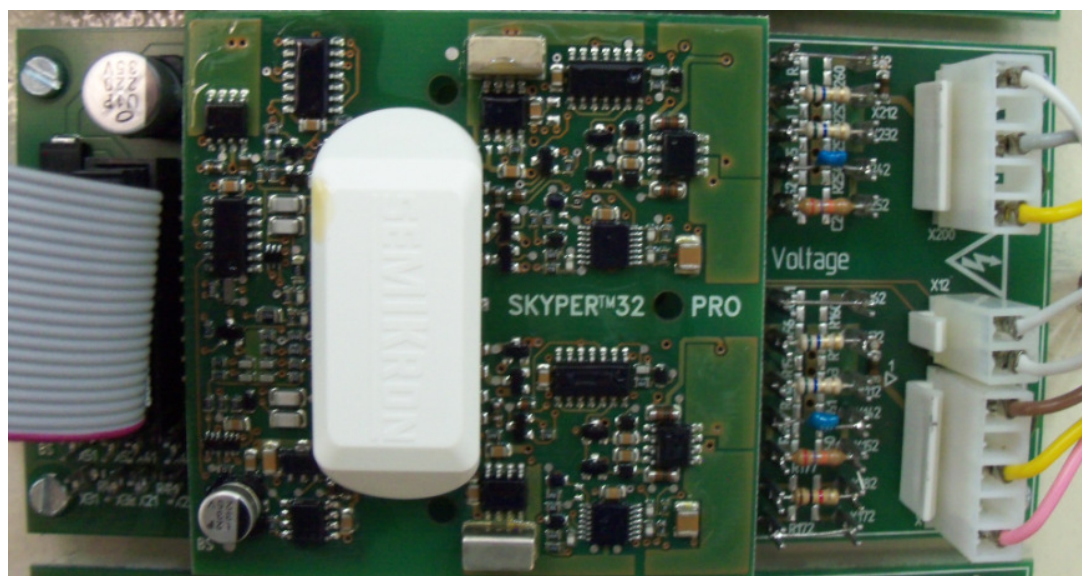
Figure 4.4 The drivers of Power module.
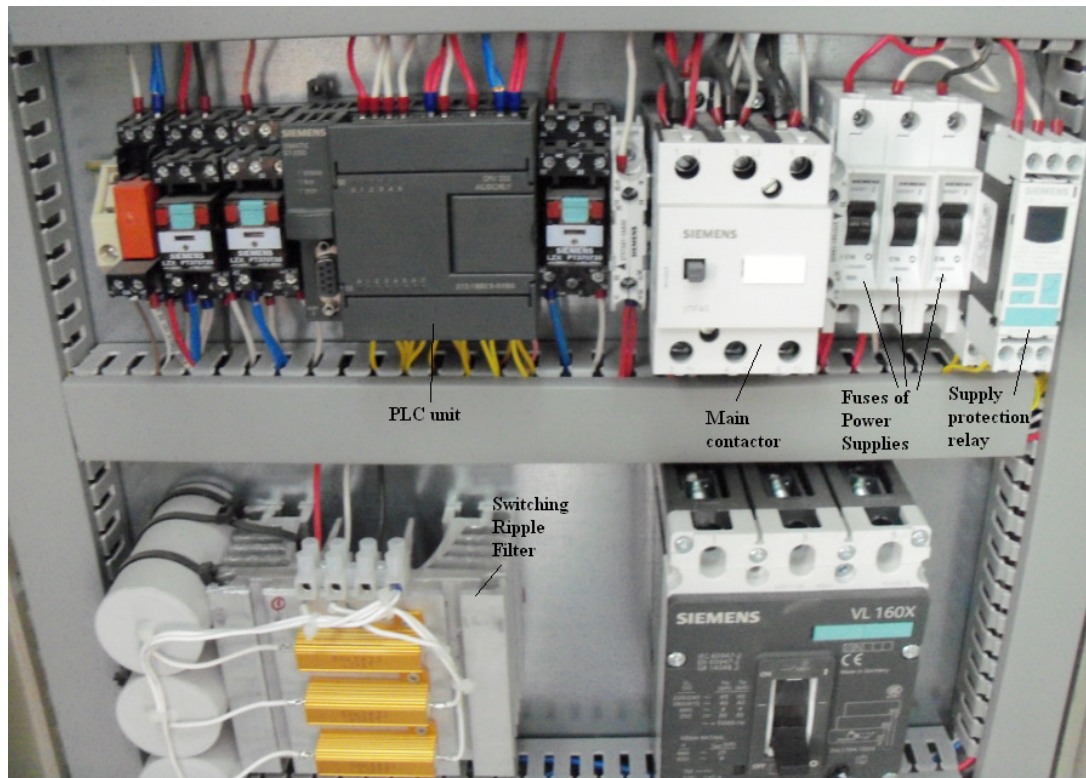
Figure 4.5 PLC control unit.
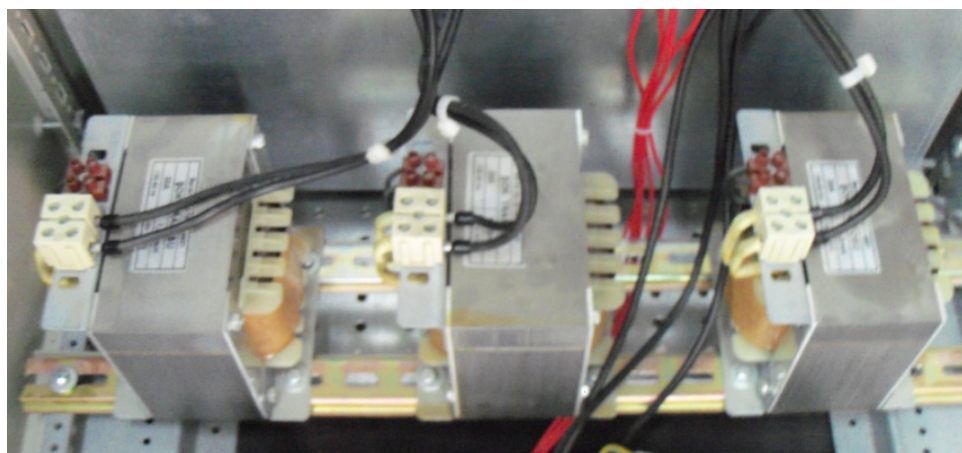
Figure 4.6 Filter Inductances.
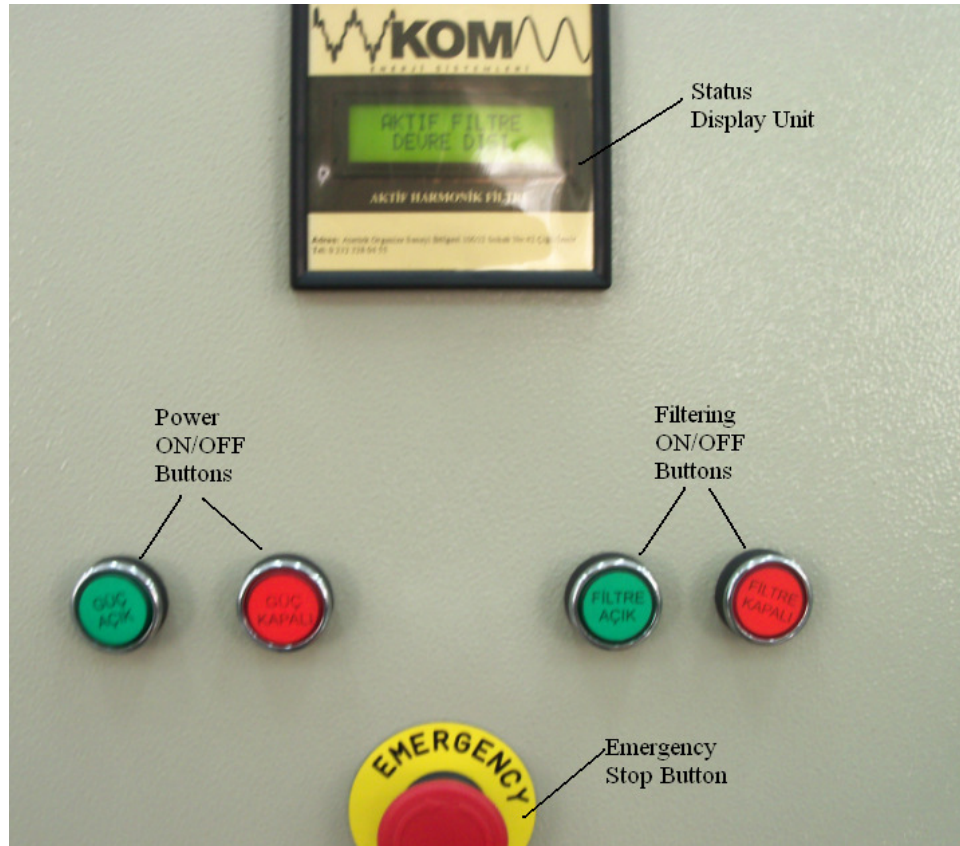
Figure 4.7 The front panel of APF.

4.2.2 Software Programming

Firstly, TMS320F2812 digital signal processor (DSP) board of Texas Instruments was used for hardware implementation of reference current generation. The F2812 DSP board contains a fixed-point processor with 150 MIPS speed, 128K Words internal flash memory, 64K Words external SRAM memory, and 12-channel PWM generator. The processor also contains two 8-channel independent analog-to-digital converters. The software implementation of reference current waveform generation was accomplished in Code Composer Studio (CCS) environment. The CCS provides a C++ compiler/linker that allows the implementation of both fixed and floating-point operations. In addition, the IQMATH library provides a powerful tool in order fulfill the floating-point operations more effectively and efficiently. The methods were implemented via floating-point operations using both standard and IQMATH libraries. Three harmonic extraction methods (IRPT, SRF and adaptive linear neuron methods) are tested on eZdsp TMS320F2812 board. The first prepared algorithms for

methods have been gradually optimized. After all, the program has been prepared to show the best performance by using SRF method and eZdsp TMS320F28335 floating-point DSP.

In the programs, the reference current generation and hysteresis current controller are operated at two independent tasks in the DSP. The value of reference current is updated with the main program cycle around 6-8 kHz, while the hysteresis current controller updates the switching signals at a 100 kHz rate in an interrupt service routine. The algorithm of the DSP program for this operation is given in Figure 4.8.

Afterward, the main program cycle was increased to 38 kHz by optimizing the algorithm for IRPT method and 32 kHz for SRF method. In ADALINE method, when the sampling time is increased, the number of neuron and program complexity increases. Therefore, the sampling time of this method has not been increased effectively.

Also, In all of the programs, offset calculations for signal conditioning circuits and each ADC channels were implemented on dsp program at start-up. Each of ADC channels have a different conversion error and resistance tolerance from signal conditioning circuits. The entire of disturbance is compensated in software.
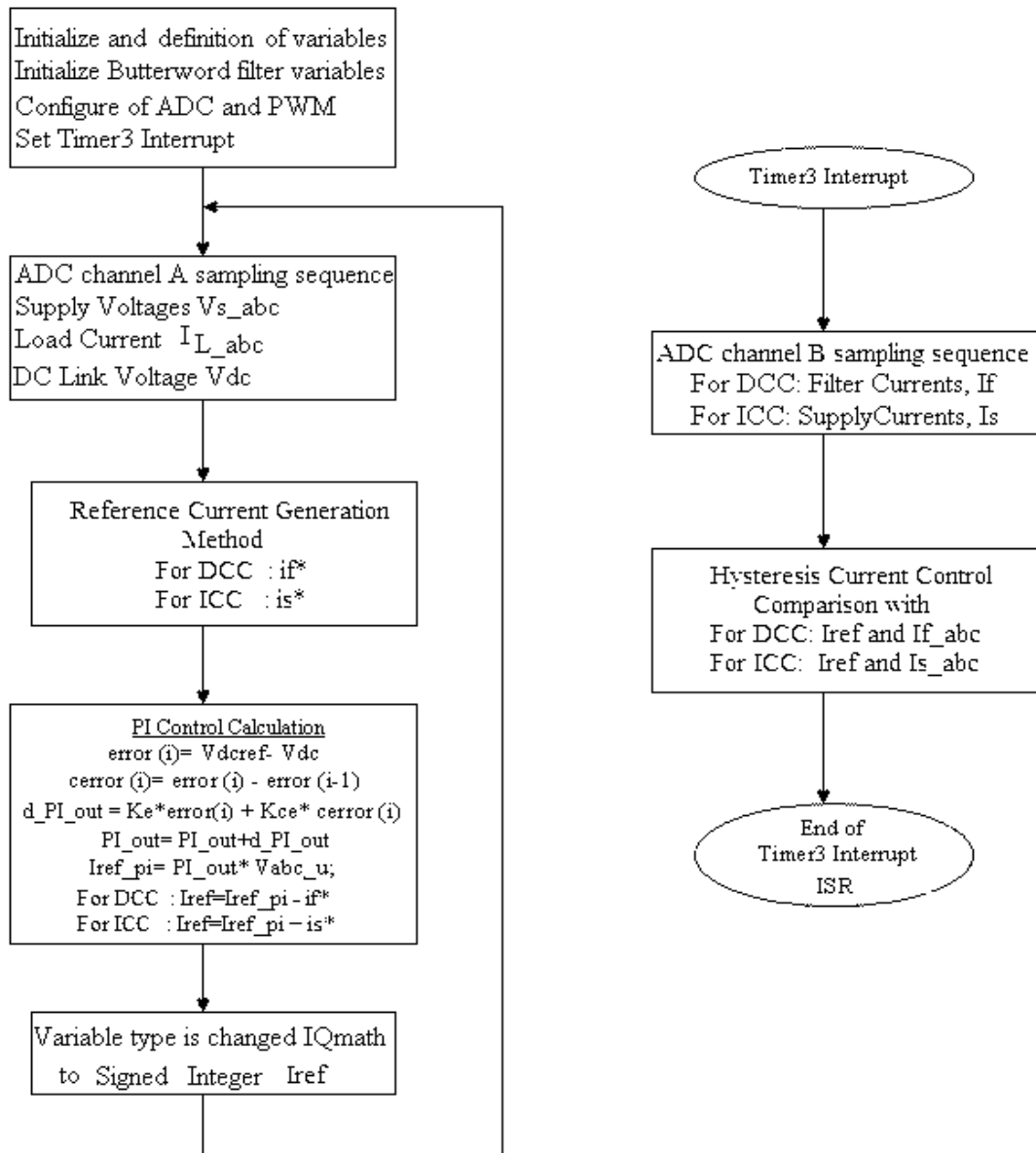
Figure 4.8 Algorithm of the shut APF for direct and indirect current control techniques.

4.2.2.1 Programming of IRPT Method

Designing of low-pass filter (LPF) is most important part of programming of IRPT method. The performance of method depends on phase error, frequency and transient response of digital filter. Therefore, 10th order Butterworth LPF has been

designed by using Matlab Filter Design Toolbox. The cut-off frequency of the filter was chosen to be 100Hz with a sampling frequency of 10 kHz. The direct form II realization of the digital LPF with the 5-cascaded blocks was used as shown in Figure 4.9. This method has the feedforward part containing the numerator coefficients and feedback part having the denominator coefficients of the filter transfer function. This method uses the minimum number of delay elements that is equal to the order of the transfer function denominator. And the algorithm of digital filter is given in Figure 4.10. Also, IRPT method was realized by using algorithm given in Figure 4.11. Timing diagram of this method is given in Table 4.1 for F28335 DSP and 38 kHz sampling time.
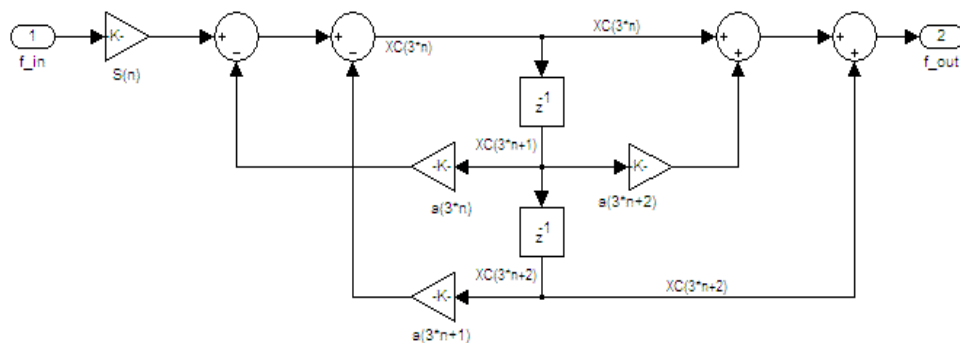
Figure 4.9 Block diagram of digital filter and variables.
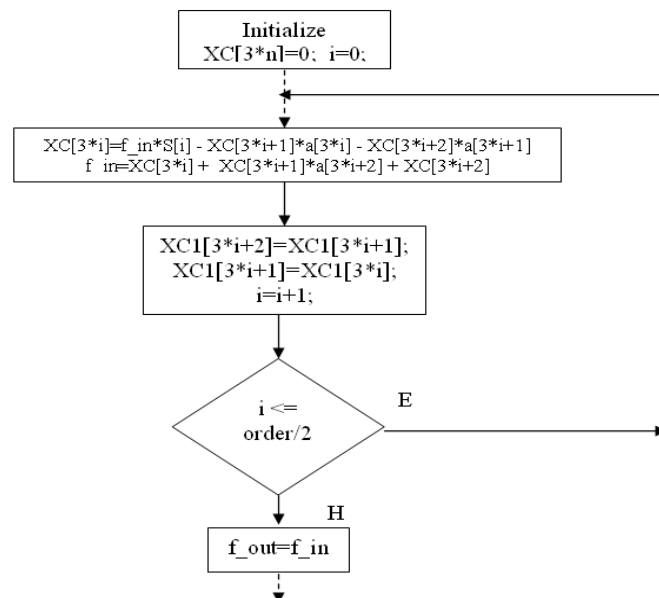
Figure 4.10 Algorithm of Butterworth IIR low pass filter
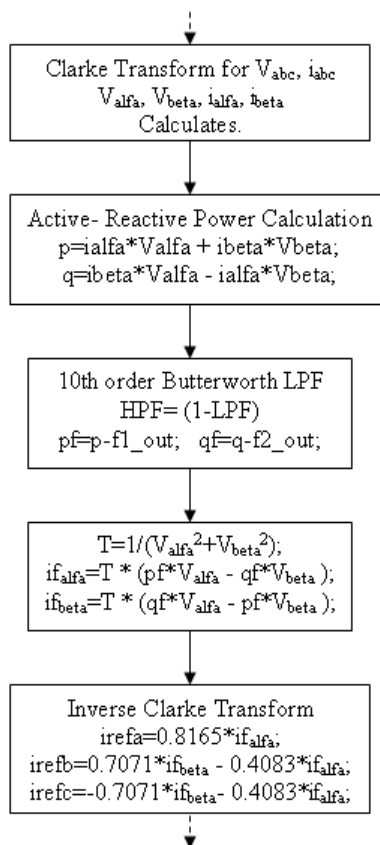
Figure 4.11 Algorithm of IRPT method.

Table 4.1 Execution times of IRPT method for each step.

Task	Execution time (µs)
ADC conversion in main program(7 channel)	0.5
Signal conditioning (Sampling is converted to real value)	2
V, I per unit calculation	0.57
V, I Clarke transform	0.82
P,Q calculation	0.21
Two 10th order Butterworth LPF	12.9
Inverse Clarke and Ref. Current	2.7
DC link PI controller	1.3
Ref. current is converted to ADC value and Ref.limiter	1.96
Internal observation variable	0.25
ADC conversion for filter current in interrupt service routine	0.37
Hysteresis current controller in interrupt service routine	1,36

4.2.2.2 Programming of ADALINE Method

When the ADALINE method is implemented in DSP, the weighting factors computed in Matlab through the training of the network have been used and these factors are given below:

w1[60]={0.33793, 0.091308, 0.60414, 0.467, -0.028711, -0.061862, 0.039123, 0.37293, 0.69523, -0.18069, 0.87735, 0.36669, 0.0017934, 0.66031, 0.27976, -0.055022, 0.27593, -0.031484, 0.20825, 0.50848, -0.298, 0.53963, -0.73417, 0.99526, -0.35752, -0.38752, 0.83009, 0.51546, -0.70713, -0.95053, 0.83916, -0.52617, -0.32566, 0.36713, -0.44794, -0.14738, -1.0078, 0.82392, 0.036318, -0.23515, -0.0068225, -0.35424, -0.18247, -0.65888, -0.028151, 0.26986, -0.21849, 0.017129, -0.80304, -0.41513, 0.41765, 0.20669, -0.26189, -0.07493, 0.38505, -1.0227, 0.18155, -0.7781, 0.08288, -0.066937};
b1=0.88073;
b2=0.11658;
w2=-0.13229;

Where w_1 and b_1 are the constants of linear neuron stated in equation (3.33), and w_2 and b_2 are the constants of the linear transfer function at the output of the neural neuron, which has the form of $y_{out} = w_2 \times y + b_2$. These weighting factors are defined as constants in software. Using these pre-calculated weighting factors, the ADALINE method was implemented in DSP and the algorithm is given in Figure 4.12.
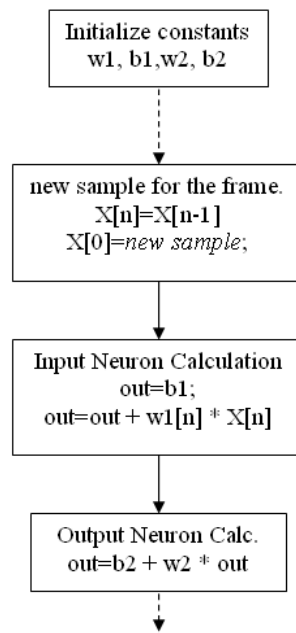
Figure 4.12 Algorithm of ADALINE Method.

4.2.2.3 Programming of SRF Method

Two different SRF methods given in Figure 3.6 and 3.7 were implemented. First one is the selective harmonic elimination method for 5th, 7th, 11th, and 13th order harmonics using F2812 DSP. In order to obtain high execution time, the structure in Figure 3.6 has been programed with F28335 floating point DSP. Thus, sampling frequency of this method was increased from 32kHz to 70 kHz. This increasing is due to property of structure. The perapared programs using F2812 and F28335 DSP were seen working same sampling frequency. The difference between two processors is that the programs can be developed more easily and stable with F28335 DSP. The timing diagram of SRF method is given in Table 4.2 for F28335 DSP and 70 kHz sampling frequency. The output of DC link PI controller and PLL have been calculated once at five cycles of main program.

The most important feature of SRF method is that it does not require high order digital filter. In our applications, only, first order digital filter was used in order to extraction DC quantity. This filter is realized using equation given below:

$$y[k] = \alpha \cdot x[k] + (1-\alpha) \cdot y[k-1] \tag{4.1}$$

Where, α is smoothing factor and $0 < \alpha < 1$, $x[k]$ and $y[k]$ are input and output of filter, respectively. In practice, $\alpha = f_c / f_s$. The structure given in Figure 4.13 is programmed as traditional three-phase PLL (Phipps et al, 2006). In application, f_c has been selected at 10 Hz and ω_{ref} is the supply frequency that is 314 rad/sec.

Table 4.2 Execution times of SRF method for each step.

| Task	Execution time (µs)
ADC conversion in main program(7 channel)	0.65
Signal conditioning (Sampling is converted to real value)	1.42
V, I per unit calculation	0.7
PLL	3.44
3/2 transform	0.72
Two first order HPF	0.52
2/3 transform	0.6
DC link PI controller	1.32
Ref. current is converted to ADC value and Ref.limiter	1.4
Internal observation variable	0.25
ADC conversion for filter current in interrupt service routine	0.37
Hysteresis current controller in interrupt service routine	1,36
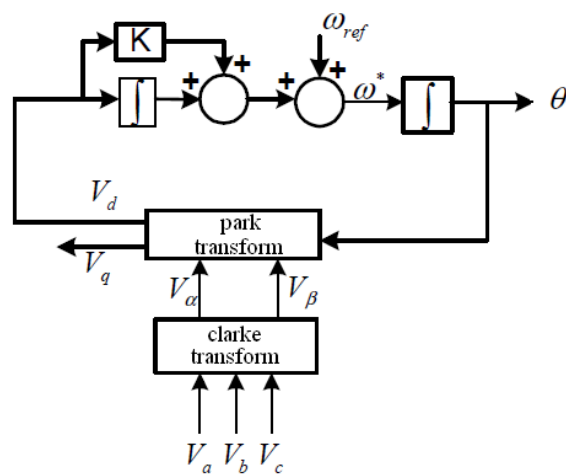
Figure 4.13 Block diagram of traditional PLL

4.3 Matlab Simulation

The computer simulations have been performed in Matlab/Simulink for the methods explained in previous chapters. The simulation program contains the dominant parameters of analog and digital circuits used in the operation of the APF. The gains of the sensors, signal conditioning circuits and analog-to-digital conversion (ADC) of implemented circuit are defined in the simulation model. All essential parameters of controllers are modeled in discrete form such that their functions can be converted into the program of the DSP. The system is also analyzed by using discrete-time solver that its integration step can be chosen according to the execution time of program in the DSP. Afterwards, the DSP and Simulink can be operated simultaneously during the test of software (Vardar et al, 2009b). Zero order hold (ZOH) blocks in the model are dedicated for the sampling parameters of currents, voltages and sampling rate of the DSP including the ADC and execution time. The simulations and corresponding experimental results are given in the same figures.

4.4 Simultaneous Operation of DSP - Matlab

In this part, the developed source code by using Code Composer Studio was tested before connecting real system. The Simulink block scheme in Figure 4.14 is used for testing the switching signals of IGBTs before connecting the DSP to IGBT block in the system. This model acquires the switching signals, which are generated by DSP, and applies them to IGBT bridge block in Simulink. The memory locations are defined on DSP for voltages, currents, and gate pulses. Simulink accesses these memory locations when simulating the system with DSP and writes the variables into the specified memory locations at each numerical solver integration step. In order to ensure the operation of DSP at the sampling rate defined in Simulink, an additional memory location, which is accessed both Simulink and DSP is also defined. The status of this memory location is toggled at the beginning of each sampling interval defined in Simulink. When the Simulink model allows the DSP to execute its code to obtain the switching states for the next sampling interval, the calculations are

performed on the DSP and switching signals are written into the memory locations. Then, the Simulink is enabled to read these values to perform the next step of simulation. Hence, the calculations for the complete system operation are performed in Simulink and DSP sequentially. This kind of operation is essential in PI controlled scheme, because the controller needs the previous values of the sampled variables.

After developing the DSP code by Simulink, the DSP Section in the Simulink model is replaced by a developed Simulink-Code Composer Studio (CCS) interface block. This interface block in the model is an s-function (The Mathwork, 2003b) that provides access to the memory locations reserved for the signals on DSP. This s-function is created for the system designed. Hence, before running the simulations with DSP, the generated code is loaded to DSP and the communication between the MATLAB and CCS was established.

While testing the DSP code with Simulink model, the sampling rate in the model is set to 100kHz, which is the rate of ADC and hysteresis current control (HCC) switching. So, the interrupt service routine for HCC is removed into main program cycle, which is not the case in the real system operation. Finally, the rate for updating reference current value was measured to be approximately 10kHz in the developed program, these values are updated in the simulations over 10 main program cycle. The Simulink model of the system is shown in Figure 4.14. A switching ripple filter is also connected to the input terminals of APF to trap the high frequency components that would appear on the filter currents and parameters of this circuit are given in Appendix.

The proper operation of DSP code for shunt APF is assured before connecting it to the gate drive circuit of IGBTs in the prototype system. The entire circuit and control parameters of shunt APF are given in Appendix. Figure 4.15 shows the results obtained from simultaneous operation of DSP with Simulink. Since the results of both MATLAB and DSP simulations are identical, the results of shunt APF are given for DSP simulation only.
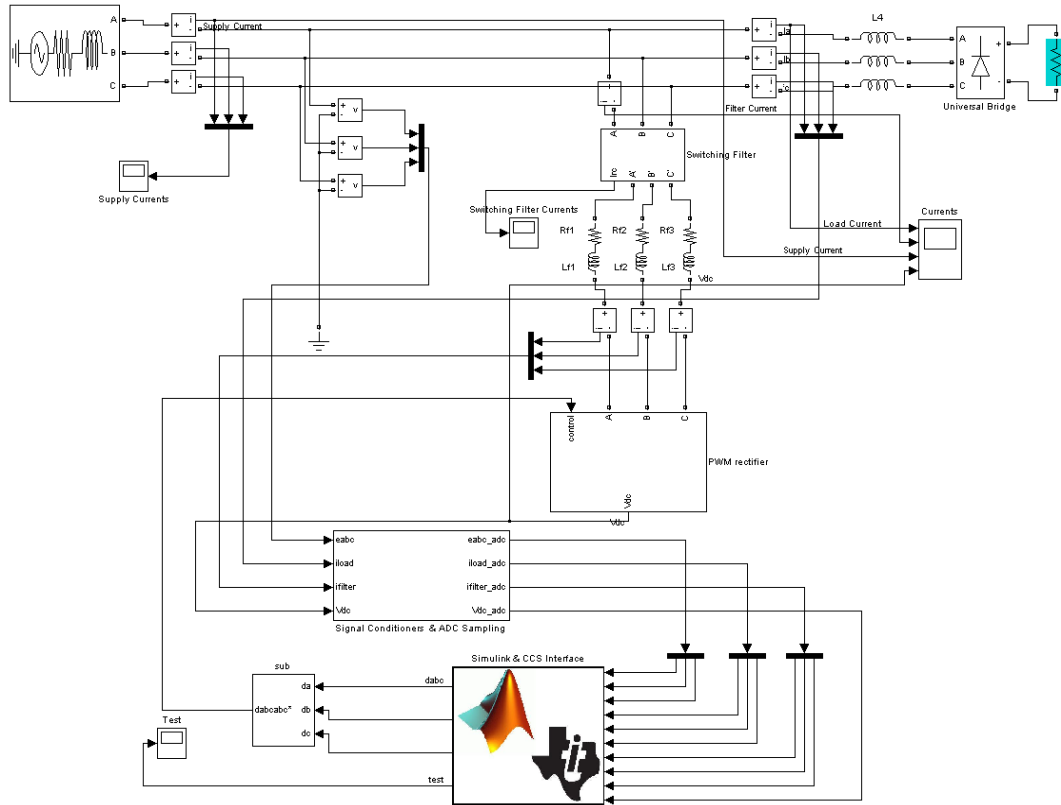
Figure 4.14 The model of simultaneous operation of shunt APF model in MATLAB/Simulink and TMS320F2812 DSP
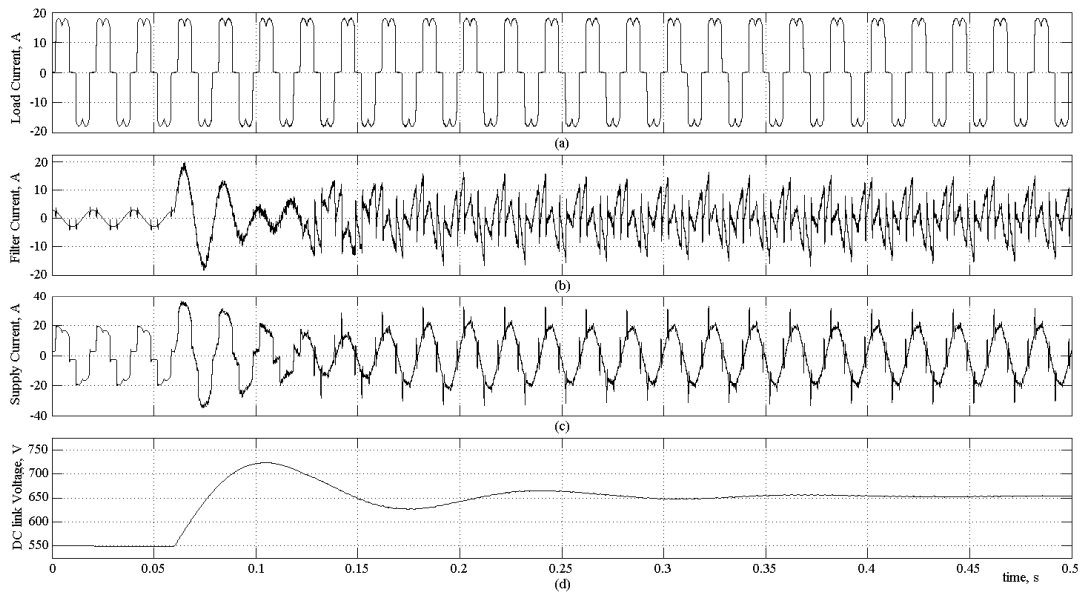
Figure 4.15 Simulation results obtained from simultaneous operation of Simulink with DSP for shunt APF a) Diode rectifier currents b) APF currents c) supply currents d) APF dc link voltage

4.5 Experimental Work in Industrial Environment with F2812

A 20 KVA, 3-phase, 380 V, 50 Hz, voltage source shunt APF is design based on the eZdsp TMS320F2812 DSP board and the photograph of prototypes are given in Figure 4.16. The rest of system parameters are given in the Appendix. The DC link voltage is set to 650 V. The reference current generation is processed at two different frequencies during the tests. One of them is around 6-8 kHz that is nearly the frequency of training of ADALINE in Matlab, the other is 38 kHz that is the maximum frequency obtained in DSP for sampling reference current.

Figure 4.16 Desinged 20 kVA shunt APF prototypes.

In the first case, the IRPT and ADALINE methods are compared on the basis of same loading conditions. In the second case, the performance of IRPT is investigated alone due to the effectiveness of sampling frequency on reference current. These filters are not programmed for reactive power compensation through out the work. The total harmonic distortion is measured by using energy analyzer, HT PQA823. The tests in this part have been done in industrial environment.

4.5.1 Shunt APF Operating at 6-8 kHz Sampling Frequency

The reference current generation and hysteresis current controller are operated at two independent tasks in the DSP. The value of reference current is updated with the main program cycle around 6-8 kHz, while the hysteresis current controller updates the switching signals at a 100 kHz rate in an interrupt service routine. The algorithm of the DSP program for this operation is given in Figure 4.8.

The shunt APF with direct current technique is tested under balanced three phase diode bridge rectifier load. In the DSP, the IRPT method is programmed for extracting load current harmonics. Figure 4.17 shows the experimental results obtained while the reference currents are generated at the sampling rate of 8 kHz. The total harmonic distortion (THD) of supply current is reduced to 18% from 30.5% in the load current with the help of APF. If the limits specified in Table 2.2 are compared to this result (when $I_{SC} > I_L \times 1000$ and $V \leq 69kV$), THD is 18% which is less than 20% given in table. Obviously, APF has brought the THD under the limit.

Figure 4.17 a) Experimental results of the direct current controlled shunt APF for IRPT Methods i) load currents ii) supply currents iii) APF dc link voltage. b) Simulation results from Matlab.

Since the training of neural network has been performed at 6 kHz, the sampling rate of reference current is also carried out at 6 kHz for ADALINE used in the implementation of APF. Mathematical complexity of this method increases the

execution time of program on DSP hence reduces sampling rate of reference current. The THD of supply current is reduced to 20% under the same loading conditions of IRPT. The THD is high in both cases because the load current commutation from one phase to the other is sharp and sampling rate is insufficient for tracking this step changes. Two effective parameters for reducing the THD which are the switching frequency and overlap angle on load currents could be adjusted, but it is not done in order to keep the operating conditions same and worst in loading conditions for ADALINE and IRPT. The THD of supply currents in the case of ADALINE is a little higher than the value in the case of IRPT, because as the IRPT responds to all harmonics, the ADALINE is expected to responding harmonics trained.

The APF is operated under unbalanced load and its results are given in Figure 4.18 for ADALINE. The unbalance operation is obtained by connecting three phase bridge rectifier in parallel to unbalanced three-phase resistive load. Therefore, the load current harmonics are generated in balanced form by the rectifier. Since ADALINE is a delayless method and extracts the harmonics on each phase independently, the content of the harmonic in each phase is predicted accurately. The APF with three-wire (without neutral line) connection responds to eliminate harmonics trained successfully because reference harmonic currents are balanced. It is obvious that if the harmonics are also unbalanced, the ADALINE can work well under 4-wire connection (one more wire can be connected between neutral point of source and center points between dc link capacitors splitting dc voltage equally).
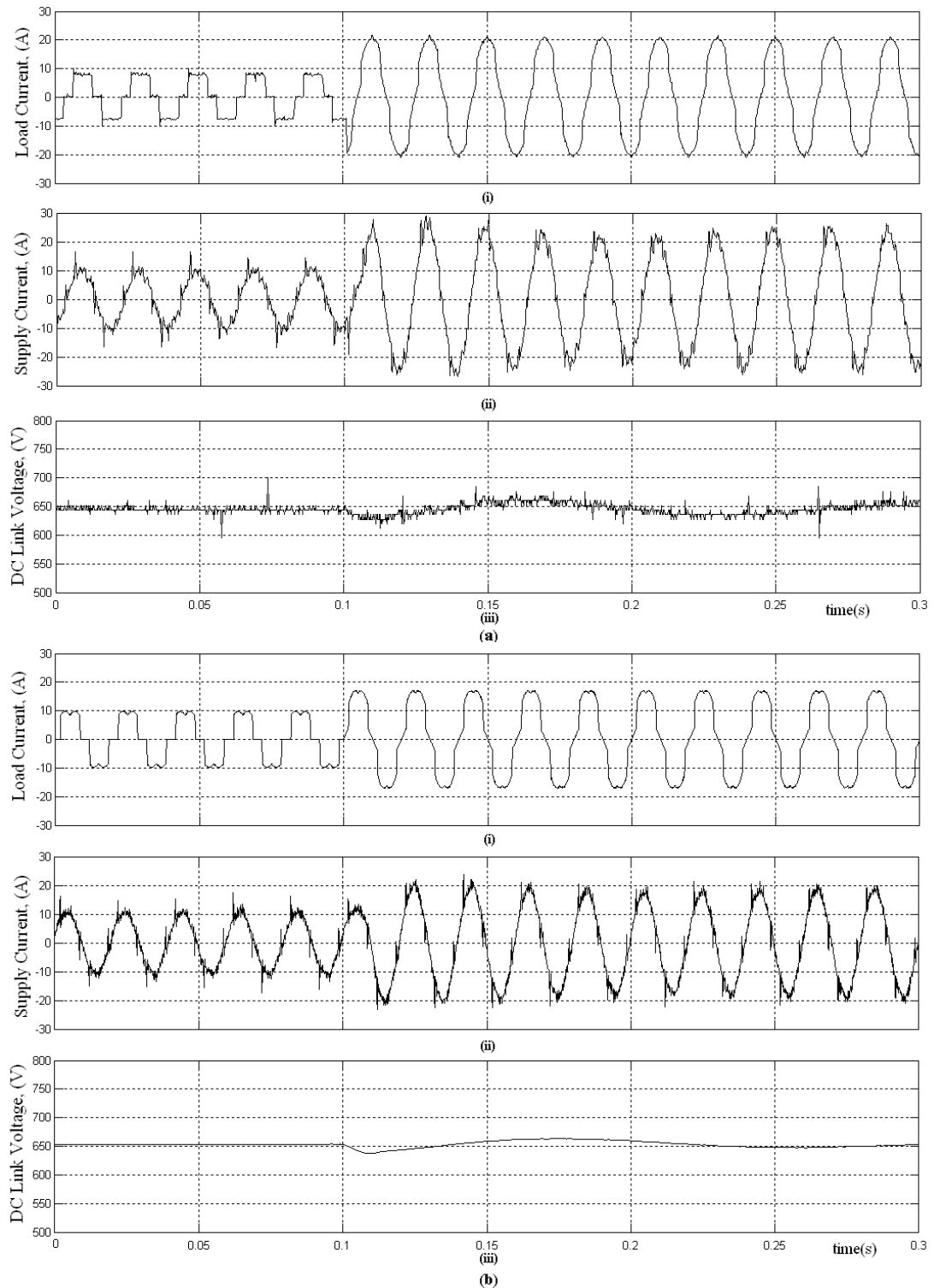
Figure 4.18 a) Experimental results of the direct current controlled shunt APF for Adaline Methods i) load currents ii) supply currents. b) Simulation results from Matlab.

The current controller has been operated by measuring current from inputs of APF (direct technique) and supply currents (indirect technique) for ADALINE under unbalanced loading condition. The result of experiment on the indirect current controller is given in Figure 4.19 for unbalanced loads. These results show that while the total harmonic distortions of the load's phase currents are 16%, 30.5%, and 16%, the THDs of supply currents becomes 4%, 6%, and 4%, respectively after operating APF. Thus, the IEEE 519 standards have been satisfied without employing the switching ripple filter and smoothing reactors. The THD of each line current in indirect current controller is lower when they are compared to the values obtained from direct current controller.
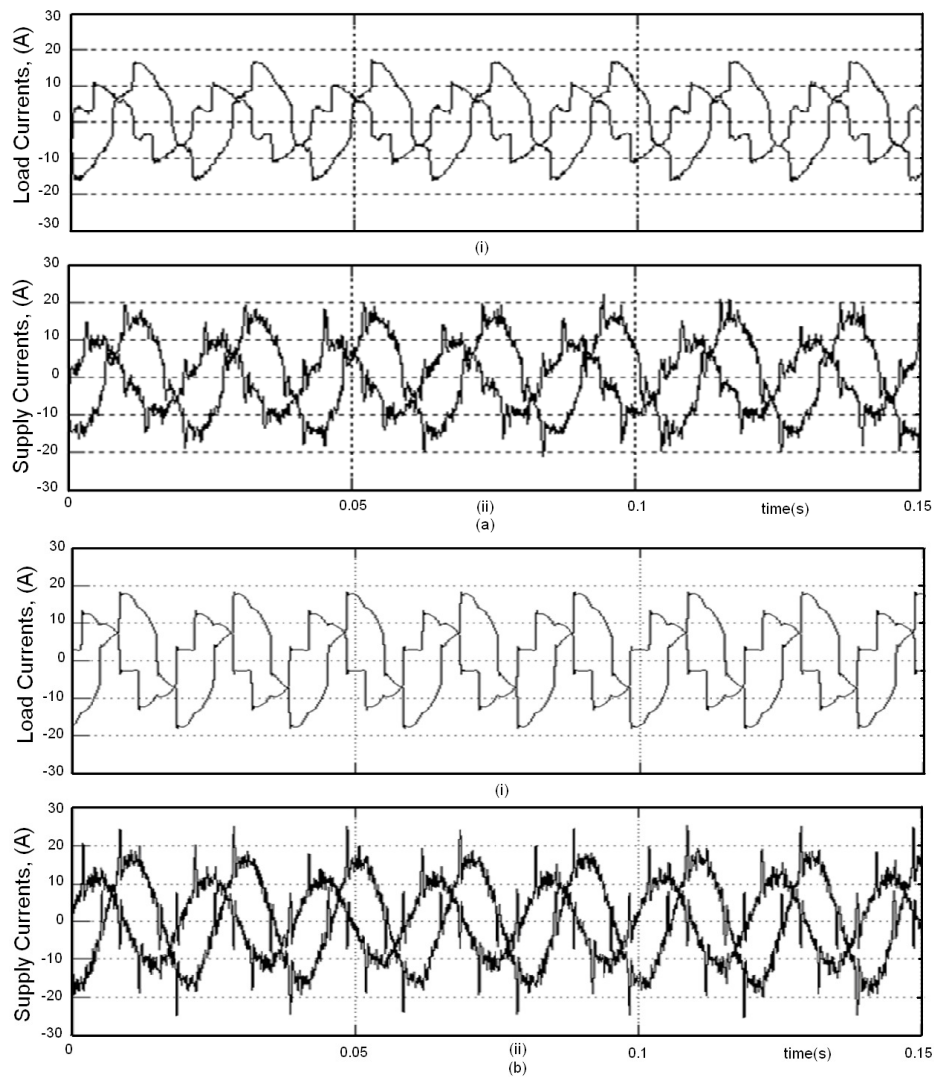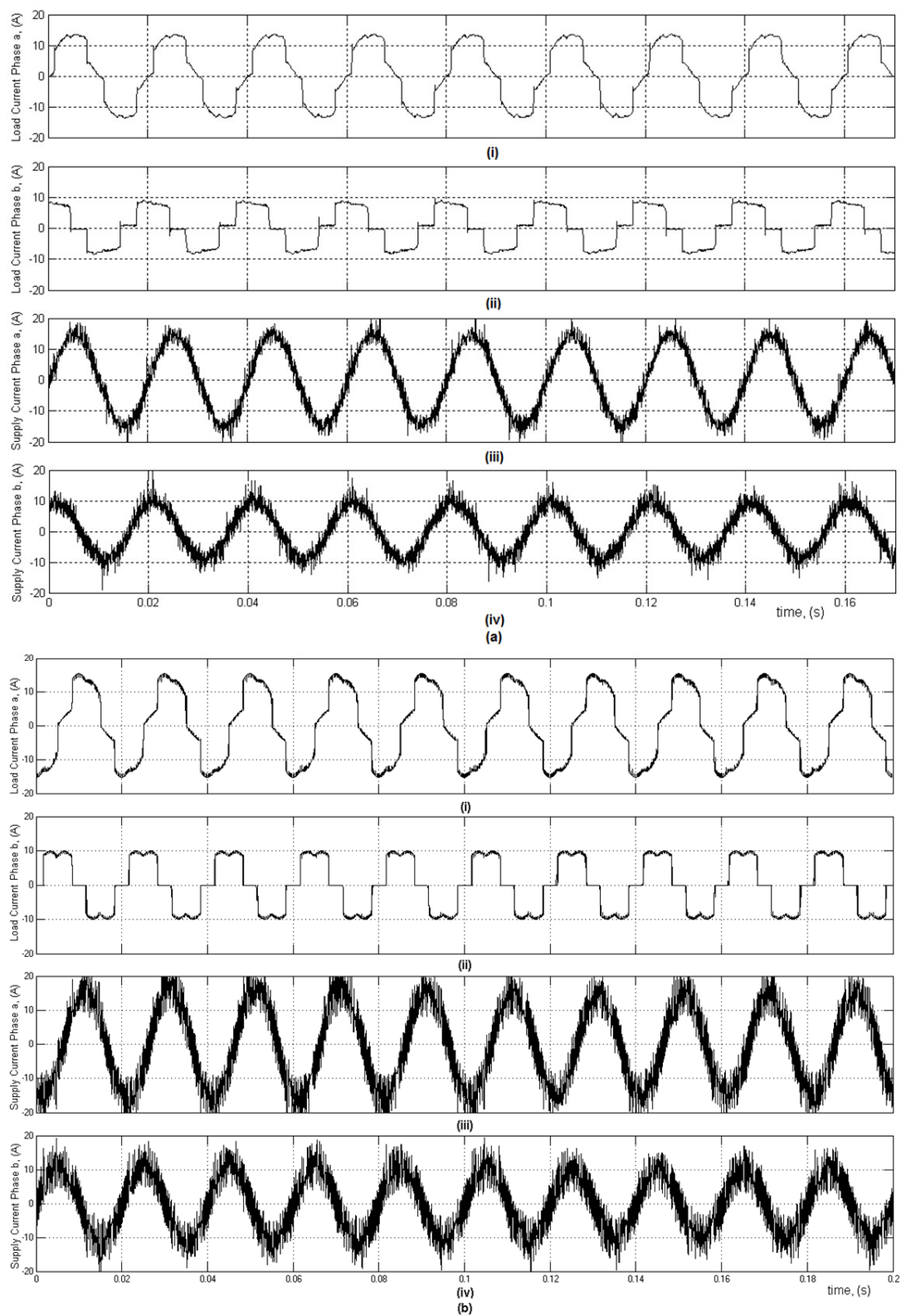
Figure 4.19 a) Experimental results of the indirect current controlled shunt APF for Adaline Methods; i) load current phase a, ii) load current phase b, iii) supply current phase a, iv) supply current phase b. b) Simulation results from Matlab.

The most important difference between direct and indirect current control techniques is that the controller in indirect algorithm works on current waveform at fundamental frequency. Therefore, the indirect current control technique may operate at lower sampling rate. The reference current which is the sum of fundamental component of load current and output of PI controller governing the dc link voltage can cause the instability, if the fundamental component of line current is not measured precisely.

4.5.2 Shunt APF Operating at 38 kHz Sampling Frequency

Most of the execution time in DSP is spent on converting the ADC reading to the variables of IQ type. In order to accelerate this process, the values between zero and 4096 at which the ADC may have converted into IQ type and prepared as a table for possible use.

The reading from ADC is captured as an index and its corresponding value in the form of IQ is obtained from table. This algorithm enables to increase the sampling frequency of reference current up to 38 kHz. The performance of the APF under IRPT is investigated and results are given in Figure 4.20 for the same loading conditions given in previously section. It is found that total harmonic distortion of supply currents are reduced from %30.5 to %6.2 by increasing sampling frequency to 38 kHz.
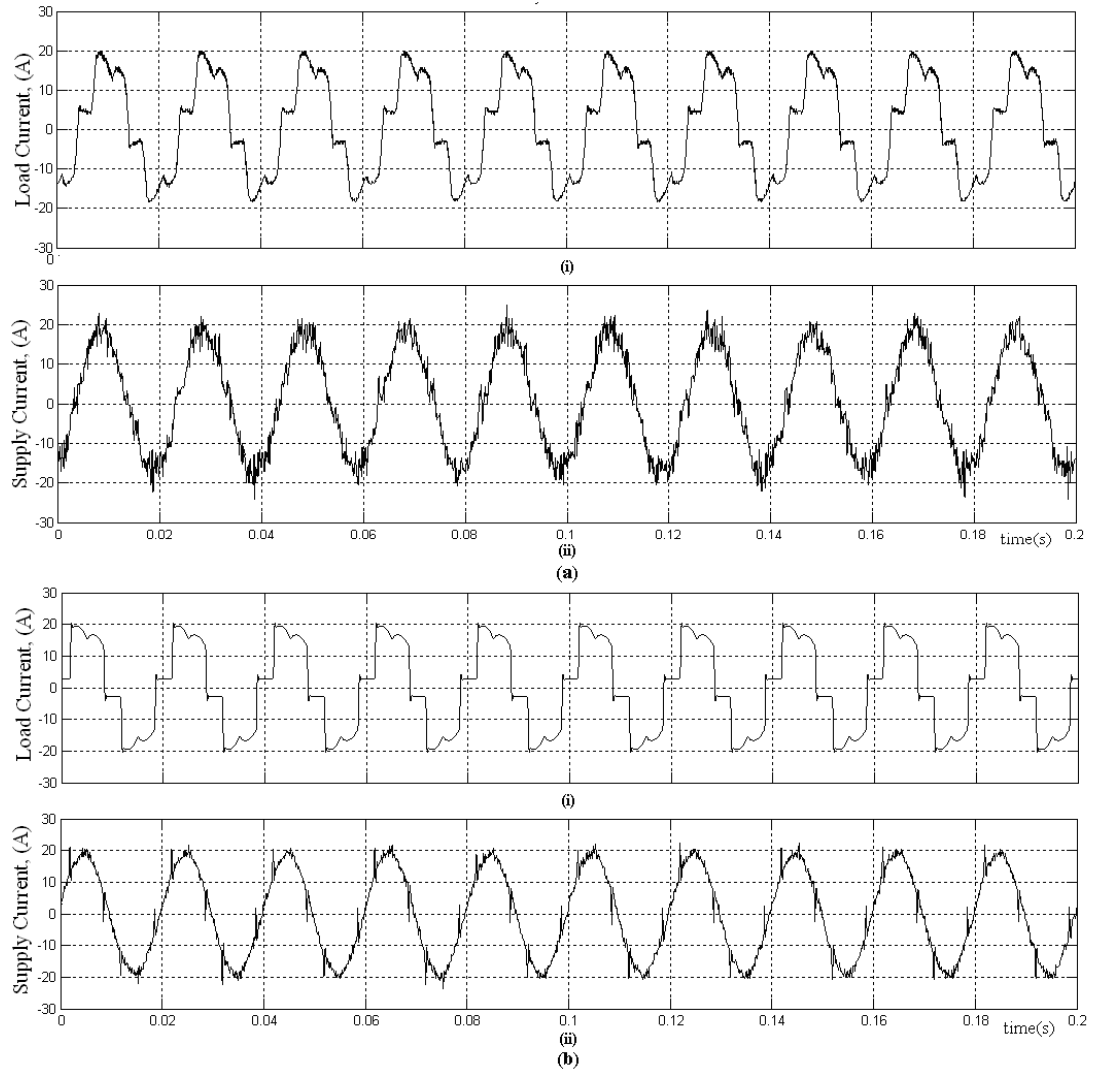
Figure 4.20 a) Steady-state currents for IRPT 38khz; i) load current ii) supply current. b) Simulation results from Matlab.

The gate signal of IGBT is shown in Figure 4.21 under the this operation condition. The harmonic spectrum of switching pulse is obtained by analyzing these signal in Matlab, is given in Figure 4.22. According to this spectrum, the avarage switching frequency is shown around of 6.5kHz.
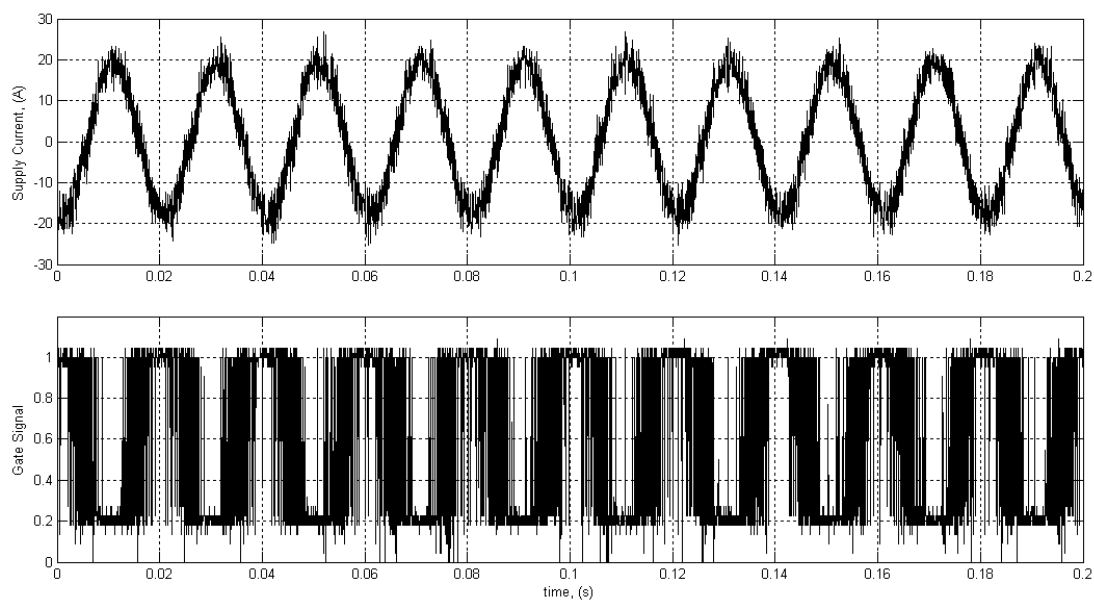
Figure 4.21 Steady-State opretion and gate signal for IRPT 38kHz algorithm.
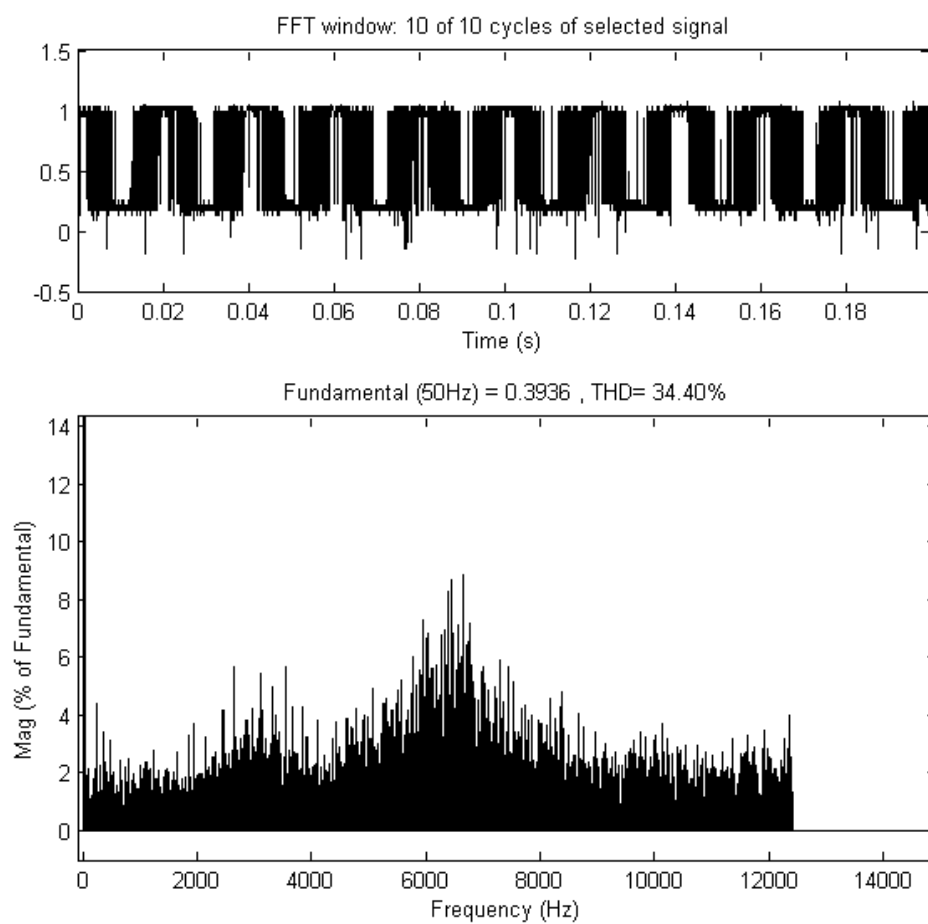
Figure 4.22 Frequency Spectrum of IGBT gate signal.

4.5.3 Transient Results for Designed IRPT Based Shunt APF

Figure 4.23 Applying load while shunt APF is running a) load current, b) supply current, c) supply voltage d) DC link voltage.

Primarily, DC link voltage is increased to a value of 650V when the shunt APF is started. While the system has no load current, the current of the active filter is sum of current for boosting DC link voltage and current of switching ripple filter. At the steady-state, the magnitude of RC switching ripple filter current is around of 3 A. While the shunt APF is operating without load, at the t=0.08sec, three phase diode rectifier load is connected to system as load. The result of experiment is given in Figure 4.23. The supply current is closer to sinusoidal in less than a quarter peroid. At this time, DC link voltage is oscillated with some small value.
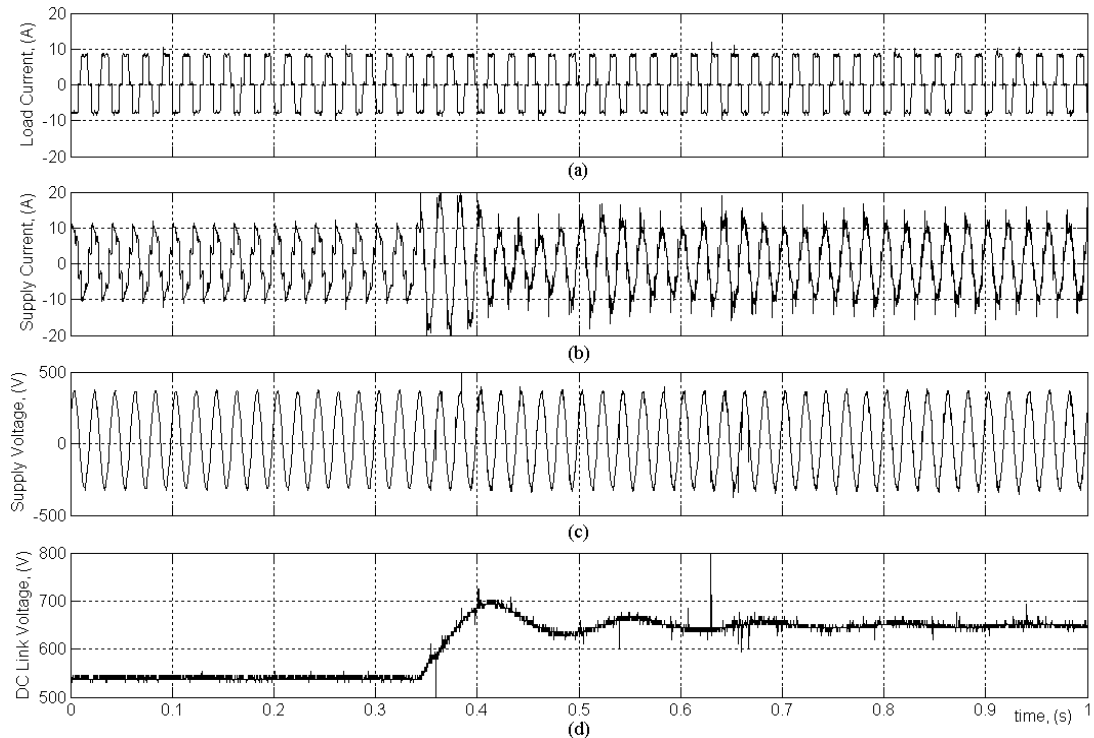
Figure 4.24 Starting of shunt APF under load a) load current, b) supply current, c) supply voltage d) DC link voltage.

When the shunt APF is started under nonlinear load at the instant t=0.35 s, the response of system can be seen in Figure 4.24. DC link voltage is initially charged to 530 V through the parallel diodes on IGBTs. Then, DC link voltage is boosted to 650V by PI controller which becomes steady-state at the instant t=0.6s. It can be observed that the maximum overshoot is around of 700V in DC link voltage. Also, this oscillation has caused distortion in supply current.

While the shunt APF has been operated with three phase diode rectifier load, the load is removed from circuit. In this case, waveforms of currents and voltages are given in Figure 4.25.

While the shunt APF has been operated in parallel to three phase diode rectifier load, the load is increased by inserting three phase resistive load in parallel. The transient response of system is given in Figure 4.26. Under these conditions, the shunt APF successfully tracks to load variations.

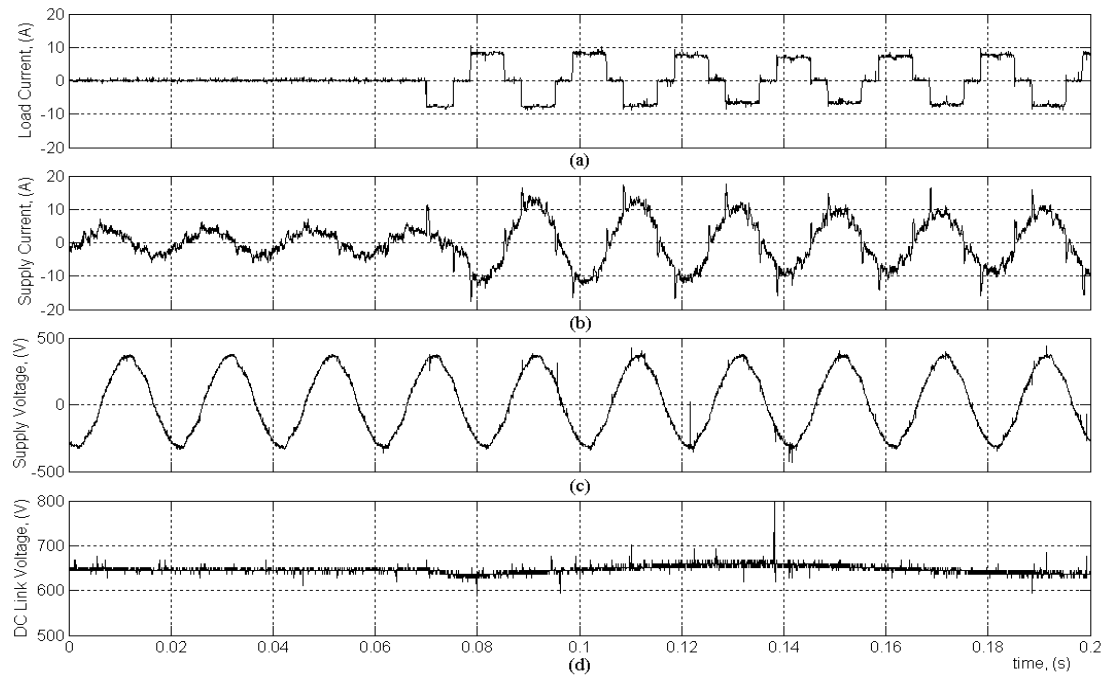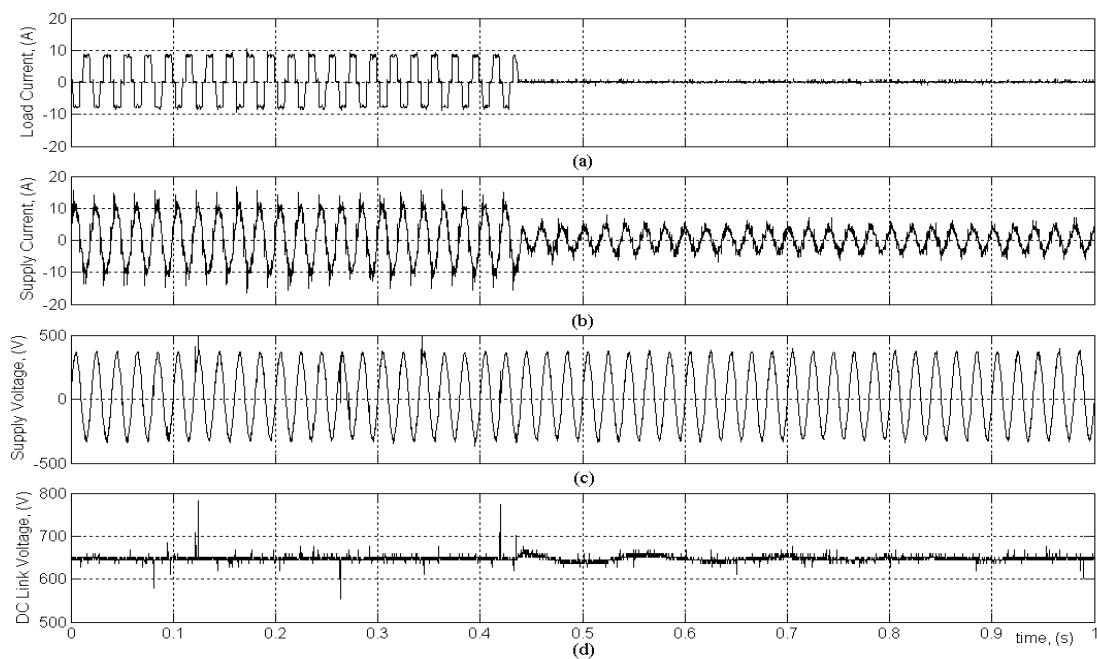Figure 4.25 Turn-off load while shunt APF running a) load current, b) supply current, c) supply voltage d) DC link voltage.
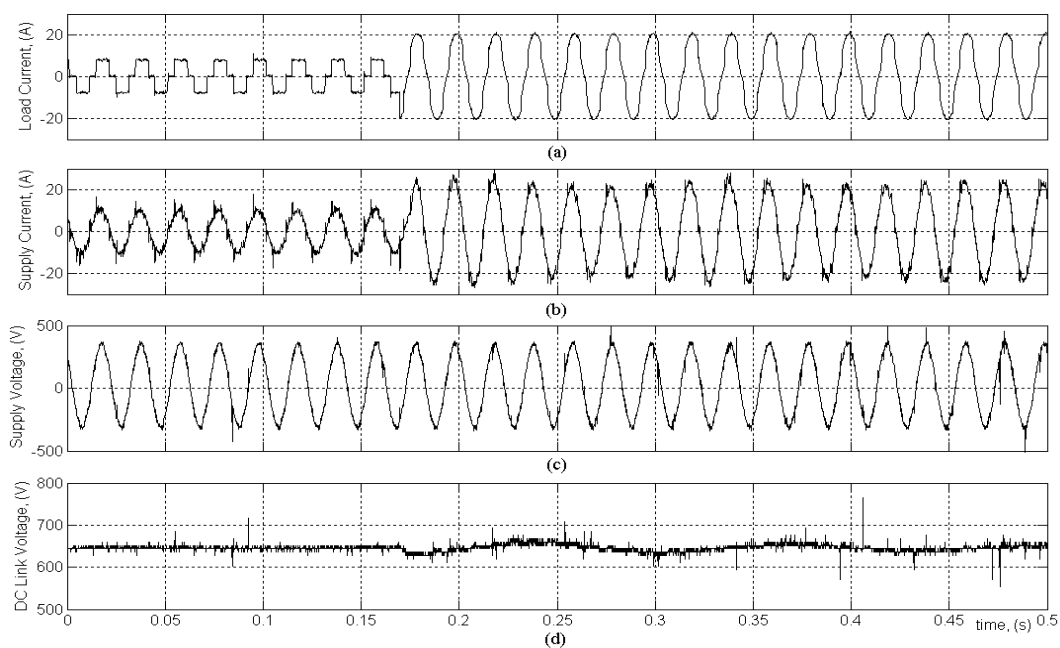
Figure 4.26 Increasing load while shunt APF running a) load current, b) supply current, c) supply voltage d) DC link voltage.
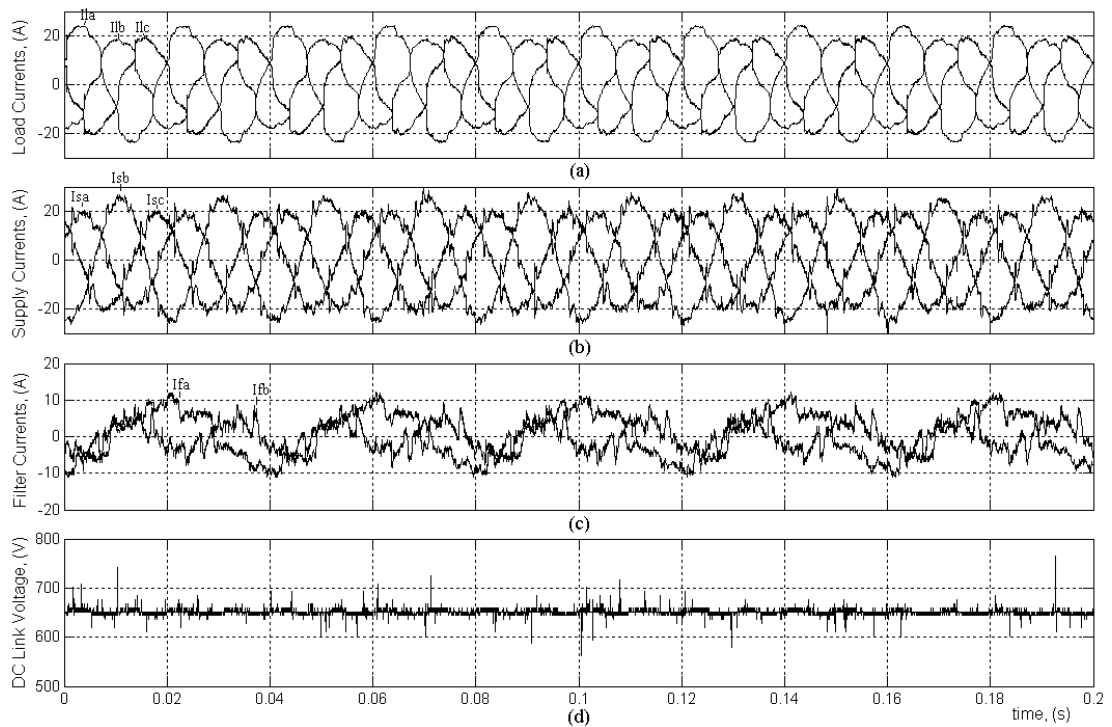
Figure 4.27 Shunt APF with IRPT method under unbalanced load a) load current, b) supply current, c) supply voltage d) DC link voltage.

The system is operated under unbalanced load by inserting three-phase unbalanced resistive load in parallel to the three-phase bridge rectifier. The variation of the load current, supply currents, filter currents and dc link voltage at steady-state is shown in Figure 4.27. As being shown in Figure 4.27c, the filter injects the current at fundamental frequency in addition to harmonics during the unbalanced operation of the load. When the reference currents of active power filter are computed from the IRPT algorithm, any imbalance in the load currents is distributed to other phases. As a result, the fundamental magnitudes of the compensated supply currents are different than the fundamental current magnitudes of the uncompensated load currents as shown in Figure 4.27a and b.

4.5.4 Shunt APF with SRF Method

The program which is prepared by using SRF method and it detects 5th, 7th, 11th, and 13th order harmonics has been tested on shunt APF protype. In experiment, the system is operated under three-phase balanced resistive load in parallel to the three-phase bridge rectifier. And the load current is smoothed by inserting line inductances in front of these loads. The smooting inductance is 3 mH, magnitude of diode rectifier current is 8A and parallel resistive load is 50 Ω. The starting transient and steady-state operation of shunt APF are given in Figure 4.28.
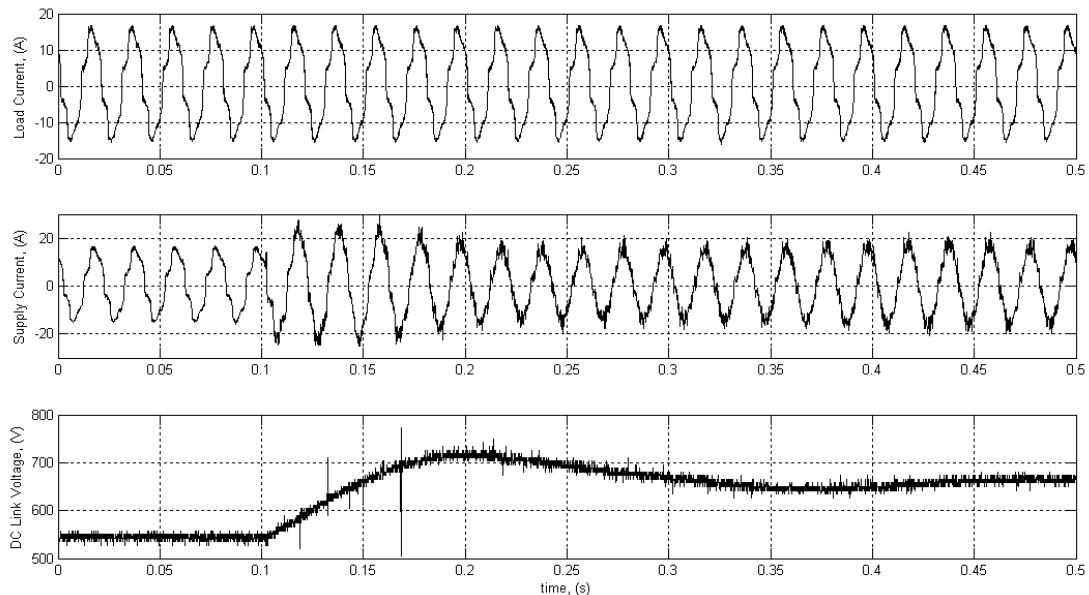
Figure 4.28 Experimental results of the direct current controlled shunt APF for SRF method a) load current, b) supply current, c) DC link voltage.

At this loading condition, the total harmonic distortion is decreased from %17 to %8 after compensation.

4.5.5 The Effect of Switching Ripple Filter

The switching ripple filter is designed in order for removing switching noise on filter currents. This high-pass filter has a serial star connected resistance and capacitance and the value of element are 3 Ω and 30 μF, respectively. The cut-off frequency of this filter is calculated as 10 kHz. A serial blocking inductance is used

between supply and RC filter which is 0.25mH. This inductance prevents high frequency currents leaking through supply . The performance of these structures are investigated with experiments. In Figure 4.29, filter current can be seen under operation without switching ripple filter. The high frequency current which is produced from hysteresis current controller is high.

In Figure 4.30, the filter current is given under RC switching ripple filter. Finally, the test result given in Figure 4.31 shows the filter current by using RC switching ripple filter and series blocking inductance.
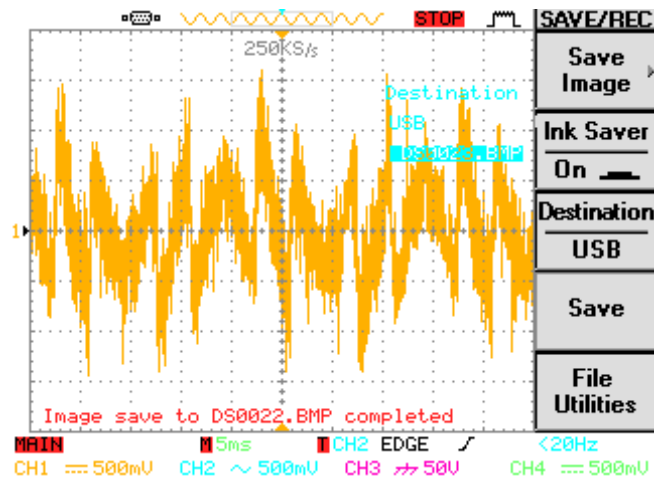
Figure 4.29 Shunt APF filter current without switching ripple filter.
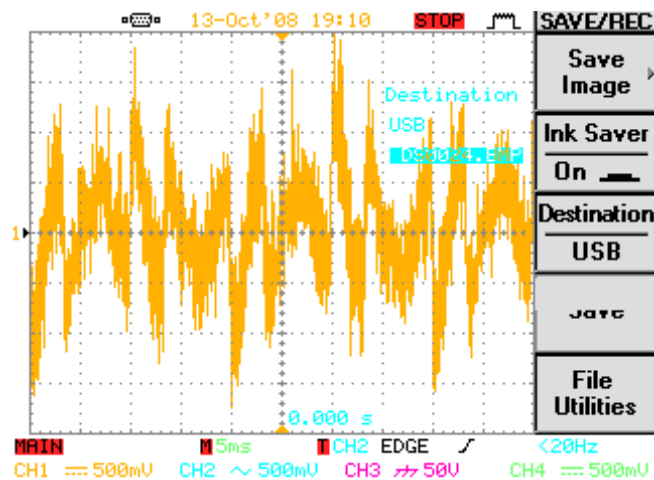
Figure 4.30 Shunt APF filter current with switching ripple filter.

According to the experimental result, high frequency compenents can be a little suppressed by only using RC filter. However, the L+RC structure eliminates almost all high-frequency components.
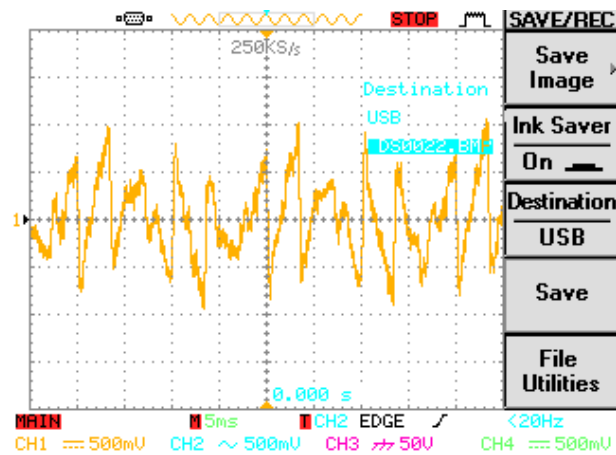
Figure 4.31 Shunt APF filter current with switching ripple filter and series inductance.

4.5.6 Comparing Three Controllers

In this work, a voltage source shunt APF is implemented by using direct and indirect current control techniques. The indirect current control technique has been applied first time with ADALINE method here. Experimental results of ADALINE are compared with IRPT method around 6 kHz. Since ADALINE method is a delayless method and works on each phase independently, it yields better results under unbalanced loading conditions. Both direct and indirect current control techniques are implemented by considering the effects of tracking capabilities on reference current. It is found that the indirect current control techniques are better to reduce the supply current harmonics but may cause instability, if the line current is not measured by the sensor with high resolution. The voltage source shunt APFs can compensate harmonics in supply currents, if the load generates current source type harmonics. If there is reactive power compensations capacitors in parallel to load, then the harmonic currents generated by the APF leaks to capacitors at the load side.

Hence, the harmonic compensation that is expected may not be successfully performed without blocking this path. It is also observed that while this situation does not cause any instability under direct current control technique, the indirect current control technique which was tested in a plant having reactive power compensation capacitors showed that HCC generates wrong switching signals and instability in shunt APF.

In application with F2812 DSP, The IRPT method produces the most accurate reference current and shows fastest response against to load variations, due to sampling time of program is 38kHz. But it can not operate under unbalanced load condition. The SRF method can be extracted four harmonic components in speed of 30kHz. By using this method, the specific harmonic elimination can be done and the power can be shared between parallel shunt APF modules.

ADALINE method produces reference current as delayless. But, the THD performance of method is limited by the sampling time. The simulation result of relationship between sampling frequency and THD performance is given in Figure 4.32 depending on load current.
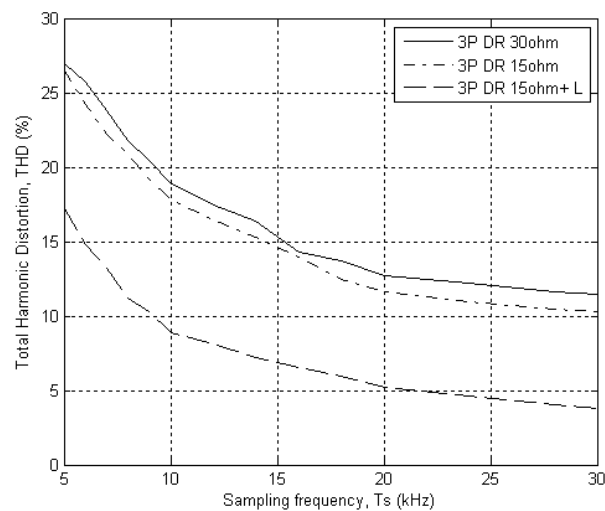
Figure 4.32 The relationship between sampling frequency and THD performance according to load for ADALINE method.

The experimental results of shunt APF by using IRPT and SRF methods are given Table 4.3 under different load conditions. Where, THD and specific harmonic distortions can be seen for after compensation and before.

Table 4.3 The performance of APF for IRPT and SRF methods under different loads.

	Load1	IRPT	SRF	Load2	IRPT	Load3	IRPT	SRF	Load4	IRPT	SRF
THD (%)	**17**	**7.5**	**8**	**24**	**6.2**	**29**	**10.7**	**14**	**16**	**6.4**	**8.2**
I_5	13.8	3	3.5	21	2	22	6.2	5	12.5	3.6	3
I_7	7	4	4	9	3.5	10.5	4	3.5	5.6	2.5	2
I_{11}	4	1	1	6	2.5	8	3	4.5	4.5	1.5	2.5
I_{13}	4	2	2.2	3	2	6.5	3	3	3.6	2	2

Load1: 8 A Diode rectifier + 3 mH L_L AC smooting line inductance + R=50Ω resistive load + Switching ripple filter.

Load2: 20 A Diode rectifier + 3 mH L_L AC smooting line inductance

Load3: 8 A Diode rectifier

Load4: 8 A Diode rectifier + R=50Ω resistive load

4.6 Experimental Work in Laboratory with F28335

The program is developed by using F28335 floating point DSP and the optimization of speed is carried out. The speed of program is increased to 70 kHz by using modified SRF method. The SRF method is programmed to generate all harmonics (not selective).

In experiment, three phase diode rectifier and three phase balanced resistances are used as load. The inductance of shunt APF is 3.2mH and the results of experiment are given in Figure 4.33. While the load current has %12.5 of total harmonic distortion before compensation, THD of supply current was measured as %4.5 (in Figure 4.33a and b) after compensation. Thus, IEEE 519 standards have been met without employing the switching ripple filter and smoothing reactors. If the smoothing reactors are used in front of tree phase diode rectifier, best performance can be obtained than current value of THD.
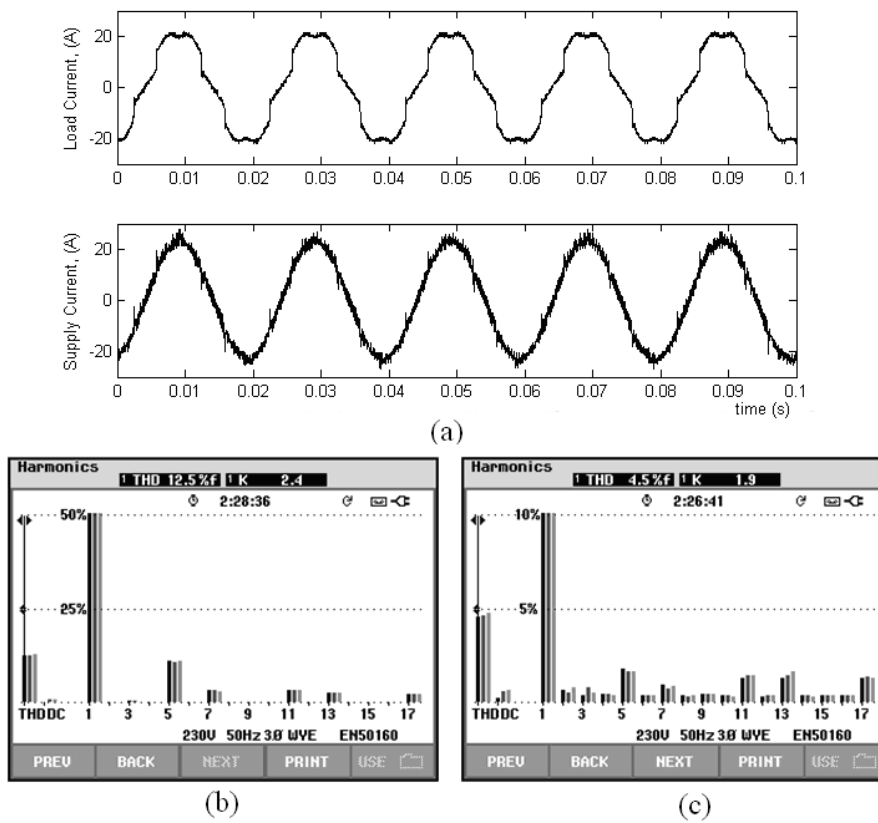
Figure 4.33 Steady-State performance of shunt APF prototype in laboratory a) Load and supply current, b) THD of load, c) THD of supply after compensation.

While three phase diode rectifier is only used as load, experiment results are shown in Figure 4.34. For this load, THD of supply are reduced from %29.4 to %11.2 after shunt APF was operated. The smoothing reactors must be used for best result of THD. Generaly, this type hard loads are not found at the coupling point of shunt APF. The total current of industrial enviroments is smoother than used load.
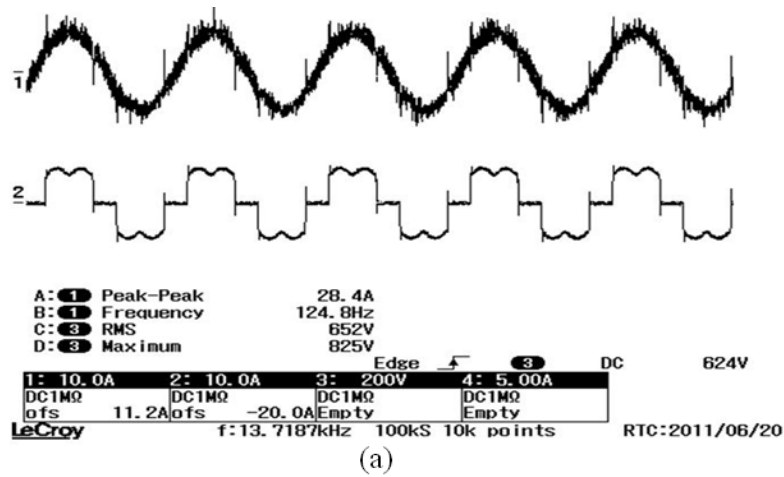
(a)
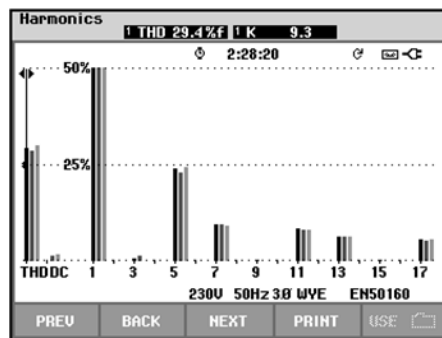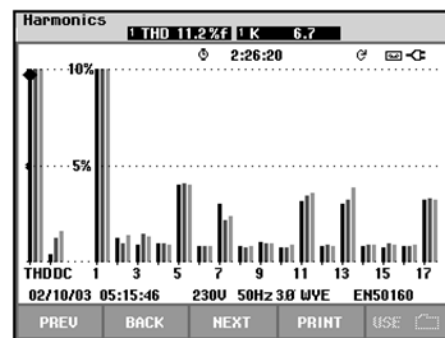
(b)   (c)

Figure 4.34 Steady-State performance of shunt APF prototype in laboratory a) Load and supply current, b) THD of load, c) THD of supply after compensation.

The performance of the shunt APF with SRF method was tested for transient conditions in laboratory. These experiment resuls are given in Figure 4.35-4.38.
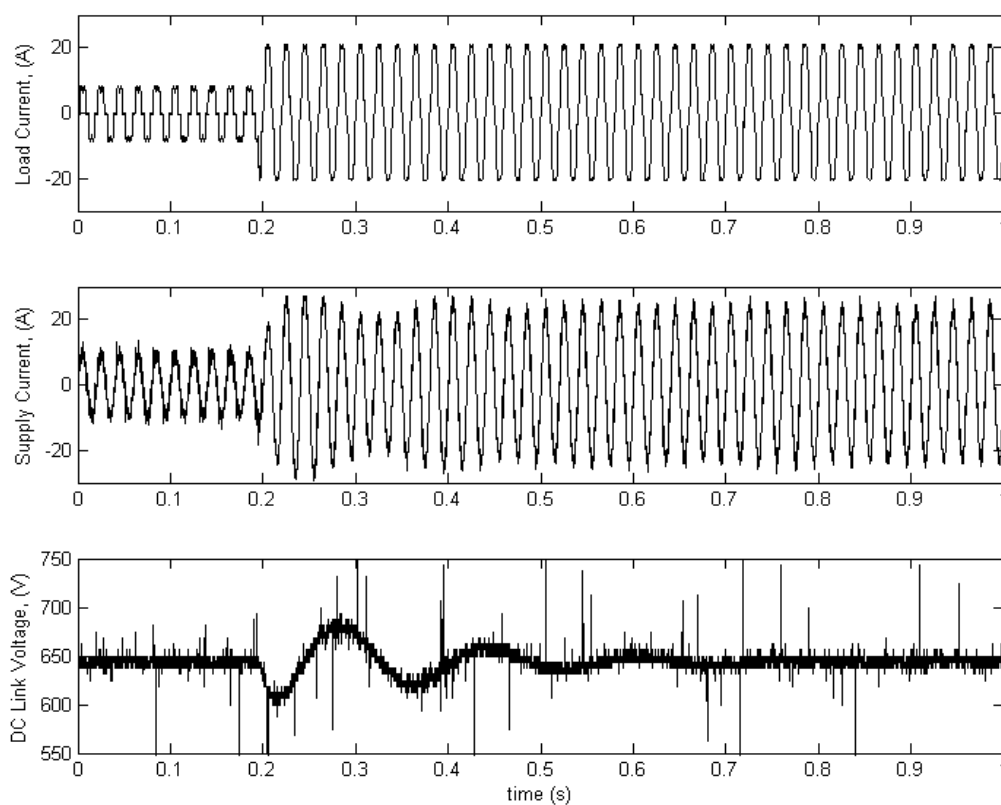
Figure 4.35 Increasing load while shunt APF running a) load current, b) supply current, c) DC link voltage.
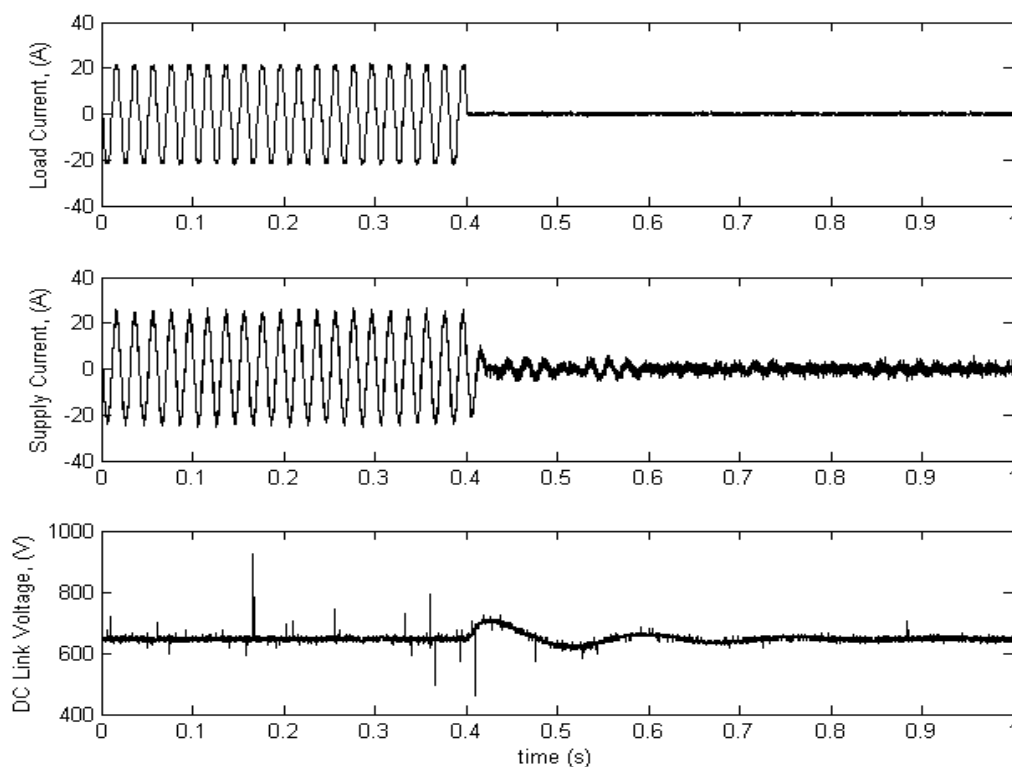
Figure 4.36 Turn-off load while shunt APF running a) load current, b) supply current, c) DC link voltage.
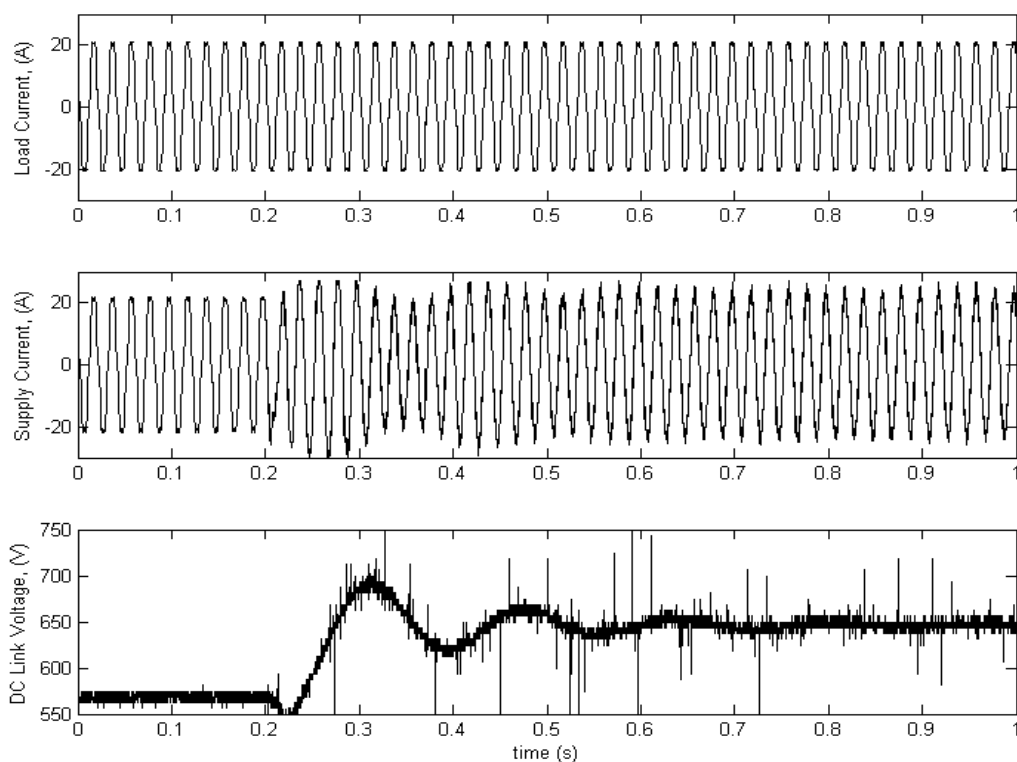
Figure 4.37 Starting of shunt APF under load a) load current, b) supply current, c) DC link voltage.
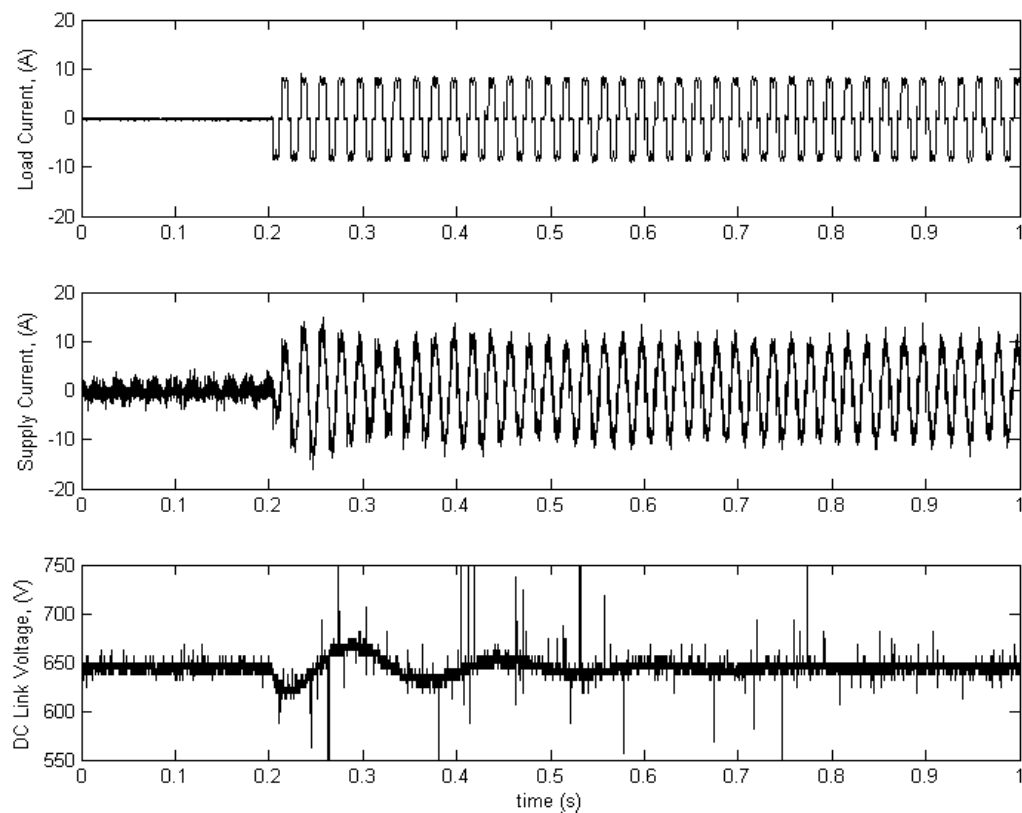
Figure 4.38 Applying load while shunt APF is running a) load current, b) supply current, c) DC link voltage.

CHAPTER FIVE
PARALLEL OPERATION

5.1 Introductory Remarks

The power rating and switching frequency of active power filter (APF) converters are determined by the magnitude of harmonic currents and required filter bandwidth. In high power applications, filtering task cannot be performed for the whole spectrum of harmonics by using a single converter due to limitations on switching frequency and power rating of the semiconductor devices (El-Shatshat et al, 1999). These limitations on the converter power rating and bandwidth affect the filtering performance as a result. The solutions suggested in the literature to this typical design problem of APFs are hybrid configuration, which reduces converter power rating; step-down transformer, which usually increases the cost; series or parallel connection of switching devices, which results in more complex gate drives; multilevel inverter, which reduces voltage rating of the switches; or splitting filtering on spectrum range among a number of APF (Peng, 1998), (Massoud et al, 2004), (Akagi, 1994, 1996).

The modular structure of shunt APF is the most advantageous feature of them. This feature allows parallel operation of number of modules to increase the kVA rating. Such an operation is also suitable especially when APFs are located in power distribution systems from the viewpoint of reliability, flexibility, and efficiency. In parallel operation of APFs; any fault in one or more APF modules is not expected to degrade the operation of whole system since other modules can tolerate it, hence system is fault tolerant and more reliable. Also, expansion capability of the APFs is an important factor depending on the increase of the harmonic polluting loads connected to the distribution system. In addition, APFs can be operated not only for harmonic compensation but also for other disturbances such as current imbalance and reactive power compensation. Finally; APFs can be optimized to minimize the switching losses as well as the total harmonic distortion of the supply currents.

Because of these reasons, modular filtering approach is quite appropriate for high power applications.

The control techniques used in parallel connection can be classified in three major categories. These are power splitting, frequency splitting, capacity limitation techniques (El-Shatshat et al, 1999), (He et al, 2006), (Chiang & Chang, 2001), (Abdelli et al, 2004), (Kuo et al, 2008). Of these methods, power and frequency splitting method requires detection of the load harmonic content and sharing the compensation currents among APF modules via a central controller. As an alternative to this approach, in a master/slave controller scheme, each APF has its own current sensor to obtain load current harmonics and master module shares the compensation currents among others (Ju et al, 2008).

The capacity limitation method aims independent operation of each APF module and provides a practical solution to power capacity enlargement problems. In APF applications, the research has mainly concentrated on voltage-source active filters, while the current-source active power filters are preferred in some applications due to their fast response as an alternative. Both configurations can be implemented for effective compensation of current harmonics injected by the load or source. The main drawbacks of the voltage source APF is the switching ripple in the source current, while the current source APF has bulk and heavy dc link inductor with high power loss (Routimo et al, 2007).

In this chapter, the voltage source APF is considered and the reference current to the APF is obtained by using Fast Fourier Transform (FFT). The configurations and suggested methods for the parallel operation of APFs are analyzed in PSCAD and results will be discussed.

5.2 APF Control Schemes for Parallel Operation

In high power applications, the APFs are usually connected in parallel. There are mainly three types of techniques for parallel operation in practice. These techniques

are based on power splitting, frequency splitting and capacity limitation on each module, which are summarized as follows:

5.2.1 Power Splitting Approach

In this approach, N identical converter modules are connected in parallel and the compensating harmonic current is equally shared among these converters (i_{Lh}/N) as shown in Figure 5.1. This approach is also known as load current distributing approach or scheme of distributed control (He et al, 2006), (Chiang & Chang, 2001). The advantage of this approach is its easiness for implementation and maintenance. The disadvantage is that any fault on the control signal bus may shut down the whole system, since it requires control interconnection among APFs for equally distributing the required compensating load current (Chiang & Chang, 2001). A central control scheme shares the total compensation currents equally among the APFs. Each APF can also be designed with its own harmonic detection and processing unit, that would eliminate dependency on single and reliable central control unit.
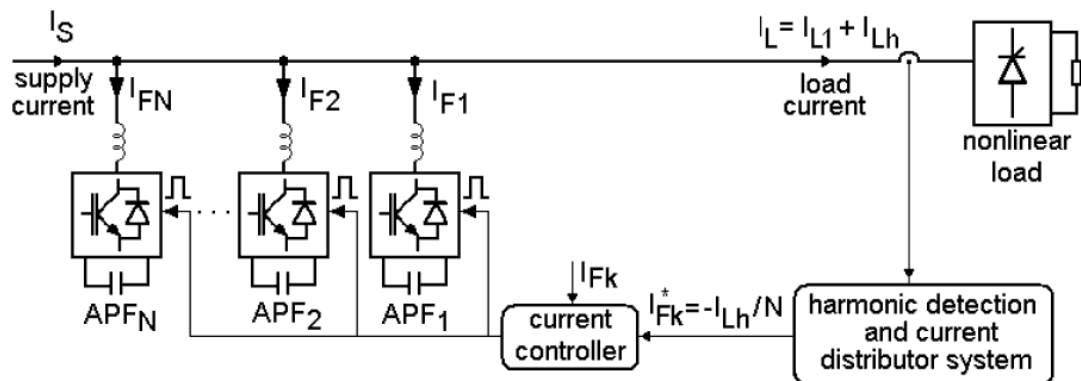
Figure 5.1 Power splitting scheme consisting of identical APF modules

5.2.2 Frequency Splitting Approach

The block scheme that represents the operation of this method is shown in Figure 5.2. In this method, each APF is assigned to compensate a specific harmonic component of a nonlinear load. Since the harmonic current magnitudes of the

nonlinear loads are inversely proportional to the harmonic order, the APF module that compensates the higher order harmonics have lower power rating and higher switching frequency, and vice versa. The switching losses of each converter are equal if the power switching frequency product is kept constant. The main disadvantage of this scheme is that the APF modules are not identical and can be replaced only by a similar module (El-Shatshat et al, 1999). Since a central control scheme that extracts load harmonic components and distributes to APF modules is required in this method, any fault on the current control signal will yield the whole system to shut down as mentioned in previous scheme.
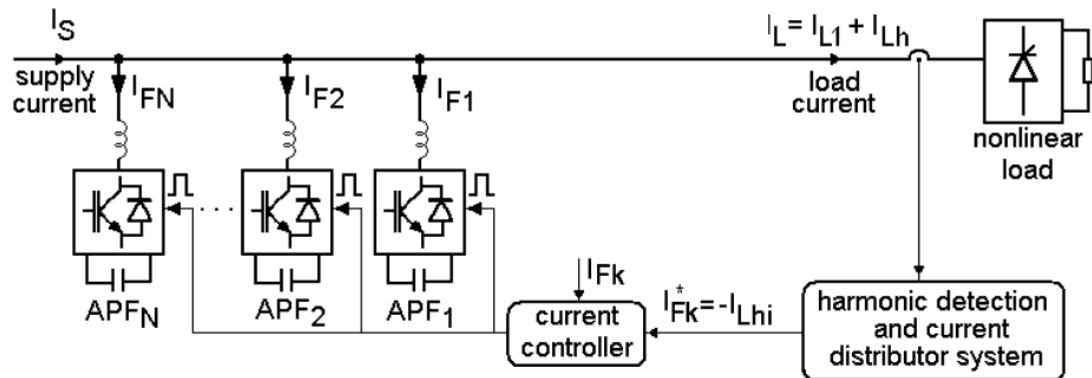
Figure 5.2 Frequency splitting scheme consisting of APF modules with different power rating and switching frequency

5.2.3 Capacity Limitation Control

In this method, each APF module injects the harmonic and/or reactive compensation current to the electrical network with limited amplitude by its own power rating (Chiang & Chang, 2001). As shown in Figure 5.3, the APF modules are distributed along the power network and each APF detects the currents at the upstream of the node, where the previous APF nearer to the load is connected. Each APF nearer to the electrical supply treats the previous APFs as on its load side and compensate the remaining part of currents. The compensated current may be at limited amplitude depending on converter's capacity. Hence, the total harmonic current and/or reactive power is shared among the APFs. In this scheme, the APF modules are not necessarily to be identical, since each module is operated

independently, therefore, allowing power capacity enlargement to be made easier. Also, there is no central control scheme that shares the total compensation currents among the APFs and as a result the APF system becomes more reliable. However, the dynamic characteristic of this method is poor (Ju et al, 2008).
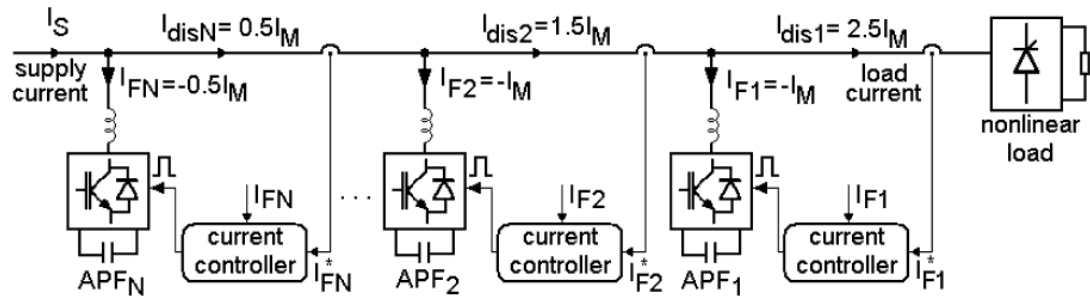
Figure 5.3 Current sensing and capacity limitation control of multimodule cascaded APFs

5.3 Simulations of Parallel Operation

Simulations for the parallel operation of APF modules are performed by using the PSCAD package program. A three-phase diode bridge rectifier with resistive load has been used as a nonlinear load. The current control loops of the APF modules contain hysteresis controller. Each APF has a switching ripple filter on its supply side and dc link PI controller.

The system parameters are summarized in Table 5.1. In simulations, harmonic compensation of the load is performed by using single-converter and multiple-converter approaches and their performances are compared. The schemes given in Figure 5.1, 5.2, and 5.3 are constructed in PSCAD package program for single-converter (N=1) and multiple-converter (N=2) approaches.

Table 5.1 System Parameters

Supply voltage (V, rms, line-to-line)	380 V
Supply frequency (fs)	50 Hz
Supply resistance (Rs)	0.001 ohm
Supply inductance (Ls)	0.1 mH
Diode rectifier load (10kW) resistance (R$_L$)	25 ohms
APF inductance (L$_F$)	1.8 mH
APF resistance of inductance (R$_F$)	0.1ohm
APF dc link capacitor (C$_f$)	2.35 mF
APF dc link reference voltage (u$_{dc}$*)	650 V
APF hysteresis current controller bandwidth (HBW)	0.2A
APF dc link voltage PI controller parameters	K$_P$=0.1 T$_I$=0.01s
Switching Ripple Filter Parameters	L=0.25mH C=30 uF R$_d$=3 sohm

5.3.1 Single-Converter Approach

When a single converter unit is implemented, the power rating of the converter can be specified by defining the constraint on total harmonic distortion or specific harmonic compensation of supply current.

5.3.1.1 Total Harmonic Distortion (THD) Approach

In this method, PAPF reference currents are generated such that they compensate the whole harmonic components in the load currents. The fundamental components of the load currents are obtained by FFT method and multiplied by reference sine waveforms, which are obtained via PLL circuit that tracks the supply voltages. Hence, the required compensation currents are simply obtained by subtracting these fundamental current waveforms from the actual load current as follows:

$$i^*_{f,i} = i_{L,i} - i_{Lh1,i} \qquad (5.1)$$

Where $i = a, b, c$ and i^*_f, i_L, and i_{Lh1} are the PAPF reference compensation current, load current, and fundamental load current of each phase, respectively. The

waveforms of supply voltages, supply currents, APF current, load current, and APF dc link voltage at steady-state after APF begins to compensate the harmonics of a 10kW load at t=0.5s are shown in Figure 5.4a. The dc link voltage of the APF is almost kept constant at 650V with a peak-to-peak ripple voltage of approximately 1V. The reference currents are updated at a sampling rate of 10 kHz considering the execution time for the process in real system. At this sampling rate, the total harmonic distortion (THD) is decreased from %29 to %11.4 after compensation. While calculating the THD, harmonic components of the supply currents upto 31st have been taken into account. Since APF acts to compensate the whole harmonic content except the fundamental, reference current waveforms contain higher order harmonics. The current injected by the APF cannot track the reference current in a strict hysteresis band. Reducing HBW or decreasing the value of the filter inductance causes the switching frequency of IGBTs increase substantially. Also, the magnitude of the filter current has effect on the switching frequency due to hysteresis controller. Hence, the waveform tracking performance of the APF degrades due to increasing switching frequency and as a result THD increases. The notches appear in the supply current waveform during commutation instants of the diode rectifier. It is seen that the APF currents are unable to track the quick variations. The reason that the supply current waveforms contain notches as shown in Figure 5.4b is the APF's current tracking error. It must be noted that the value of the supply reactance is taken as a small value in simulations. In practice, the notches in the supply currents are also affected by the magnitude of source reactance.

5.3.1.2 Specific Harmonic Elimination Approach

In this method, compensation of specific harmonics that the load current contains is aimed. The amplitude and phase information of specific harmonic components of the load currents are obtained by FFT method. A PLL circuit is used to obtain the phase information of the supply voltages. The reference compensation currents are obtained as follows:

$$i_{f,i}^* = -\sum_h i_{Lh,i} \tag{5.2}$$

Where $i = a, b, c$ and i_f^* and i_{Lh} are the PAPF reference compensation current and specific harmonic component of the load current for one phase, respectively. In simulations, APF is assigned for the compensation of 5th, 7th, 11th, and 13th harmonics. The waveforms of supply voltages, supply currents, APF current, load current, and APF dc link voltage at steady-state after compensation are shown in Figure 5.4b. The dc link voltage of the APF is almost kept constant at 650V with a peak-to-peak ripple voltage of 4 V. THD value is decreased from %29 to %11.7 after compensation of 10kW diode rectifier load current harmonics.
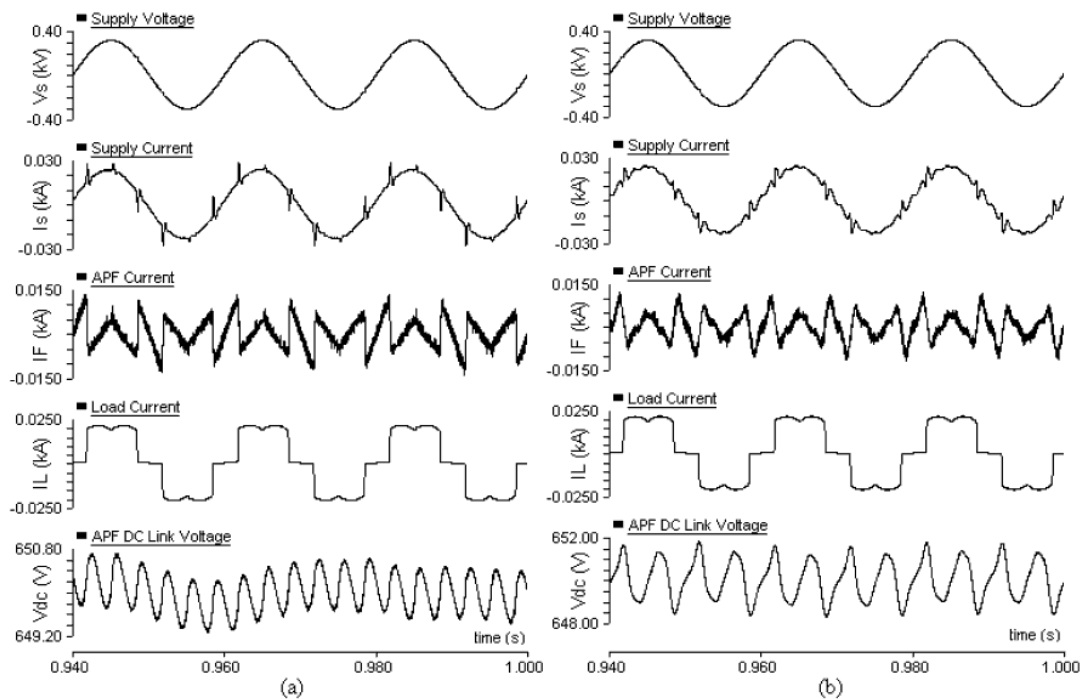
Figure 5.4 Simulation results obtained from single-converter at steady-state a) THD approach b) specific harmonic elimination approach.

5.3.2 Multiple Converter Approach

In this part, the methods of power splitting and frequency splitting are examined. Each converter is employed for predefined harmonic compensation or power sharing. In this simulation, two APFs are connected in parallel for the load.

5.3.2.1 Power Splitting Approach

In this method, reference compensation currents are generated in the same way as mentioned for single converter approach. This calculated reference current is divided by the number of APF modules and shared to APF modules equally as follows:

$$i_{fk,i}^* = \frac{i_{L,i} - i_{Lh1,i}}{N}$$

(5.3)

Where $i = a, b, c$ and $k = 1,.., N$ is the number of APF module. Simulations are performed with $N = 2$ parallel APFs. The waveforms of supply voltages, supply currents, load current, and APF currents at steady-state after APFs begin to compensate the harmonics of a 10kW load at t=0.5s are shown in Figure 5.5a. THD value is decreased from 29% to 10.2%, which is slightly beter than the one obtained from single-converter approach.
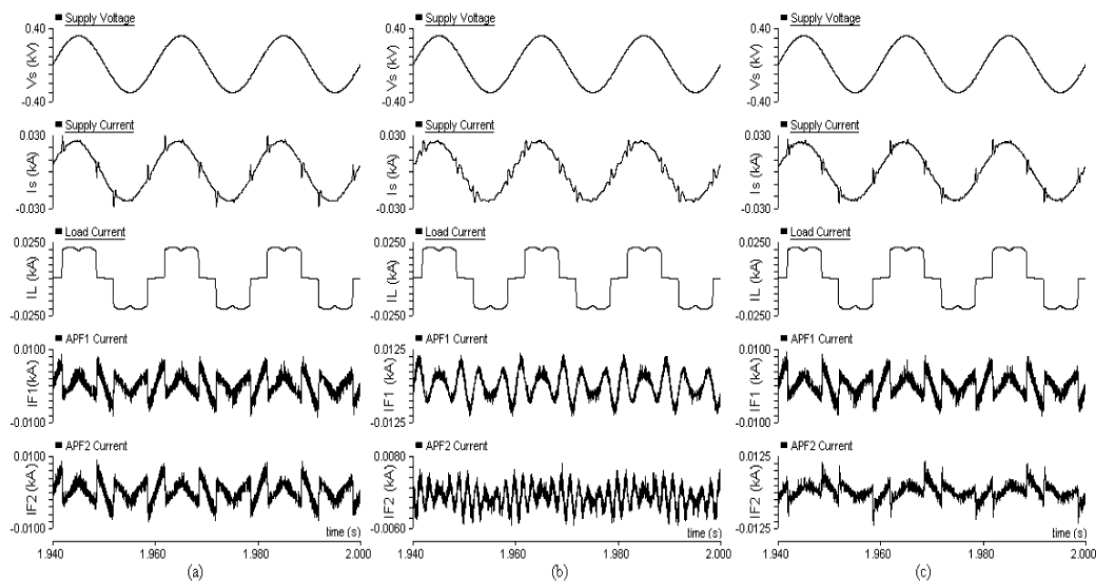

Figure 5.5 Simulation results obtained from multiple-converter at steady-state a) power-splitting approach b) frequency-splitting approach c) capacity- limitation control approach.

5.3.2.2 Frequency Splitting Approach

In this method, the waveforms of specific harmonic components of the load current are generated in the same way as mentioned in single converter approach. The required compensation current consisting of specific harmonic components is shared among the APF modules. In simulations, two APF modules are used; the APF1 is assigned to compensate 5th and 7th harmonics, while APF2 compensates 11th and 13th harmonics. The waveforms of supply voltages, supply currents, load current, and APF currents at steady-state after APFs begin to compensate the harmonics of a 10kW load at t=0.5s are shown in Figure 5.5b. The THD value of the supply current is decreased from 29% to 11.6% after both APFs compensates in simulations. The THD performance of this configuration is almost the same as the result obtained from single-converter specific harmonic elimination approach.

5.3.2.3. Capacity Limitation Control

In this method, reference compensation currents are generated in the same way as mentioned in single-converter approach. The peak value of the compensation currents is limited according to the current limit of each APF module. In order to limit the compensation currents in PSCAD simulations, the rms value of the reference compensation current is calculated first. The power rating of each APF module is determined by the following formula (Akagi, 1996):

$$P = \sqrt{3} \cdot \frac{V_{dc}}{\sqrt{2}} \cdot \frac{i_{f\,\max}}{\sqrt{2}} \tag{5.4}$$

Where, V_{dc} is the dc link voltage value and $i_{f\,\max}$ is the peak value of the compensation currents. Under regulated dc link voltage conditions, the capacity of each APF module is determined by the peak (or rms) filter current. Hence, a gain factor for each APF, which represents the fraction of APF capacity, is calculated as follows:

$$i_{fk,gain} = \begin{cases} 1, & i_{fk}^* \leq i_{fk\,max,rms} \\ \dfrac{i_{fk\,max,rms}}{i_{fk}^*}, & i_{fk}^* > i_{fk\,max,rms} \end{cases} \qquad (5.5)$$

Where, $i_{fk\,max,rms}$ represents the rms current limit of kth APF and i_{fk}^* is the rms value of the calculated reference compensation current. In simulations, the rms current limit of each APF is chosen to be 2.5A. In Figure 5.5c, the waveforms of supply voltages and currents, the current waveforms on the APF2 load side, and APF compensation currents are shown at steady-state. THD value is decreased from 29% to 7.3%, which is slightly better than the one obtained from multiple-converter power-splitting approach. For THD approach of single-converter and 10kW diode rectifier load, the peak value of the filter reference currents is approximately 10.7A (excluding the amount of fundamental current that is required for APF operation). Due to tracking error of APF, instantaneous filter currents may become higher than this value, which means required APF power rating is somewhat higher. For single-converter specific harmonic elimination approach, the peak value of the filter reference currents is approximately 9.4A (excluding the amount of fundamental current that is required for APF operation). For power splitting approach with multiple-converter, the peak values of the reference currents of both APF converters are at the half value of the single-converter.

For frequency splitting approach with multiple-converter, the peak values of the reference currents of APF1 and APF2 are 7.4A and 3.2A, respectively. For multiple converter capacity limitation control, the peak value of the reference currents of APF1 and APF2 are calculated as 6A and 10A in simulations, respectively. Although the rms compensating currents are limited such that both APFs almost equally share the compensating currents, the instantaneous filter current of APF2 is higher than that of APF1 in capacitylimitation control method. This is because of the supply currents' containing high frequency components that APF1 cannot properly compensate during diode rectifier commutation instants. As a result, the actual VA capacity of the APF2 is increased.
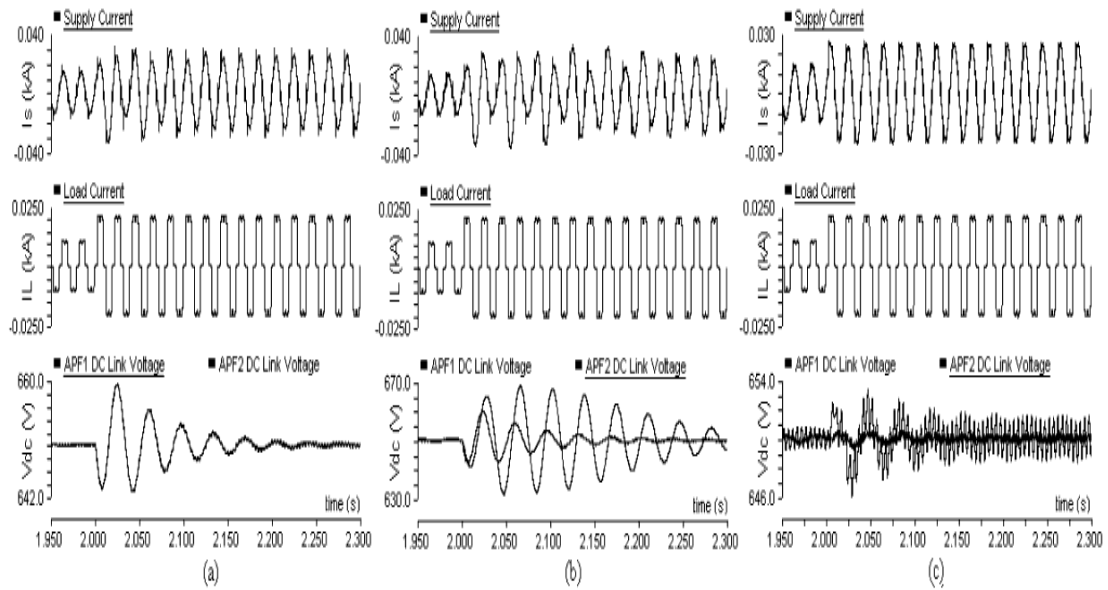
Figure 5.6 Responses of the multiple-converter APF systems to a step load change a) power-splitting approach b) frequency-splitting approach c) capacity- limitation control approach.

The performances of multiple-converter APF systems were also tested against a step load change from 5kW to 10kW at t=2s. The simulation results for three multiple-converter aproaches are shown in Figure 5.6, which includes the variations of supply current, load current, and APF dc link voltages. The specific harmonic elmination with frequency-splitting method gives the fastest transient response, while the capacity limitation is the slowest.

5.4 Results of Simulations

When the power ratings of the converters are considered for the compensation of diode rectifier load current harmonics, it can be seen that the total VA rating of the installed APFs are highest in multiple-converter capacity limitation control approach and lowest in single-converter specific harmonic elimination approach.

Simulation results show that the multipleconverter power-splitting and capacity limitation control methods give the best THD performance in the suppression of the lower order dominant harmonics. Single-converter specific harmonic elimination and

frequency-splitting methods give almost the same performance, however, since the peak amplitude of the sum of harmonics is lower than that of an individual harmonic, assigning an APF for the compensation of only one harmonic is not effective and this yields to a larger total APF VA rating. The THD performance of single-converter THD method worsens as the nonlinear load increases, because of the increase in required switching frequency of the converter. When the compensating currents are shared as shown in multiple-converter power-splitting approach, the THD performance of the system is observed to improve.

Table 5.2 VA Ratings of APFs

		The peak value of the filter reference currents	
Single Converter	THD approach	10.7 A	
	Specific harmonic elimination approach	9.4A	
Multiple Converter	Power splitting approach	5.35A	5.35A
	Frequency splitting approach	7.4 A	3.2A
	Capacity limitation control	6 A	10A

Table 5.3 Compensation characteristic of methods

		THD of supply
Single Converter	THD approach	%11.4
	Specific harmonic elimination approach	%11.7
Multiple Converter	Power splitting approach	%10.2
	Frequency splitting approach	%11.6
	Capacity limitation control	%7.3

The actual VA capacity of the forthcoming APFs is increased due to insufficient compensation of the previous APF modules in capacity-limitation technique, if the

modular system is subjected to compensate high frequency components in the load currents such as in the case analyzed with a diode rectifier feeding a resistive load.

5.5 Experimental Results on Parallel Operation

Designed 20kVA shunt APF prototype can produces harmonic currents that it has value of 30A amplitude. There are several methods for parallel operation in order to meet the need for high power. One of them is power sharing method. Parallel connected filters reads same load current and extracted reference current that is divided by number of APF unit.

Two 20-kVA shunt APF are connected in parallel and these filter reads same load current. The first filter is namely as SN01 has 1.5mH filter inductance. The other filter is namely as SN2 and it has 4mH filter inductance. The filters uses IRPT method and the produced reference current equaly shared. There is a swicthing ripple filter connected to PCC.

Figure 5.7 Supply current at parallel operation of APF modules under noload a) Only SN2 operates b) Only SN1 operates c) Both of units operates.

Firstly, these shunt APF units have been tested under no-load condition. The results of filter currents are given in Figure 5.7. The active filters draw the currents from supply as they are given in Figure 5.7a and b. The total current supplied from source is given in Figure 5.7 c.
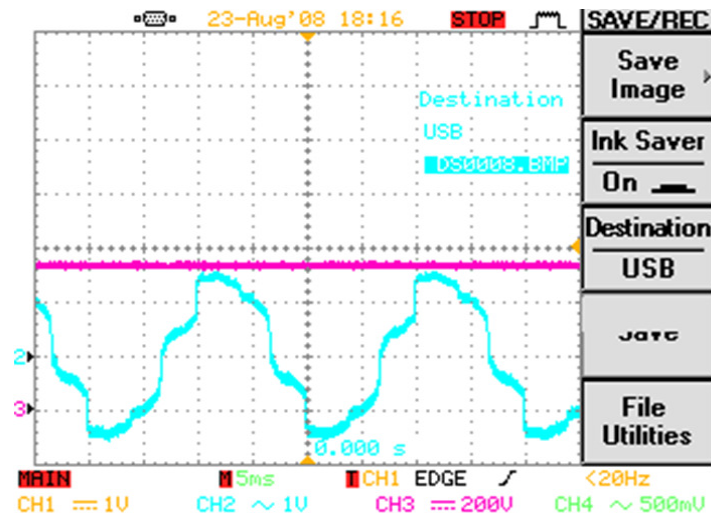
Figure 5.8 Supply current at the applied load current (Three phase rectifier and resistive balanced load)

The non-linear load draws the current from supply as it is seen in Figure 5.8. The load, here, contins three phase bridge rectifier in parallel to resistances. Each unit compansates the half of the harmonic content as it is given in Figure 5.9a and b. The whole load current harmonics are compansated properly and the waveform of supply is given Figure 5.9c.
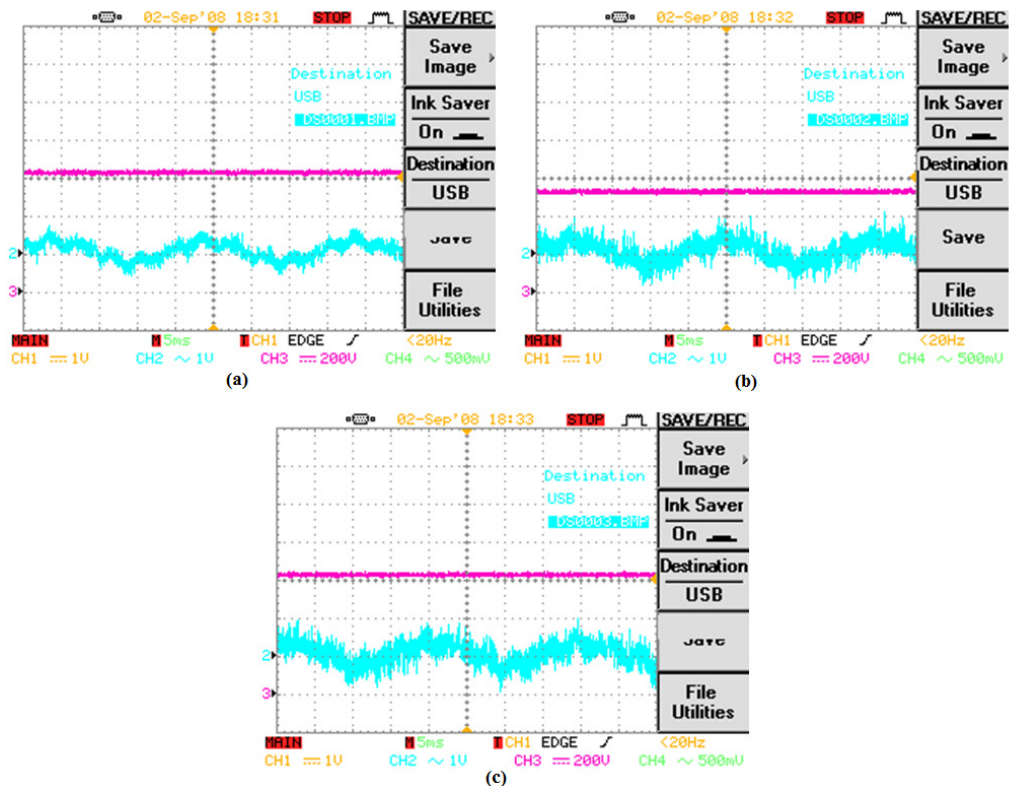
Figure 5.9 Supply current at parallel operation of APF modules under load a) Only SN2 operates b) Only SN1 operates c) Both of units operates.

SN01 and ve SN02 are properly sharing the harmonics as it is expected. Therefore, the parallel connection can be implemented for high power applications.

CHAPTER SIX

MODELLING OF SHUNT ACTIVE POWER FILTER
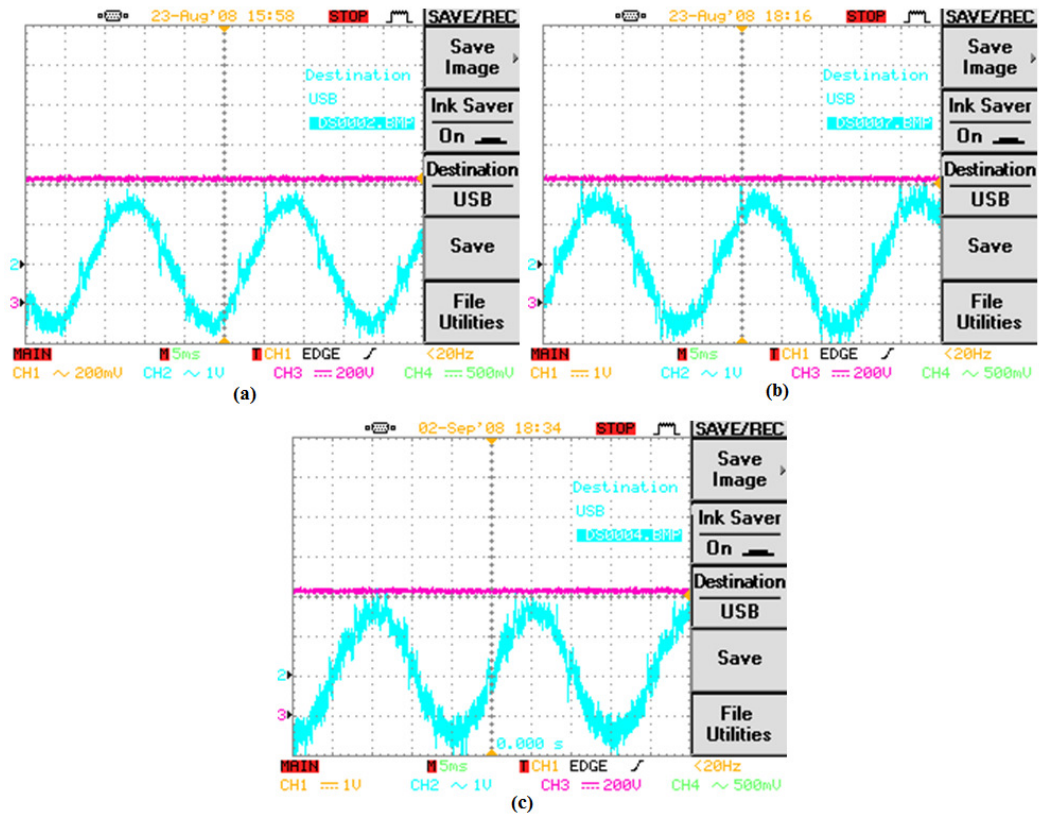
6.1 Introductory Remarks

The approaches for modeling of active power filters can be classified under the topics of switching function model, DC model and analytical model (Emadi, 2005). Switching function model is preferred for faster analysis during computer simulation. DC model provides a simple harmonic equivalent circuit, but does not include the mutual effects between the three-phases, however, offers the analysis of transient response on DC link.

An analytical model can be obtained for active power filters by using switching functions of the PWM waveform (Emadi, 2005). An average value model provides a simple harmonic equivalent circuit, but does not cover the mutual couplings between the three-phases. It offers the analysis for transient response of DC link voltage. Analytical model, which can be derived at different reference frames by using generalized machine theory. It utilizes the basic Kirchhoff's voltages laws and differential equations written on entire system. The design of current controller and DC link PI controller are carried out by using this model. The design and analysis of controllers are usually performed at synchronously rotating reference frame (SRF). Most of the studies in the literature consider the PWM current control techniques having switching functions that is proper in q-d model. The overall system is frequently decoupled on d and q axis. Two independent control loops which are voltage and current loops at outer and inner blocks respectively are obtained. The PI controller of dc voltage is tuned according to only DC link capacitor regardless of other system parameters (Tsang & Chan, 2006).

The current control technique selected is the most important part for satisfactory performance in practical applications. The hysteresis current controllers have been

frequently used for tracking the reference harmonic currents in APFs. While the hysteresis current controller generates the switching signals according to comparison of the scalar current error with a fixed hysteresis band, it could be also implemented with the vector of current error. The most important advantage of the scalar method is simplicity and robustness. The main disadvantage is that it causes the varying switching frequency and may lead a resonance problem on supply (Buso et al,1998), (Li & Tan, 2005).

In this chapter, a detailed model for shunt active power filter is presented in synchronously rotating reference frame. Then, the hysteresis loop is linearized around of operating point. The hysteresis current controller is modeled with active power filter (APF) for stability analysis and design of dc link PI controller. The results of linear model are compared with results of the detailed analytical model The stable operating ranges of system parameters like hysteresis band width, filter inductance, dc link capacitor and sampling frequency are verified by the detailed simulation program in Matlab/Simulink and experiments.

6.2 Analytical Model of Shunt Active Power Filter

The block scheme of a three-phase shunt active power filter (APF) compensating the current harmonics of a non-linear load is shown in Figure 6.1. The APF power circuit topology is a PWM type converter in parallel with the load. The load current waveforms are measured by means of current sensors and their harmonic contents are extracted by using several method (Emadi, 2005),(Vardar et al, 2009). The compensating currents for harmonics are injected to the electrical network by the APF. This is achieved by an inner current control loop to force the APF currents track the reference current waveforms. The PI controller regulates the DC bus voltage on the reference level.
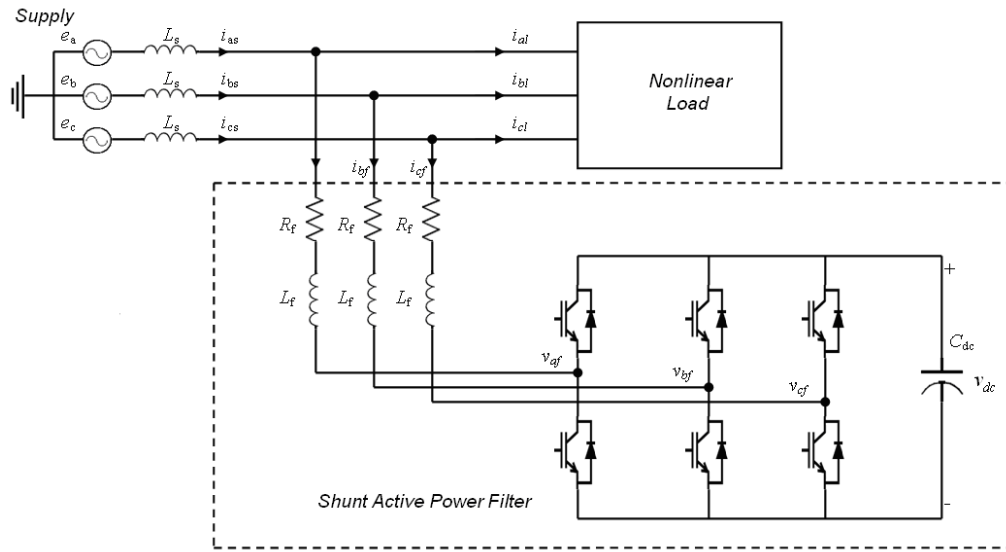
Figure 6.1 Circuit diagram of APF with a non-linear load.

The set of differential equations are written for three-phase active power filter below (Blasko & Kaura, 1997), (Kuo, 2001).

$$L_f \frac{d}{dt} i_{af} = e_a - R_f i_{af} - v_{af} \tag{6.1}$$

$$L_f \frac{d}{dt} i_{bf} = e_b - R_f i_{bf} - v_{bf} \tag{6.2}$$

$$L_f \frac{d}{dt} i_{cf} = e_c - R_f i_{cf} - v_{cf} \tag{6.3}$$

$$C_{dc} \frac{d}{dt} v_{dc} = f_a i_{af} + f_b i_{bf} + f_c i_{cf} \tag{6.4}$$

Where f_a, f_b and f_c are switching functions. L_f and R_f are filter inductances and resistances, respectively. C_{dc} is the value of DC link capacitor.

Three phase voltages, currents and switching functions can be transformed to synchronously rotating reference frame by using the following equation (6.5).

$$\begin{bmatrix} x_d \\ x_q \\ x_0 \end{bmatrix} = \frac{2}{3} \begin{bmatrix} \sin\theta_e & \sin(\theta_e - \frac{2\pi}{3}) & \sin(\theta_e + \frac{2\pi}{3}) \\ \cos\theta_e & \cos(\theta_e - \frac{2\pi}{3}) & \cos(\theta_e + \frac{2\pi}{3}) \\ \frac{1}{2} & \frac{1}{2} & \frac{1}{2} \end{bmatrix} \begin{bmatrix} x_a \\ x_b \\ x_c \end{bmatrix}$$

(6.5)

If $\lambda_{abc} = L \cdot i_{abc}$;

$$p \cdot \lambda_{abcf} = e_{abc} - r_f i_{abcf} - v_{abcf}$$

Where: $r_f = \begin{vmatrix} R_f & 0 & 0 \\ 0 & R_f & 0 \\ 0 & 0 & R_f \end{vmatrix}$, $L = \begin{vmatrix} L_f & 0 & 0 \\ 0 & L_f & 0 \\ 0 & 0 & L_f \end{vmatrix}$.

In equation (6.6), transformed synchronously rotating reference frame variables are used.

$$pK_S^{-1}\lambda_{dqf} = K_S^{-1}e_{dq} - K_S^{-1}r_f i_{dqf} - K_S^{-1}v_{dqf}$$

(6.6)

If both two sides are multiplied by K_S :

$$K_S pK_S^{-1}\lambda_{dqf} = K_S K_S^{-1}e_{dq} - K_S r_f K_S^{-1}i_{dqf} - K_S K_S^{-1}v_{dqf}$$

(6.7)

$$K_S pK_S^{-1}\lambda_{dqf} = e_{dq} - K_S r_f K_S^{-1}i_{dqf} - v_{dqf}$$

(6.8)

$$K_S(p[K_S^{-1}])\lambda_{qdf} + K_S K_S^{-1}(p\lambda_{dqf}) = e_{dq} - K_S r_f K_S^{-1}i_{dqf} - v_{dqf}$$

(6.9)

$$p[K_S^{-1}] = \omega \cdot \begin{bmatrix} \cos\theta_e & -\sin\theta_e & 0 \\ \cos(\theta_e - \frac{2\pi}{3}) & -\sin(\theta_e - \frac{2\pi}{3}) & 0 \\ \cos(\theta_e + \frac{2\pi}{3}) & -\sin(\theta_e + \frac{2\pi}{3}) & 0 \end{bmatrix}$$

(6.10)

$$K_S p[K_S^{-1}] = \omega \cdot \begin{bmatrix} 0 & -1 & 0 \\ 1 & 0 & 0 \\ 0 & 0 & 0 \end{bmatrix}$$

(6.11)

$$\omega\lambda_{qdf} + p\lambda_{dqf} = e_{dq} - K_S r_f K_S^{-1}i_{dqf} - v_{dqf}$$

(6.12)

$$K_S r_f K_S^{-1} = r_f$$

(6.13)

The sum of phase currents is zero at three-phase three-wire systems. The equations in (6.1-6.4) transformed to the synchronously rotating reference frame are given in (6.14-6.16).

$$L_f \frac{d}{dt} i_{df}^e = e_d - R_f i_{df}^e + \omega_e L_f i_{qf}^e - v_{df}^e \tag{6.14}$$

$$L_f \frac{d}{dt} i_{qf}^e = e_q - R_f i_{qf}^e - \omega_e L_f i_{df}^e - v_{qf}^e \tag{6.15}$$

$$C_{dc} \frac{d}{dt} v_{dc} = \frac{3}{2}(f_d i_{df}^e + f_q i_{qf}^e) \tag{6.16}$$

$$v_{df}^e = f_d \cdot v_{dc} \tag{6.17}$$

$$v_{qf}^e = f_q \cdot v_{dc} \tag{6.18}$$

D-axis of supply voltage is positioned such that it coincides with the positive peak value of phase-a voltage of supply. In this case, q axis component of supply voltages will be zero. This transformation yields the active and reactive power equations for the load as follows.

$$e_d = V_m \tag{6.19}$$

$$e_q = 0 \tag{6.20}$$

$$p_L = \frac{3}{2} V_m i_{dL}^e \tag{6.21}$$

$$q_L = -\frac{3}{2} V_m i_{qL}^e \tag{6.22}$$

$$i_{df}^{e^*} = i_1 - i_{dL}^e \tag{6.23}$$

$$i_{qf}^{e^*} = -i_{qL}^e \tag{6.24}$$

$$i_{df}^{e^*} = i_1 - i_{dL}^e + i_{dc} \tag{6.25}$$

$$I_{dc} = G_{dc}(s)(v_{dc}^* - v_{dc}) \tag{6.26}$$

Where, I_{dc}, is the output of DC link PI controller. v_{dc}^* and v_{dc} are reference and actual DC Link voltages, respectively. The reactive power demand of the load is supplied by the source, hence the reference current of the APF does not have quadrature component of current, $i_{qf}^{e\,*}$ =0. In the model, the harmonic extraction method is carried out by a lowpass filter as being shown in Figure 6.2. The cutoff frequency, ωa affects the stability of control loop, settling time of DC link voltage, and compensation characteristic of active power filter (Akagi, 1994, 1996).

Figure 6.2 shows the block diagram of shunt APF in synchronously rotating reference frame. But, hysteresis current controller is operated in abc coordinates. Hysteresis current controller can be represented in dq coordinates such as given in Figure 6.3.
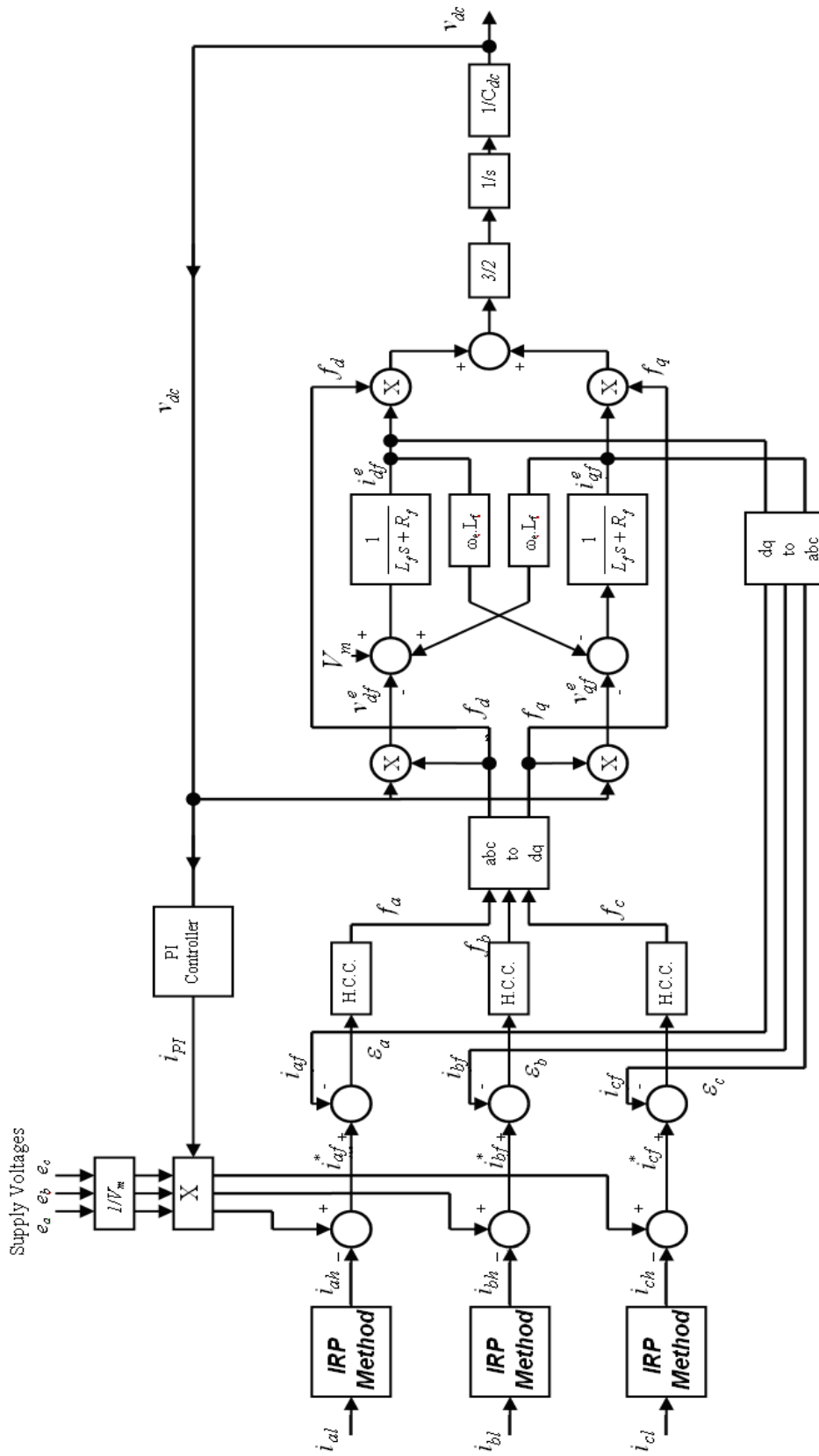
Figure 6.2 The block diagram of shunt active power filters and HCC is allocated in abc coordinates.
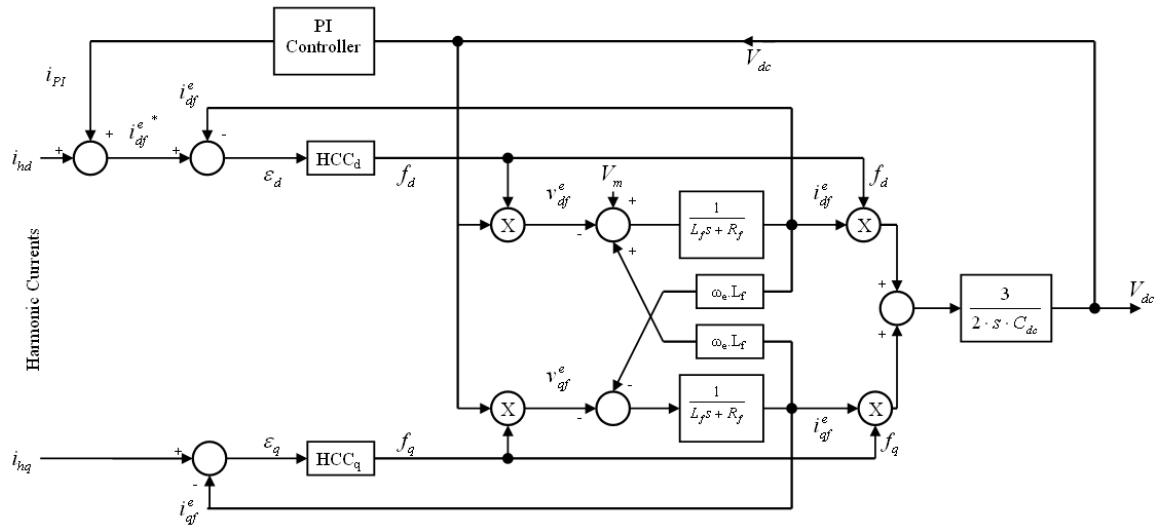
Figure 6.3 The block diagram of shunt active power filters at synchronously rotating reference frame.

6.3 Modeling of Hysteresis Current Controller

In literature, various models have been proposed to describe hysteresis operator (Blasko & Kaura, 1997). Some of them are Preisach model, Krasnosel'skii-Pokrovkii hysteron, Islinskii hysteresis operator and neural networks models. The performance of trained neural network depends on frequency of input error signal used during training. Therefore, tracking error of this model depends on frequency of input error signal and it does not show the same performance under all operation conditions.

Hysteresis current controller (H.C.C) shows a nonlinear characteristic. Here, the hysteresis is modeled with a sigmoid function as it is given below (Xiu & Liu, 2009).

$$f(s,\alpha) = \frac{1}{1 + e^{-c.(s+\alpha.\Delta s)}} \tag{6.27}$$

Where α is a scaling parameter which affects the area in the hysteresis. For instance, when α is equal to zero the hysteresis characteristic disappears. When α is increased, the hysteresis band expands. And c is the shape parameter which presents

the slope of function. The parameters of equation (6.27) are replaced by the variables of the APF and the equation obtained in equation (6.28) apparently shows that the switching function dependents on the error between reference and actual currents. The system given in Figure 6.2 is analyzed in Matlab with the switching function given in equation (6.28) and it is observed that the simulation results of APF using the "relay model" in Simulink (Vardar & Akpinar, 2011) are identical.

$$f_a(\varepsilon_a, HB) = \frac{1}{1 + e^{-c.(\varepsilon_a + HB.\Delta\varepsilon_a)}} \tag{6.28}$$

Due to existence of $\Delta\varepsilon_a$, the response of switching function also depends on change of error. Hysteresis function modeled in equation (6.28) is shown in Figure 6.4 for sinusoidal input signal with HB=1 and c=10 parameters. It should be pointed out that the error ε_a is not sinusoidal in the APF, therefore, the shape of hysteresis loop changes in every switching period.
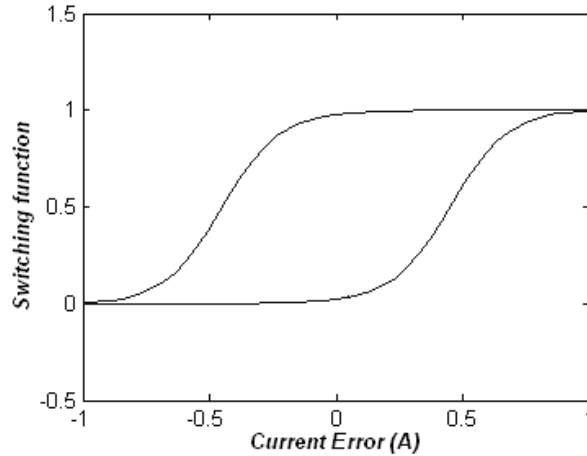

Figure 6.4 Sinusoidal response of proposed hysteresis function

6.3.1 Linear Model of Hysteresis Current Controller

The simulation results of APF using the "relay model" in Simulink are given in Figure 6.5a for error and switching functions at synchronously rotating reference

frame. These results are expanded in Figure 6.5b for observation of switching ripples how they are synchronized with hysteresis band. Figure 6.5a shows that the d-axis component of error varies between $\pm$ HB, while f_d is almost constant and its magnitude is equal to V_m/V_{dc}. The ripples on f_d can be resolved into two components. One of them is created by ε_d forcing f_d to be zero during the time when ε_d violates the upper limit of hysteresis band. When ε_d violates the lower limit of the hysteresis band, then f_d becomes V_m/V_{dc}. This ripple component on f_d features the hysteresis loop.
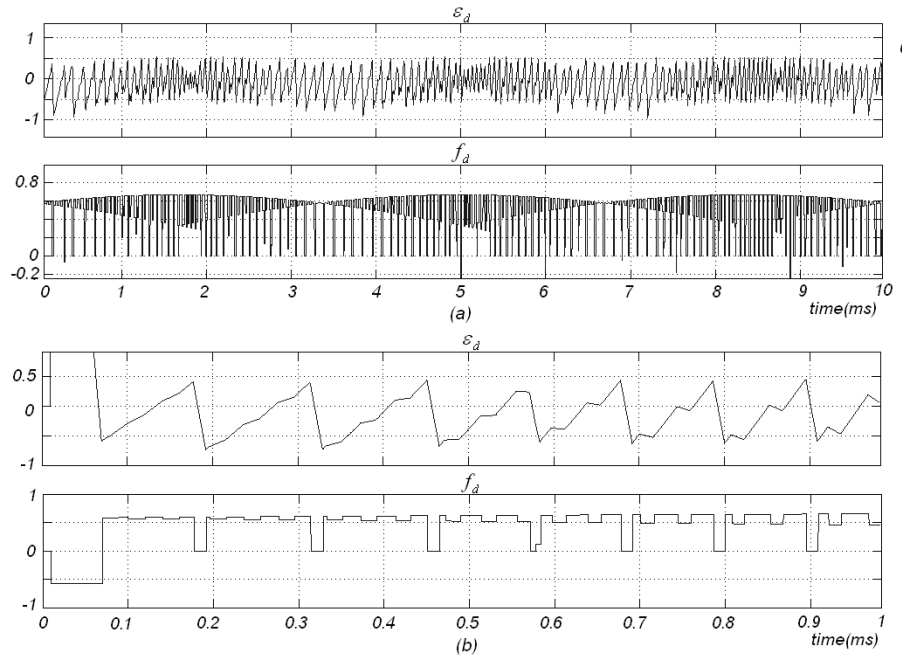

Figure 6.5 The d axis switching functions and the reference current errors a) During the half of the fundamental supply frequency b) Results are expanded for high resolution.

The latter ripple component is created by ε_q in a shape of sawtooth. The switching function on d-axis, f_d can be expressed as follows by neglecting the effect of ε_q.

$$f_d = \frac{V_m}{V_{dc}} \cdot f_a(\varepsilon_d, HB) \qquad (6.29)$$

The model of converter is established on the basis that the q-axis component of supply voltage and filter current are zero ($e_q = 0$ and $i_{qf}^e{}^* = 0$). By neglecting the voltage drop on the inductance between the supply voltage and converter at fundamental frequency, the average value of v_{qf}^e can be assumed to be zero, hence f_q is zero from equation (6.18). The hysteresis effect links the error to the f_d component and the block diagram of APF can be reconstructed by taking this analysis into consideration as shown in Figure 6.6.
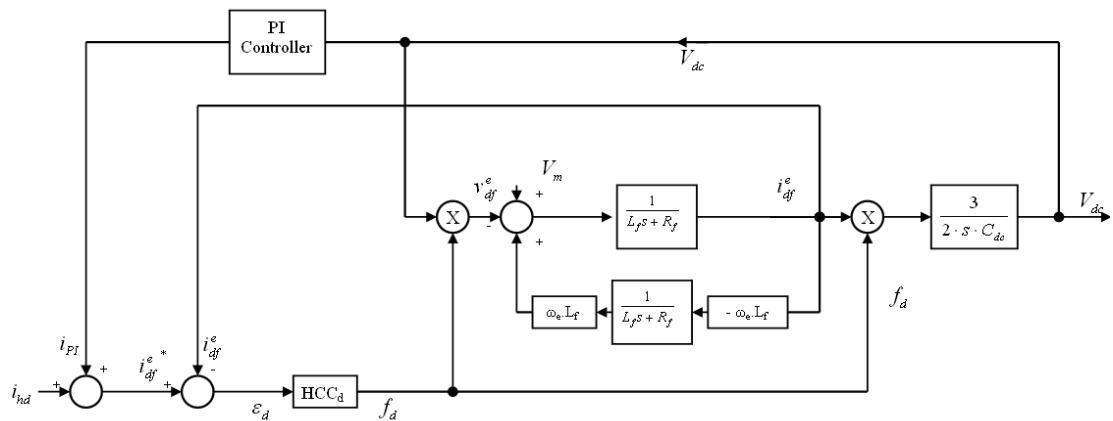

Figure 6.6 Block diagram of active power filter on d axes

The non-linear effect of hysteresis function on d axis is linearized between two switching intervals as it is depicted in Figure 6.7.
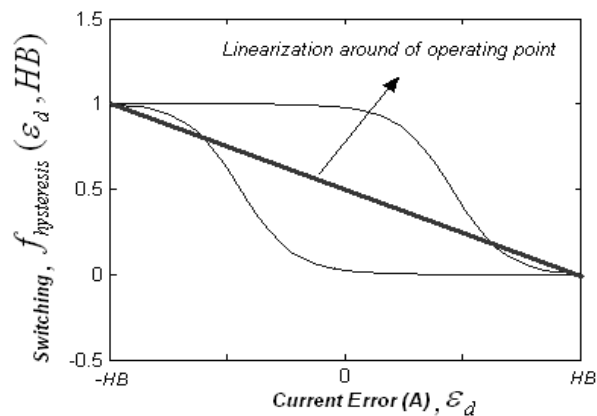

Figure 6.7 Linearization of hysteresis band

The linear model of hysteresis function between two consecutive switching is given in equation (6.30).

$$f_a(\varepsilon_d, HB) = \frac{HB - \varepsilon_d}{2 \cdot HB}$$

(6.30)

The blocks of active power filter can be established by using this linearized hysteresis current controller as given in Figure 6.9. It should be noted that two multiplication units in Figure 6.6 are replaced by a linear gain in Figure 6.9 by taking the reference DC link voltage instead of its actual value and V_m / V_{dc} for f_d. These modifications are given in linear model at Figure 6.8
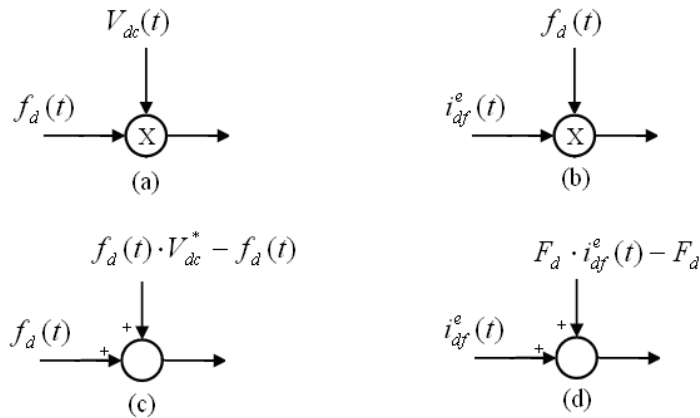

Figure 6.8 Multiplication blocks converted to summaries

The analysis of this model is carried out in Matlab and results are compared to ones obtained from the synchronously rotating reference frame (SRF) model within Figure 6.2. The waveforms of DC link voltage and reference filter current from both models are given in Figure 6.10 for the system parameters in below. Neglecting the effect of f_q in the linear model may yield an increase on the settling time of capacitor voltage during start-up under no-load.
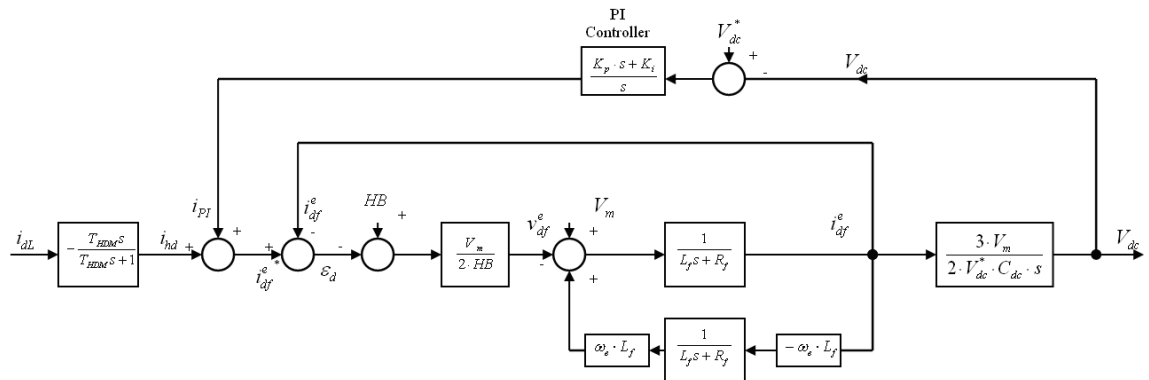
Figure 6.9 Block diagram of active power filter on qd axes with linearized hysteresis current controller.

System parameters:

L_f =1.8mH, C_{dc} =2300μF, ω_e =314 rad/s, v_m =310 V, v_{dc}^* =650 V, K_E = 0.0001, K_{CE} = 0.05

6.4 Design of DC Link PI Controller

In a closed-loop feedback system, the error is the difference between the reference and actual values. The controller output for analog proportional-integral (PI) is expressed as:

$$u(t) = K_P \cdot \varepsilon(t) + K_i \cdot \int \varepsilon(t) \cdot dt \qquad (6.31)$$

Where, K_P and K_I are the proportional and integral error gain gains. Digital PI controller, which is used in the DSP, is the discrete form of the analog PI controller. The output of digital PI controller is expressed as a difference equation for a given sampling time (T_S) as follows (Dote & Kinoshita, 1990):

$$\Delta u(n \cdot T_S) = K_{CE} \cdot \Delta\varepsilon(n \cdot T_S) + K_E \cdot \varepsilon(n \cdot T_S) \qquad (6.32)$$

Where,

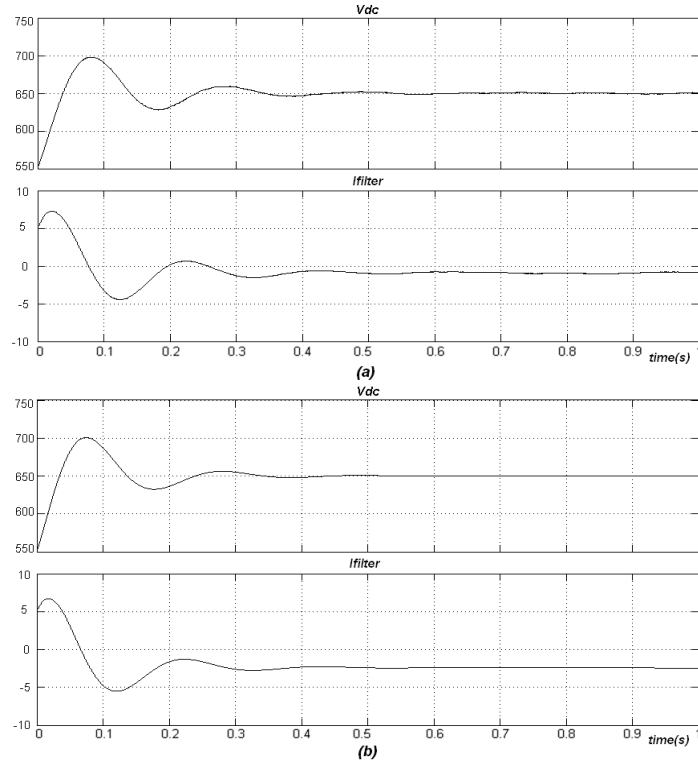$$K_{CE} = K_P \text{ and } K_E = K_i \cdot T_S \qquad (6.33)$$

Figure 6.10 Simulation results with HB= 4A, a) SRF model b) linearized model.

In order to design a PI controller used for dc voltage regulation, it is necessary to obtain transfer function between input and output variables and disturbance signal. The dc link voltage and load current are considered here as the output and input variables, respectively. The variation and stability condition of dc link voltage governed by PI controller is investigated as a function load current. The linear relation between direct axis converter input voltage and error signal ε_d can be obtained by using equation (6.29) and equation (6.30) as follows.

$$v_{df} \cong f_d \cdot V_{dc}^* = \frac{V_m \cdot (HB - \varepsilon_d)}{2 \cdot HB} \tag{6.34}$$

The reference dc link voltage V_{dc}^* and peak supply voltage V_m can be kept constant. The resistance of inductance at the input of converter is neglected for simplification of transfer functions.

The software used for the APF is a time consuming program due to use of digital filters and transformations. The execution time of digital signal processing unit may cause significant limitation on sampling time and performance of the system. Therefore, a complete cycle between the sampling and switching of the dc link capacitor voltage can be represented by a delay of T_s which is the sampling time. A low-pass filter with the time constant T_s is located between reference and measured dc link voltage as being shown in Figure 6.11.
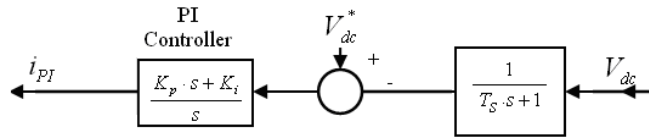

Figure 6.11 Time delay for execution time

By including the processing time, the transfer function between the capacitor voltage and load current can be obtained as given in equation (6.35).

$$\frac{\Delta V_{dc}(s)}{\Delta I_{dL}(s)} = \frac{-3 \cdot V_m^2 \cdot T_{HDM} \cdot (1 + T_s \cdot s) \cdot s^2}{(T_{HDM} \cdot s + 1) \cdot \Delta(s)} \tag{6.35}$$

The characteristic equation and its coefficients are as follows:

$$\Delta(s) = b_4 \cdot s^4 + b_3 \cdot s^3 + b_2 \cdot s^2 + b_1 \cdot s + b_0 \tag{6.36}$$

$$b_4 = 4 \cdot HB \cdot L_f \cdot V_{dc}^* \cdot C_{dc} \cdot T_s$$

$$b_3 = 4 \cdot HB \cdot L_f \cdot V_{dc}^* \cdot C_{dc} + 2 \cdot V_m \cdot V_{dc}^* \cdot C_{dc} \cdot T_s$$

$$b_2 = 2 \cdot V_m \cdot V_{dc}^* \cdot C_{dc} + 4 \cdot \omega_e^2 \cdot HB \cdot L_f \cdot V_{dc}^* \cdot C_{dc} \cdot T_s$$

$$b_1 = 4 \cdot \omega_e^2 \cdot HB \cdot L_f \cdot V_{dc}^* \cdot C_{dc} + 3 \cdot V_m^2 \cdot K_p$$

$$b_0 = 3 \cdot V_m^2 \cdot K_i$$

The stability is guaranteed if the transfer function does not have any pole in the right half plane. The stability range of dc link voltage PI controller parameters are determined by applying Routh-Hurwitz method (Kuo,1987). Therefore the following three constraints are calculated.

i) $3 \cdot V_m^2 \cdot K_i > 0 \Rightarrow K_i > 0$ (6.37)

ii) $4 \cdot \omega_e^2 \cdot HB \cdot L_f \cdot V_{dc}^* \cdot C_{dc} + 3 \cdot V_m^2 \cdot K_p > 0$

$$\Rightarrow K_p > -\frac{4 \cdot \omega_e^2 \cdot HB \cdot L_f \cdot V_{dc}^* \cdot C_{dc}}{3 \cdot V_m^2}$$ (6.38)

The entries of the Routh array are formed from the coefficients of characteristic equation in s-domain equation (6.36).

$$
\begin{array}{ll}
s^3 & b_4 \\
s^3 & b_3 \\
s^2 & b_2 - b_4 b_1 / b_3 \\
s^1 & b_1 - \left(\dfrac{b_3 b_0}{b_2 - (b_4 b_1 / b_3)} \right) \\
s^0 & b_0
\end{array}
$$ (6.39)

For a given a set variables, their effect on stability can be checked by evaluating the entries of Routh array to determine the signs. Each column of Routh array must be positive and not changed sign for stability.

iii) $b_1 - \left(\dfrac{b_3 b_0}{b_2 - (b_4 b_1 / b_3)} \right) > 0$ (6.40)

The stability range of K_{CE} and K_E parameters of DC link controller are determined by applying Routh-Hurwitz criteria and given in Figure 6.12. The prepared Matlab m-files for this analysis are given in appendix.
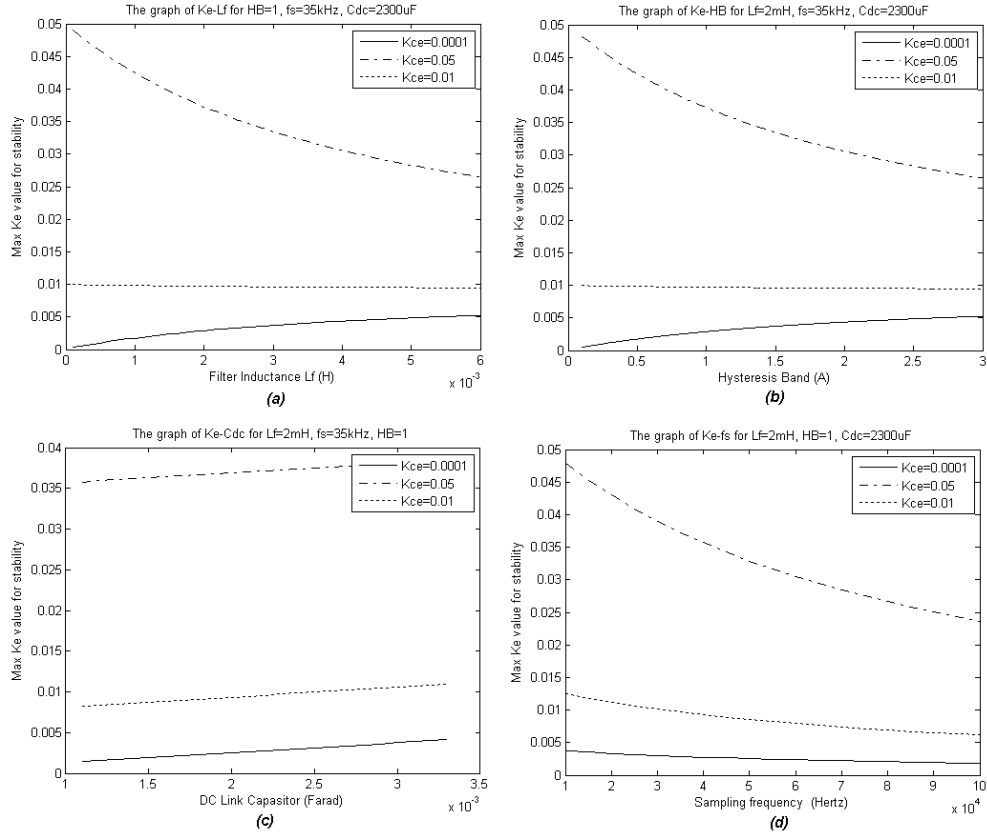
Figure 6.12 Stability range of DC link digital PI controller parameter according to system parameters.

The transfer functions between direct axis components of load current, filter current and load harmonic current are obtained by using Figure 6.9 as follows.

$$\frac{\Delta i_d(s)}{\Delta I_{dL}(s)} = \frac{-2 \cdot V_m \cdot V_{dc}^* \cdot C_{dc} \cdot T_{HDM} \cdot (1 + T_s \cdot s) \cdot s^3}{(T_{HDM} \cdot s + 1) \cdot \Delta(s)} \tag{6.41}$$

$$\frac{\Delta i_d(s)}{\Delta i_{hd}(s)} = \frac{2 \cdot V_m \cdot V_{dc}^* \cdot C_{dc} (1 + T_s \cdot s) \cdot s^2}{\Delta(s)} \tag{6.42}$$

Figures 6.13a and 6.13b show the bode diagrams of equations (6.41) and (6.42) respectively. The magnitude of the gain is almost constant while the frequency changes between around 100 rad/s and 10000 rad/s. The phase difference is zero between the reference current and filter current, while it is 180 degrees between the load current and filter current for harmonic harmonics compensation. This

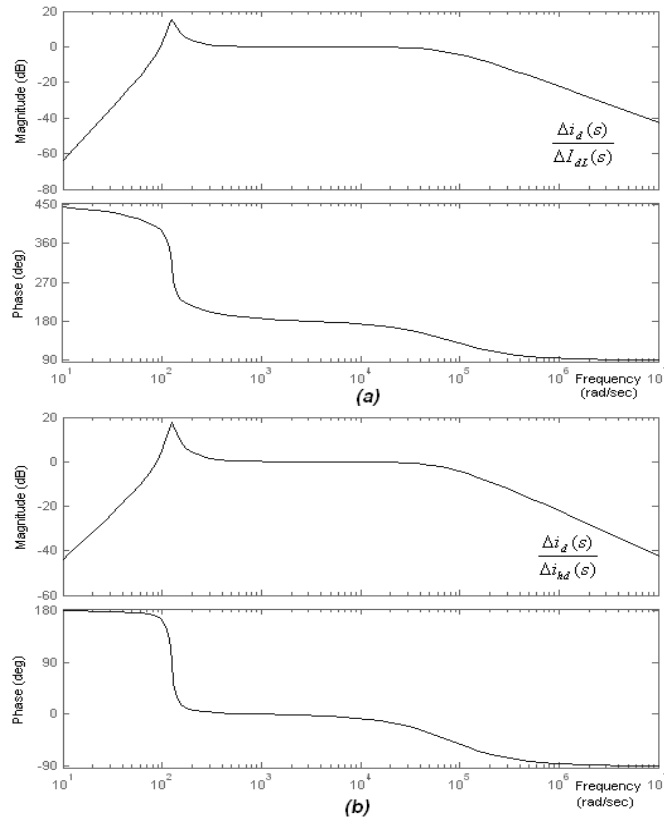observation on the bode plots is validated with the help of detailed simulation results in Matlab-Simulink.

Figure 6.13 Gain and phase variations according to frequency

The validity of SRF and linear models was tested by selecting the Ke and Kce parameters above stability limit curves on the stability region, the border of stability region, and the unstability region. At the linearized model, the results are given in Figure 6.14. At the Figure 6.14a, the direct axes current of filter and DC link voltage are damped by oscillating for a point a little low from stability limit. In Figure 6.14b, at a point in the region over the stability limit, the oscillations on the DC link voltage and filter current gradually increases and the instability occurs. On the point of stability limit, outputs of system are oscillating shown in Figure 6.14c. These parameters are applied to SRF model and results are given in Figure 6.15. The results of SRF and linearized model are similar to each other.

Figure 6.14 Simulation result of linearized model a) for Ke= 0.02 , Kce=0.05, a little low from of stability limit b) Ke= 0.05 , Kce=0.05, a little high from stability limit c) Ke= 0.042 , Kce=0.05, on the stability limit.
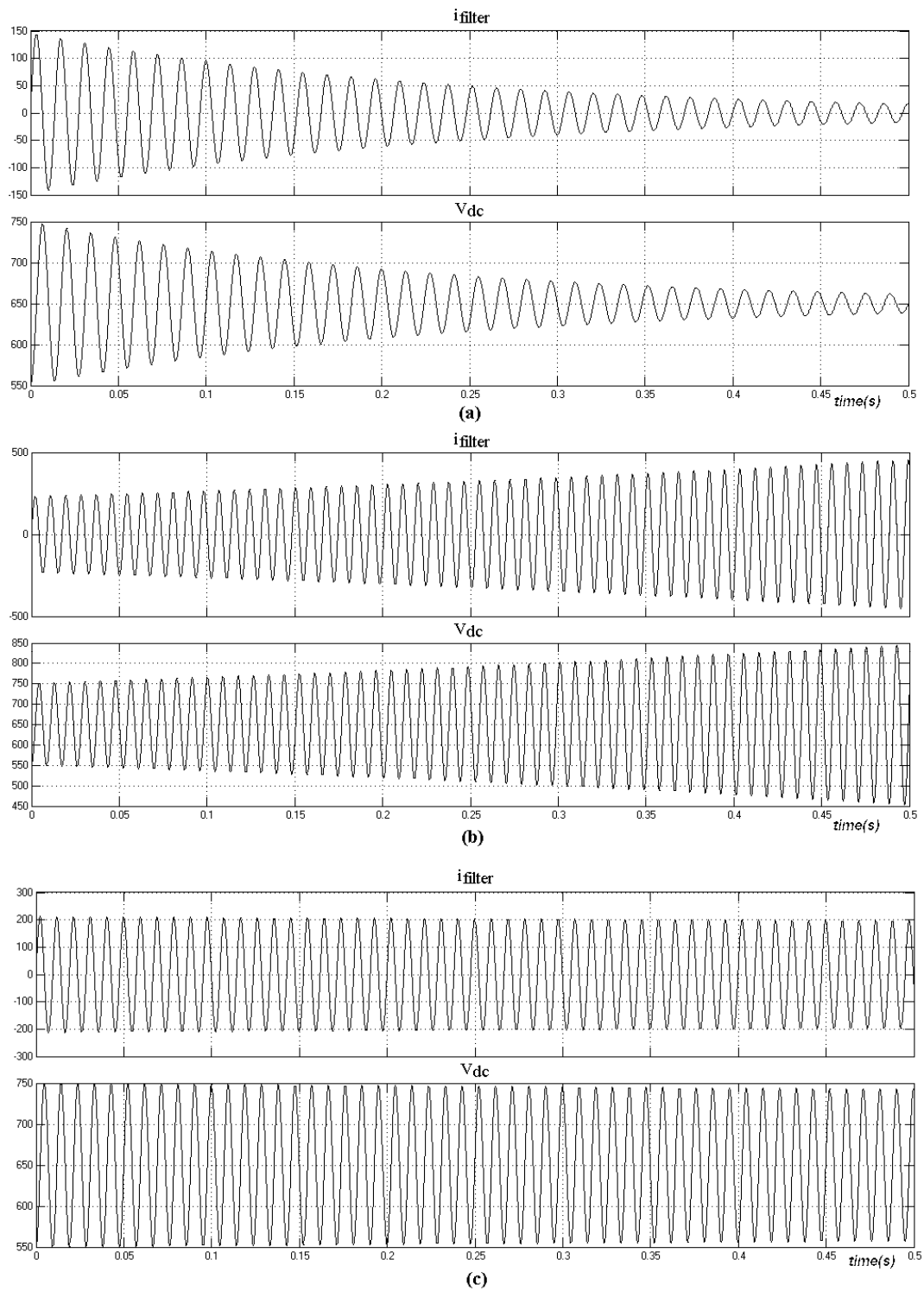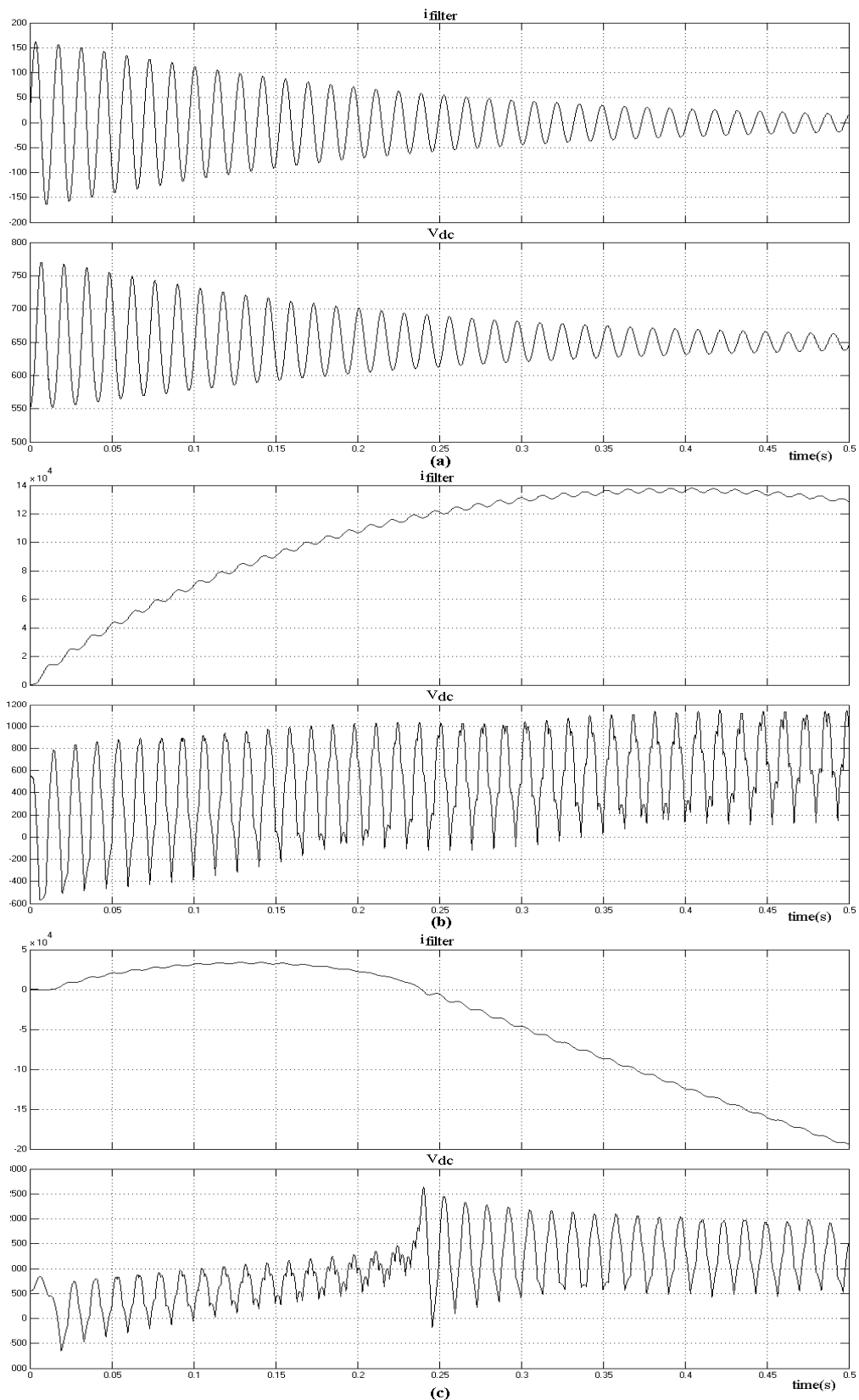
Figure 6.15 Simulation result of SRF model a) for Ke= 0.02, Kce=0.05, a little low from of stability limit b) Ke= 0.05 , Kce=0.05, a little high from stability limit c) Ke= 0.042, Kce=0.05, on the stability limit.
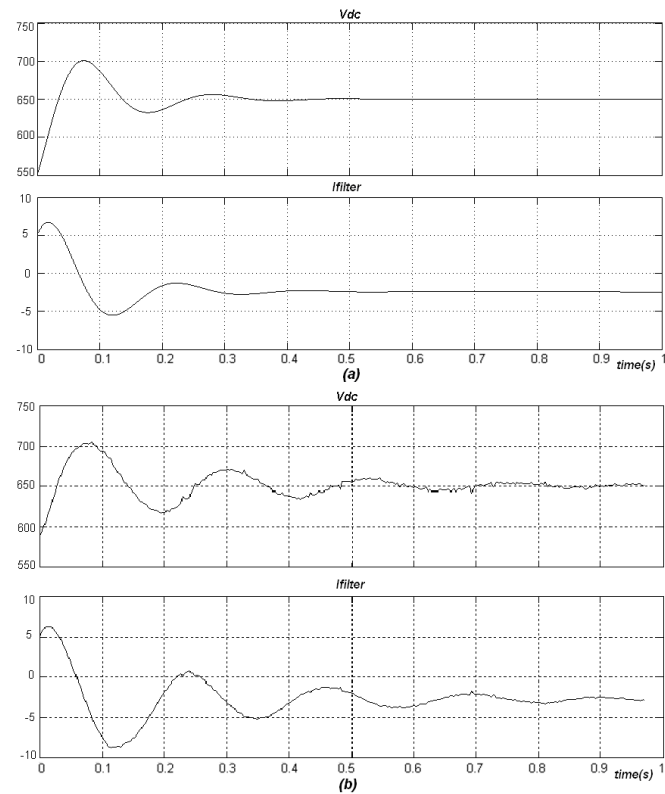
Figure 6.16 DC Link Voltage and reference filter current during
charging up capacitor a) linearized model, b)experiment.

The DC link voltage is directly measured over the capacitor while the filter reference current is obtained inside the program loaded in the DSP, they are both given in Figure 6.16. The ripples on the filter current do not exist during the charging up (starting) period under no-load (non-linear load is not connected). The experimental result of filter current, which is the output of DC link PI controller, contains a dc bias because of direction of active power, but linear model does not include DC link capacitor loss, switching losses and switching filter loss. It is clear that ac component of measured waveform and results of linear model are compatible.

This seems to be a reasonable assumption during this linearization because switching frequency is very high with respect to the power frequency therefore the relative speed is still nearby switching frequency. This model is used to find out stability limits according to filter inter inductance, hysteresis band width and switching frequency. The stability range of DC link PI controller is found by applying Routh-Hurwitz criteria. The transfer functions between the load current and

filter current are obtained and the bode plots are given. The appearance of gain and phase are verified in detailed simulation results. The experimental records have shown that linear model can be successfully used to design the dc link PI controller.

6.5 Effect of System Parameters on Performance of the Shunt APF

In power system, capacitors are widely used in order to compensate reactive power or passive filtering, which generally cause resonance problems in harmonic distorted network. Looking from the load side, the source impedance and the reactive power compensation capacitor constitute a parallel resonance circuit. So, harmonic currents can be amplified to critical values at the resonant frequency drawn by the load or by the active filter. Looking from the source side, the source impedance and the reactive power compensation capacitors create a series resonance circuit. The harmonic voltages injected by the supply side transformer can cause inadmissible high harmonic source currents. The parallel and series resonance are very dangerous for power system. The inductors are connected in series with the reactive power compensation capacitors in order to solve the resonance problem, shifting the resonant frequency to an uncritical area. Also, instead of compensation capacitor, the using of a passive filter may cause in the same way resonant problem.

In this chapter, the effect of system parameters is investigated for the performance of APF. The general block scheme is given in Figure 6.17. This model can be used for a hybrid parallel active filter with passive filter, a compensation capacitor, or any complex loads. Where, Z_S is source impedance, Z_L is impedance of the desired passive filter or compensation capacitor. The load has been represented as a current source (Fang et al, 2009), (Peng, 1998).
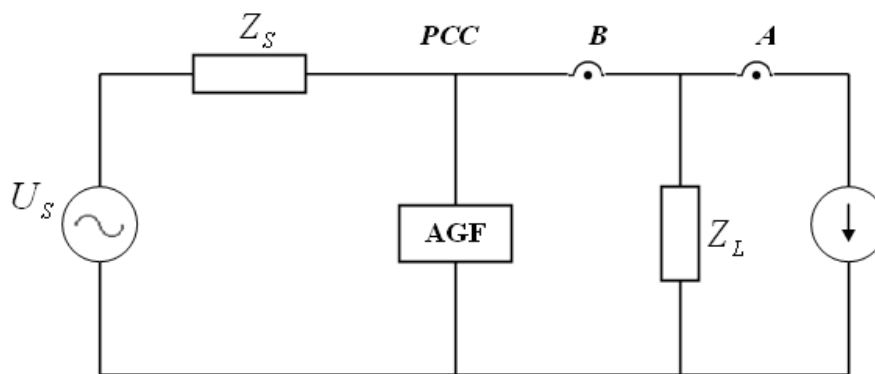
Figure 6.17 Equivalent circuit of a hybrid system.

The single line control block diagram of APF with hysteresis current controller is given in Figure 6.18. Here, the equation (6.41) is used as the transfer function of shunt active power filter.
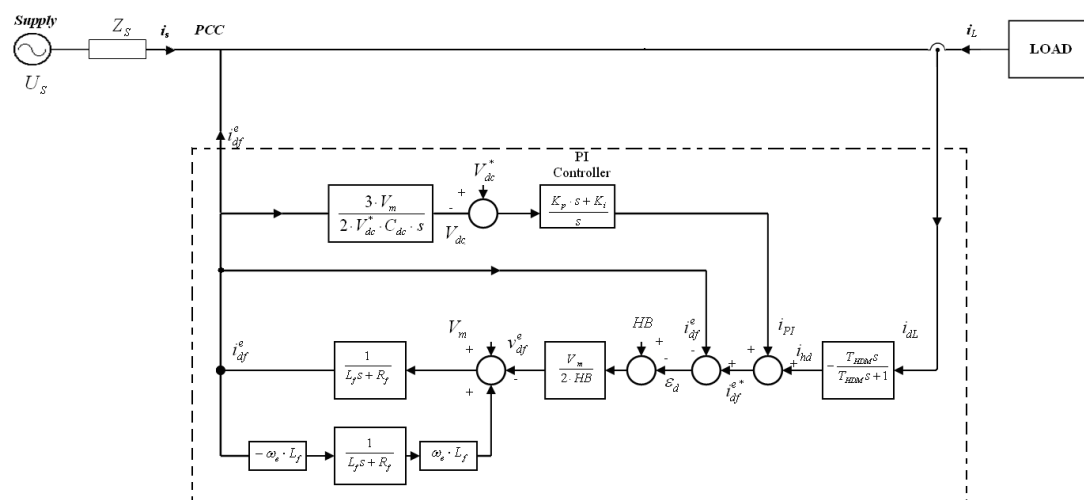
Figure 6.18 Control block diagram of APF

The transfer function of active filter can be defined as follow:

$$G_{APF}(s) = \frac{\Delta i_d(s)}{\Delta I_{dL}(s)} = \frac{-2 \cdot V_m \cdot V_{dc}^* \cdot C_{dc} \cdot T_{HDM} \cdot (1 + T_s \cdot s) \cdot s^3}{(T_{HDM} \cdot s + 1) \cdot \Delta(s)} \qquad (6.43)$$

The load current detecting method may obtain signal from the point A or B as pointed on Figure 6.17. By getting signal from point A, the compensation capacitor

is left on the source side. Therefore, the compensation capacitor current is not detected by the current controller. These two current control detections techniques yield different results. These two situations are analyzed in the following subsections.

6.5.1 The Measurement is taken from Point A

When the APF gets sampling from point A for harmonic detection, currents of compensation capacitor or passive filter are not included in the detected load current. In this situation, the equivalent circuit of system is shown in Figure 6.19. The transfer function of APF is defined as $G_{APF}(s)$, the produced current by filter can be written as:

$$i_f = G_{APF}(s) \cdot i_L \tag{6.44}$$

Figure 6.19 Equivalent circuit when the detecting point is A.

When the Kirchhoff's current law is applied on PCC in circuit, the equation (6.45) can be written. If the voltage on the PCC (V_{PCC}) is solved from this equation, equation (6.46) can be obtained. Here, the current of supply can be expressed by equation (6.47).

$$\frac{V_S - V_{PCC}}{Z_S} - i_L + G_{APF}(s) \cdot i_L - \frac{V_{PCC}}{Z_L} = 0 \tag{6.45}$$

$$-\frac{V_{PCC}}{Z_S} - \frac{V_{PCC}}{Z_L} + \frac{V_S}{Z_S} - \left(1 - G_{APF}(s)\right) \cdot i_L = 0$$

$$-\frac{V_{PCC} \cdot \left(Z_S + Z_L\right)}{Z_S \cdot Z_L} = -\frac{V_S}{Z_S} + \left(1 - G_{APF}(s)\right) \cdot i_L$$

$$V_{PCC} = \frac{V_S \cdot Z_L}{Z_S + Z_L} - \frac{\left(1 - G_{APF}(s)\right) \cdot \left(Z_S \cdot Z_L\right) \cdot i_L}{Z_S + Z_L} \tag{6.46}$$

$$i_s = \frac{V_S - V_{PCC}}{Z_s} \tag{6.47}$$

When, the equation (6.46) is substitute into equation (6.47), equation (6.48) can be obtained after simplification.

$$i_s = \frac{V_S}{Z_s} - \frac{V_S \cdot Z_L}{\left(Z_S + Z_L\right) \cdot Z_S} + \frac{\left(1 - G_{APF}(s)\right) \cdot \left(Z_S \cdot Z_L\right) \cdot i_L}{\left(Z_S + Z_L\right) \cdot Z_S}$$

$$i_s = \frac{V_S \cdot \left(Z_S + Z_L\right) - V_S \cdot Z_L}{\left(Z_S + Z_L\right) \cdot Z_S} + \left(1 - G_{APF}(s)\right) \cdot \frac{Z_L}{\left(Z_S + Z_L\right)} \cdot i_L$$

$$i_s = \frac{1}{\left(Z_S + Z_L\right)} \cdot V_S + \left(1 - G_{APF}(s)\right) \cdot \frac{Z_L}{\left(Z_S + Z_L\right)} \cdot i_L \tag{6.48}$$

This equation provides the transfer function between load and supply current.

6.5.2 The Measurement is taken from Point B

When the APF gets sampling from point B for harmonic detection, currents of compensation capacitor or passive filter are included in the detected load current. In this situation, the equivalent circuit of system is shown in Figure 6.20. The transfer function of APF is defined as $G_{APF}(s)$, the produced current by filter can be written as:
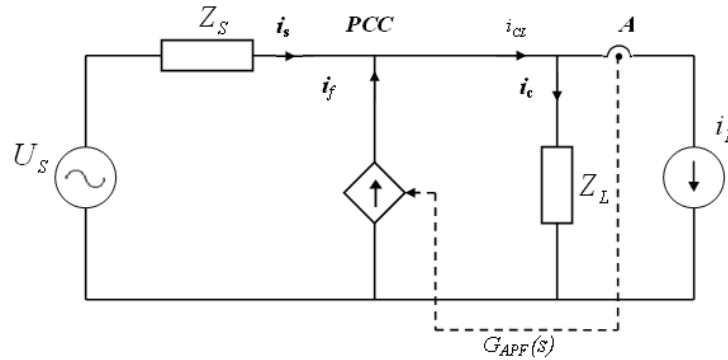
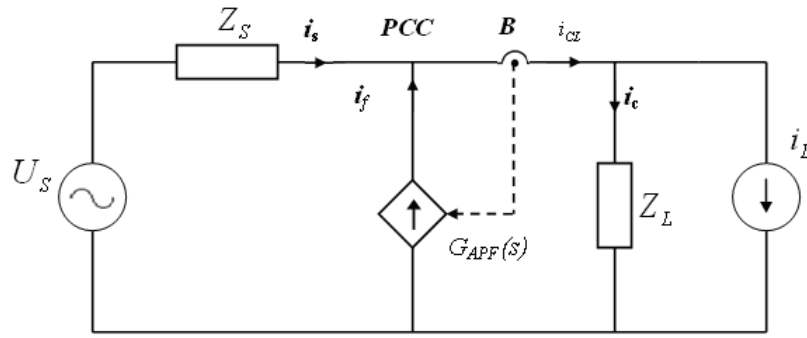$$i_f = G_{APF}(s) \cdot i_{CL} \tag{6.49}$$

Figure 6.20 Equivalent circuit when the detecting point is B.

If the Kirchhoff's current law is applied on PCC in circuit, the equation (6.50) can be written. When V_{PCC} is solved from this equation, equation (6.51) can be obtained. Where, the current of supply can be expressed by equation (6.52).

$$\frac{V_S - V_{PCC}}{Z_S} - i_L + G_{APF}(s) \cdot i_{CL} - \frac{V_{PCC}}{Z_L} = 0 \tag{6.50}$$

$$\frac{V_S - V_{PCC}}{Z_S} - i_L + G_{APF}(s) \cdot \left(i_L + \frac{V_{PCC}}{Z_L} \right) - \frac{V_{PCC}}{Z_L} = 0$$

$$\frac{V_S}{Z_S} - \frac{V_{PCC}}{Z_S} - \left(1 - G_{APF}(s) \right) \cdot i_L - \left(1 - G_{APF}(s) \right) \cdot \frac{V_{PCC}}{Z_L} = 0$$

$$\frac{V_{PCC} \cdot \left(\left(1 - G_{APF}(s) \right) \cdot Z_S + Z_L \right)}{Z_S \cdot Z_L} = \frac{V_S}{Z_S} - \left(1 + G_{APF}(s) \right) \cdot i_L$$

$$V_{PCC} = \frac{Z_S \cdot Z_L}{\left(1 - G_{APF}(s) \right) \cdot Z_S + Z_L} \cdot \left[\frac{V_s}{Z_S} - \left(1 - G_{APF}(s) \right) \cdot i_L \right] \tag{6.51}$$

$$i_s = \frac{V_S - V_{PCC}}{Z_s} \tag{6.52}$$

When, the equation (6.51) is substituted into equation (6.52), the equation (6.53) is obtained after simplification.

$$i_s = \frac{V_S}{Z_s} - \frac{Z_L}{Z_S \cdot \left[\left(1 - G_{APF}(s) \right) \cdot Z_S + Z_L \right]} \cdot V_S + \frac{\left(1 - G_{APF}(s) \right) \cdot Z_L}{\left(1 - G_{APF}(s) \right) \cdot Z_S + Z_L} \cdot i_L$$

$$i_s = \frac{V_S \cdot Z_L + (1 - G_{APF}(s)) \cdot V_S \cdot Z_S - V_S \cdot Z_L}{Z_S \cdot [(1 - G_{APF}(s)) \cdot Z_S + Z_L]} + \frac{(1 - G_{APF}(s)) \cdot Z_L}{((1 - G_{APF}(s)) \cdot Z_S + Z_L)} \cdot i_L$$

$$i_s = \frac{(1 - G_{APF}(s))}{((1 - G_{APF}(s)) \cdot Z_S + Z_L)} \cdot V_S + \frac{(1 - G_{APF}(s)) \cdot Z_L}{((1 - G_{APF}(s)) \cdot Z_S + Z_L)} \cdot i_L$$

$$i_s = \frac{1}{\left(Z_S + \dfrac{Z_L}{(1 - G_{APF}(s))} \right)} \cdot V_S + \frac{Z_L}{\left(Z_S + \dfrac{Z_L}{(1 - G_{APF}(s))} \right)} \cdot i_L \tag{6.53}$$

This equation provides the transfer function between load and supply current.

6.5.3 Response of the Shunt APF with Compensation Capacitor

In this section, the effect of reactive power compensation capacitor on performance of harmonic elimination characteristic is analyzed with shunt APF. The values of series internal resistance and the capacitance of the capacitor are R=85mΩ and C=656µF. The equivalent impedance of compensation capacitor is $Z_L(s) = \dfrac{RCs}{RCs + 1}$.
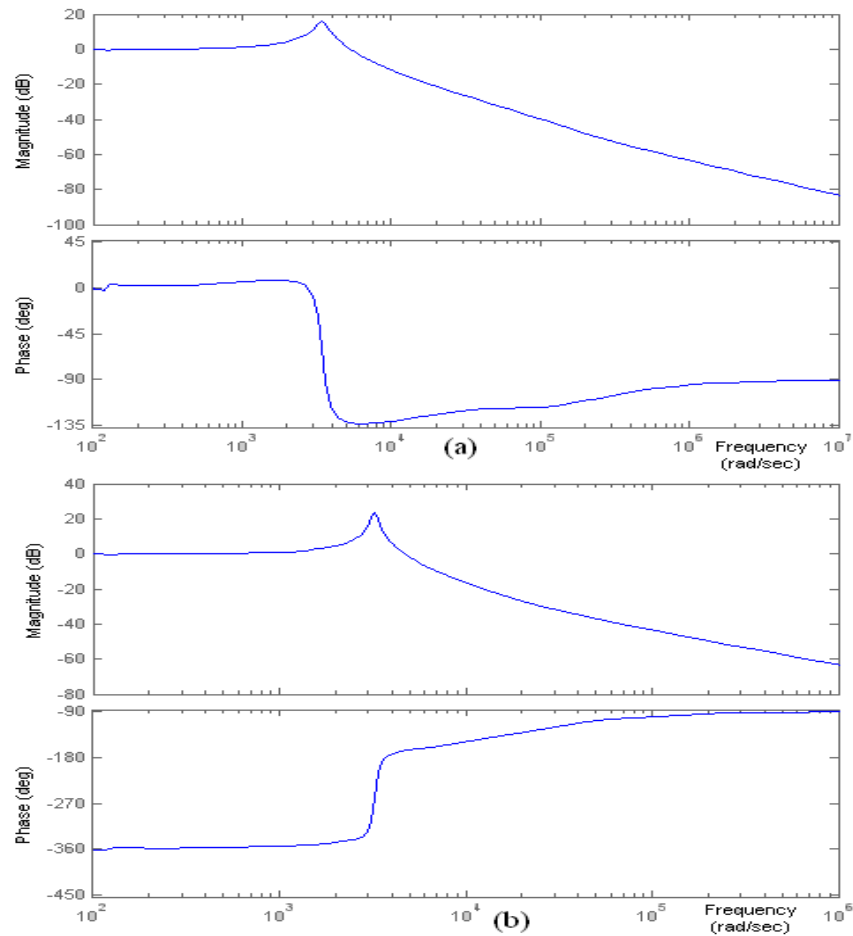
Figure 6.21 Frequency response of whole system, I_s/I_L a) when the detecting point is A , b) when the detecting point is B.

The frequency response of whole system is shown in Figure 6.21 for taking measurement from points of A and B. According to these responses, when the current measurement is done from point A, the peak of the gain at parallel resonance frequency is lower than that of the value obtained by using the measurement from point B. The response of the system is depending on entire parameters used in the equations (6.48) and (6.53). Therefore, the magnification of the harmonic currents at the parallel resonance frequency is a serious application problem of the active power filters with the reactive power compensation capacitors. The measurement of the current either from point A or from point B does not avoid this problem.

CHAPTER SEVEN
CONCLUSION

The performance of ten different harmonic extraction methods have been evaluated by using Matlab simulations and three of them, which are IRPT method, SRF method, and ADALINE method have been implemented in DSP unit in order evaluate their performance as well as identify the programming difficulties with the methods. The IRPT method has a faster response to load variations. However, it is not effectively compensating harmonics of unbalanced loads and not effective for load balancing. ADALINE method gives better performance against the load current variations in amplitude and frequency. Its computational time is the longest among three tested algorithms in the digital signal processor. But it should be noted that the SRF method can also be preferred to eliminate the specific harmonics at estimated frequencies instead of injecting whole spectrum of harmonics as being done by IRPT.

The DSP program of shunt APF application is prepared by using MATLAB package program. The simultaneous operation of the DSP with the Simulink models has been also established by the developed model structure. The developed source code for DSP is tested with co-operating DSP and-Simulink. The approaches given here can be implemented for rapid prototyping of the system in industrial applications. The proper operation of the DSP is guaranteed through simulations before testing the code on physical system.

In experimental work, ADALINE based shunt APF is implemented by using direct and indirect current control techniques. The indirect current control technique has been applied first time with Adaline Method in this work. Experimental results of ADALINE are compared with IRPT method. Since ADALINE method is a delayless method and works on each phase independently, it yields better results under unbalanced loading conditions.

The sampling frequency of reference current is limited by the execution time of DSP unit. The sampling period should be lower to reduce the THD value. Both direct and indirect current control techniques are implemented by considering the effects of tracking capabilities on reference current. It is found that the indirect current control techniques is better to reduce the supply current harmonics but may cause instability, if the line current is not measured by the sensor with high resolution.

ADALINE method produces reference current as delayless. But, the THD performance of method is limited by the sampling time. This problem can be overcome by sampling the load current at 6 kHz and passing through the ADALINE in order to get fundamental component. In addition to that the load current is also sampled around 100 kHz. The output of ADALINE is subtrected from the sampled values around 100 kHz in order reference current for harmonics. Thus, the harmonic currents are received at sampled values from high frequency. This technique is implemented in MATLAB simulation. The experimental work is left to future works.

The 20kVA shunt APF prototype was tested successfully for ADALINE, IRPT, and SRF methods. The IRPT and SRF methods have 38 kHz and 32 kHz sampling rate by using F2812 DSP, respectively. But, sampling rate of SRF method is increased to 70 kHz by replacing the DSP with F28335 floating point one. Thus, performance of APF is improved.

In modularity of shunt APF, when the power ratings of the converters are considered for the compensation of diode rectifier load current harmonics, it can be seen that the total VA rating of the installed APFs are highest in multiple-converter capacity limitation control approach and lowest in single-converter specific harmonic elimination approach. Simulation results show that the multiple converter power-splitting and capacity limitation control methods give the best THD performance in the suppression of the lower order dominant harmonics. Single-converter specific harmonic elimination and frequency-splitting methods give almost the same performance, however, since the peak amplitude of the sum of harmonics is lower

than that of an individual harmonic, assigning an APF for the compensation of only one harmonic is not effective and this yields to a larger total APF VA rating. The THD performance of single-converter THD method worsens as the nonlinear load increases, because of the increase in required switching frequency of the converter. When the compensating currents are shared as shown in multiple-converter power-splitting approach, the THD performance of the system is observed to improve. The actual VA capacity of the forthcoming APFs is increased due to insufficient compensation of the previous APF modules in capacity-limitation technique, if the modular system is subjected to compensate high frequency components in the load currents such as in the case analyzed with a diode rectifier feeding a resistive load.

A linear model of a shut active power filter which contains hysteresis current controller is obtained using the synchronously rotating reference frame. The switching frequency is left as a variable in the d-axis model even the reference frame speed is selected at the fundamental frequency. This seems to be a reasonable assumption during this linearization because switching frequency is very high with respect to the power frequency therefore the relative speed is still nearby switching frequency. This model is used to find out stability limits according to filter inter inductance, hysteresis band width and switching frequency. The stability range of DC link PI controller is found by applying Routh-Hurwitz criteria. The transfer functions between the load current and filter current are obtained and the bode plots are given. The appearance of gain and phase are verified in detailed simulation results. The experimental records have shown that linear model can be successfully used to design the dc link PI controller.

REFERENCES

Abdelli, Y., Machoum, M., & Khoor, M.S. (2004). Control of a multimodule parallelable three-phase active power filters. *11th International Conference on Harmonics and Quality of Power*, New York, USA, 543-548.

Abdeslam, DU, Merckle, J, & Wira, P. (2005). Adaline-based estimation of power harmonics. *ESANN'2005 Proceedings European Symposium on Artificial Neural Network*, Belgium, 571–576. ISBN 2-930307-05-6.

Aiello, M., Cataliotti, A., Cosentino, V., & Nuccio, S.(2007). Synchronization techniques for power quality instruments. *IEEE Trans. Instrument. Meas.*, *56* (5), 1511–1519.

Akagi, H. (1994). Trends in Active Power Line Conditioners. *IEEE Trans. on Power Electronics*, *9* (3), 263-268.

Akagi, H. (1996). New trends in active filters for power conditioning. *IEEE Trans on Industry Applications*, *32* (6), 1312–1322, DOI:10.1109/28.556633.

Akagi, H. (2002). *Active filters for power conditioning.* T.L. Skvarerina (Ed.), The Power Electronics Handbook, New York, CRC Pres.

Akagi, H. (2004). Trends in active power line conditioners. *IEEE Trans. on Power Electronics*, *9 (3),* 263–268, DOI: 10.1109/63.311258.

Akagi, H. (2005). Active harmonic filters. *Proc. IEEE*, *93* (12), 2128–2141.

Aredes, M., Neto, J.A.M., Ferreira, J.C.C., Monteiro, L.F.C., Fernandes R.M., & Siqueira, M.J.V. (2005). A simplified control strategy for a unified power quality conditioner prototype. *Proc. IEEE Power Electronics Specialist Conf., Brasil, June*, 2592-2597.

Arrillaga J., Bradley D. A.and Bodger P. S. (1985). *Power system harmonics*. John Wiley & Sons.

Asiminoaei, L., Blaabjerg, F., & Hansen, S.(2005). Evaluation of harmonic detection methods for active power filter applications. *Applied Power Electronics Conference and Exposition.*, *1*, 635–641.

Balog, R. S., Sorchini, Z., Kimball, J. W., Chapman, P. L., & Krein, P. T. (2005). Modern Laboratory-based education for power electronics and electric machines. *IEEE Trans. Power Systems*, *20* (2), 538–547.

Blasko, V., & Kaura, V.(1997). A new mathematical model and control of a three-phase ac–dc voltage source converter. *IEEE Trans. on Power Electronics*, *12* (1), 116–123.

Bhattachharya, S., Frank, T.M., Divan, D.M., & Banerjee, B.(1998). Active filter system implementation. *IEEE Ind. Appl. Magazine*, *4*, 47–63.

Boudjedaimi, M, Wira, P, Abdeslam, DO, Djennoune, S & Urban, JP. (2008). Voltage source inverter control with adaline approach for the compensation of harmonic currents in electrical power systems. *34th Annual Conference of the IEEE Industrial Electronics Society IECON08*, USA, 2708–2713. DOI: 10.1109/IECON.2008.4758386.

Brod, D. M. & Novotny, D. W. (1985). Current control of VSI-PWM inverters. *IEEE Transactions on Industry Applications.*, *21* (4), 562–570.

Buso, S., Malesani, L, & Mattavelli, P.(1998). Comparison of current control techniques for active filter applications. *IEEE Trans. on Industrial Electronics*, *45* (5), 722-729.

Casaravilla, G., Salvia, A., Briozzo, C. & Watanabe, E. (2002). Control strategies of selective Harmonics current shunt active filter. *IEE Proc.-Generation, Transmission and Distribution*, *149* (6): 689–694.

Chiang, S.J., & Chang, J.M. (2001). Parallel operation of shunt active power filters with capacity limitation control. *IEEE Trans. On Aerospace and Electronic Systems*, *37* (4),1312–1320.

Dawande, M., Donescu, V., Yao, Z., & Rajagopalan, V. (1997). Recent advances in simulation of power electronics converter systems. *Springer India*, 20 (6), 689-704.

Defour, C., Abourida, S., & Belanger, J. (2005). Hardware-in-the-loop simulation of power drives with RT-LAB. *Proc. Int. Conf Power Electr. and Drives Systems*, 1646–1651.

Dixon, JW. & Ooi BT. (1988). Indirect current control of a unity power factor a sinusoidal current boost type three-phase rectifier. *IEEE Transactions on Industrial Electronics*, *35* (4), 508–515, DOI:10.1109/41.9172.

Dote, Y., & Kinoshita S. (1990). *Brushless Servomotors: Fundamentals and Applications.* Claredon, Oxford, ISBN-10: 0198593724.

Dubey, S.P., Singh, P., & Manjunath, H.V. (2005). DSP based neural network controlled parallel hybrid active power filter, *Int. J. Emerg. Electr. Power Syst.*, *4*, 1–14.

El-Habrouk, M., Darwish, M.K., & Mehta, P.(2000). Active power filters: a review, IEE Proc. Electron. Power Appl., *147* (5), 403–413.

El-Shatshat, R., Kazerani, M., & Slama, M.M.A. (1999). Modular active power filtering approaches: power splitting verses frequency splitting. *Proc. of IEEE Canadian Conference on Electrical and Computer Engineering*, Alberta, Canada, 1304- 1308.

Emadi, A., Nasiri, A., & Bekiarov, S.B.(2005). *Uninterruptible power supplies and active filters*. USA: CRC Press.

Fang, Z., Longhui, W. Zhe, C., Xianwei, W., & Zhaoan, W. (2009). Study on a control method of PAPF for resonance damping and harmonics compensation in power system. *Power Electronics and Motion Control Conference, 2009. IPEMC '09. IEEE 6th International*, DOI: 10.1109/IPEMC.2009.5157558, 1161 – 1167.

Girgis, A.A., Chang, W.B., & Markam, E.B. (1991). A digital recursive measurement scheme for on-line tracking of power system harmonics. *IEEE Trans. Power Deliv.*, *6* (3), 1153–1160.

Grady, W.M., Samotyj, & M.J., Noyola, A.H. (1990). Survey of active line conditioning methodologies. *IEEE Trans. Power Deliv., 5* (3), 1536–1542.

Greenwood, A. (1999). *Electrical Transients in Power Systems*, John Wiley & Sons, Inc. New York.

Gyugyi L. & Strycula E. C. (1976). Active AC power filters. *IEEE Industrial applications Society Annual Meeting*, 529-535.

Han, B.M., Bae, B.Y., & Ovaska, S.J. (2005). Reference signal generator for active power filters using improved adaptive predictive filter. *IEEE Trans. Ind. Electron.*, *52* (2), 576–584.

Haque, M.T., & Ise, T.(2002). Implementation of single-phase pq theory. *Power Convers. Conf.*, *2*, 761–765.

He, Y., Zou, Y., Liu, F., Wang, C., & Huan, Z. (2006). Research on parallel operation of active power filters. *IEEE Power Engineering Society General Meeting*.

Holtz J. & Stadtfeld S. (1983) A predictive controller for the stator current vector of ac machines fed from a switched voltage source. *in Proceeding of International Power Electronics Conference (IPEC'83),* Tokyo, 1665–1675.

Ingram, D.M.E. & Round, S.D.A. (1997) Novel digital hysteresis current controller for an active power filter. *Proceedings 1997 International Conference on Power Electronics and Drive Systems*, *2*, 744-749.

Ju, J., Chen, M., Xu, J., Xu, D., Wang, Q., & Zhang, F. (2008). Design issues of multi-modular shunt active power filter system. *Proc. Of Applied Power Electronics Conference and Exposition*, Texas, USA, 1914-1919.

Kazmierkowski M. P. & Malesani L. (1998). Current Control Techniques for Three-Phase Voltage-Source PWM Converters: A Survey. *IEEE Transactions on Industrial Electronics*, *45*(5), 691–703.

Kennel, R. & Linder, A. (2000). Predictive Control of Inverter Supplied Electrical Drives. *in Proceeding of Power Electronics Specialists Conference (PESC' 2000), 2*, 761–766.

Khadkikar, V., Chandra, A., & Singh, B.N. (2009). Generalised single-phase p-q theory for active power filtering: simulation and DSP-based experimental investigation. *IET Power Electron., 2* (1), 67–78.

Kuo, B.C.(1987). *Automatic Control Systems* (5th ed.). USA, Prentice-Hall.

Kuo, H.H., Yeh, S.N., & Hwang, J.C. (2001). Novel analytical model for design and implementation of three-phase active power filter controller. *IEE Proc.-Electr. Power Appl., 148* (4), 369-383.

Kuo, Y., Chiueh, M., & Hsu, W. (2008). Modularized three-phase four wire active power filter. *3rd International Conf. on Electric Utility Deregulation and Restructuring and Power Technologies*, Nanjing, China, 1853-1858.

Li, C., & Tan, Y.(2005). A hybrid neural network based modeling for hysteresis. *Proceedings of the IEEE Int. Symposium on Intelligent Control*, Limassol, Cyprus, 53-58.

Liu, H., Liu, G., & Shen, Y. (2006). A novel harmonics detection method based on wavelet algorithm for active power filter. *World Congress on Intelligent Control and Automation*, 7617–7621.

Massoud, A.M., Finney, S.J., & Williams, B.W. (2004). Practical issues of three-phase, three-wire, voltage source inverter based shunt active power filters. *11th International Conference on Harmonics and Quality of Power*, New York, USA, 436-441.

The Mathworks, Inc. (2003a). *Embedded Target for the TI TMS320C2000TM DSP Platform for use with Simulink-User's Guide Version 1*.

The Mathworks, Inc. (2003b). *Writing s-functions*.

Malesani, L., & Tomasin P. (1993). PWM current control techniques of voltage source converters - A Survey. *Industrial Electronics, Control, and Instrument*, *2*, 670-675.

Moreno, V., Pigazo, A., Diego, R.I. (2002). Reference estimation technique for active power filters using a digital Kalman algorithm. *Harmonics and Quality of Power 10th International Conference*, *2*, 490-494.

Nabae, A., Ogasawara, S. & Akagi, H. (1986). A novel control scheme for current-controlled PWM inverters. *IEEE Transactions on Industry Applications*, *22*(4): 697-701.

Ovaska, S.J., Bose, T., & Vainio, O. (2005). Genetic algorithm-assisted design of adaptive predictive filters for 50/60 Hz power systems instrumentation. *IEEE Trans. Inst. Meas.*, *54* (5), 2041–2048.

Osowski, S. (1992). Neural network for estimation of harmonic components in a power system. *IEE Proceedings-C*, *139* (2), 129–135.

Ozdemir, A. (2004). A digital adaptive filter for detecting harmonic, active and reactive currents. *Meas. Sci. Technol., 5* , 1316–1322.

Ozdemir, E., Ucar, M., Kesler, M., & Kale, M. (2007). The design and implementation of a shunt active power filter based on source current measurement. *Proc. IEEE Int. Electric Machines & Drives Conf., Antalya, Turkey, May.* 608-613.

Pecharanin, N., Sone, M, & Mitsui, H. (1994). An application of neural network for harmonic detection in active filter. *IEEE World Congress on Computational Intelligence; IEEE International Conference on Neural Networks*, 6, 3756–3760. DOI: 10.1109/ICNN. 1994. 374807.

Peng, F.Z. (1998). Application issues of active power filters. *IEEE Industry Applications Magazine*, September/October, 21-30.

Pinto, J.G., Neves, P., Pregitzer, R., Monterio, L.F.C., & Afonso, J.L. (2007). Single-phase shunt active filter with digital control. *ICREPQ'07, 28–30 March, Spain*.

Rahmani, S., Al-Haddad, K., Hadi Kanan, H., & Fnaiech, F. (2006). Modified PWM with a new indirect current control technique applied to a single-phase shunt active power filter. *Canadian Journal of Electrical and Computer Engineering*, *31* (3), 135–144, DOI:10.1109/CJECE.2006.259208.

Rechka, S., Ngandui, E., Xu, J., & Sicard, P. (2002a). A comparative study of harmonic detection algorithms for active filters and hybrid active filters. *IEEE PESC* , *1*, 357–363.

Rechka, S., Ngandui, E., Xu, J., & Sicard, P. (2002b). Performance evaluation of harmonics detection methods applied to harmonics in presence of common power quality problems. *ELECTRIMACS,* 363–375.

Rechka, S., Ngandui, E., Xu, J., & Sicard, P. (2003). Analysis of harmonic detection algorithms and their application to active power filters for harmonic compensation and resonance damping. *Can. J. Elect. Comp. Eng.*, *28*, 41–51.

Rojas, R. (1996). *Neural networks - a systematic introduction.* Berlin, New-York, Springer-Verlag.

Routimo, M., Salo, M., & Tuusa, H. (2007). Comparison of the voltage source and current-source shunt active power filters. *IEEE Trans. on Power Electronics*, *22* (2), 636-643.

Phipps, W., Harrison, M.J., & Duke, R.M. (2006). Three-phase phase-locked loop control of a new Generation power converter. *Industrial Electronics and Applications, 1ST IEEE Conference.*

Sasaki, H., & Machida, T. (1971). A new method to eliminate AC harmonic currents by magnetic flux compensation consideration on basic design. *IEEE Trans. Power App. Syst.*, 2009-2019.

Singh, BN, Chandra, A, & AI-Haddad, K. (1998). Performance comparison of two current control techniques applied to an active filter. *8th International Conference on Harmonics and Quality of Power (ICHQP'98), 1*, 133–138, Athens, Greece;. DOI:10.1109/ICHQP.1998.759859.

Singh, B., Al-Haddad, K., & Chandra, A. (1999). A review of active filters for power quality improvement. *IEEE Trans. Ind. Electron., 46* (5), 960–971.

Singh, BN., Singh, B., Chandra, A., Rastgoufard, P., & Al-Haddad, K. (2007). An improved control algorithm for active filters. *IEEE Transactions on Power Delivery, 22* (2), 1009–1020, DOI: 10.1109/TPWRD.2006.886790.

Surgevil, T., Vardar, K., & Akpinar, E. (2009). Analysis of shunt active power filters using PSCAD for parallel operation. *6th International Conference on Electrical And Electronics Engineering (ELECO'09),* Bursa, ISBN: 978-1-4244-5106-7.

Terbobri, G.G., Sadison, M.F., & Khanniche, M.S. (2000). Trends of real time controlled active power filters, *International Conference on Power Electronics and Variable Speed Drives*, 410–415.

Tsang, K.M., & Chan, W.L.(2006). Design of single phase active power filter analogue cascade controller. *IEE Proc.-Electr. Power Appl.*, *153* (5), 735-741.

Teper, J.S., Dixon, J.W., Venegas, G., & Moran, L.(1996). A simple frequency-independent method for calculating the reactive and harmonic current in a nonlinear load. *IEEE Trans. Ind. Electron.*, *43* (6), 647–654.

Valiviita, S., & Ovaska, S.J.(1998). Delayless method to generate current reference for active filters. *IEEE Trans. Ind. Electron., 45* (4), 559–567.

Vardar, K., Surgevil, T., & Akpinar, E. (2009a). Evaluation of reference current extraction methods for DSP implementation in active power filters. *Electric Power Systems Research, 79*, 1342-1352.

Vardar, K., Surgevil, T., & Akpinar, E. (2009b). Rapid prototyping applications on three-phase PWM rectifier and shunt active power filter. *6th International Conference on Electrical And Electronics Engineering (ELECO'09),* Bursa, 258–262. ISBN: 978-1-4244-5106-7.

Vardar, K., & Akpinar, E. (2011). Comparing ADALINE and IRPT methods based on shunt active power filters. *European Transaction on Electrical Power*, *21*, 924–936.

Vazquez, JR, & Salmeron, P. (2003). Active power filter control using neural network technologies. *IEE Proceedings—Electric Power Applications, 150* (2), 139–145, DOI: 10.1049/ip-epa:20030009.

Yalazan, H.T., Sürgevil, T., & Akpınar E. (2007). Wavelet transform application in active power filter used for slip energy recovery drives. *ACEMP'07*, 398–402.

Yanbo, C., Fudan, Z., and Cheng, K.W.E. (2006). Shunt active power filter-SIMULINK simulation and DSP-based hardware realization. *Proc. Int. Conf. on Power Electronics Systems and Applications, Hong Kong, November.* 120-125.

Xiu, C., & Liu Y.(2009). Hysteresis response neural network and ıts applications. *ISECS International Colloquium on Computing, Communication, Control, and Management*, 361–364.

Zhao, J., & Bose, B.K. (2004). Neural-network-based waveform processing and delayless filtering in power electronics and AC drives. *IEEE Trans. Ind. Electron*, *51* (5), 981–991.

APPENDIX A

MATLAB SIMALATIONS OF HARMONIC EXTRACTION METHOD AND
ACTIVE POWER FILTER TOPOLOGIES

The designed model libraries of shunt APF by using Matlab
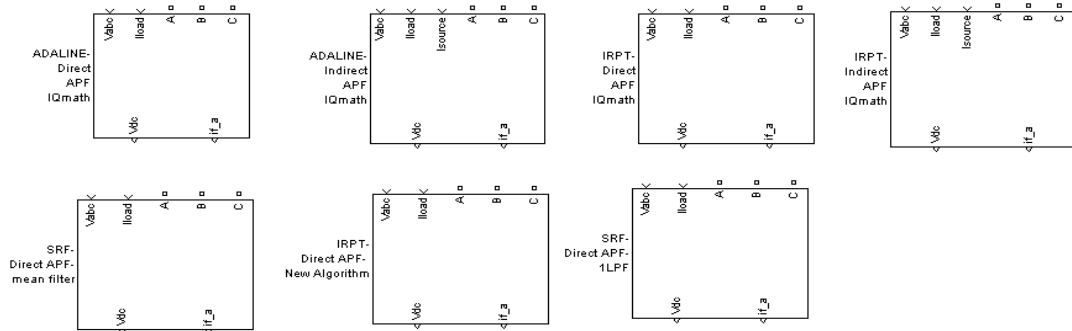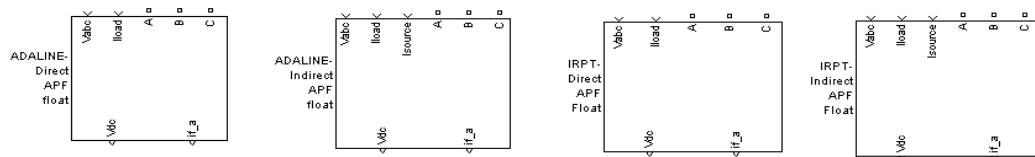
General model
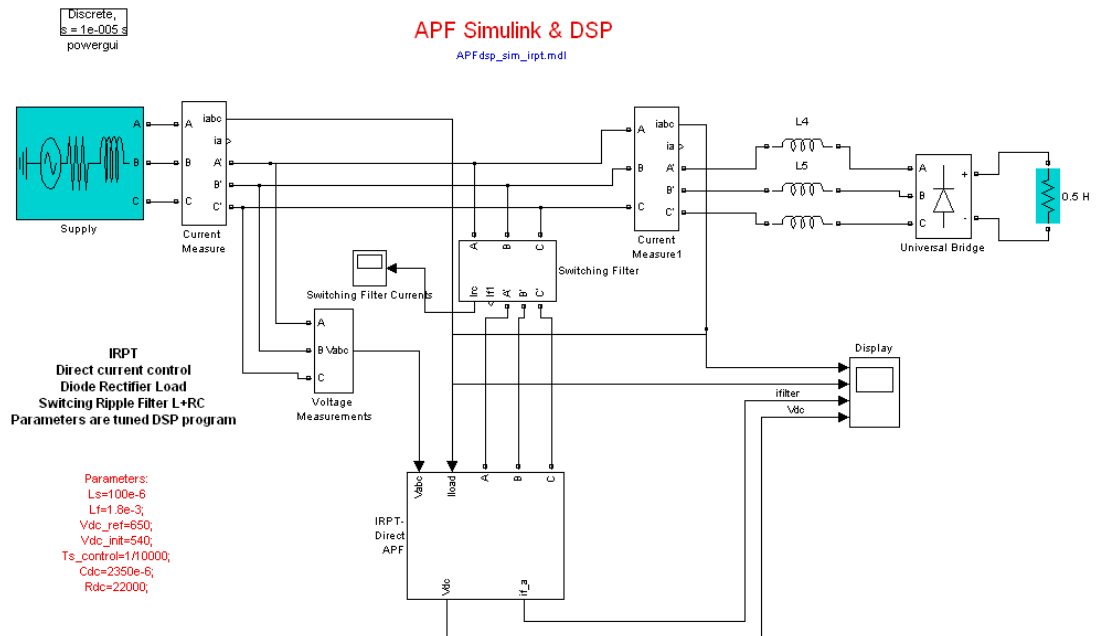
Parameter Adjustment of shunt APF model.

Block Parameters: ADALINE- Direct APF IQmath

Direct ADALINE PAPF (mask)

Direct Current Controlled Parallel Active Power Filter with ADALINE Methods. TMS28F12 with IQmath.

Parameters

Filter Inductance (H)
1.8e-3

DC Link Referance Voltage (V)
650

DC Link Initialize Voltage (V)
540

DC Link Capacity (F)
2300e-6

Ts_control
1/6000

Iload gain
1*21.5

Ifilter gain
1*25.64102

Base Current (A)
50

Hysteresis Band (ADC value)
15

OK | Cancel | Help | Apply

Block Parameters: ADALINE- Indirect APF IQmath

Indirect ADALINE PAPF (mask)

Indirect Current Controlled Parallel Active Power Filter with ADALINE Methods. TMS28F12 with IQmath.

Parameters

Filter Inductance (H)
1.8e-3

DC Link Referance Voltage (V)
650

DC Link Initialize Voltage (V)
540

DC Link Capacity (F)
2300e-6

Ts_control
1/6000

Iload gain
12*21.5

Ifilter gain
20*25.64102

Base Current (A)
50

Hysteresis Band (ADC value)
15

OK | Cancel | Help | Apply

Block Parameters: IRPT- Direct APF IQmath

Direct IRPT PAPF (mask)

Direct Current Controlled Parallel Active Power Filter with IRPT Methods. TMS28F12 with IQmath.

Parameters

Filter Inductance (H)
1.8e-3

DC Link Referance Voltage (V)
650

DC Link Initialize Voltage (V)
540

DC Link Capacity (F)
2300e-6

Ts_control
1/10000

Iload gain
1*21.5

Ifilter gain
1*25.64102

Base Current (A)
50

Hysteresis Band (ADC value)
15

OK | Cancel | Help | Apply

Block Parameters: SRF- Direct APF- mean filter

Direct IRPT PAPF (mask)

Direct Current Controlled Parallel Active Power Filter with SRF Methods. TMS28F12 with IQmath.

Parameters

Filter Inductance (H)
5e-3

DC Link Referance Voltage (V)
650

DC Link Initialize Voltage (V)
540

DC Link Capacity (F)
2300e-6

Ts_control
1/12800

Iload gain
1*21.5

Ifilter gain
1*25.64102

Base Current (A)
50

Hysteresis Band (ADC value)
15

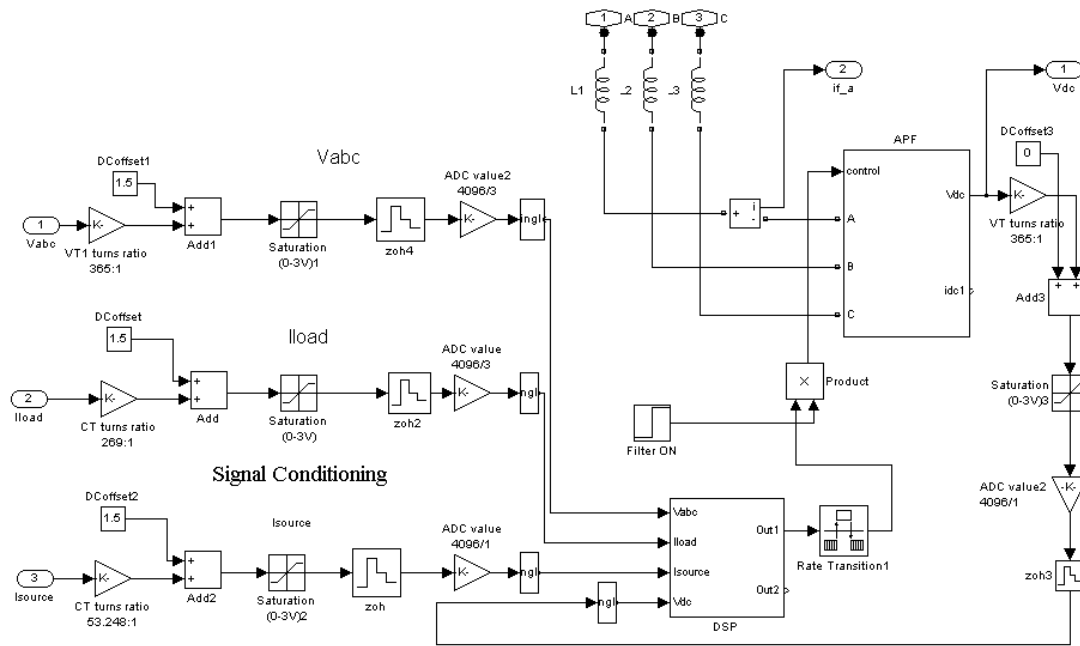Mean Filter number of point
128

OK | Cancel | Help | Apply

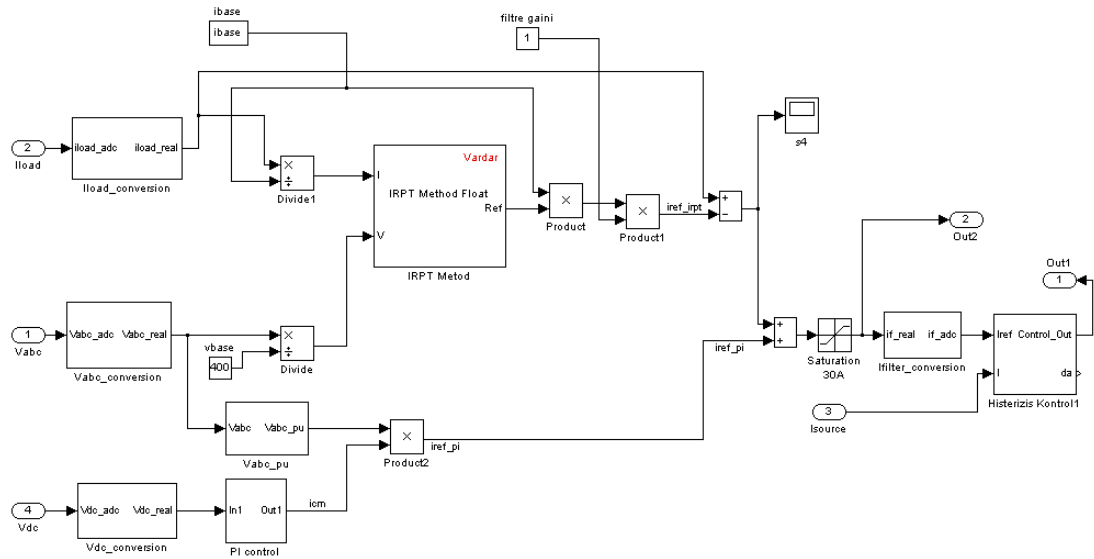APF models with Direct current control
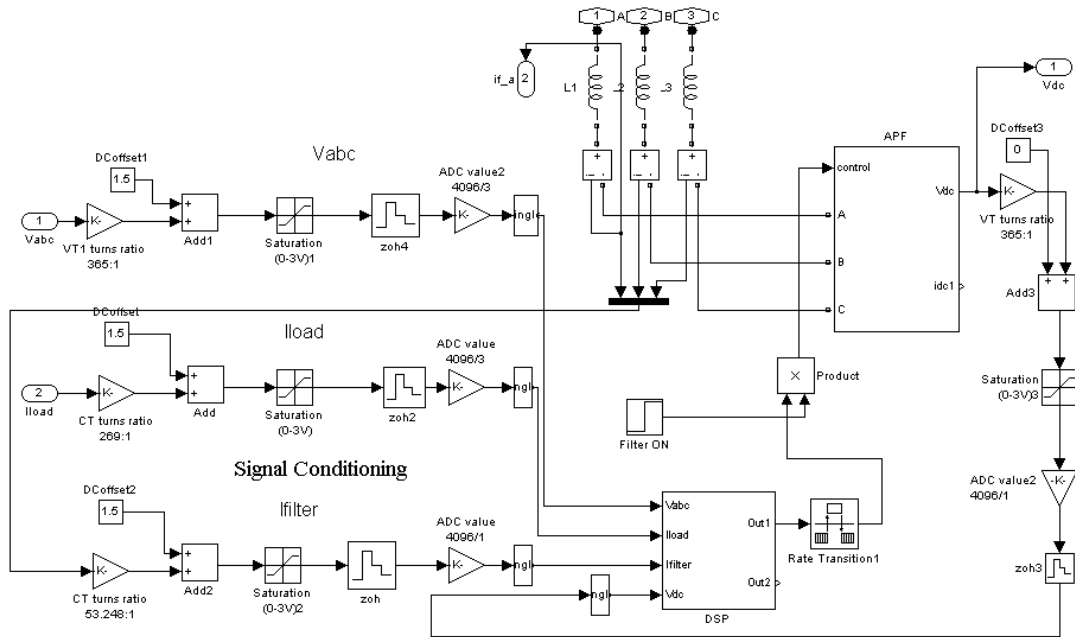
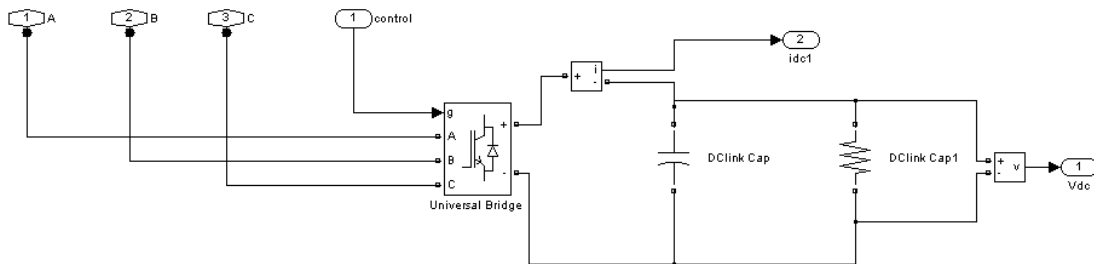APF models with Direct current control – DSP Block
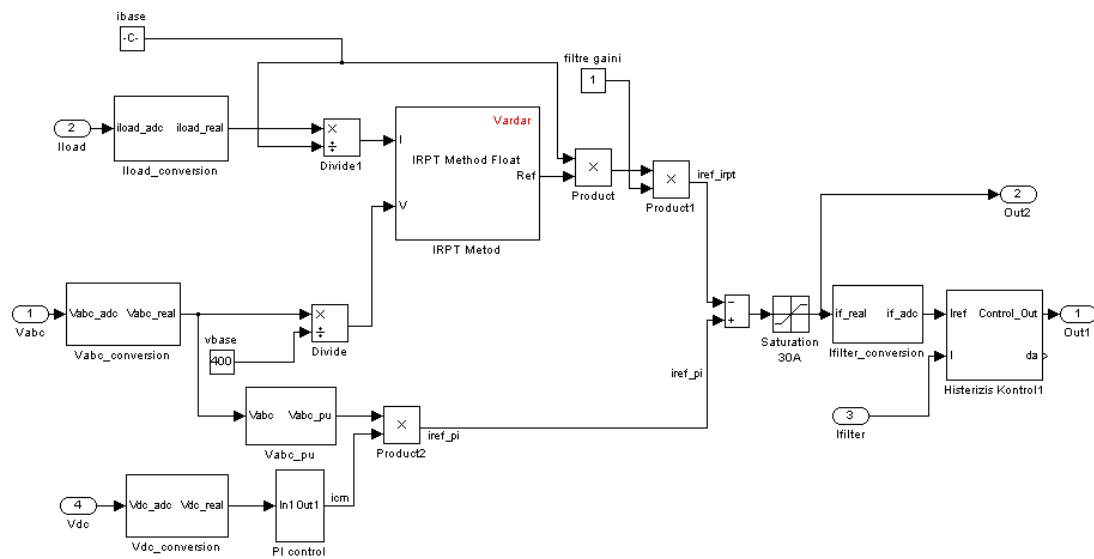
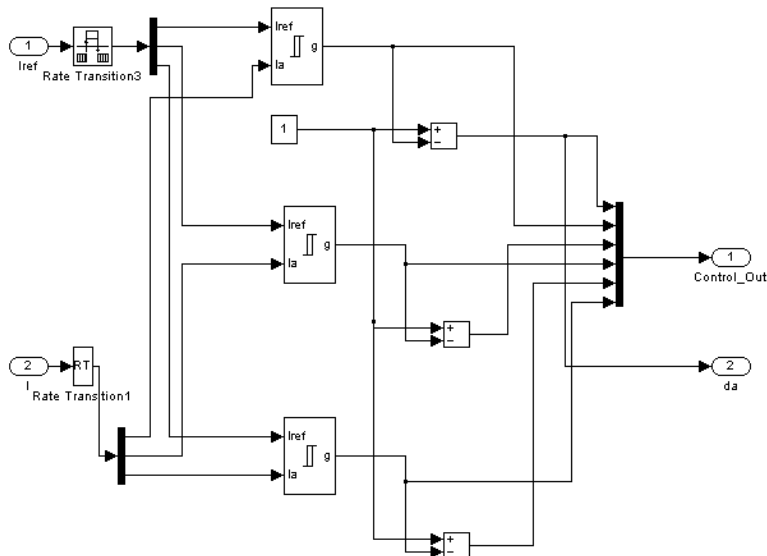APF models with Indirect current control
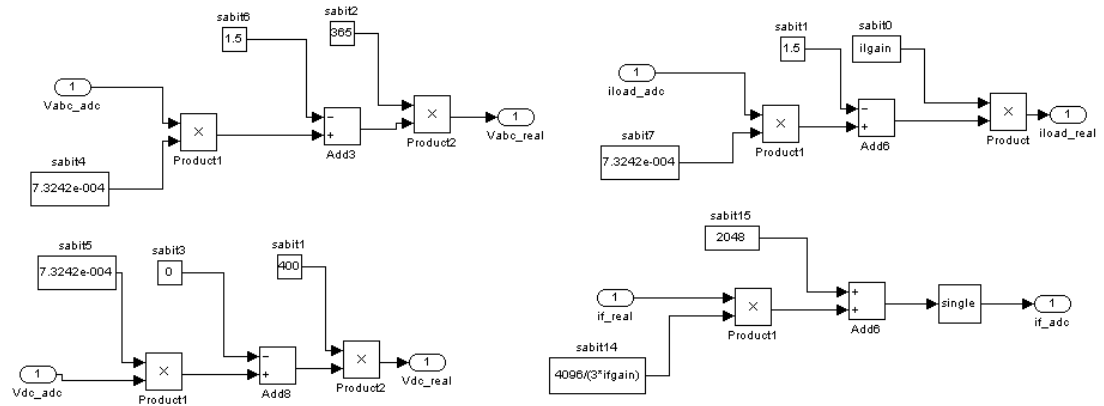

APF models with Indirect current control– DSP Block

APF Block for all models

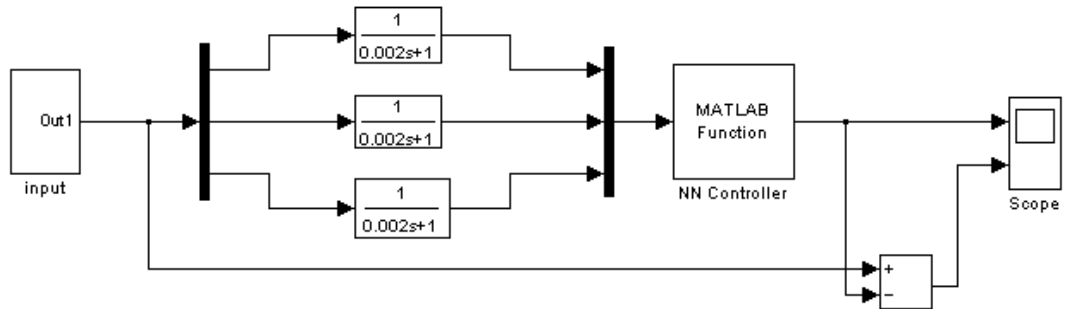## Hysteresis Current Controller block for all models

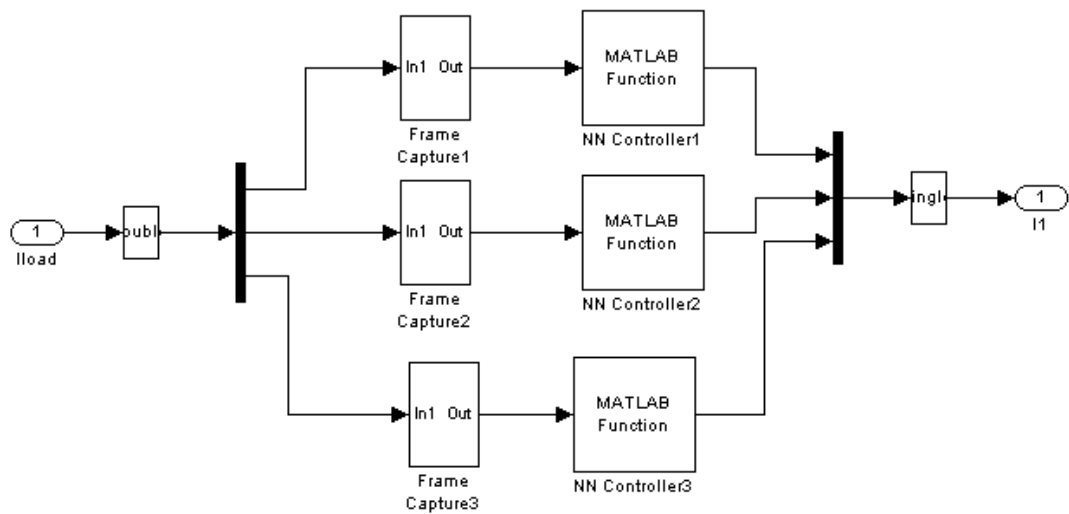## Real Datas from reading ADC conversion block into the DSP block

Note: Constants are same namely at the DSP program source code.
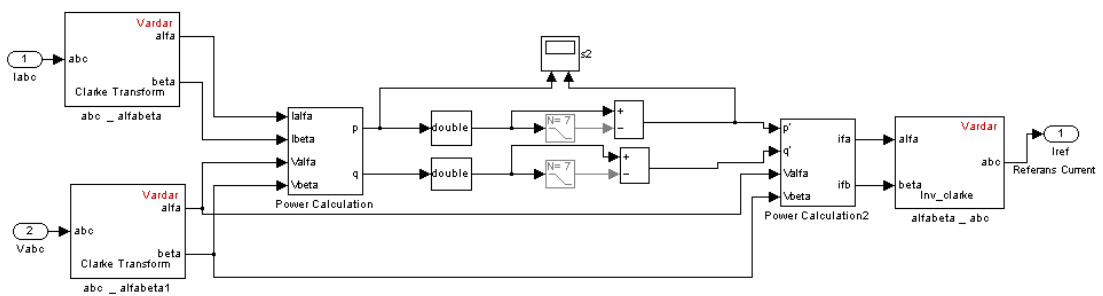
Block diagrams of Harmonic Extraction Methods

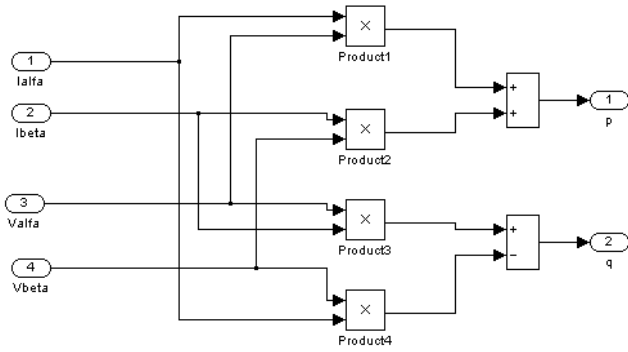Delayless filtering based on Neural Network

Simulation of Adaline Method

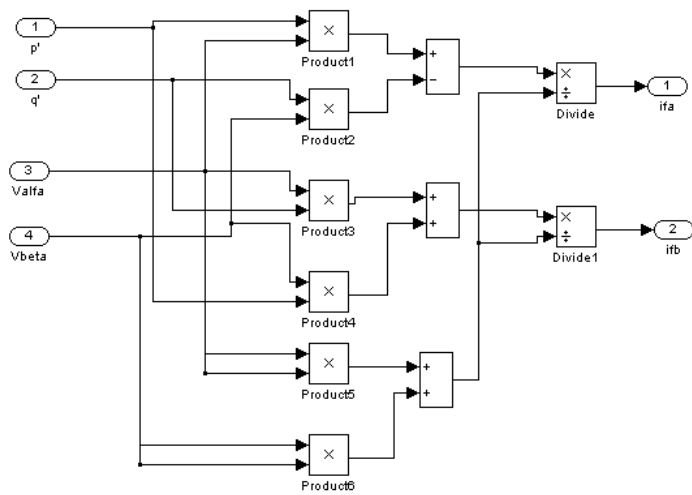
Simulation of IRPT Method

Clarke Transform Block
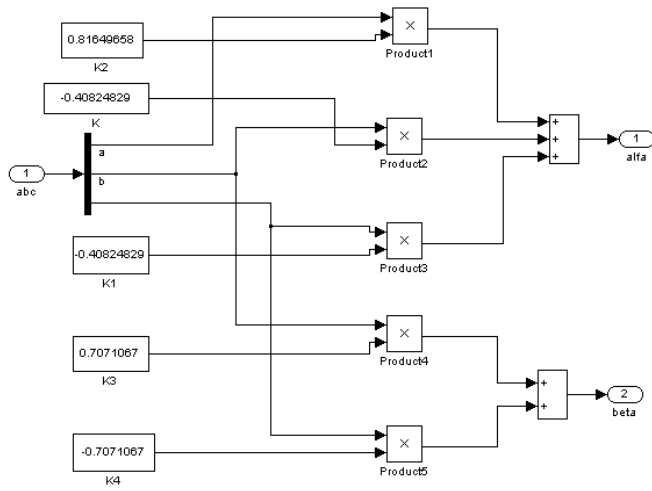
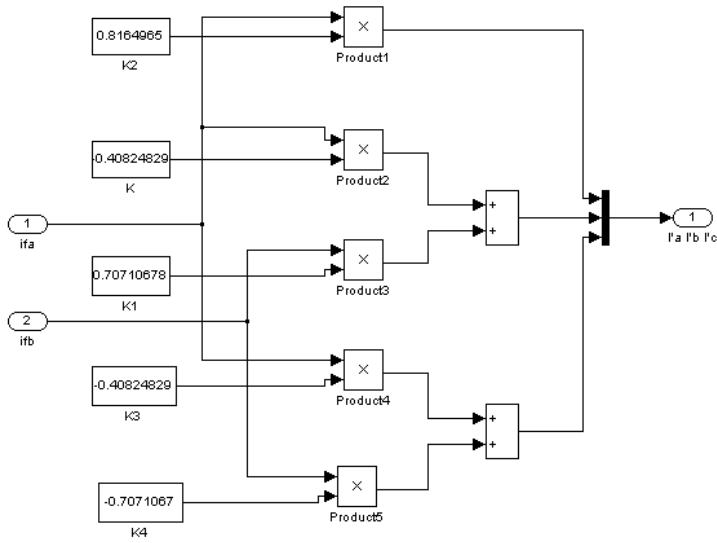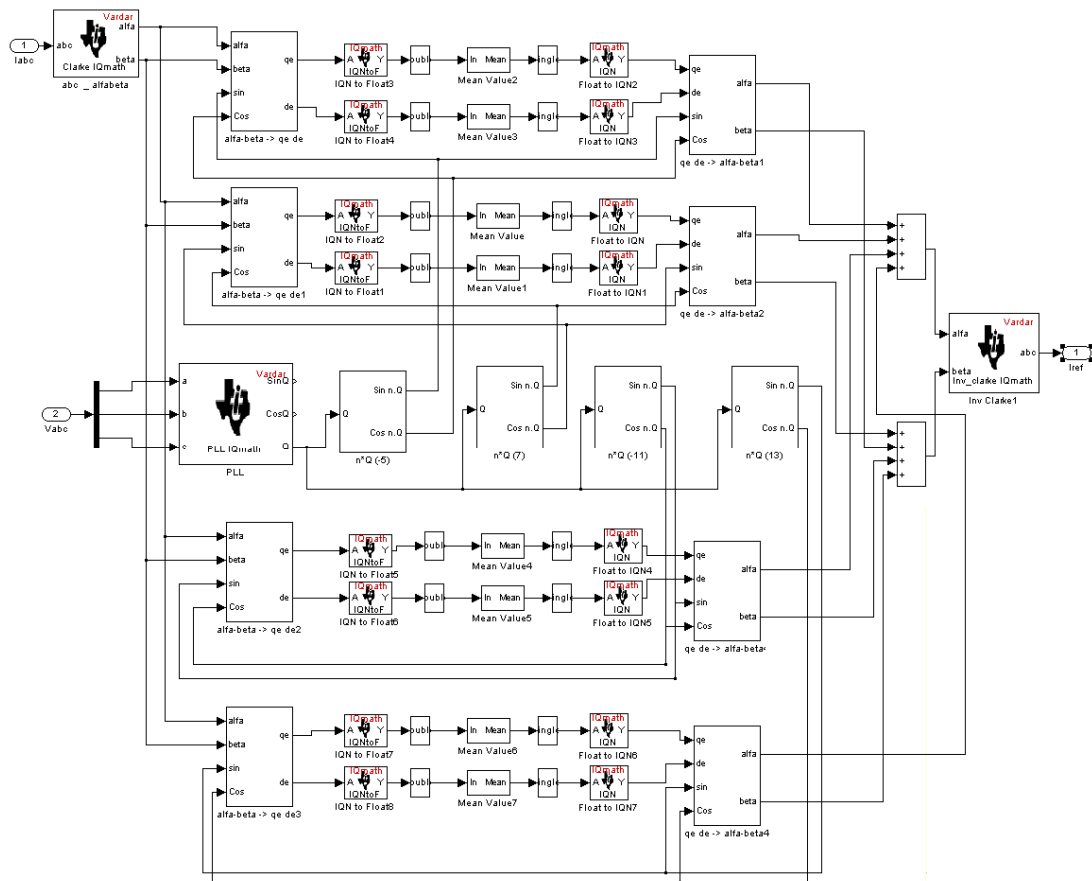## Power Calculation Block

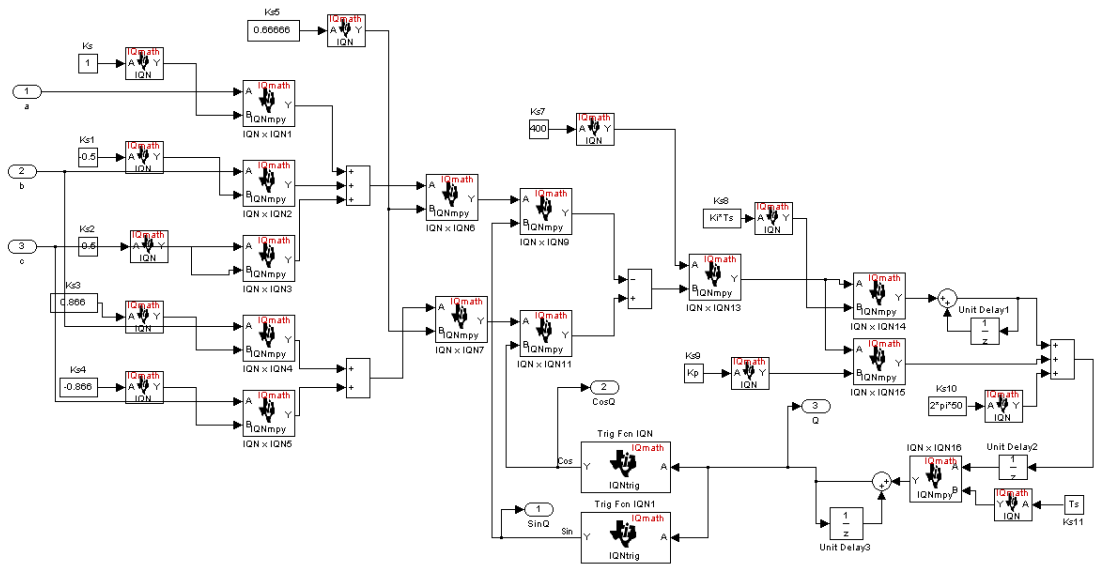## Power Calculation2 Block
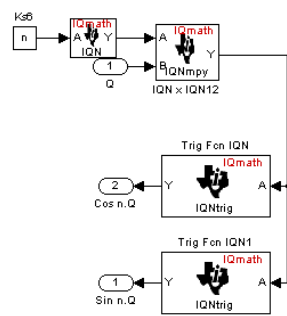
Inverse Clarke Block

Simulation of SFR Method by using Iqmath library
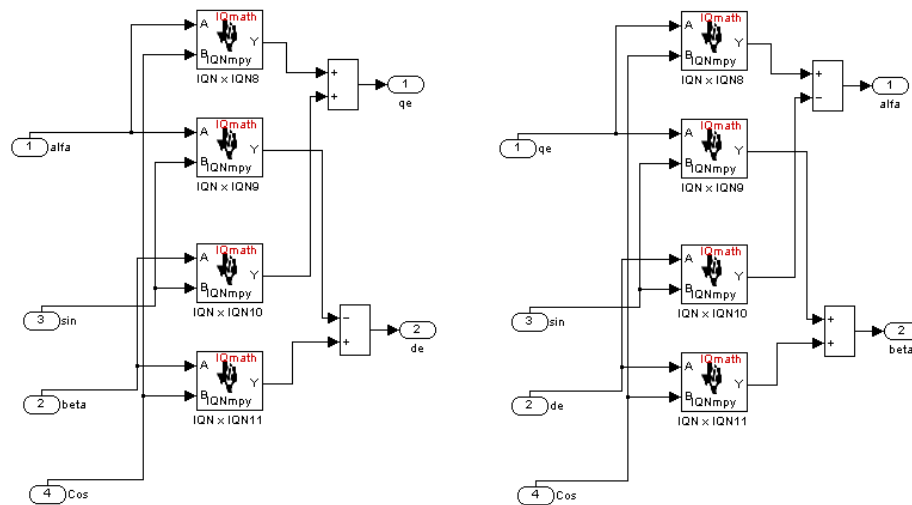
PLL Block

N*Theta Block

alfa-beta to dq and dq to alfa-beta Block

APPENDIX B

Designed circuits for shunt APF prototype.

The signal conditioning circuit for sampling of filter currents.
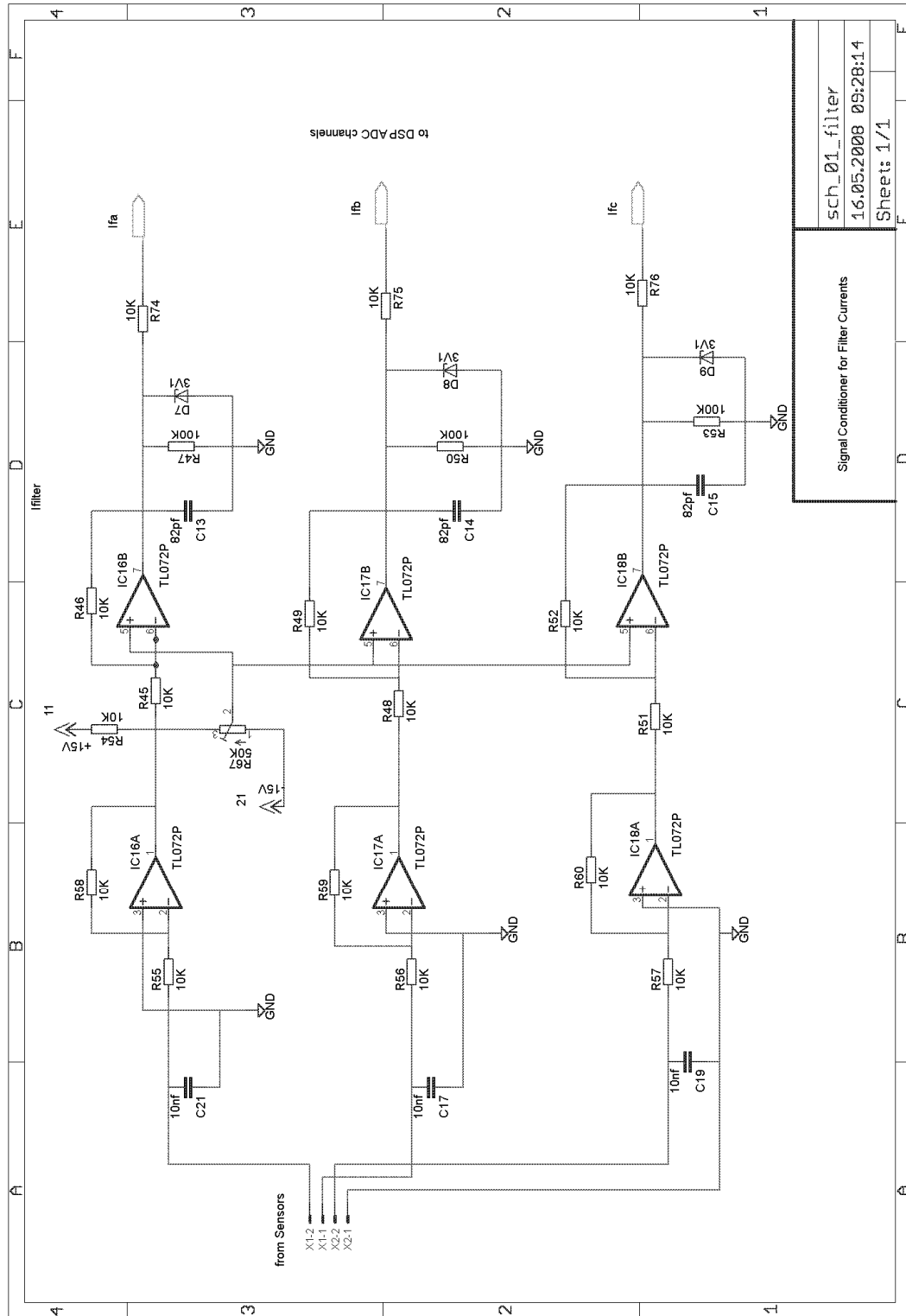
The signal conditioning circuit for sampling of load currents
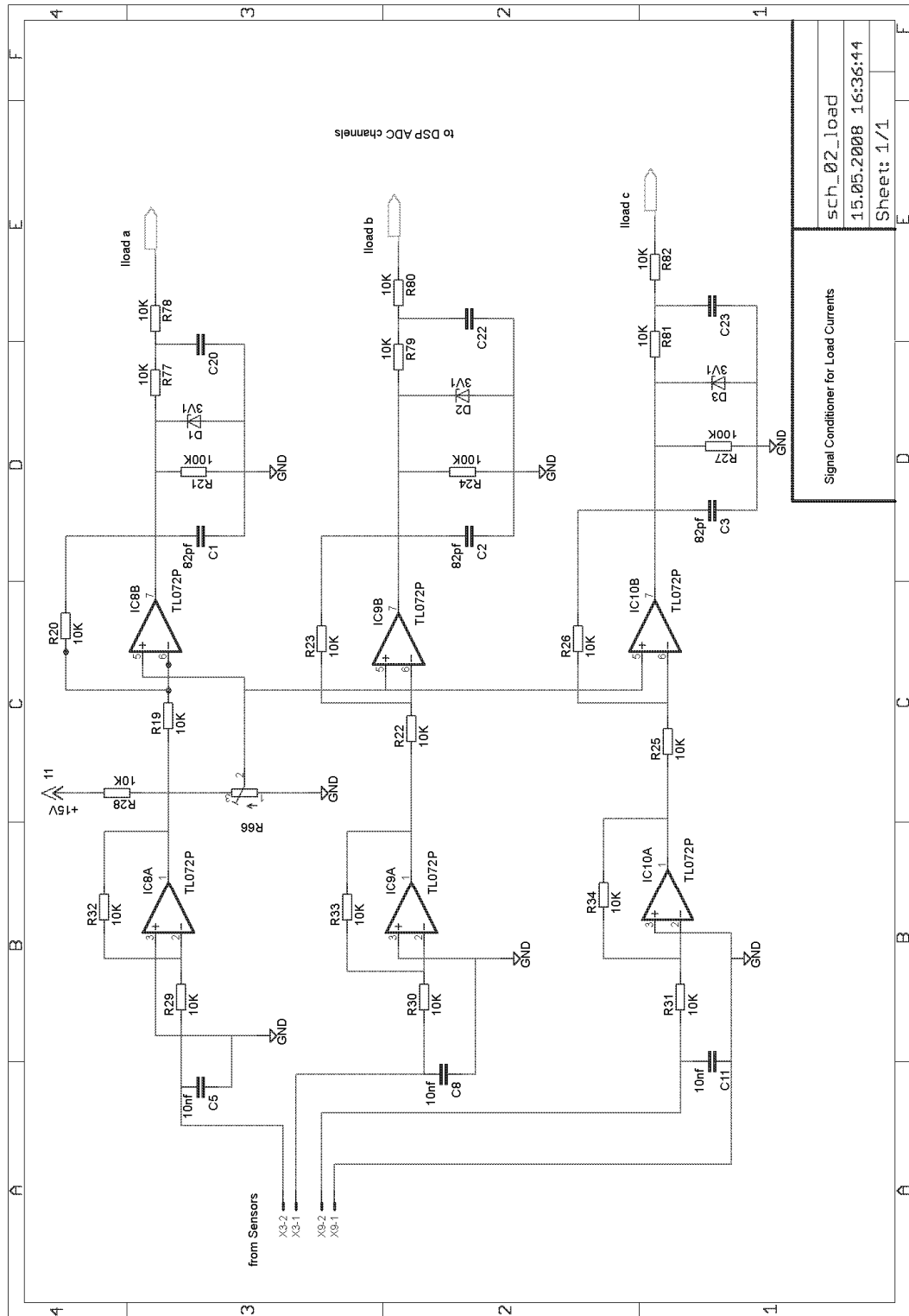
The signal conditioning circuit for sampling of supply voltages.
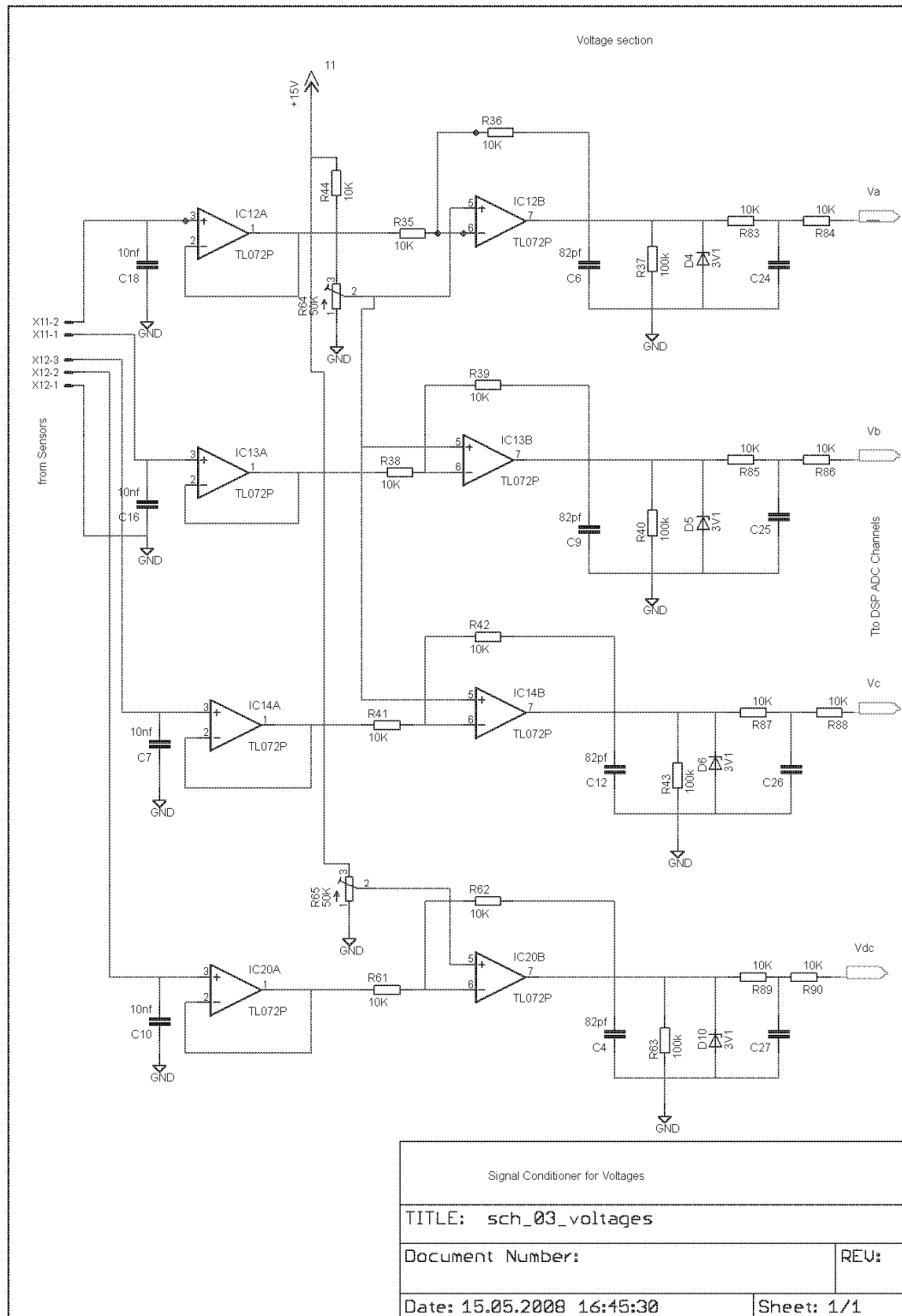
Analog protection circuits for IGBT gate pulses.
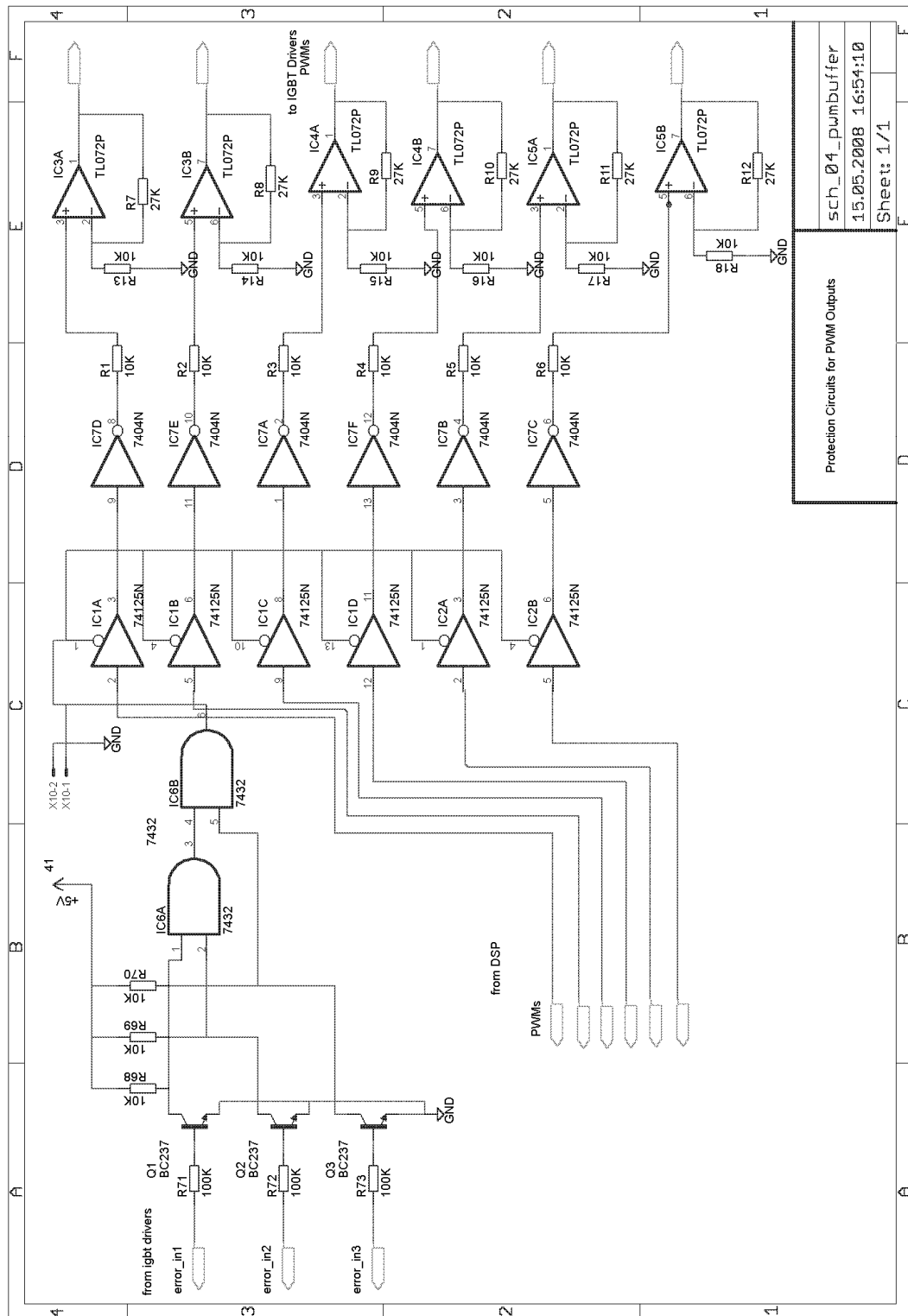
Current measument circuit.

Voltage measurement circuit.

LV25P Voltage Transducer Circuit

TITLE: sch_20_vtcard00

Document Number:

REV:

Date: 15.05.2008 19:00:18

Sheet: 1/1

APPENDIX C

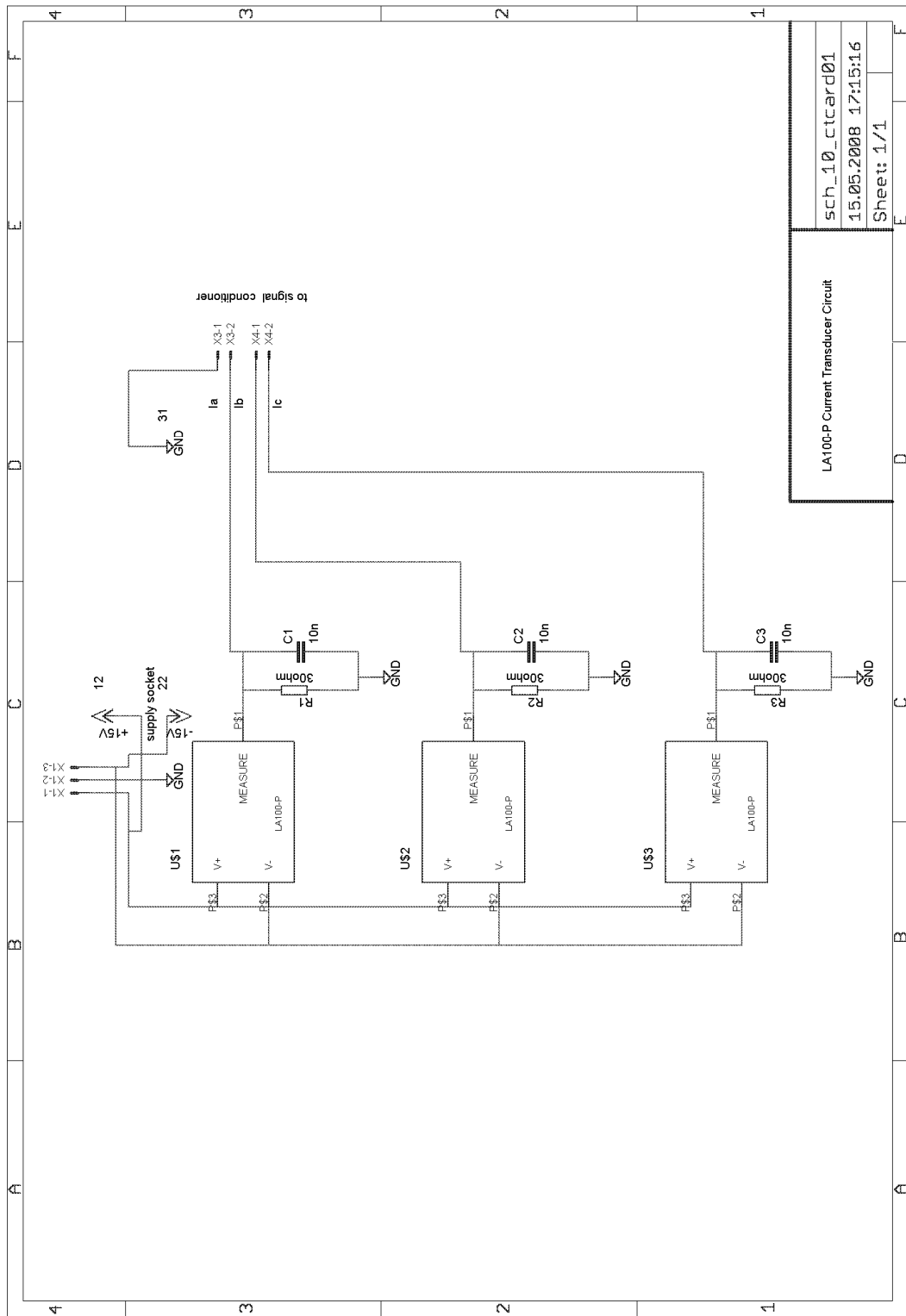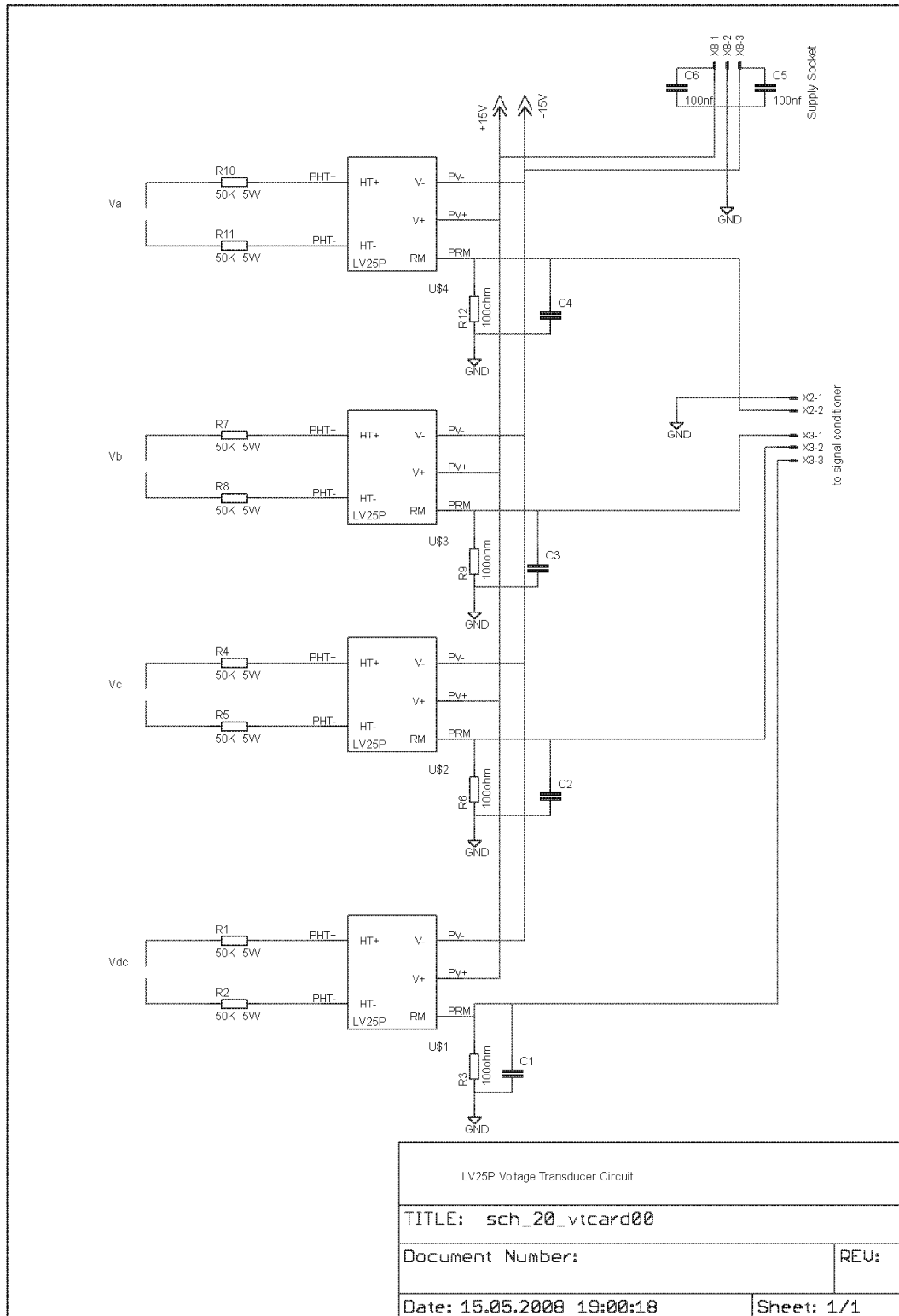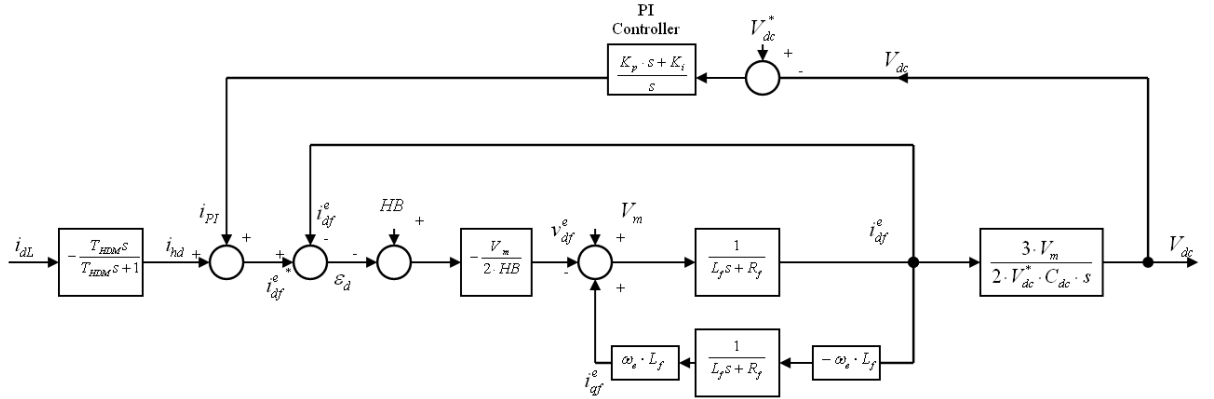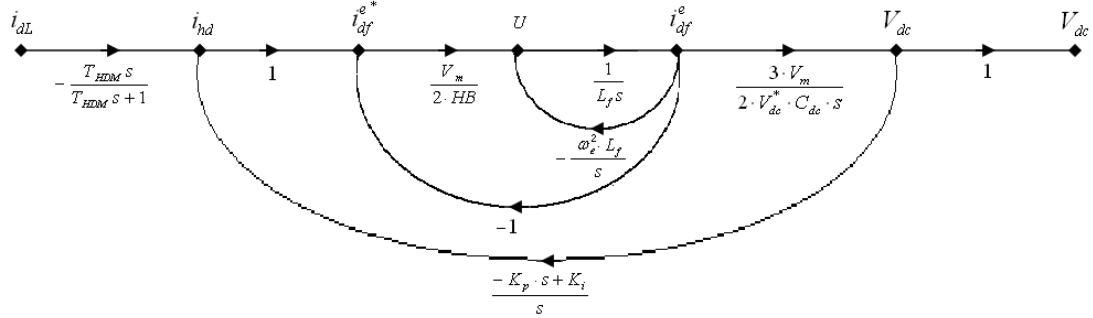## Finding of Linear Transfer function of shunt active power filter with hysterisis

By using $R_f \cong 0$, $F_d = \dfrac{V_m}{V_{dc}^*}$ and $v_{df} = f_d \cdot V_{dc}^* = \dfrac{V_m \cdot (HB - \varepsilon_d)}{2 \cdot HB}$ equations for obtain a

simple transfer function, signal-flow graph of system is as follows.

$$\frac{\Delta Output(s)}{\Delta Input(s)} = \frac{\Delta V_{dc}(s)}{\Delta I_{dL}(s)} = \frac{-\dfrac{T_{HDM} \cdot s}{T_{HDM} \cdot s + 1} \cdot \dfrac{V_m}{2 \cdot HB} \cdot \dfrac{1}{L_f \cdot s} \cdot \dfrac{3 \cdot V_m}{2 \cdot V_{dc}^* \cdot C_{dc} \cdot s}}{1 + \dfrac{\omega_e^2 \cdot L_f^2}{L_f \cdot s} \cdot \dfrac{1}{L_f \cdot s} + \dfrac{V_m}{2 \cdot HB} \cdot \dfrac{1}{L_f \cdot s} + \dfrac{V_m}{2 \cdot HB} \cdot \dfrac{1}{L_f \cdot s} \cdot \dfrac{3 \cdot V_m}{2 \cdot V_{dc}^* \cdot C_{dc} \cdot s} \cdot \dfrac{K_p \cdot s + K_i}{s}}$$

$$= \frac{\dfrac{-3 \cdot V_m^2 \cdot T_{HDM} \cdot s}{(T_{HDM} \cdot s + 1) \cdot 4 \cdot HB \cdot L_f \cdot V_{dc}^* \cdot C_{dc} \cdot s^2}}{1 + \dfrac{\omega_e^2}{s^2} + \dfrac{V_m}{2 \cdot HB \cdot L_f \cdot s} + \dfrac{3 \cdot V_m^2 \cdot K_p \cdot s + 3 \cdot V_m^2 \cdot K_i}{4 \cdot HB \cdot L_f \cdot V_{dc}^* \cdot C_{dc} \cdot s^3}}$$

$$= \frac{\dfrac{-3 \cdot V_m^2 \cdot T_{HDM} \cdot s}{(T_{HDM} \cdot s + 1) \cdot 4 \cdot HB \cdot L_f \cdot V_{dc}^* \cdot C_{dc} \cdot s^2}}{\dfrac{4 \cdot HB \cdot L_f \cdot V_{dc}^* \cdot C_{dc} \cdot s^3 + 4 \cdot \omega_e^2 \cdot HB \cdot L_f \cdot V_{dc}^* \cdot C_{dc} \cdot s + 2 \cdot V_m \cdot V_{dc}^* \cdot C_{dc} \cdot s^2 + 3 \cdot V_m^2 \cdot K_p \cdot s + 3 \cdot V_m^2 \cdot K_i}{4 \cdot HB \cdot L_f \cdot V_{dc}^* \cdot C_{dc} \cdot s^3}}$$

$$= \frac{-3 \cdot V_m^2 \cdot T_{HDM} \cdot s^2}{(T_{HDM} \cdot s + 1) \cdot [4 \cdot HB \cdot L_f \cdot V_{dc}^* \cdot C_{dc} \cdot s^3 + 2 \cdot V_m \cdot V_{dc}^* \cdot C_{dc} \cdot s^2 + 4 \cdot \omega_e^2 \cdot HB \cdot L_f \cdot V_{dc}^* \cdot C_{dc} \cdot s + 3 \cdot V_m^2 \cdot K_p \cdot s + 3 \cdot V_m^2 \cdot K_i]}$$

By not including the processing time, the transfer function between the capacitor voltage and load current can be obtained as follow.

$$\frac{\Delta V_{dc}(s)}{\Delta I_{dL}(s)} = \frac{-3 \cdot V_m^2 \cdot T_{HDM} \cdot s^2}{(T_{HDM} \cdot s + 1) \cdot \Delta(s)}$$

The characteristic equation :

$$\Delta(s) = 4 \cdot HB \cdot L_f \cdot V_{dc}^* \cdot C_{dc} \cdot s^3 + 2 \cdot V_m \cdot V_{dc}^* \cdot C_{dc} \cdot s^2 + 4 \cdot \omega_e^2 \cdot HB \cdot L_f \cdot V_{dc}^* \cdot C_{dc} \cdot s + 3 \cdot V_m^2 \cdot K_p \cdot s + 3 \cdot V_m^2 \cdot K_i$$

The stability is guaranteed if the transfer function does not have any pole in the right half plane. The stability range of dc link voltage PI controller parameters are determined by applying Routh-Hurwitz.

All coefficients of characteristic equation must be great to zero.

i) $3 \cdot V_m^2 \cdot K_i < 0 \Rightarrow K_i > 0$

ii) $8 \cdot \omega_e \cdot HB \cdot V_{dc}^* \cdot C_{dc} + 3 \cdot V_m^2 \cdot K_p > 0 \Rightarrow K_p > -\dfrac{4 \cdot \omega_e^2 \cdot HB \cdot L_f \cdot V_{dc}^* \cdot C_{dc}}{3 \cdot V_m^2}$

Routh-Hurwitz list

s^3	a_3	a_1
s^2	a_2	a_0
s^1	$\dfrac{a_2 \cdot a_1 - a_3 \cdot a_0}{a_2}$	0
s^0	a_0	0

All terms of Routh list must be great to zero.

iii)

$$\frac{a_2 \cdot a_1 - a_3 \cdot a_0}{a_2} > 0$$

$$\Rightarrow \frac{(2 \cdot V_m \cdot V_{dc}^* \cdot C_{dc}) \cdot (4 \cdot \omega_e^2 \cdot HB \cdot L_f \cdot V_{dc}^* \cdot C_{dc} + 3 \cdot V_m^2 \cdot K_p) - (4 \cdot HB \cdot L_f \cdot V_{dc}^* \cdot C_{dc}) \cdot 3 \cdot V_m^2 \cdot K_i}{2 \cdot V_m \cdot V_{dc}^* \cdot C_{dc}} > 0$$

$$\Rightarrow (4 \cdot \omega_e^2 \cdot HB \cdot L_f \cdot V_{dc}^* \cdot C_{dc} + 3 \cdot V_m^2 \cdot K_p) - (2 \cdot HB \cdot L_f) \cdot 3 \cdot V_m \cdot K_i > 0$$

$$\Rightarrow (2 \cdot HB \cdot L_f) \cdot 3 \cdot V_m \cdot K_i < (4 \cdot \omega_e^2 \cdot HB \cdot L_f \cdot V_{dc}^* \cdot C_{dc} + 3 \cdot V_m^2 \cdot K_p)$$

$$\Rightarrow K_i < \frac{(4 \cdot \omega_e^2 \cdot HB \cdot L_f \cdot V_{dc}^* \cdot C_{dc} + 3 \cdot V_m^2 \cdot K_p)}{6 \cdot HB \cdot L_f \cdot V_m}$$

$$\Rightarrow K_i < \frac{2 \cdot \omega_e^2 \cdot V_{dc}^* \cdot C_{dc}}{3 \cdot V_m} + \frac{V_m \cdot K_p}{2 \cdot HB \cdot L_f}$$

Range of stability area of DC Link PI controller can be determined by three equations given in above.

Matlab analysis of linear transfer function for shunt active power filter:

```
format long
clear all
w=2*pi*50;
HB=1;
Cdc=2300e-6;
Vm=310;
Vdc=650;
ts=1/100000;
tdc=0;
th=0.0001;
Lf=0.002;


Kp=0.05;
Ki=0.0005/ts;

a0=3*Vm*Vm*Ki
a1=3*Vm*Vm*Kp+4*w*w*HB.*Lf*Vdc*Cdc
a2=2*Vm*Vdc*Cdc
a3=4*HB*Lf*Vdc*Cdc
% vdc/idl
tf0=tf([1],[1 ])
tf1=tf([ 3*Vm*Vm],[ a3 a2 a1 a0])
tf2=tf([1 0   ],[1 ])
tf3=tf([tdc 1],[1 ])
tf4=tf([-th 0],[th 1 ])
tf5=tf1*tf2*tf0*tf4
bode(tf5)
```

```
% vdc/idh
tf0=tf([1],[1 ])
tf1=tf([ 3*Vm*Vm],[ a3 a2 a1 a0])
tf2=tf([1 0  ],[1 ])
tf3=tf([tdc 1],[1 ])
tf4=tf([-th 0],[th 1 ])
tf5=tf1*tf2*tf0*tf0
bode(tf5)


% idf/idl
tf0=tf([1],[1 ])
tf1=tf([ 2*Vm*Vdc*Cdc],[ a3 a2 a1 a0])
tf2=tf([1 0 0 ],[1 ])
tf3=tf([tdc 1],[1 ])
tf4=tf([-th 0],[th 1 ])
tf5=tf1*tf2*tf0*tf4
bode(tf5)


% idf/idh
tf0=tf([1],[1 ])
tf1=tf([ 2*Vm*Vdc*Cdc],[ a3 a2 a1 a0])
tf2=tf([1 0 0  ],[1 ])
tf3=tf([tdc 1],[1 ])
tf4=tf([-th 0],[th 1 ])
tf5=tf1*tf2*tf0*tf0
bode(tf5)
```

Finding stability ranges of linear model by Matlab:

```
%% For Ke-Lf
clear all
w=2*pi*50;
HB=1;
Cdc=2300e-6;
Vm=310;
Vdc=650;
ts=1/35000;
tdc=1/35000;
Kp=0.01;
Lf=0.0001:0.0001:0.006;

Kp=0.0001;
%b0=3*Vm*Vm*Ki
b1=3*Vm*Vm*Kp+4*w*w*HB.*Lf*Vdc*Cdc
b2=2*Vm*Vdc*Cdc+4*w*w*HB.*Lf*Vdc*Cdc*tdc
b3=4*HB.*Lf*Vdc*Cdc+2*Vm*Vdc*Cdc*tdc
b4=4*HB.*Lf*Vdc*Cdc*tdc
ki=ts*(((b2 - (b4./b3).*b1)./b3).*b1)./(3*Vm*Vm);

Kp=0.05
%b0=3*Vm*Vm*Ki
b1=3*Vm*Vm*Kp+4*w*w*HB.*Lf*Vdc*Cdc
b2=2*Vm*Vdc*Cdc+4*w*w*HB.*Lf*Vdc*Cdc*tdc
b3=4*HB.*Lf*Vdc*Cdc+2*Vm*Vdc*Cdc*tdc
```

```
b4=4*HB.*Lf*Vdc*Cdc*tdc
ki1=ts*(((b2 - (b4./b3).*b1)./b3).*b1)./(3*Vm*Vm);


Kp=0.01;
%b0=3*Vm*Vm*Ki
b1=3*Vm*Vm*Kp+4*w*w*HB.*Lf*Vdc*Cdc
b2=2*Vm*Vdc*Cdc+4*w*w*HB.*Lf*Vdc*Cdc*tdc
b3=4*HB.*Lf*Vdc*Cdc+2*Vm*Vdc*Cdc*tdc
b4=4*HB.*Lf*Vdc*Cdc*tdc
ki2=ts*(((b2 - (b4./b3).*b1)./b3).*b1)./(3*Vm*Vm);


figure
plot(Lf,ki,'-',Lf,ki1,'-.',Lf,ki2,':')
title('The graph of Kce-Lf for HB=1, fs=35kHz, Cdc=2300uF')
xlabel('Filter Inductance Lf (H)')
ylabel('Max Ke value for stability')
legend('Kce=0.0001','Kce=0.05','Kce=0.01')


%% for Ke-HB
clear all
w=2*pi*50;
HB=1;
Cdc=2300e-6;
Vm=310;
Vdc=650;
ts=1/35000;
tdc=1/35000;
Kp=0.0001;
Lf=0.002;


HB=0.1:0.01:3;


Kp=0.0001;
%b0=3*Vm*Vm*Ki
b1=3*Vm*Vm*Kp+8*w.*HB*Vdc*Cdc
b2=2*Vm*Vdc*Cdc+8*w.*HB*Vdc*Cdc*tdc
b3=4.*HB*Lf*Vdc*Cdc+2*Vm*Vdc*Cdc*tdc
b4=4.*HB*Lf*Vdc*Cdc*tdc
ki=ts*(((b2 - (b4./b3).*b1)./b3).*b1)./(3*Vm*Vm);


Kp=0.05
%b0=3*Vm*Vm*Ki
b1=3*Vm*Vm*Kp+8*w.*HB*Vdc*Cdc
b2=2*Vm*Vdc*Cdc+8*w.*HB*Vdc*Cdc*tdc
b3=4.*HB*Lf*Vdc*Cdc+2*Vm*Vdc*Cdc*tdc
b4=4.*HB*Lf*Vdc*Cdc*tdc
ki1=ts*(((b2 - (b4./b3).*b1)./b3).*b1)./(3*Vm*Vm);


Kp=0.01;
%b0=3*Vm*Vm*Ki
b1=3*Vm*Vm*Kp+8*w.*HB*Vdc*Cdc
b2=2*Vm*Vdc*Cdc+8*w.*HB*Vdc*Cdc*tdc
b3=4.*HB*Lf*Vdc*Cdc+2*Vm*Vdc*Cdc*tdc
b4=4.*HB*Lf*Vdc*Cdc*tdc
ki2=ts*(((b2 - (b4./b3).*b1)./b3).*b1)./(3*Vm*Vm);


figure
```

```
plot(HB,ki,'-',HB,ki1,'-.',HB,ki2,':')
title('The graph of Kce-HB for Lf=2mH, fs=35kHz, Cdc=2300uF')
xlabel('Hysteresis Band (A)')
ylabel('Max Ke value for stability')
legend('Kce=0.0001','Kce=0.05','Kce=0.01')


%% For Ke-Cdc
clear all
w=2*pi*50;
HB=1;
Cdc=2300e-6;
Vm=310;
Vdc=650;
ts=1/35000;
tdc=1/35000;
Kp=0.0001;
Lf=0.002;
Cdc=1100e-6:100e-6:3300e-6;


Kp=0.0001;
%b0=3*Vm*Vm*Ki
b1=3*Vm*Vm*Kp+8*w.*HB*Vdc.*Cdc
b2=2*Vm*Vdc.*Cdc+8*w.*HB*Vdc.*Cdc*tdc
b3=4.*HB*Lf*Vdc.*Cdc+2*Vm*Vdc.*Cdc*tdc
b4=4.*HB*Lf*Vdc.*Cdc*tdc
ki=ts*(((b2 - (b4./b3).*b1)./b3).*b1)./(3*Vm*Vm);

Kp=0.05
%b0=3*Vm*Vm*Ki
b1=3*Vm*Vm*Kp+8*w.*HB*Vdc.*Cdc
b2=2*Vm*Vdc.*Cdc+8*w.*HB*Vdc.*Cdc*tdc
b3=4.*HB*Lf*Vdc.*Cdc+2*Vm*Vdc.*Cdc*tdc
b4=4.*HB*Lf*Vdc.*Cdc*tdc
ki1=ts*(((b2 - (b4./b3).*b1)./b3).*b1)./(3*Vm*Vm);

Kp=0.01;
%b0=3*Vm*Vm*Ki
b1=3*Vm*Vm*Kp+8*w.*HB*Vdc.*Cdc
b2=2*Vm*Vdc.*Cdc+8*w.*HB*Vdc.*Cdc*tdc
b3=4.*HB*Lf*Vdc.*Cdc+2*Vm*Vdc.*Cdc*tdc
b4=4.*HB*Lf*Vdc.*Cdc*tdc
ki2=ts*(((b2 - (b4./b3).*b1)./b3).*b1)./(3*Vm*Vm);

figure
plot(Cdc,ki,'-',Cdc,ki1,'-.',Cdc,ki2,':')
title('The graph of Kce-Cdc for Lf=2mH, fs=35kHz, HB=1')
xlabel('DC Link Capacitor (Farad)')
ylabel('Max Ke value for stability')
legend('Kce=0.0001','Kce=0.05','Kce=0.01')

%% For Ke-fs
clear all
w=2*pi*50;
HB=1;
Cdc=2300e-6;
Vm=310;
```

```
Vdc=650;
ts=1/35000;
tdc=1/35000;
Kp=0.0001;
Lf=0.002;
fs=10000:5000:100000;
ts=1./fs;
tdc=ts;


Kp=0.0001;
%b0=3*Vm*Vm*Ki
b1=3*Vm*Vm*Kp+8*w.*HB*Vdc.*Cdc
b2=2*Vm*Vdc.*Cdc+8*w.*HB*Vdc.*Cdc.*tdc
b3=4.*HB*Lf*Vdc.*Cdc+2*Vm*Vdc.*Cdc.*tdc
b4=4.*HB*Lf*Vdc.*Cdc.*tdc
%for ii=1:lenght(Lf)
ki=ts.*(((b2 - (b4./b3).*b1)./b3).*b1)./(3*Vm*Vm);


Kp=0.05
%b0=3*Vm*Vm*Ki
b1=3*Vm*Vm*Kp+8*w.*HB*Vdc.*Cdc
b2=2*Vm*Vdc.*Cdc+8*w.*HB*Vdc.*Cdc.*tdc
b3=4.*HB*Lf*Vdc.*Cdc+2*Vm*Vdc.*Cdc.*tdc
b4=4.*HB*Lf*Vdc.*Cdc.*tdc
ki1=ts.*(((b2 - (b4./b3).*b1)./b3).*b1)./(3*Vm*Vm);


Kp=0.01;
%b0=3*Vm*Vm*Ki
b1=3*Vm*Vm*Kp+8*w.*HB*Vdc.*Cdc
b2=2*Vm*Vdc.*Cdc+8*w.*HB*Vdc.*Cdc.*tdc
b3=4.*HB*Lf*Vdc.*Cdc+2*Vm*Vdc.*Cdc.*tdc
b4=4.*HB*Lf*Vdc.*Cdc.*tdc
ki2=ts.*(((b2 - (b4./b3).*b1)./b3).*b1)./(3*Vm*Vm);


figure
plot(fs,ki,'-',fs,ki1,'-.',fs,ki2,':')
title('The graph of Kce-fs for Lf=2mH, HB=1, Cdc=2300uF')
xlabel('Sampling frequency  (Hertz)')
ylabel('Max Ke value for stability')
legend('Kce=0.0001','Kce=0.05','Kce=0.01')
```

Developed Matlab code for analysing effect of system elements.

```
format long
clear all
w=2*pi*50;
HB=1;
Cdc=2300e-6;
Vm=310;
Vdc=650;
ts=1/100000;
tdc=0;
th=0.0001;
Lf=0.002;
Kp=0.05;
Ki=0.0005/ts;
a0=3*Vm*Vm*Ki
a1=3*Vm*Vm*Kp+4*w*w*HB.*Lf*Vdc*Cdc
a2=2*Vm*Vdc*Cdc
a3=4*HB*Lf*Vdc*Cdc


% Supply side impedance
Ls=127.5e-6;
Zs=tf([Ls 0], [1])
%%%%%%%%%%%%%%%%%%%%%%%%%%%%%%%%%%%%%%%%%%
% Load side impedance

% for RC circuit
Rl=85e-3
Cl=1500.76e-6
Zl=tf([Rl*Cl 1], [Cl 0])


%%%%%%%%%%%%%%%%%%%%%%%%%%%%%%%%%%%%%%%%%%%
tf0=tf([1],[1 ]);
tf1=tf([ 2*Vm*Vdc*Cdc],[ a3 a2 a1 a0]);
tf2=tf([1 0 0 ],[1 ]);
tf3=tf([tdc 1],[1 ]);
tf4=tf([-th 0],[th 1 ]);
tf5=tf1*tf2*tf3*tf4;
Gapf= tf5;
%%%%%%%%%%%%%%%%%%%%%%%%%%%%%%%%%%%%%%%%%%%

% measurement from A point
Ga=(1-Gapf)*Zl/(Zl+Zs)
bode(Ga)

figure
% measurement from B point
Gb=(1-Gapf)*Zl/(Zl+(1-Gapf)*Zs)
bode(Gb)
axes([1 10^4  -150 10])
```
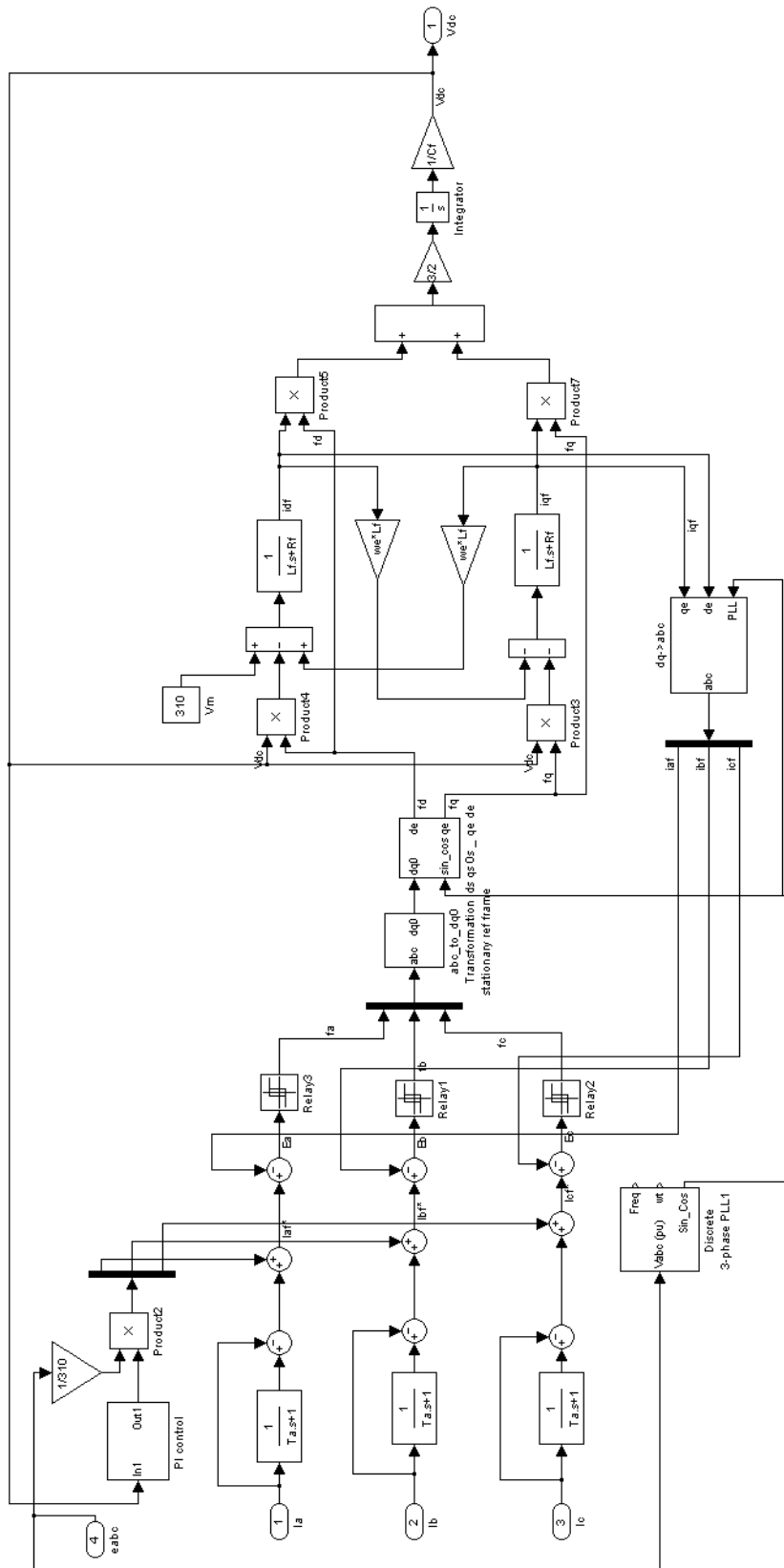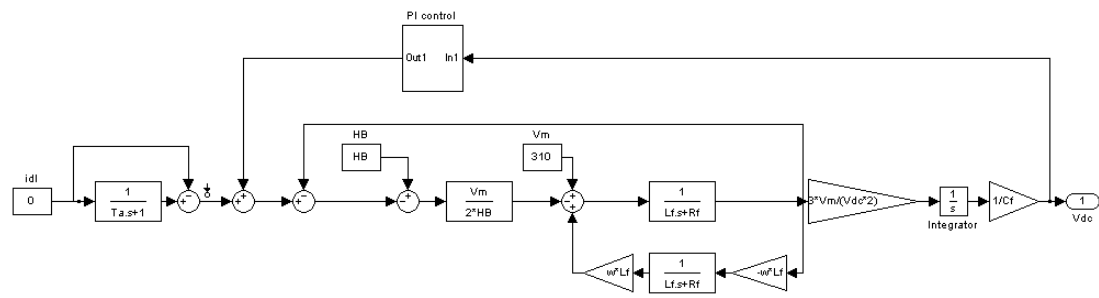
Matlab Simulation of Analytic Model of Shunt Active Power Filter

Matlab Simulation of Linear Model of Shunt Active Power Filter

LIST OF SYMBOLS

L_f	Filter inductance
R_f	Filter resistance
C_{dc}	DC link capacitor
e_a, e_b, e_c	Supply voltages
v_{af}, v_{bf}, v_{cf}	Terminal voltages of active power filter
i_{af}, i_{bf}, i_{cf}	Filter currents
i_{al}, i_{bl}, i_{cl}	Load currents
i_{ah}, i_{bh}, i_{ch}	Harmonic currents from generated by load
f_a, f_b, f_c	Switching functions of each phase
f_d, f_q	d, q components of switching functions
F_d, F_q	Simplifying on f_d, f_q
i_{df}^e, i_{qf}^e	d, q components of filter currents in SRF
$i_{df}^{e'}$	Decomposed d axis current of filter
i_{df}^{e*}, i_{qf}^{e*}	Reference currents in SRF
i_{dL}^e, i_{qL}^e	d,q components of load current
v_{df}^e, v_{qf}^e	d,q components of terminal voltages
i_{dc}	DC link current
ω_e	Synchronously angular velocity
HB	Hysteresis Band
$\varepsilon_a, \varepsilon_b, \varepsilon_c$	The current tracking errors of each phase.
c	Shape parameter of hysteresis function
α	Scaling parameter of hysteresis function
ε_{PI}	PI controller error
ε_i	Current error of decomposed current

v_{dc}, v_{dc}^*	DC link actual and reference voltages
v_m	Peak voltage of supply
K_p, K_i	Proportional and integral gains of PI controller.
K_E, K_{CE}	Proportional and integral gains of digital PI controller.
W_n	the weighting values
X_n	inputs of neuron
n	number of inputs
b	bias value
$\hat{y}(k)$	reference output of system
$u(k)$	input of system.
y	output of Adaline
f_1	fundemantel frequency
f_S	sampling frequency
T_S	sampling period
E	error between output and desired output.
γ	learning constant
∇E	gradient of error
∇W_n	change of weights
MSE	Mean square error